2-1-2019

Deferred Cooling System

Maha Farouk El Bedaiwy

The American University in Cairo
School of Sciences and Engineering
Environmental Engineering Program

Deferred Cooling System

BY
Maha Bedaiwy
B.Sc. in Mechanical Engineering

A thesis submitted in the partial fulfillment of the requirements for the degree of

Master of Science in Engineering
With specialization in
Environmental Engineering

Under the Supervision of

Dr. Amr Serag Eldin
Professor, Department of Mechanical Engineering
The American University in Cairo

Dr. Mohamed El Morsi
Associate Professor, Department of Mechanical Engineering
The American University in Cairo

Fall 2018

Abstract:

The thesis is concerned with the development of a system for dissipating heat from a thermodynamic cycle operating in environments where fresh water is scare and ambient temperatures are high, therefore evaporative cooling is not an option whereas ambient temperatures are too high most of the day for adequate air cooling. An example of this is solar driven vapor compression cycles in desert climates. The proposed system exploits the substantially cooler night time ambient temperatures and the highly effective net radiation exchange with night sky.

Since solar driven equipment require to operate during daytime when solar energy is available and hence their cycle heat is being rejected during day time hours when ambient temperatures are high, and the environment is hostile to cooling , the proposed system resorts to deferred cooling with the aid of thermal storage which can be in the form of sensible heat and water storage , however this water need not be potable and is re-usable.

The thesis presents the details of implementation of the proposed system and mathematical model which can be used in its simulation and design. An experimental rig was purposely designed and built from which valuable measurements were obtained and used to demonstrate the application of the concept.

Comparison between the model prediction and measurement revealed further important results. Theoretical investigation was also conducted using the proposed model to explore the system response and behavior under various weather and loading conditions. The model acts as a tool to evaluate any site's suitability for the Deferred Cooling System (DCS) or possibly any other similar system employing radiative cooling.

The results of those investigations revealed that the system is only recommended to be used under the right weather condition, in those conditions it is highly effective and efficient; indeed, it was adopted for the very hostile environment of Shallatin, Upper Egypt (23.1 °N latitude , 35.56 °E longitude) , for a solar driven ice production project for fish preservation and proved to be quite successful.

Acknowledgement

I am very grateful to have been given the opportunity to work with my advisors Professor Mohamed Amr Serag El-din who has trusted me with his innovative idea and guided me through and Associate Professor Mohamed El Morsi whose thorough support and guidance in every step of the way have made it possible for me to accomplish this work. Thank you, it has been a true honor to have you as my advisors.

I would like to dedicate this research work to the memory of my late mother Carmen Thabet who has been an inspiration for me throughout and hope to be able to provide the same drive for my kids Nora and Omar Helal who have been the most understanding and supportive kids. I would also like to thank my father Farouk Bedaiwy and my brother Sharif Bedaiwy for helping when their help was most needed.

The American University in Cairo has been my home as an undergraduate and now as a graduate student. I would like to thank all of its staff and especially the Fluids lab technicians and engineers (particularly technician Haythem) for their help. A special thanks to Professor Salah El Haggar who has been my professor as an undergraduate student and has encouraged me throughout my masters.

I would like to acknowledge the financial support received from the Egyptian Academy of Scientific Research and Technology, through the ASRT prototyping, Technological Development and Marketing Support Program, 2015-2016.

Finally, I would like to thank the Deutsche Gesellschaft für Internationale Zusammenarbeit (GIZ) GmbH Egyptian-German Private Sector Development Programme (GIZ-PSDP) and the Egyptian National Cleaner Production Center-Ministry of Trade and Industry (ENCPC-MTI) for the use of the weather station provided by them.

Table of Contents:

List of Figures:

List of Tables:

Nomenclature:

A	Surface area
c_p	Specific heat
D	Diffusion Coefficient
DR	Diffuse radiation
E	Emissive power
Fps	Shape factor
G	Global radiation
Gr	Grashof number
h	Heat transfer coefficient
J	Radiosity
K	Thermal conductivity
Kd	Diffuse percent
T	Temperature
t	Time
m	Mass
Nu	Nusslet number
P	Pressure
Pr	Prandtl No.
$\dot{Q}$	Rate of heat flow
R	Resistance
Ra	Rayleigh No.
Re	Reynolds No.
Ri	Richardson no.
Sc	Schmidt
Sh	Sherwood Number
V	Volume
V	Wind speed
X	Distance/gap

Greek Symbols

α	Thermal Diffusivity
ε	Evaporation coefficient
ϵ	Emissivity
ρ	Density
σ	Boltzmann constant
ϕ	Relative humidity

Subscripts

∞	Ambient
bot	Bottom of the pool
cl-sky	Clear sky
conv	Convection
dp	Dew point
evp	Evaporation
htg	Heating
Gr	Ground
p	Pool
LWrad	Long wave radiation
mid	Middle
raw	Right above the pool
s	Shield
Sat	Saturated
sf	Surface
sim	Simulated
sp	Space
SWrad	Short wave radiation
s,i	Shield inside
s,o	Shield outside
ins	Insulation
St	Steam
Gr	Ground
ws	Weather station

Abbreviations

ASRT	Egyptian Academy for Scientific Research and Technology
COP	Coefficient Of Performance
DCS	Deferred Cooling System
ECAC	Evaporative Condenser Cooled Air Conditioners
EER	Energy Efficiency Ratio
EPS	Expanded Polystyrene

Chapter 1: Introduction

Engineering systems which follow thermodynamic cycles need to continuously reject heat during their operation. Heat rejection is achieved employing various cooling media; whether air, water or any other cooling agent. The choice of the cooling media depends on the application requirement, location, climate and abundance of resources. Cooling water is a popular choice because of its excellent thermodynamic properties and its general availability and low price, however the latter is not always the case, e.g. in desert environments. This is the very reason why large power plants tend to be located next to natural water sources.

In desert climates, where fresh water is scarce and air temperatures are high, the need for an innovative design that does not require much water consumption or transportation (being pipes or other means) is a key to the success of new projects in remote areas; many being solar energy driven systems that require cooling during operation. Solar energy applications are particularly important for many developing countries under the Sunbelt, as a key step towards achieving sustainable development and avoiding the use of polluting, expensive and potentially diminishing conventional fuel sources. The challenge of employing solar energy driven applications is the need to operate during daytime hours when solar energy is abundant and hence ambient air temperature is high, thus posing heat rejection difficulties. The day time ambient air is too hot for direct air-cooling; moreover, most countries under the Sunbelt feature desert like climates, where fresh water is scarce and hence use of evaporative cooling is an expensive proposition, as water consumption is high and water is scarce. Sensible heat water cooling is definitely ruled out because of the scarcity of water.

One of the very common cooling needs is the heat rejection in vapor compression cycle for condenser cooling used in many applications such as refrigeration and air conditioning, whether for residential buildings, industrial facilities, or for electronic equipment and chiller operation in refrigeration. Air conditioning systems represent around one third of electricity consumption in some large cities (such as California in the US) during peak hours , which makes any gain in the efficiency of their energy consumption increasingly attractive,(Faramarzi, Lutton, and Gouw 2010)

Heat rejection from refrigeration cycle is not the only application where cooling water is required, in fact applications for heat exchangers that employ cool water go far beyond air conditioning. An example of this would be the possible use of heat exchangers at the back of PV panels to enhance their performance when operating at lower temperatures in hot climates. A simulation of electricity generating PV system performance using TRNSYS reported an average annual efficiency increase from 2.8% to 7.7 % when operating at lower temperature at the recommended optimum cooling flow rate(Kalogirou 2001)

The purpose of the condenser is exchanging the rejected heat by the refrigerant to the cooling fluid, with air and water being the most commonly used media for cooling. The air-cooled condensers are simple heat exchangers that allow sensible heat transfer from the refrigerant inside the coil at a higher temperature and pressure to outside air at dry bulb temperature. Though efficiency (represented in COP (coefficient of performance)) drops with the rise in dry bulb temperature, switching to other higher efficiency alternatives, such as water cooling, has been stalled by the water system consumption and maintenance requirements. There is also the evaporative condenser

cooling where the condenser coil is basically covered with a water film that absorbs some of the heat from the refrigerant inside, then ambient air passing across the coil leads to latent heat and mass transfer due to evaporation that depends on the air wet bulb temperature. Since they depend mainly on evaporation, their suitability for various climates with high humidity is questionable. (Faramarzi, Lutton, and Gouw 2010) ; moreover because of the high rates of water consumption they are also not well suited to desert environments.

The initial and running cost of air versus water cooled chillers have been the focus of many studies in different cities to try and compare their pros, cons and suitability for different climates. Naguib (Naguib 2009) compared the total ownership cost of both systems of size ranging from 100 to 500 tons refrigeration for various US cities representing different climates to see the impact on installation, maintenance and running costs. The initial cost of water-cooled system was always higher, the energy cost comparable for 100 tons, but less than air cooled for larger capacities and the maintenance cost slightly higher for low tonnage water cooled systems. This makes water cooled chiller more attractive for larger capacities, especially that they normally have longer life than air cooled chillers. Of course, water cooled chillers have better efficiencies, so they are more favorable with longer daily operational hours to overshadow the higher installation cost.

One of the main contributors of the high installation cost of the water cooled systems that prevent benefiting from its better efficiencies in small projects is the high cost of the cooling tower of the water cooled chiller, that does not even last as long as the chiller itself (Naguib 2009). This creates a need for a simpler, less expensive way to feed water cooled condensers that would make them more attractive for smaller capacity projects, where the choice of air cooled condenser might not be favorable due to high ambient temperatures with negative impact on COP and thus higher power requirements; especially in projects with scarce energy resources, in remote areas that rely mainly on solar power supplemented with battery storage for parts of the day where there is no sun.

Another comparison between evaporative condenser cooled air conditioners (ECAC) and air-cooled type (A/C) was conducted at the technology test center in the laboratories of southern California Edison. The study revealed that evaporative cooled condensers operating in very hot and dry climate conditions, had a 51% better energy efficiency ratio (EER) than air cooled (A/C) type. The normalized (at 95 °F) net cooling capacity, total power consumption and EER of both cooling air conditioning systems were compared against ambient DB temperature, showing a clear deterioration in all three performance measures of the air-cooled systems with the increase in dry bulb (DB) temperature, which was not the case for the ECAC. However, the water consumption requirements to cover for evaporation losses and purging capacity for the ECAC were estimated to be 2.1 to 2.8 gallons per hour per ton of air conditioning capacity for the unit under test (3 tons capacity). (Faramarzi, Lutton, and Gouw 2010) This represents a clear obstacle against their use in locations with limited water resources.

Condenser cooling options for engineering projects are normally evaluated at the start of the projects to come up with the most feasible solution. A theoretical study of the available techniques for condenser cooling of seawater greenhouses was done in Aachen University in Germany with the following outcomes. The study started by listing all the possible cooling techniques and evaluating their feasibility for the application. Air was first considered but was disregarded since it is as hot as or even hotter than the humid air entering the condenser. So the only option would be to use a

cooling machine to cool the air, but cooling water is more technically sound due to its heat transfer capabilities and of course pumping water is a better choice than pumping gas, with overall less power requirements.

The second option is to use water as the coolant either from deep or surface sea water, if a nearby source is available. Deep water from the sea is quite cold, whereas surface water would need cooling which could be achieved by employing an evaporative cooler. The main drawback of using sea water is the negative effect it can create on heat transfer mechanisms due to the biological deposit of sea organisms on surfaces that can cause fouling and would require high frequency maintenance with elevated costs. Water cooling could be achieved either through heat exchanger or using direct contact spray condenser (DCSC) that is not subject to fouling and employs both mass and heat transfer. In the DCSC, part of the condensate is cooled externally (using heat exchanger) and is sprayed from automatically controlled nozzles along the passage of humid air. Again a source of cold water is needed for the external heat exchanger so the surface seawater has to be cooled by evaporation or by using a cooling machine.(Dawoud et al. 2006)

Evaporative cooling was also considered with different types of cooling towers; however, this cooling method is highly dependent on both the air-dry bulb temperature and the relative humidity of the site. The study reported maximum allowable humidity levels versus ambient air temperatures for specific temperature difference between air and water leaving the cooling tower and air leaving the condenser. For example, 65% humidity levels was found to be the maximum acceptable limit for evaporative cooling to produce an effective cooling media for the condenser at a temperature of 45°C, where as 18% would be the maximum acceptable limit at 30°C. (Dawoud et al. 2006) So even if the cooling tower cost is justifiable for engineering projects , climate conditions of high humidity sites could render that option completely invalid for the site.

From the above discussion, we can clearly conclude that the need for cooled water always finds its way one way or another in heat rejection applications, so the presence of a simple, cost effective solution that does not require high water or power consumption for cooling the water is always favorable. This is where the concept of deferred cooling system that is the focus of this work comes to play.

1.1: Deferred cooling system:

In hot desert climates, though ambient air temperature is high, it drops significantly during the night to levels (10-25°C below day time temperatures), and thus can be used to dissipate the rejected heat from the condenser of a reverse cycle much more effectively. Another feature of desert climates is the clear, cool night time skies with temperatures reaching 25 $°C$ below ambient. To exploit this phenomenon, all what is needed is to devise a simple system to defer the dissipation of the condenser heat to the environment, until night time, when the ambient temperature is much cooler, and infra–red radiation exchange with the sky can be exploited. The present work is concerned with the design, implementation and testing of such a system. The system relies on sensible heat storage through storing unpotable, reusable cooling water to cool the condenser during day time operational hours, and deferring the heat dissipation from the cooling water to night time; because of the high thermal capacity of the cooling water, the water cooled during nighttime may be

expected to retain its cool temperature until it is used next day; provided a proper implementation design is made of course.

Since the main reason of elevated temperatures in sunny climates is the absorption of short-wave radiation from the sun, proper shading of water surface during the day could eliminate most of the beam component part of solar radiation that contains the bigger percentage of solar radiation energy on a sunny day. On the other hand, exposing the water surface to night time cold skies greatly enhance cooling of the stored water during the night through heat loss by long wave radiation. The deferred cooling system comprises an artificial shallow pond with a removable shield as a thermal store.

The system under study is mostly suitable for desert environment that features high temperature swings between day and night that is mostly affected by the clearness of the desert sky. Though the desert climate is a dry climate that could be suitable for evaporative cooling, shortage of water, power and initial capital cost makes the simple deferred cooling system more favorable for desert climates.

The purpose of this research work is to investigate the novel idea of a" Deferred Cooling System˝ and its ability to provide cooling water to be used in typical desert climates , either in refrigeration and air-conditioning systems or for general equipment cooling through heat exchangers to enhance their performance in hot climates This is done by analyzing the system cooling performance using a lumped capacity mathematical model with its results compared to experimental work for validation. The aim is to provide a simple model that is able to use the metrological weather data of any site to evaluate the system suitability for the site under consideration with a possibility to study the effect of different running scenarios on the system performance. The model could also provide an indication for the suitability of any site for radiative cooling systems in general using its relevant weather data. On the other hand, the experimental work was used to demonstrate the deferred cooling concept of the system.

This introductory chapter is followed by a literature review in chapter 2, then a description of the system and its implementation in chapter 3; followed by the developed mathematical model presented in chapter 4, theoretical investigation in chapter 5, the experimental rig in chapter 6; the results of the measurements and their simulations are discussed in chapter 7. Finally, the conclusion and recommendations are presented in chapter 8. The appendix includes the MATLAB code developed as well as supplementary information on the experimental work that was used in validating assumptions and demonstrating some research highlights. The appendix also includes some supplementary information for different sections of the thesis as will be pointed out throughout the different chapters. Figure 1-1 presents an outline for the thesis to clarify the link between the different sections of this work.

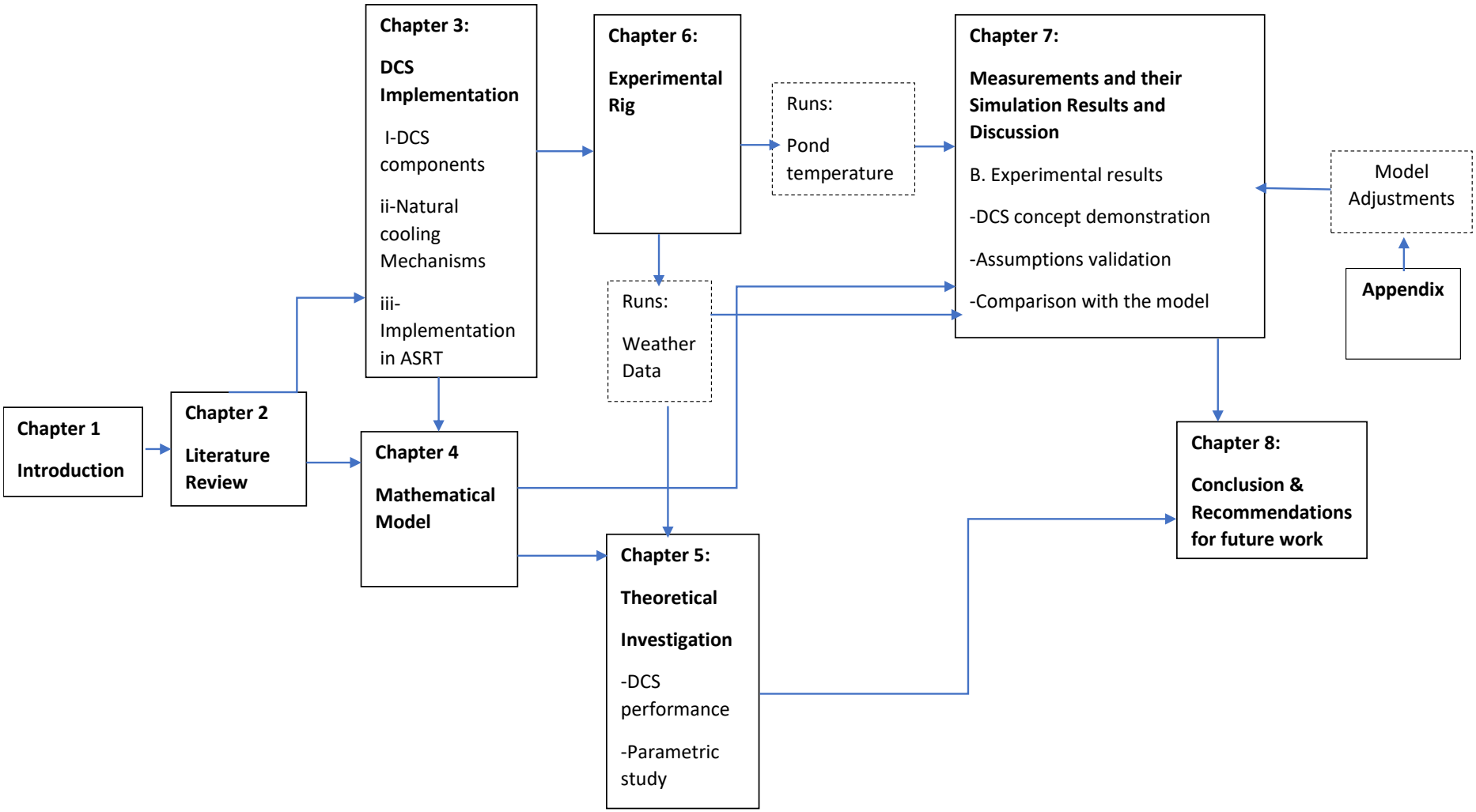

Figure 1-1: Thesis outline

Chapter 2: Literature Review

The concept of using a ground heat sink in absorbing thermal cooling load has been first introduced by Serag-Eldin (Serag-Eldin 2011) to be used mainly in desert climates for the cooling of air conditioning systems. The proposed design involved alternating the use of the cool water in the ground sink to absorb the heat load in the circulating water from the condenser with air cooled cross-flow heat exchanger to decrease the thermal load that the ground heat sink is required to absorb in its daily cycle. Though the natural cooling mechanisms of the heat sink are similar to those of the deferred cooling system under study, it differs from it mainly in that it is required to absorb the full thermal load of the engineering system it is required to cool in its daily cycle to avoid the heat up of these systems since there is no alternative cooling mechanism. Also, in the deferred cooling system, the cooler water goes directly from the sink to be used as the cooling water and does not pass through heat exchangers or ducts. The system under study does not have to be buried in the ground, has different shading positions that could be more flexibly operated and could involve more than one heat sink at a time.

2.1: Radiative cooling systems:

While solar energy provides natural heat energy that is universally exploited in building space heating, there exist enormous cooling potential from various ambient cold energy sources that can be exploited as cold sinks in air conditioning applications. Depending on weather conditions, these cool sources could be atmospheric air at either wet or dry bulb temperatures, geothermal and night sky radiation energy .Dogtrot houses in US homes shield sun rays and use air to create a cool breeze .Humidity levels define the limits for the potential use of wet bulb air in evaporative cooling, especially for space heating where safe humidity levels cannot be crossed, this encourages its use only in low humidity climates. It also common for the temperature to be lower than ambient air deep into the ground, this is where cooling via geothermal energy through earth to air heat exchangers provide big cooling potential. (Robinson, Dorwart, and Sharp 2015)

Radiative cooling happens when bodies on earth emit long wave radiation in the infrared region that ranges from 18 to 13μm, so called “atmosphere infrared window”. This phenomena allows the passage of energy through the atmosphere without warming it, since the wavelength is directly dependant on the body temperature, with radiation emitted from earth surface falling in the infrared region.(Vall and Castell 2017)

The estimation of infrared atmospheric radiation from clear skies is either derived from irradiance and radiation spectrum measurements or considering the composition of gases in the atmosphere under relevant temperature, pressure and density that vary considerably with heights and affect their radiation absorption Clouds have a great effect on increasing the received atmospheric radiation on earth, since they could act as a blackbody that emits radiation near the infrared window. (Vall and Castell 2017)

Ideally to achieve maximum cooling in radiators, it needs to be horizontally placed on earth’s surface as to maximize its sky and minimize its ground view factor. Being tilted allows more exposure to the horizon, being the warmer part of the sky. This is simply not possible in most cases, since a tilt angle

is needed for mounting on roofs or to achieve a favourable natural gravity circulation.(Vall and Castell 2017)

Every place on earth has a specific radiative cooling potential that has to be matched to the cooling needs of the application under study. As early as 1978, Atwater and Ball (Atwater and Ball 1978), created a method to obtain the temperature of the sky from infrared radiation in the atmosphere, creating maps for US cities showing both the sky and difference between air and sky temperature distribution for different seasons of the year . The temperature difference (so called depressions) ranged from 6 to 18 $°C$.Other studies reported that radiative cooling would be suitable for certain climates rather than others, highlighting the suitability of a place like California for radiative cooling (Martin and Berdahl 1984). In Thailand, a difference of near 8 $°C$ between effective sky temperature and daily minimum ambient temperature was reported, highlighting an opportunity for benefits from radiative cooling in the area.(Vall and Castell 2017) AS for Malaysia, analysis estimated the potential of radiative cooling to elevate up to 11% of cooling energy requirement. (Hanif et al. 2014)A research gap still exist in standardizing and simplifying the methods used to select suitable sites for radiative cooling by creating some sort of a world map matching suitable radiative cooling climates with their cooling needs.(Vall and Castell 2017)

If through the use of selective materials, we could create an" ideal emitter " in the optical window of (8-13) μm and an "ideal reflector" outside this range, the power of reflective cooling, at ambient temperature , could be in the range of 100 W/m^2, theoretically reaching temperatures of 50 $°C$ below ambient if radiation energy was the sole energy affecting the perfect emitter.(Granqvist, Hjortsberg, and Eriksson 1982) Though the existence of such a material is unrealistic, ongoing efforts to create conditions that would get radiative cooling to operate as close as possible to ideal conditions do exist, through the use of selective surfaces or screens, cover screens, paints, reflecting mirrors (for unwanted radiation outside that range) or the replacement of radiator surrounding air with either vacuum or another gas to supress convection between cover and radiator surfaces. (Vall and Castell 2017)

Several research attempts have been made to test prototypes of radiative cooling systems, both experimentally and numerically. The majority of which are modified flat plates solar collectors, used as radiators for cooling. At first, the main aim of radiative cooling was to assist in roof cooling of buildings, by achieving some nocturnal cooling and reflecting sun rays during the day.(Vall and Castell 2017) Air was used as the operating fluid , white painting over steel and Tedlar coated Aluminum were used ,all provided radiative cooling power not more than 22 $\frac{W}{m^2}$, with temperature reaching 6 $°C$ below ambient during the night. (Michell and Biggs 1979)Other systems involved circulating air from buildings into Aluminum painted tubes during the night , achieving 2.5-4$°C$ reduction in temperature when compared to buildings without radiative precooling.(Bagiorgas and Mihalakakou 2008)Then water ,with its higher thermal capacity and easier operation and control replaced air as the operating fluid in recent research , either in closed or open radiator systems, with the latter having evaporation and convection cooling effects in addition to radiation .As mentioned earlier, solar collectors were used for radiative cooling , an experimental investigation of night sky cooling of a flat plate type solar water heater (2.2 x1.3 m) after removing the glazing reported an average cooling of $80W/m^2$ for an eight hour span. (Erell and Etzion 1996)Then attempts were made to combine heating and cooling in closed system solar collectors , achieving up

to 610 $\frac{W}{m^2}$ of heating and 51$\frac{W}{m^2}$ of cooling .Another study attempted supplying radiative cooling power of around 628 $\frac{kJ}{m^2 night}$ for a small scale refrigerator achieving temperature of 7 °C lower than ambient air.(Matsuta, Terada, and Ito 1987)

The need for combining thermal storage with radiative cooling was first highlighted by Ito and Miura (S. Ito and N. Miura 1989) due to the fact that though cooling happens at night , it is needed during the day. They were able to cool their storage tank 2-5 °C below ambient, with cooling rate of 40-60 W/m^2 during summer and 60-80 $\frac{W}{m^2}$ in winter nights.

Another experiment highlighting the significance of the existence of heat storage as well as its physical location in radiative cooling systems was done by Erell and Etzion (Etzion and Erell 1991) .Night time sky radiation cooling happens in around ten hours out of a whole day , so in order to be able to use it during the day, a heat sink is needed to absorb the effect of heat gains that happen mostly during day light hours .On the other hand , as the radiator gets cooler , the effective temperature difference between its surface and the sky gets smaller , reducing the radiative cooling rate and increasing the chances of additional surface temperature reduction due to water condensation . So in other words, thermal storage, keeps the radiator warmer which enhances cooling of its surface. In the experiment four boxes with a floor area of 1.85 m^2 were used, made out of two layers of plywood with 5 cm polystyrene panels in between and painted white. During the day, a thicker panel made with the same material of the box was used to seal the radiator on top of the box's roof (1.35 m^2) . Air temperature inside the box were measured at different heights as well as the temperature of radiator's surface. The roof of the four boxes were made of 0.5 mm metal sheet or a concrete slab and inside the box a concrete slab, used as a form of thermal storage was put in different positions in two boxes, coupled with the concrete roof in the third and removed from the fourth, in order to compare the effect of its mere existence and location. Results showed that not only the presence of thermal storage was important, but its location and coupling with the radiator is of great significance, the closer the coupling (conduction better than convection through air), the improved the cooling effect.(Etzion and Erell 1991)

According to Al-NIMR(Al-Nimr, Kodah, and Nassar 1998) , the night sky radiation can be used to cool the surface of a radiator and the cool radiator surface can then be used for condensing the refrigerant in refrigeration or heat pump cycle. The point is once this fluid is cooled, it has enormous potential to be used in many cooling and heating applications. Lowering the surface temperature by radiation implies that the absorbed energy needs to be less than that emitted, which means that it all depends on having an effective black body emitter, as well as an atmospheric condition that would enhance transmissivity of long wave radiation through both clean and clear skies. Others climate conditions negatively affect the thermal loss, such as high solar intensity or high wind speed on a hot day that creates strong convection currents. (Al-Nimr, Kodah, and Nassar 1998)

The solar heat gain can be controlled through the use of selective surfaces such as Polyethylene that is known to be nearly opaque in the short wave length region(the region of solar energy), and is excellent in transmitting long wave radiation(lower temperature range). (Andretta et al. 1981)Convection can be reduced by either evacuating the air or creating an air gap around the radiator. During the night, though sun is not there, its energy could be reflected through the moon

that also could be countered by the use of reflective coating covering the selective material. (Al-Nimr, Kodah, and Nassar 1998)

The use of night sky radiation cooling by radiators has been investigated through various experimental studies. An early study done in 1975 shows that if a surface material is selectively matched with the radiation window of the atmosphere (8-13 μm) , it can be effectively cooled through the exposal to clear sky radiation both during the day and night. This bare root to Stefan-Boltzmann law that indicates that a black body emits radiation at σT^4, so a black body at 300 $°K$ will lose heat at 450 W/m^2 when exposed to the space temperature of near zero $°K$. However when a body is at sea level, it does not just lose energy to the outer space, it also gains energy from the diffuse and beam sun radiation , convection and conduction as well as radiation emitted back from the atmosphere.(Catalanotti et al. 1975)

The emissivity of the atmosphere differs according to both climatic and geographic conditions, ranging from one in cloudy skies , 0.5 to 0.6 for dry climates at high elevations and around 0.8 to 0.9 in clear skies at the level of the sea.(Bell et al. 1960)

While the first source of heat gain from the sun is mostly eliminated after sunset, convection and conduction can be controlled by proper insulation. The diffuse radiation is in a wave length window less than 4 μm.(Craig 1965) A polyethylene covered Aluminum radiator , with a deposited film of polyvinyl fluoride, achieve selective optical properties in the range of 8-13μm (atmospheric window), showing a major improvement in cooling levels achieved by the radiator in comparison with a black body, both numerically and experimentally. Even during daylight hours , a temperature drop of 10-15$°C$ could be achieved to ambient air .(Catalanotti et al. 1975)

Another comparison done between the effect of material and colour of radiators on cooling levels achieved below ambient temperature by night sky radiation report 6 $°C$ for Aluminum , 2.5 $°C$ for black paint, 11 $°C$ for white paint over a polyethylene covered Aluminum radiator and 6 $°C$ for the same radiator with a black paint. The losses were relatively small for the month of July and August. The lowest night sky radiation loss was about 1.5MJ/m^2, which was almost $\frac{1}{20}$ of the solar gain during the day. So if the design of the radiator ensured high reflectivity of solar energy and good insulation to avoid heating up during the day, the night sky cooling could be used effectively in space cooling. (Kimball 1985)

Again, in an effort to utilize the clean cooling potential of night sky radiation, while avoiding the use of polluting, expensive conventional methods, an experimental and theoretical investigation of the cooling potential of radiation to the night skies was done in Irbid-Jordan. A 0.6 m^2 , specially made radiation panel built of mild steel and covered with polyethylene with rock-wool rear and side insulation also achieved a temperature regression to air of 15$°C$. The experimental set up included the steel panel with black coating and covered with thin film (40 μm)of Polyethylene , a pump and a storage tank (Al-Nimr, Kodah, and Nassar 1998). Though natural circulation of fluid from the panel to the Rockwool insulated storage tank was possible, a pump was used for flow control that is useful in temperature measurements. The temperature decreases of fluid flowing in and out of the panel and the minimum achieved temperature in the tank throughout two different nights were measured. Results showed that cooling of average tank (1201 capacity) temperature by 15$°C$ was possible in a 12 hours night, in spring (range of temperature and humidity are: 16-27$°C$ and 28-55%

respectively)), with the 0.6 m^2 panel. This is equivalent to 13 $\frac{MJ}{m^2}$ per night. With the effective sky temperature being the lowest temperature attainable, the temperature reduction could be altered by reducing the area ration between the panel and the tank. (Al-Nimr, Kodah, and Nassar 1998)It is worth mentioning that the effective sky temperature used in calculation was that proposed by Duffie and Beckman (Duffie and Beckman 2013) as follows:

$$T_{sky} = T_{\infty}\left[0.711 + 0.0056T_{dp} + 0.000073T_{dp}^2 + 0.013\cos 15t_{since\ midnight}\right] \quad 2\text{-}1)$$

The idea of using roof ponds on top of buildings to reduce temperature inside the buildings through improved conduction of special ceiling material with the water in the pond in hot dry climates, has been investigated by several researchers. To achieve space cooling, the heat gained by the pond should be lost to the environment through natural cooling by radiation, evaporation and convection. Faced with same problems, the need to avoid thermal gain from the environment, during hot sunny days, solutions were investigated. Alternating between the use of insulation material that would float on the pond surface when isolation from the surrounding is favourable, or water circulation through radiators for cooling when temperatures permit, was proposed. The majority of these radiators were modified commercially available flat plate collectors, mainly by just removing their glazing, which provided an easy way for rough testing. The main aim for the collector design is to collect heat, so using it to test cooling defies the purpose when attention is made to design details. Analytical study of the use of those collectors in cooling found them performing less than radiators made of just pipes, without fins .(Erell and Etzion 2000)

An example of the studies on using flat plate collectors for radiative cooling is a study done in Beijing, where night circulation of water was done through a 2 m^2 flat plate collector used as radiator. The experiment was composed of galvanized iron plate, insulated from its backside, tubes made of copper with white painting, tank for storage and a pump. Usually, these radiators are installed as a replacement for the roof cover, slightly inclined with respect to the roof top. Fluid then flows, normally by gravity, rejecting heat on its path through the channels of the radiator, then makes its way back to the storage tank. Automatic control stops the circulation in case passive cooling is unachievable to avoid negative impact on the temperature of water in the reservoir. The system achieved an average net cooling of 26 W/m^2. (Xu, Niu, and Feng 2015)

A review done by Sergi and castell (Vall and Castell 2017)on the topic of radiative cooling in 2017 suggested that though it research on the matter go back decades ago, it has not been widely analyzed and they concluded the following

a) Wider analysis of radiative cooling phenomena is needed since any small change in the system heat flux, affect its cooling behaviours with such small cooling energy densities.
b) Cooler temperatures are achieved through covers.
c) Better system control is achieved when water is used as the thermal-carrier as compared to air.
d) Higher cooling rates are achieved through thermal storage.

2.2: Scope of work:

Since the effectiveness of the deferred cooling system is affected by weather conditions, shield position and other system features, monitoring and analyzing the temperatures achieved under various conditions and creating a model of the system for predicting and exploring other possibilities such as varying the hours of shield, number of pools, climate change was necessary to identify its features.

A lumped capacity MATLAB model was employed to verify the performance of the deferred cooling. The model is explained in detail in chapter 4.

The purpose of the current research is to:

a) Present a design for deferring the cooling of thermodynamic cycles operating during daytime to nighttime, with particular relevance to solar driven cycles (that need to operate during daytime) in desert environment where ambient conditions are hostile to cooling.
b) Develop a computational tool to aid in the design and sizing of the system, which is capable of predicting the temperatures achieved by the deferred cooling system under different weather conditions and shield positions
c) To demonstrate the application of this system experimentally and gain practical experiences in its application.
d) To provide guidelines and recommendations for practical implementations based on both experimental results and model predictions.
e) Investigate the performance of the DCS under different operating modes, based on both predictions and measurements.

Chapter 3: Deferred Cooling System Implementation

3.1: The deferred cooling system components:

The deferred cooling system comprises a shallow, shielded artificial pond (such as a commercial swimming pool) filled with either fresh or salty/brackish water that uses natural cooling mechanisms to lower the temperatures of previously heated water from prior use as a cooling agent. Three shading positions of the system are proposed, shield upper position (1m above the pool) or shield lower position (right above the pool) during the day and no shield during the night. During cooler days, and if the ambient air is colder than previously heated water, the shield could be brought to the higher shield upper position exposing the water surface to cooler convection currents, while still obstructing direct beam radiation as well as most of the diffuse.

(a) No shield

(b) Shield upper position

(c) Shield lower position

Figure 3-1: Shield positions of the deferred cooling system

3.2: Shield design:

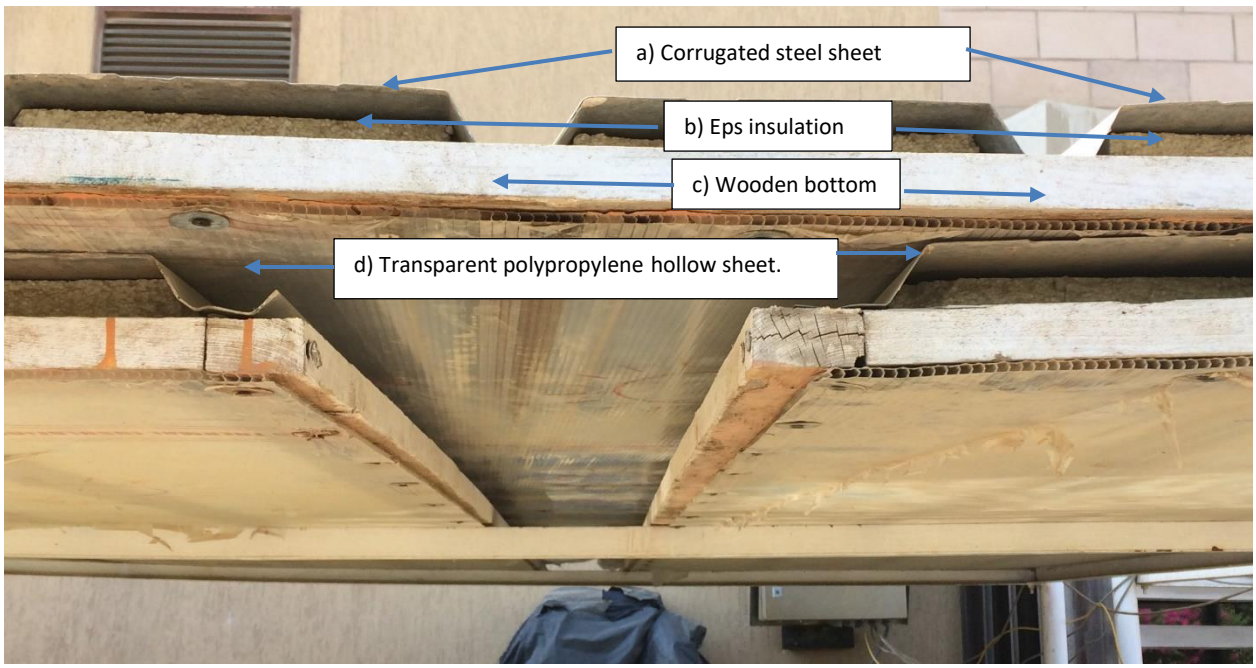

Figure 3-2: Shield components

The function of the shield was to prevent short wave solar radiation from entering the pond during daytime to avoid increasing the temperature of the water during the day due to the heat gain associated with it. The shield shape and materials are designed especially for effective reflectance of sun rays away from the shield and pool, as well as providing high thermal insulation from the top layer to the bottom to avoid heat transfer to the bottom surface facing the pool and consequently to the pool. The shield is 3.3 m wide and 4 m long and is composed of sections, each 1.1 m wide. Each section has 4 layers listed from top to bottom as follows:

a) Corrugated, 1 mm steel sheet in the top most part facing the sun (k=54 W/$m°C$) (Shield Outside (So))

b) 5 cm Foam slabs, made of expanded polystyrene (EPS) beads (k=0.03 W/$m°C$), used as filling for thermal insulation inside to avoid heat transfer to the bottom part. (Shield insulation)

c) Wood bottom, 3 cm thick (k=0.13 W/$m°C$) covered with 5 mm thick polypropylene hollow sheet (k=0.055W/$m°C$). (Shield inside (SI))

The overall thermal resistance of the shield ($\sum \delta x/KA$) is calculated as (2.5/A in $\frac{°C}{w}.m^2$ or 0.57$\frac{°C}{w}$per shield section) where the area A is total area of the shield sections used during the run(as per calculations in Appendix B)

II-Natural Cooling phenomena and their estimation:

The natural cooling mechanisms of the deferred cooling system include convection (natural or forced), surface evaporation and night time radiation exchange with the sky. The effectiveness of these mechanisms depends on the shading position, the difference between air to water surface temperature as well as the clearness index and the relative humidity.

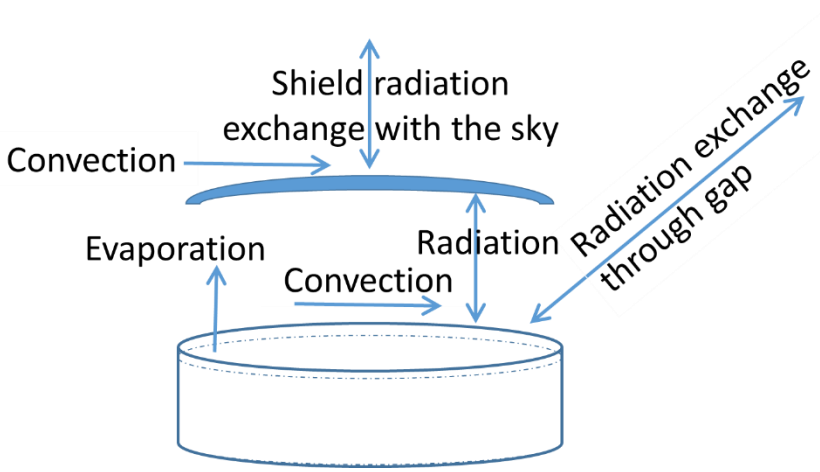

Figure 3-3(a)Shield upper position heat flow

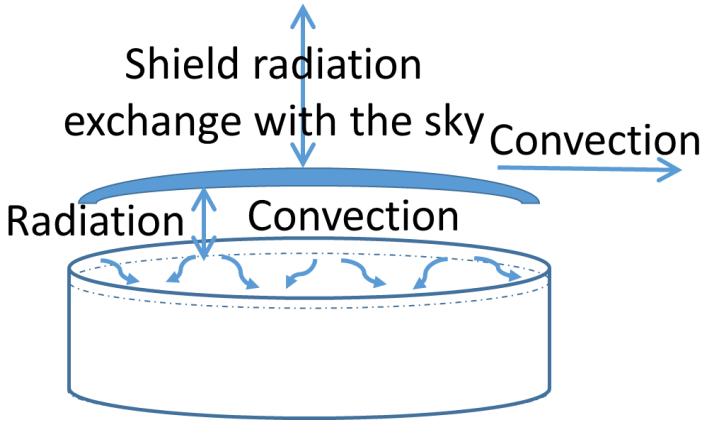

Figure 3-3(b) Shield lower position heat flow

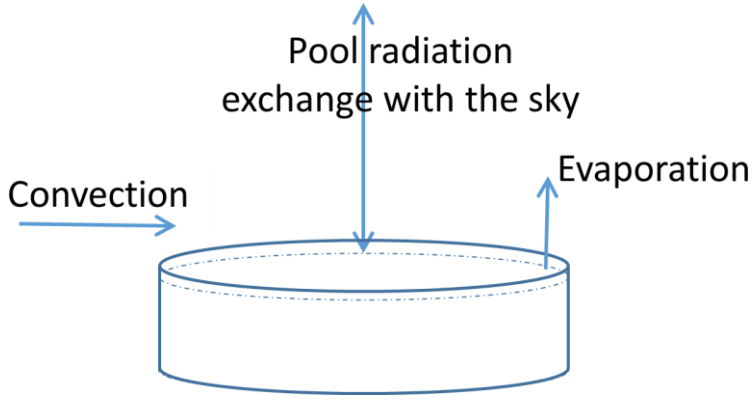

Figure 3-3(c)No shield position heat flow

Figure 3-3 : Heat flow for different shield positions of the DCS

Infrared Radiation Exchange with the Sky:

Radiation exchange between horizontal surfaces operating at temperatures close to ambient and exposed to cold sky is one of the main causes of heat loss that designers are aware of when calculating energy losses in air conditioning systems, solar collectors or even building heating systems. (Bliss 1961) Asymmetrical gases in the air that absorb and re-radiates incident solar radiation have a great effect on this phenomenon. According to Bliss(Bliss 1961), the most important among these gases is water vapor after which comes carbon dioxide and ozone, with much less importance. If these gases were not present and air was completely dry, temperature of the sky would be around 290 °C below ambient air temperature, but in reality, it ranges from 10 to 25 degrees below ambient due to the effect of atmospheric re-radiation. Bliss suggested that the emissivity of the gas mixture used in the determination of atmospheric radiation is a function of dew point, air temperature, pressure, altitude and the composition of the gas mixture.(Bliss 1961)

3.3: Implementation in ASRT research project:

A renewable energy research project implemented in Shallatin , southern Egypt (23.1 °N latitude , 35.56 °E longitude) and funded by the ” Egyptian Academy for Scientific Research and Technology(ASRT)” (Serag-Eldin and El Morsi 2015) involved the design, installation and commissioning of a solar driven ice production facility. The project faced the need for an innovative, simple, inexpensive design of cooling water source for condenser heat rejection in a remote , hot , fairly humid area(depending on the distance from the sea) with no grid connection and no fresh water resources.(Huzayyin et al. 2017)

The project was to provide fishermen with the ice needed to preserve fish using salt water, either from the sea or widely spread saline wells in the area without the need for electrical power from the grid. PV panels were to power the ice production facility with battery storage as a backup(Huzayyin et al. 2017).The ice making system employed standard components of Freon vapor compression cycle that required the rejection of heat (almost 7.3 kw) absorbed from sea water by chiller(2.6 kw chiller with 1.8 COP) as well as compression work done by the compressor via the condenser coolant. (Serag-Eldin and El Morsi 2015)

Air cooling through finned tube, cross flow heat exchanger that would require around 300 W fan power to blow air across the heat exchanger was considered but found unsuitable for the site climate with temperature exceeding 45° C in summer, since the minimum condenser temperature achievable is 5°C below ambient. This elevated condenser operating temperature creates a risk of equipment shutting off or operating at much reduced efficiency which would affect the ice production and reduce equipment lifetime. (Serag-Eldin and El Morsi 2015)

Water cooling was then considered for the condenser heat exchanger with alternatives ways to reject the heat from the water coolant into the surrounding. The first alternative was to use sea water, but that would require considerable cost for piping to get to reasonable water depth and would limit the design of the prototype to sites close to the sea and would also create a negative environmental impact on marine life. The option of cooling towers was also eliminated due to the elevated humidity levels of the site that greatly decrease the cooling effectiveness of those towers since they rely on evaporation to cool the water. Even if the climate was suitable for cooling towers,

the lack of fresh water to compensate for evaporation, the high cost and fan power demand of those towers make them only feasible for larger projects.(Serag-Eldin and El Morsi 2015)

Similar to many small scale, solar energy projects happening in remote areas where water, electricity and initial investments are limited, there was a need for unconventional way to reject the heat of the cooling water into the surrounding in a much simpler way, this is why the deferred cooling system was considered. The chiller condenser was cooled employing high salinity brackish water that was cooled employing the system proposed here.

3.4: Operational procedure in the ASRT project:

The estimated heat rejection required for the project was 7.3 kW. The temperature rise across the condenser was estimated to be 5°C degrees with a 0.00034 m^3/s volumetric flow rate and 9 hours operation with a total required volume of cooling water of 11 m^3/day.(Serag-Eldin and El Morsi 2015)

During operation, one of the three pools must have available space to store the returned warm water. At start this pool would be empty and the other two would have enough volume to store the overall daily consumption of the pool. A 3.6m diameter pool with a 0.76m height was used. The required height of the two pools to store the 11 m3 is 0.522 m, which is less than the 0.76 m height of the pool. (Serag-Eldin and El Morsi 2015)

At night, the total volume of cooling water (estimated as 12 m^3/day) will be equally distributed among the 3 pools. During the day, when the condenser operation will be required, one of the pools will be emptied distributing its water content among the other two that will be feeding the condenser during its operation, with the empty pool receiving the reject water. At mid-day, one of the feeding pools will become empty, a switch will then be made to store the reject water in it and feed the condenser form the other available feeding pool that had not been yet used. At the end of the day, water will be redistributed among the three pools for optimum night cooling. (Serag-Eldin and El Morsi 2015)

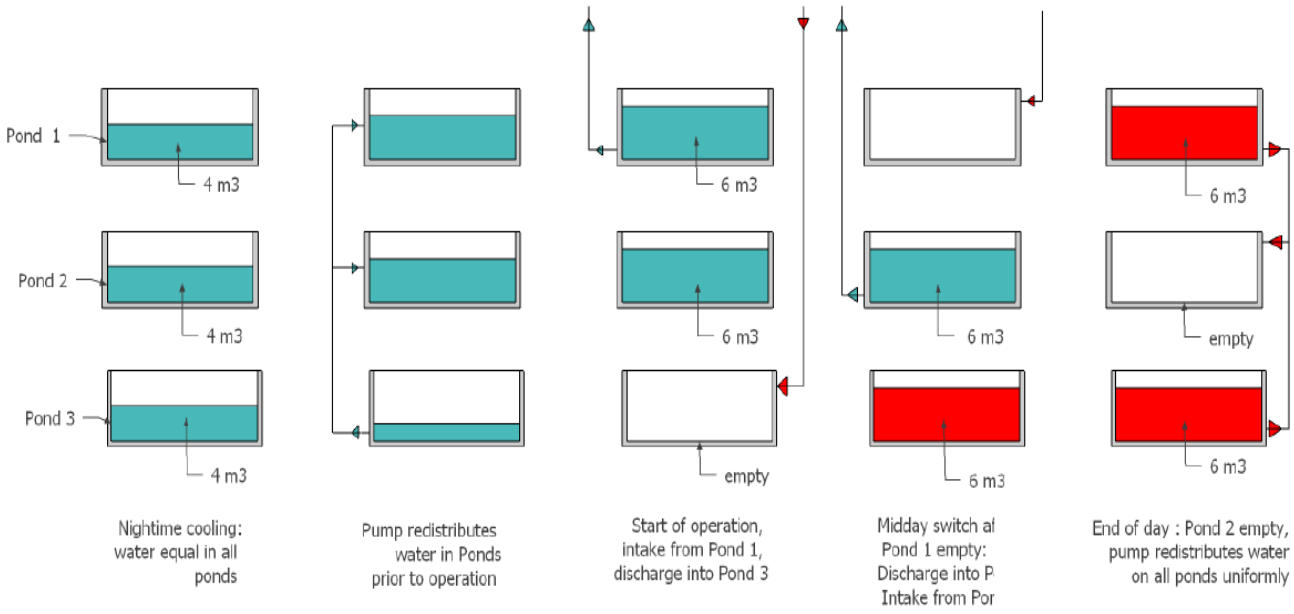

Figure 3-4: Sequence of operation in the cooling ponds for 8 hours of condenser operation

Chapter 4: Mathematical Model

In order to evaluate the different possible scenarios of running the deferred cooling system and recommend best run scenarios that would minimize pool temperature for optimum cooling daily, a lumped capacity, time dependent model implemented on MATLAB was created. The model starts by:

Shield status determination (shield/ no shield) and heating according to required time schedule (ideally sunrise to sunset) for every time interval. Then it implements the relevant model for one of the chosen following scenarios:

Unshielded scenario:

This is similar to that of an outdoor swimming pool. This is the case when the pool surface is totally exposed to the sky. This would occur during the hours between sunset and sunrise as the solar radiation would be absent and long wave radiation exchange with the sky would be beneficial in reducing the pool temperature and dissipating the heat. Moreover, during night time hours, particularly in the desert environment, the atmospheric temperature is generally considerably lower than the pool surface temperature and thus additional cooling can be obtained by exposing the pool surface.

Shielded scenario:

The shield is placed over the pool during day time, ideally between sunrise to sunset or during normal working hours (9am to 5 pm) for simplicity. The shield is mainly there to prevent solar radiation from entering the pool to avoid the associated heat gain.

The choice of day time shield positions is according to the relative ambient to pool temperature. There are two shield positions:

Upper shield position:

Approximately 1meter above the pool, allowing forced convection heat transfer between the pool surface and ambient air while targeting to block beam radiation. The upper shield position is selected by the model when cooler ambient temperature exists to make use of cool convention currents in decreasing the temperature of the water in the pool during day time.

Lower shield position:

On the contrary, lower shield position is selected when the ambient air is not much less than the pool temperature or even higher since it acts as wind shield, blocking forced convection currents in addition to its superior ability to prevent both beam and diffuse solar radiation from entering the pool (being physically closer to its surface).The shield in the lower position is right above the pool water, but not touching it.

4.1: Mathematical model:

The mathematical model comprises heat balance equations for the shield and the pool. Three different model categories are considered, namely the unshielded model, shield upper position model and the shield lower position. According to the physical phenomena under consideration, being radiation, convection, evaporation or solar heat gain, sometimes these models meet, following similar solution procedures.

4.1.1: Unshielded pool:

A heat balance for the pool water treated as a lumped capacity yields:

$$\frac{dE}{dt} = \sum \dot{Q} \tag{4-1}$$

where $\sum \dot{Q}$ is the sum of heat losses and gains, introduced by the following heat sources/sinks while neglecting pumping power:.

a) $\dot{Q}_{\mathrm{SWrad}}$: heat gain from daytime solar short-wave radiation.

b) $\dot{Q}_{\mathrm{LWrad}}$: night time cooling by long-wave radiation losses to the sky.

c) $\dot{Q}_{\mathrm{conv}}$: convection heat flow that is either a gain or loss according to the relative temperature of the pool water as compared to the ambient air. In the presence of strong wind, forced convection generally dominates over free convection. It is also possible to have mixed convection with lower wind speeds.

d) $\dot{Q}_{\mathrm{evp}}$: heat required to evaporate the water from the surface of the pool. Evaporation losses are affected by humidity level, pool water surface temperature, surface area to volume ratio and wind speed.

e) $\dot{Q}_{\mathrm{htg}}$: heat flow from direct heating of the water.

f) $\dot{Q}_{\mathrm{fresh}}$: additional term is added to accommodate the heat flow from either the addition of fresh water to the pool to compensate for evaporation or loss of mass due to leakage. This term could also be used when hot return water from the condenser is added to the pool. In the MATLAB code, this term appears in the mass balance together with mass loss due to evaporation or leakage indirectly affecting the heat flow.

The method of estimation of the various heat flows is explained later in the section on the calculation of heat flows for different shield status and positions.

The general differential equation solved, in absence of $\dot{Q}_{\mathrm{fresh}}$ is:

$$m_w C \frac{dT_p}{dt} = \dot{Q}_{\mathrm{SWrad}_{sun-p}} - \dot{Q}_{\mathrm{LWrad}_{p-sky}} - \dot{Q}_{\mathrm{conv}_{p-\infty}} - \dot{Q}_{\mathrm{evp}} + \dot{Q}_{\mathrm{htg}} \tag{4-2}$$

where m_w, C, and dT_p/dt, are the mass, thermal capacity of water in the pool and the rate of change of pool temperature.

4.1.2: Shielded pool:

Figure 4-1 depicts the heat balance for the combined shield and pool.

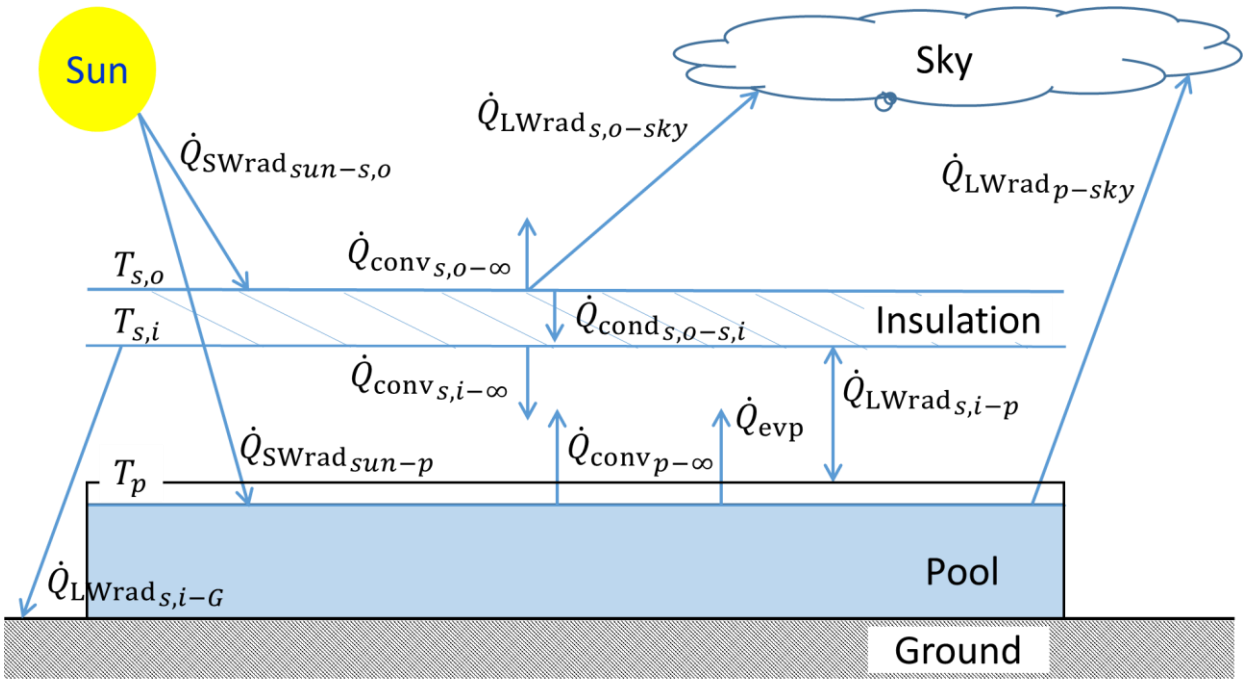

Figure 4-1: Heat Balance of shield and pool

Heat Balance on the upper surface of the shield:

A heat balance for the upper surface of the shield, neglecting its thermal inertia due to its low heat capacity ($m.C$), results in neglect of the rate of thermal energy storage in the shield, yielding Eq. (4-3)

$$\dot{Q}_{\mathrm{cond}_{s,o-s,i}} = \dot{Q}_{\mathrm{SWrad}_{sun-s,o}} - \dot{Q}_{\mathrm{LWrad}_{s,o-sky}} - \dot{Q}_{\mathrm{conv}_{s,o-\infty}} \quad (4\text{-}3)$$

Heat balance on the lower surface of the shield:

A heat balance for the lower surface of the shield (facing the pool), again neglecting its thermal inertia due to its low heat capacity, yields Eq.(4-4):

$$\dot{Q}_{\text{cond}_{s,o-s,i}} = \dot{Q}_{\text{conv}_{s,i-\infty}} + \frac{\sigma T_{s,i}^4 - J_s}{\frac{1-\epsilon_s}{\epsilon_s A_s}} \tag{4-4}$$

where, $T_{s,i}$ is the temperature of the shield inside surface facing the pool and the ground and J_s is the radiosity of the shield, as illustrated in Figure 4-2 and Figure 4-3.

4.1.3: Heat balance for the water in the pool:

A lumped capacity analysis is employed for the heat balance of the water in the pool. It merely expresses the first law of thermodynamics, stating that the net heat gained by the pool at any instant of time equals the rate of change in its internal energy, as expressed in Eq.(4-5).

$$m_w\, C\, \frac{dT_p}{dt} = \dot{Q}_{\text{SWrad}_{sun-p}} - \frac{\sigma T_p^4 - J_p}{\frac{1-\epsilon_p}{\epsilon_p A_p}} - \dot{Q}_{\text{conv}_{p-\infty}} - \dot{Q}_{\text{evp}} + \dot{Q}_{\text{htg}} \tag{4-5}$$

where, J_p is the radiosity of the pool, as depicted in Figure 4-2 and Figure 4-3.The following section explains the method of estimation of the various heat flows for different shield status (unshielded, upper and lower shield positions).

4.1.4: Calculation of heat Flows:

4.1.4.1: Short-wave radiation heat gain:

a) Gains for the unshielded pool:

The short-wave thermal gain is calculated according to Eq. (4-6), where the solar heat flux (q''_{sol}) is measured using the weather station pyranometer, which measures the global radiation and is read by MATLAB through the “shield weather data” subprogram (MATLAB function).

$$\dot{Q}_{\text{SWrad}_{sun-p}} = \propto_p A_p\, q''_{sol} \tag{4-6}$$

b) Gains for the shielded pool:

Same as the “unshielded” scenario, the global radiation is obtained from the weather station and fed into the MATLAB code. The short-wave thermal gain is calculated according to Eq. (4-7). Ideal conditions are simulated in the upper shield position, assuming the shield is effective enough to block all beam radiation and most of the diffuse radiation.

$$\dot{Q}_{\text{SWrad}_{sun-s,o}} = \propto_s A_s\, q''_{sol} \tag{4-7}$$

In the ideal lower shield position, it is assumed that the shield is completely covering the pool, blocking both solar radiation components. During the experimental runs, there is an air gap, allowing part of the ground reflected diffuse radiation

4.1.4.2: Long-wave radiation exchange:

a) Unshielded pool:

For the unshielded scenario, radiation losses to the sky are calculated directly from Eq. (4-8):

$$\dot{Q}_{\mathrm{LWrad}_{p-sky}} = \sigma\, \epsilon_p\, A_p \left(T_p^4 - T_{sky}^4\right) \tag{4-8}$$

The clear sky emissivity used in calculation was that proposed by (Berdahl, Paul and Martin 1984; Berdahl and Fromberg 1982; Staley and Jurica 1972) as per Eq.(4-9):

$$\begin{aligned}\epsilon_{cl-sky} = T_{Amb}.\big[&0.711 + 0.0056.T_{dp} + 0.000073.T_{dp}^2 \\ &+ 0.013\cos\big((2.\pi.t_{since\ midnight}\,)/24\big) + 12^{-5}(P_\infty - 1013)\big]\end{aligned} \tag{4-9}$$

where T_{dp} is the dew point temperature estimated according to Eq.((4-10)

$$T_{dp} = \left(\frac{\Phi_\infty}{100}\right)^{\frac{1}{8}}.(112 + 0.9T_\infty) + 0.1T_\infty - 112 \tag{4-10}$$

The effect of clouds is then introduced through Eq. (4-11)

$$\epsilon_{sky} = \epsilon_{cl-sky} + \left(1 - \epsilon_{cl-sky}\right).N.\tau \tag{4-11}$$

Where τ is cloud factor that depends on cloud base temperature and is usually estimated from weather data (taken as 0.8 in this research work) (Martin and Berdahl 1984). N is calculated based on the relevant diffuse to global radiation for the site as per Eq. (4-12)(Kasten and Czeplak 1980):

$$\frac{DR(N)}{G(N)} = 0.3 + 0.7\left(\frac{N}{8}\right)^2 \tag{4-12}$$

where DR and G are di

ffuse and global radiation respectively.

The effective sky temperature used in calculation is that proposed by (Bliss 1961)&(Berdahl, Paul and Martin 1984), as shown in Eq. (4-13)

$$T_{sky} = T_\infty.\epsilon_{sky}^{\frac{1}{4}} \tag{4-13}$$

There is also the possibility to estimate T_{sky} to be lower than ambient air by 10 to 25°C(Bliss 1961), the higher difference would represent desert climates. This approach could be used to represent virtual running scenario of desert climate where the sky temperature is estimated to be 25°C below ambient.

Similarly, for the shielded scenario, the radiation losses from the upper surface of the shield facing the sky to the sky is calculated directly from Eq. ((4-14)

$$\dot{Q}_{\mathrm{LWrad}_{s,o-sky}} = \sigma\, \epsilon_s\, A_s \left(T_{s,o}^4 - T_{sky}^4\right) \tag{4-14}$$

b) Upper shield position:

For the upper shield position, radiation losses from the pool are calculated using the radiation network method, shown in Figure 4-2 as per Holman (Holman, J.P. and White 1992) to solve two equations for radiation exchange between the pool, shield inside surface, ground and sky.

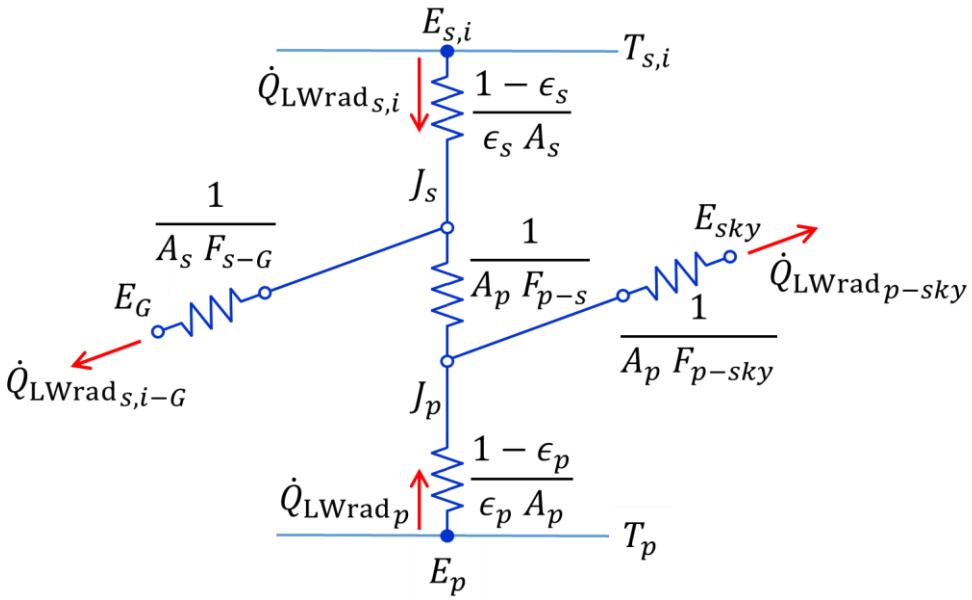

Figure 4-2: Radiation network for the shield in the upper position

The radiosity of the shield and the plate are calculated from Equations (4-15) and (4-16).

$$\frac{E_{s,i}-J_s}{R_{sf_s}}+\frac{J_p-J_s}{R_{sp_{p-s}}}+\frac{E_G-J_s}{R_{sp_{s-G}}}=0 \tag{4-15}$$

$$\frac{J_S-J_p}{R_{sp_{p-s}}}+\frac{E_{sky}-J_p}{R_{sp_{p-sky}}}+\frac{E_p-J_p}{R_{sf_p}}=0 \tag{4-16}$$

where $R_{sp_{p-s}}$, R_{sf_s} and R_{sf_p} are the space resistance for pool-to-sky, surface resistance of the shield and surface resistance of the pool, respectively. These resistances are defined by Eqs. (4-17)(4-18) and (4-19).

$$R_{sp_{p-s}}=\frac{1}{A_p F_{p-s}}=\frac{1}{A_s F_{s-p}} \tag{4-17}$$

$$R_{sf_s}=\frac{1-\epsilon_s}{\epsilon_s A_s} \tag{4-18}$$

$$R_{sf_p}=\frac{1-\epsilon_p}{\epsilon_p A_p} \tag{4-19}$$

The surface resistance of the ground and sky are taken as zero as it is an infinite area. Thus, the radiosity of the ground (J_G) and the sky (J_{sky}) are:

$$J_{Gr} = E_{Gr} = \sigma T_{Gr}^4 \tag{4-20}$$

$$J_{sky} = E_{sky} = \sigma T_{Sky}^4 \tag{4-21}$$

The radiation heat flow out of the pool ($\dot{Q}_{\mathrm{LWrad}_p}$) and the shield inside surface $\dot{Q}_{\mathrm{LWrad}_{s,i}}$ are then calculated as shown by Eqs. (4-22) and (4-23), respectively:

$$\dot{Q}_{\mathrm{LWrad}_p} = \frac{\sigma\, T_p^4 \; - J_p}{\frac{1-\epsilon_p}{\epsilon_p\, A_P}} \tag{4-22}$$

$$\dot{Q}_{\mathrm{LWrad}_{s,i}} = \frac{\sigma\, T_{s,i}^4 - J_s}{\frac{1-\epsilon_s}{\epsilon_s\, A_s}} \tag{4-23}$$

The shape factor used to calculate the space resistances, F_{p-s}, for the shield in the upper position, is 0.55 (Holman, J.P. and White 1992).

c) Lower shield position:

For the shield in the lower position, long-wave radiation losses from the pool are calculated according to Eq. (4-24) as shown by the radiation network shown in Figure 4-3.

$$\dot{Q}_{\mathrm{LWrad}_{p-s,i}} = \frac{\sigma\, T_p^4 \; - \sigma\, T_{s,i}^4}{\frac{1-\epsilon_p}{\epsilon_p\, A_p} + \frac{1}{A_p\, F_{ps}} + \frac{1-\epsilon_s}{\epsilon_s\, A_s}} \tag{4-24}$$

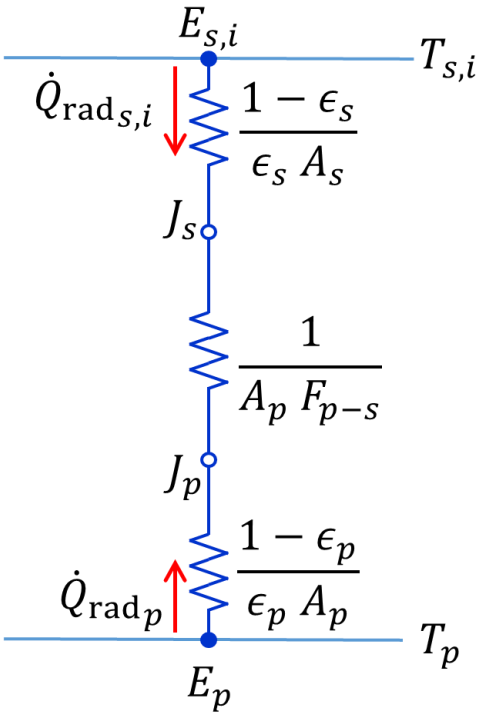

Figure 4-3:Radiation network for the shield in the lower position.

4.1.4.3: Convection/Evaporation heat flow:

a) Convection/Evaporation for unshielded and upper shield position:

Convection/Evaporation exchange with the environment for the unshielded and the shield in the upper position is modeled according to Eq. (4-25) and (4-26), respectively:

$$\dot{Q}_{\mathrm{conv}_{p-\infty}} = h_p\, A_p \left(T_p - T_\infty\right) \tag{4-25}$$

The heat transfer coefficient (h_p) of an outdoor pool is given by Eq. (4-26) as proposed (Auer 1996; Czarnecki 1978; Hahne and Kübler 1994)

$$h_p = 3.1 + 4.1 V_\infty \tag{4-26}$$

The heat required to evaporate the water from the surface of the pool is given by Eq.(4-27)

$$\dot{Q}_{\mathrm{evp}} = \alpha_{\mathrm{evp}}\, A_p \left(P_{Sat}(T_p) - P_{St}(T_\infty)\right) \tag{4-27}$$

The modified evaporation coefficient (α_{evp}) of an outdoor pool is given by Eq.(4-28), as proposed by(Hahne and Kübler 1994; Richter 1969). Eq.(4-28) is validated by the Thermodynamics and Heat Technology Institute at Stuttgart University in Germany after validating its ability to represent temperature changes of an outdoor pool at Leonberg(Guidati 1992). This equation provided the best fit with the measured data since the wind speed used to derive it was recorded 2 meters above the pool(Hahne and Kübler 1994) , similar to our experimental rig and weather station position.

$$\alpha_{evp} = 4.523 + 5.088\omega_{Amb}^{0.84} \tag{4-28}$$

The relative humidity is then used to calculate the pressure of steam(Hahne and Kübler 1994) P_{St}, as shown in Eq. (4-29).

$$P_{St} = \varphi_\infty\, P_{Sat}(T_\infty) \tag{4-29}$$

P_{Sat} is the saturation pressure given by Eq.(4-30) according to (Hahne and Kübler 1994)

$$P_{Sat} = c1.\, e^{\frac{c2.T}{C3+T}} \tag{4-30}$$

where c1=6.1, c2=17.08, c3=234

Similarly, for the shielded scenario, the convection losses from the lower and upper surfaces of the shield to the environment and are calculated directly from Eqs. (4-31) and (4-32), respectively:

$$\dot{Q}_{\mathrm{conv}_{s,i-\infty}} = h_p\, A_s \left(T_{s,i} - T_\infty\right) \tag{4-31}$$

$$\dot{Q}_{\mathrm{conv}_{s,o-\infty}} = h_{s,o}\, A_s \left(T_{s,o} - T_\infty\right) \tag{4-32}$$

where $h_{s,o}$ is calculated in a similar manner as h_p.

b) Convection/Evaporation for the lower shield position:

In the ideal shield lower position, it is assumed that the shield is completely covering the pool, blocking both solar radiation components, with condensation and evaporation effects cancelling out during daytime, leaving just free convection effects in the enclosed space between the pool and shield. The shield temperature must be less than the pool temperature for free convection to occur, which is predetermined from the calculation of Rayleigh number (Ra).

As per Holman(Holman, J.P. and White 1992), the method of calculation of free convection in an enclosed space between two parallel plates is as follows:

Rayleigh number (product of Grashof(Gr) and Prandtl(Pr), determines the method of calculation of Nusselt number(Nu). For Ra less than 1700, Nusselt (Nu) equals one, which means that heat is transferred by conduction only, otherwise different coefficients are used to calculate (Nu). as a function of Ra as presented in Eqs.(4-33)-(4-36)

In case $Ra < 1700, Nu = 1$ (4-33)

In case $1700 < Ra < 7000, Nu = 0.059Ra^{0.4}$ (4-34)

In case $7000 < Ra < 3.2 * 10^5, Nu = 0.212Ra^{1/4}$ (4-35)

In case $Ra > 3.2 * 10^5, Nu = 0.061Ra^{1/3}$ (4-36)

$h_p = (\mathrm{Nu}\ \mathrm{K})/X$ (4-37)

where K is thermal conductivity of moist air, calculated at film temperature and *X* is the height of the air gap between the shield and the water surface. Free convection effect is then calculated as a function of the difference in temperature between the water and shield, as presented by Eq. (4-38)

$$\dot{Q}_{\mathrm{conv}_{p-s,i}} = A_p\, h_p \left(T_p - T_{s,i}\right) \quad (4\text{-}38)$$

4.1.4.4: Additional heat flow from incoming fresh water added to the system:

An additional term is added to simulate the heat flow from either the addition of fresh water to the pool to compensate for evaporation, or loss of mass due to leakage. This term would also be used to represent field implementation of condenser cooling during the day, where hot reject water from condenser cooling is added to the pool to be cooled throughout the night when the condenser is not operational. In the MATLAB code, this term appears in the mass balance together with mass loss due to evaporation or leakage indirectly affecting the heat flow.

4.1.4.5: Conduction heat flow in the shield:

$$\dot{Q}_{\text{cond}_{s,o-s,i}} = \frac{T_{s,o} - T_{s,i}}{\sum R_{ins}} \tag{4-39}$$

where $\sum R_{ins} = A \sum_{i=1}^{n} \frac{\delta x_i}{K_i}$ is the equivalent resistance of the shield taken as the summation of thermal resistances in series of the various layers. $T_{s,o}$ and $T_{s,i}$ are the temperatures of the shield outside surface facing the sky and the ambient air and the inside surface facing the pool and the ground, respectively.

4.2: Solution algorithm:

Figure 4-4 and Figure 4-5 display the solution algorithms for the upper and lower shield positions, respectively.

4.2.1: Solution procedure for upper shield position:

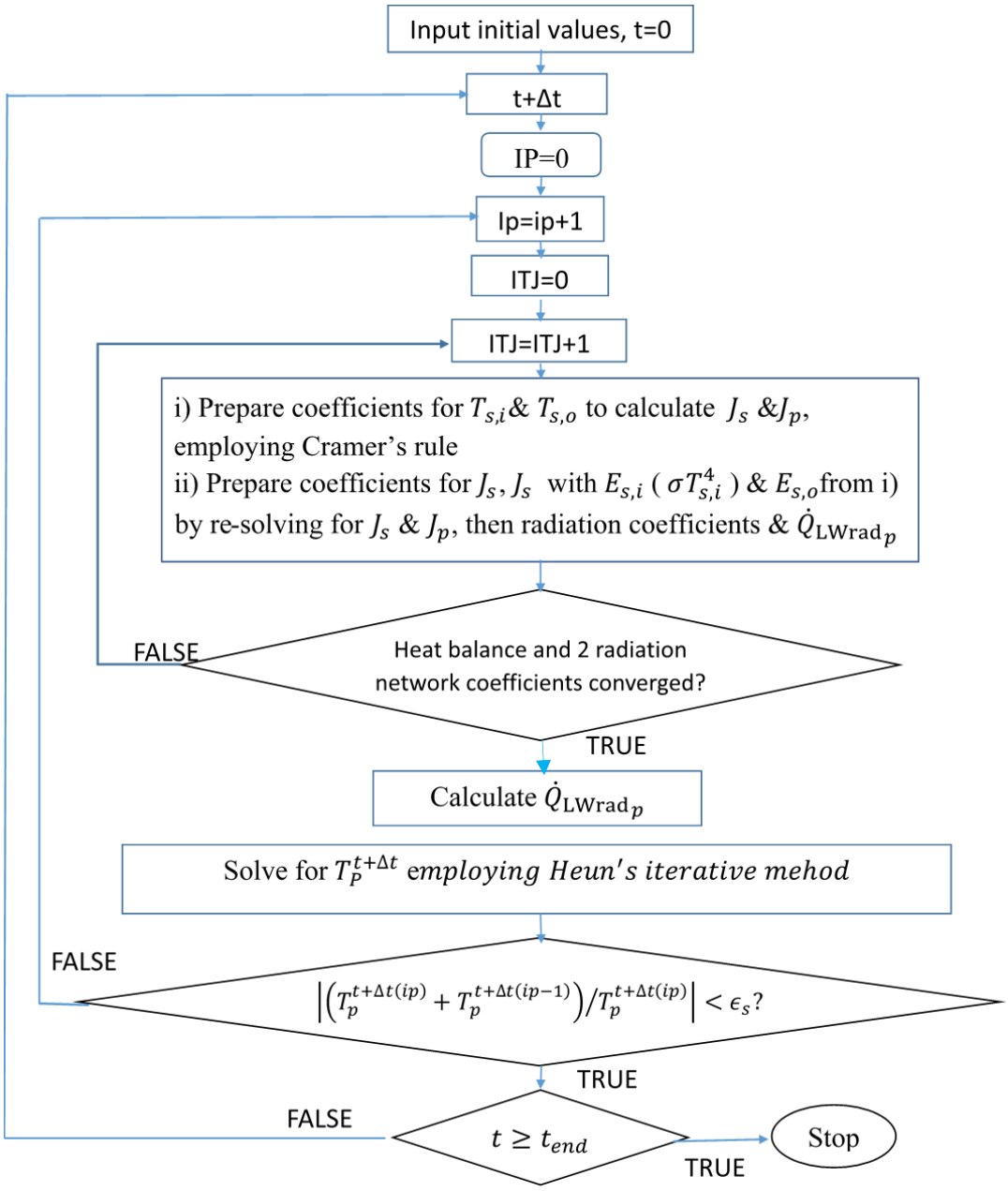

Figure 4-4: Solution procedure for shield upper position

4.2.2: Solution procedure for lower shield position:

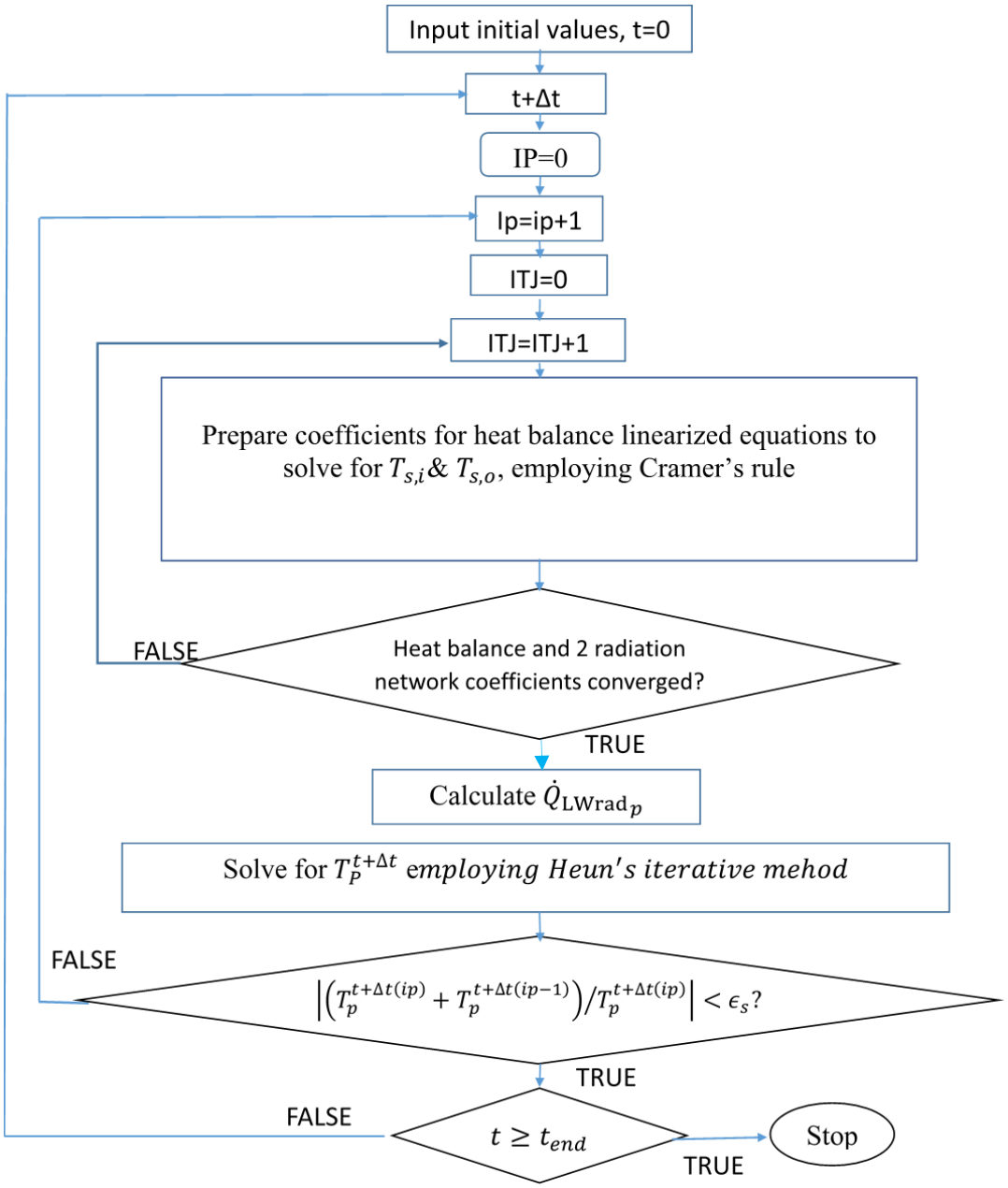

Figure 4-5: Solution procedure for shield lower position

The program flow description and code are listed in detail in appendix A

Chapter 5: Theoretical investigation

This chapter starts by discussing the possible operational scenarios of the DCS based on the total number of cooling to be provided by the system daily in the first section of the chapter (section 5.1). The section highlights the number of pools required for each scenario and the proposed sequence of operation. It starts by referring to the scenario of the ASRT project with 3 pools(Serag-Eldin and El Morsi 2015) (introduced at the beginning of chapter 3), followed by a detailed explanation of the maximum possible, 12 hours cooling scenario with 4 pools, then the minimum proposed 4 hours of daily cooling for small demand with 2 pools, used in the simulation model in section 5.2.

Section 5.2 demonstrates the model's prediction for the water temperature in one representative pool of the DCS, using actual weather data measured at AUC campus in New Cairo (30.02 ° N latitude, 31.5 ° E longitude) during the months of April, May and June 2017. The section presents the data for 3 cycles, then concludes with a parametric study for selected parameters, to study their effect on the DCS performance. Finally, section 5.3 presents the model's prediction for the DCS performance when operating with 4 pools to provide a total of daily cooling of 12 hours, representing a more practical approach than that used for analysis in section 5. 2

5.1: DCS operational procedure for 12 hours cooling daily:

At the beginning of chapter 3, the operational procedure of the DCS system as implemented in the ASRT project was demonstrated using 3 pools and 8 hours condenser operation. This sequence was suitable for the ASRT project requirements, however alternative operational sequence could be required for longer operational hours or different condenser load. An example of this is the 12 hours of cooling demand from the DCS illustrated in in Figure 5-1.

For the DCS running scenario presented in Figure 5-1 , 12 hours condenser operation is required, based on 12 hours of sun shine in summer for solar driven equipment in desert climates. The pool volume is designed to have enough volume to match the 4 hours of condenser operation. This DCS system design provides operational flexibility since all what is needed in case of a different load, is to match the pool volume with the new design load.

The DCS system is recommended as a substitute for air cooling in desert climates, mostly for solar driven equipment, its maximum number of operational hours would be the 12 hours of sunshine. So, this maximum 12-hour scenario and that explained at the beginning of chapter 3 (the ASRT 8 hours operation scenario), are the most likely scenarios of DCS operation.

Figure 5-1 and Figure 5-2 presents the operational sequence of four pools, feeding the condenser with cooled water for 3 cycles, each cycle provides 4 hours of condenser cooling as follows:

i. On the first day, at 6 am, the condenser starts its daily operation, withdrawing cooled water from the previous night from pool 2 and rejecting hot water to pool 1.
ii. At 10 am, pool 1 is full of hot, "condenser reject" water. Pool 2 is empty, and the condenser starts withdrawing water from pool 3 and rejecting water to pool 2 for the next 4 hours.
iii. At 2 pm, pool 2 if full of hot, "condenser reject" water. Pool 3 is empty, and the condenser starts withdrawing water from pool 4 and rejecting water to pool 2 for the next 4 hours.

iv. At 6 pm, we have 3 hot pools full of" condenser reject" water, the first one (pool 1) is filled at 10 am and starts its cooling cycle since then to be cooled throughout the whole night. Pool 2 starts to cool at 2 pm throughout the night. Pool 3 is filled and left to cool starting 6 pm throughout the night.

v. Right after 6 pm, the total volume of the 3 pools (3V) is redistributed over the 4 pools (3/4 V each) to increase the surface area to volume ratio and increase heat losses. This along with, the high temperature difference between the hot water and cool ambient air contribute to the highest heat loss rate throughout the night.

vi. Before 6 am, pool 1 is emptied and its volume, which is quarter of the whole volume is redistributed over the other three pools that are filled in full to their original water level. Then the operational cycle repeats itself starting 6 am daily.

Though the three pools have different cooling periods during the day, they are all left to cool from 6 pm till 6 am the next day, which is the most effective cooling period. From sunset to sunrise, the pools are exposed to nighttime cool skies and the high long wave radiation heat losses associated with it, especially for desert climates. This is in addition to cool convection currents due to the high difference between day and night ambient air temperatures of desert climates.

In the DCS, the condenser is not operational during the night since it is mainly designed for cooling of solar driven systems in desert climates to replace air cooling. The DCS operation is not recommended at night since for such night time operation, air cooling would be favourable, and the system needs night time cooling to provide the required water temperature drop. This will be illustrated in the continuous operation section of this chapter, by simulating continuous night time operation with the numerical model and discussing its effect on the system.

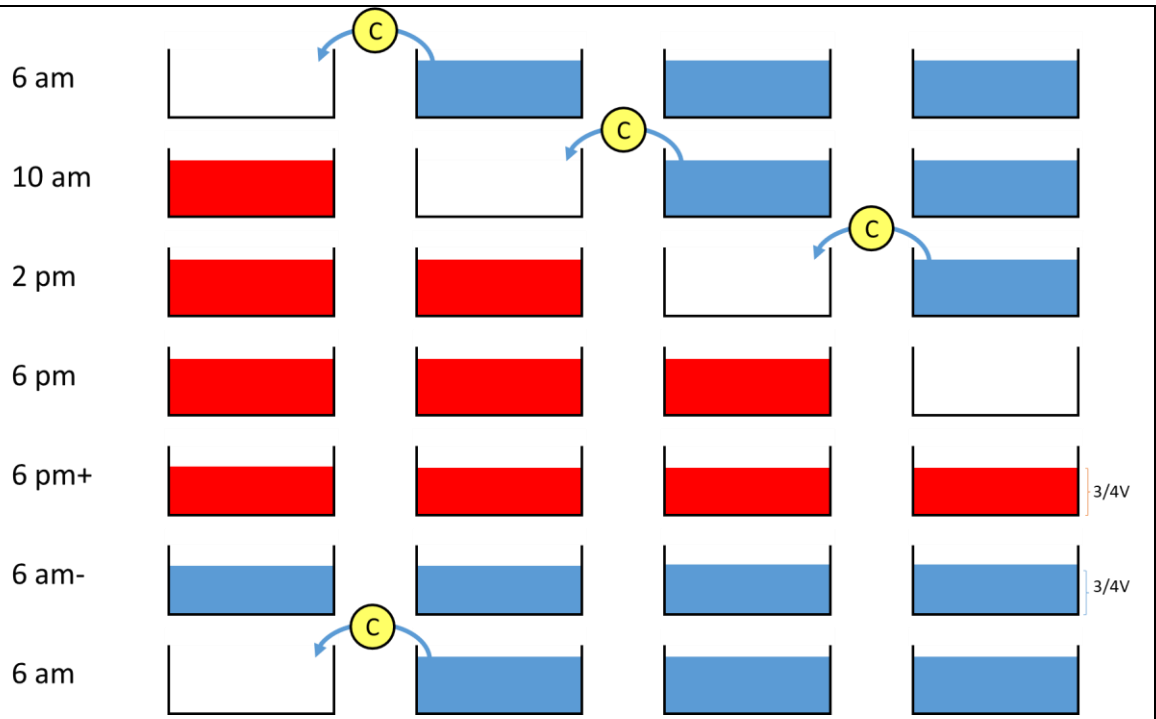

At 6 am: C_{in} : from pool 2 C_{out} : to pool 1
At 10 am: C_{in} : from pool 3 C_{out} : to pool 2
At 2 pm: C_{in} : from pool 4 C_{out} : to pool 3
At 6 pm: 3 hot pools(3xV)
At 6+ pm: 4 x(3/4V) hot pools
At 6- am next day: 4 x(3/4V) cooled pools
At 6 am next day: 3 x V cooled pools Cycle repeats

Figure 5-1: DCS "12 hours operational cycle"

As shown in Figure 5-2 that displays the height of water in the 4 pools versus time, the total overall cycle time of each of the four pools is 24 hours, distributed as follows:

Table 5-1: cooling, emptying and filling duration for the 4 pools in 12 DCS hours operation

Event	Pool 1	Pool 2	Pool 3	Pool 4
Cooling start:	10 am on day 1	2 pm on day 1	6 pm on day 1	6 pm on day 1
Cooling end:	6 am on day 2	6 am on day 2	10 am on day 2	2 pm on day 2
Cooling duration:	20 hours	16 hours	16 hours	20 hours
Filling:	6 till 10 am daily (from condenser)	10 am till 2 pm daily (from condenser)	2 till 6 pm daily (from condenser)	6pm daily (from other pools)
Emptying:	6 am daily (to other pools)	6 till 10 am daily (to condenser)	10 am till 2 pm daily (to condenser)	2 till 6 pm daily (to condenser)
Fill/empty duration:	4 hours	8 hours	8 hours	4 hours
Overall cycle time:	24 hours	24 hours	24 hours	24 hours

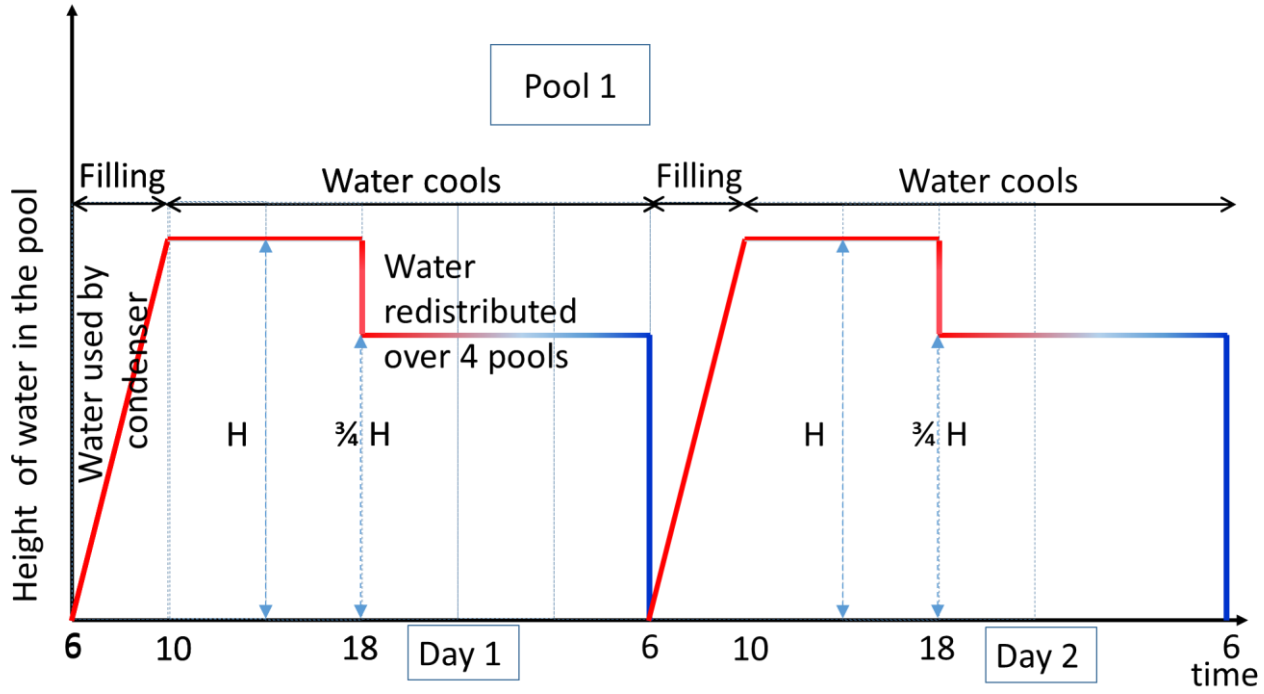
Pool 1
Filling
Water cools
Filling
Water cools
Height of water in the pool
Water used by condenser
Water redistributed over 4 pools
H
¾ H
H
¾ H
6
10
18
Day 1
6
10
18
Day 2
6
time

(a)

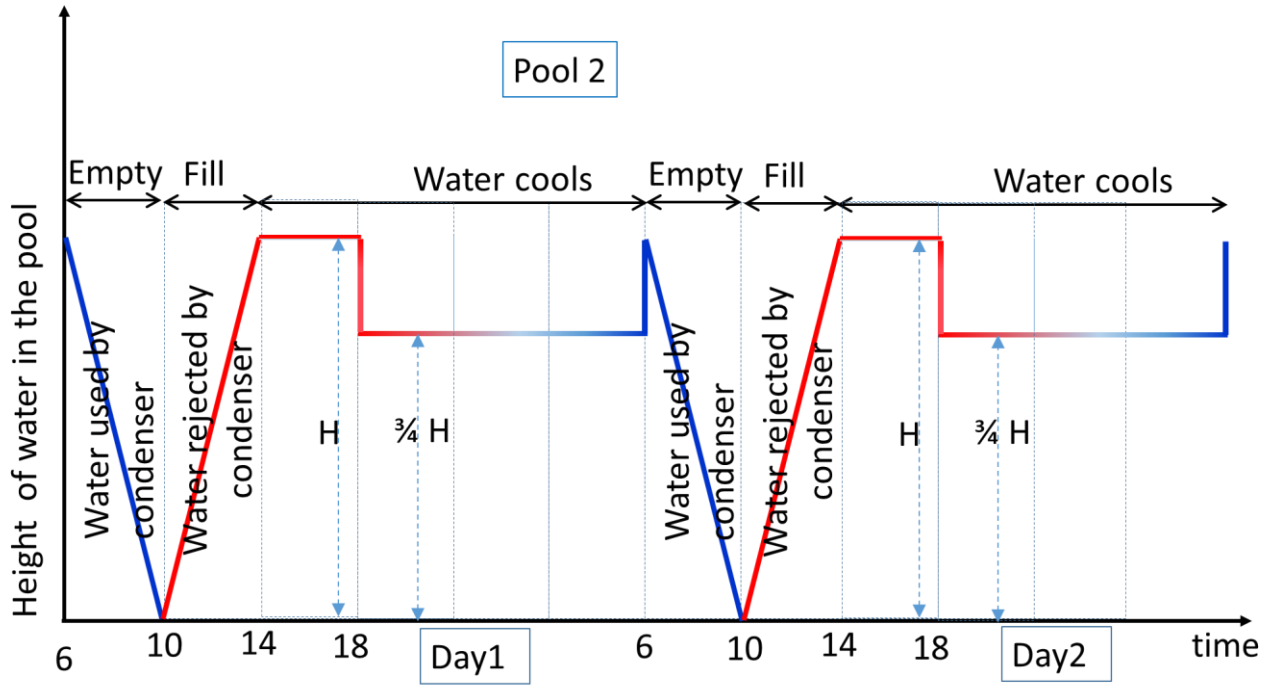
Pool 2
Empty
Fill
Water cools
Empty
Fill
Water cools
Height of water in the pool
Water used by condenser
Water rejected by condenser
H
¾ H
Water used by condenser
Water rejected by condenser
H
¾ H
6
10
14
18
Day1
6
10
14
18
Day2
time

(b)

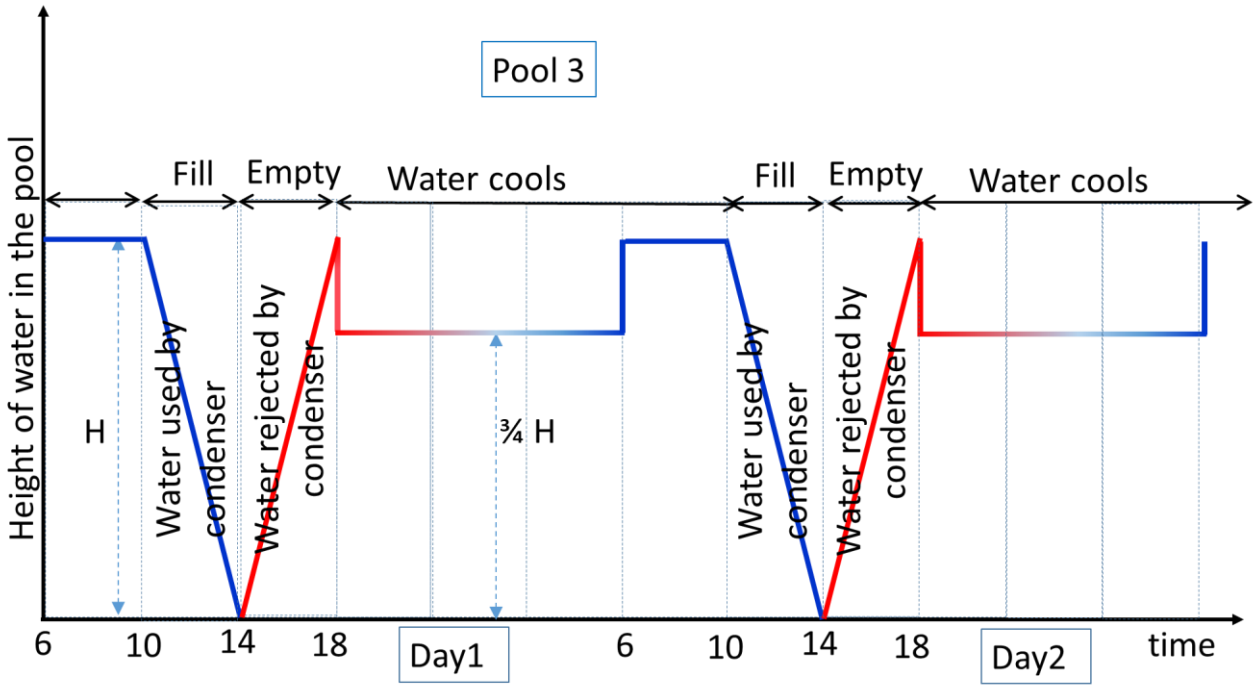

(c)

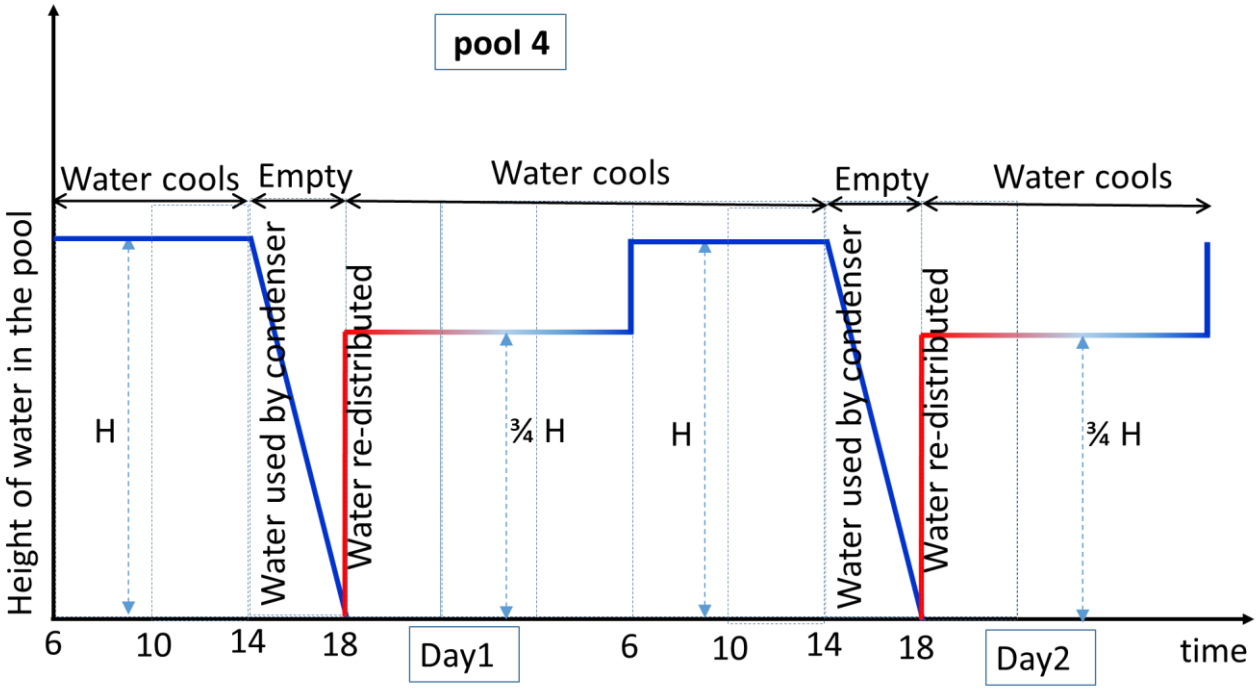

(d)

Figure 5-2: Height of water in the 4 pools of the DCS 12 hours operation

5.2: DCS operation/simulation for 4 hours cooling daily:

The simplest mode of operation for the DCS system is when only one cycle of 4 hours of cooling is required daily with 2 operational pools. In this case, only one pool will be used for cooling daily and the other will be used as a storage for the hot rejected water out of the condenser. In practice the cooling cycle start will depend on the required hours of operation and could range from 10 am (for 6 am condenser operation) to 6 pm for late afternoon condenser operation. The operational hours could change from day to day and consequently the start of the cooling cycle.

For simulation purposes, one pool is considered to represent the DCS performance providing 4 hours of cooling daily. For this pool, the cooling cycle is taken as 20 hours similar to pool 2 and 3 in the "12 hours cooling "operation discussed earlier. There is also 8 hours of emptying and filling every operational cycle, that makes the overall cycle time 28 hours. The 28 hours cycle creates 4 hours shift every day, making the cooling period starts at 10 am on the first day(similar to pool 1 in the" 12 hours cooling "scenario), 2 pm on the 2nd day (similar to pool 2 in the 12 hours scenario)and 6 pm on the 3rd((similar to pool 3) in the "12 hours cooling " scenario, representing the 3 cooling cycles start times of the 4 pools in the 12 hours operational sequence, reflecting the relevant different weather conditions and thermal losses for morning , afternoon and evening hours.

In the next section of this chapter (section 5.3), this simple mode of operation is used as a building block for the simulation of one representative pool for the DCS operation using the theoretical model, to better understand the system performance. Since at the beginning of each of the three cycles to be modeled, the pool starts cooling at the start of one of the pools in the "12 hours cooling "operation, it is used as a representation of the cooling cycle of the 3 pools in the "12 hours cooling" scenario. The main difference is that the volume was not reduced to quarter at 6 pm as recommended. This is because the refilling of the pool would be a function of the other pool temperatures, which could not be accurately estimated while simulating only one pool.

For simulation purposes,Figure 5-3 displays the pool filling cycle for a DCS using 2 pools and 20 hours cooling. The pool starts with hot water at initial temperature of 40°C, $T_{p_{i_1}}$ .The pool water is then left to cool for 20 hours, followed by 4 hours to empty the water in the pool, during which it is used to cool the condenser. During those four hours, the condenser rejects the hot water to the second pool at a predetermined temperature$T_{p_{f_1}}$. The temperature is either calculated from a predetermined temperature difference ΔT or is set to the initial temperature 40°C. The predetermined temperature difference ΔT is calculated from the value obtained from the first day, where $\Delta T = T_{p_{i_1}} - T_{p_{f_1}}$. The cycle takes another four hours, making the overall cycle time 28 hours, as shown in Figure 5-3 .

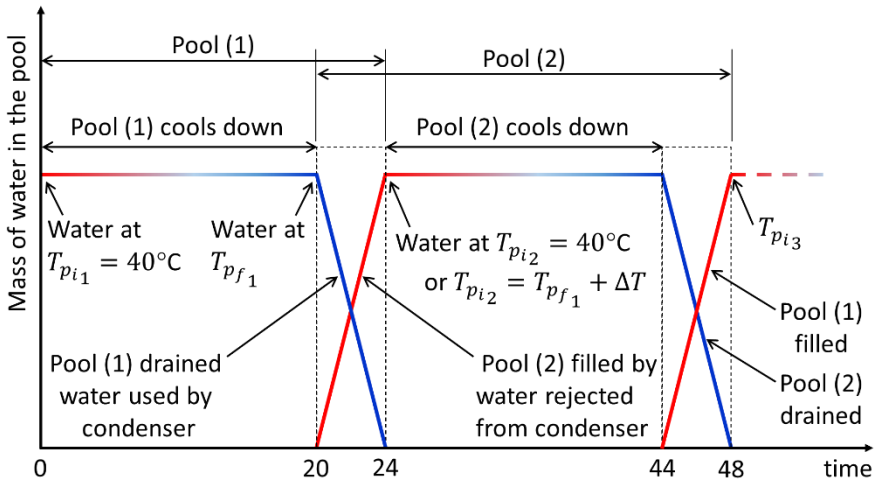

Figure 5-3:Pool filling cycle for the DCS system using two pools.

5.3: DCS performance simulation (single pool):

The simulation demonstrates the use of the program and the main features of flow and heat transfer using single pool calculation in which the cycle covers the 4 main operations mainly gradual filling of the pool, gradual emptying of the pool, night-time cooling, daytime exposure. In actual reality, the there are multi number of pools and their operation start, and end times differ, and they do not necessarily go through the four outlined operations. Thus, the cycle time is 24 hours that is repeated every new day.

Because only one pool is simulated, the cycle time has to include filling and emptying, therefore extends to 28 hours. Three cycles are considered to span all the possible operating hours.

In this simulation, the water temperature of one of the pools used to cool the reject water out of a condenser in a refrigeration cycle is predicted against time using the site's weather boundary conditions (wind speed, humidity, solar radiation, ambient air temperature), measured two meters above the pool, every minute. During daytime operational hours the shield is placed above the pool. Its vertical height being either above the pool rim or flush with it, according to the relative temperature of pool water and ambient air. The shield upper position (shield above the pool rim) is adopted when the ambient air temperature is lower than the pool temperature by at least 5 ℃ to make use of cool convention currents in reducing the water temperature; otherwise the model adopts shield down position (shield flush with pool rim) during the day. After sunset and throughout the night, the shield is removed, simulating the unshielded scenario till sunrise (set at 7 pm till 5 am in the model for simplicity).

Ideal conditions are simulated for the shield upper position, assuming the shield is effective enough to block all beam radiation and most diffuse radiation. Evaporation and convection effects are accounted for in relation to the measured wind speed.

For the ideal shield lower position, it is assumed that the shield is completely covering the pool, blocking both solar radiation components, with condensation and evaporation effects cancelling out during daytime, leaving just free convection effects in the enclosed space between the pool and shield.

Figure 5-4 displays the pool filling cycle for a DCS using one pool. The pool starts with hot water at initial temperature of 40°C, $T_{p_{i_1}}$. The pool water is then left to cool for 20 hours, followed by 4 hours to empty the water in the pool, during which it is used to cool the condenser. After those four hours, the condenser rejects the hot water to the pool at a predetermined temperature$T_{p_{f_1}}$. The temperature is either calculated from a predetermined temperature difference ΔT or is set to the initial temperature 40°C. The predetermined temperature difference ΔT is calculated from the value obtained from the first day, where $\Delta T = T_{p_{i_1}} - T_{p_{f_1}}$. The cycle takes another four hours, making the overall cycle time 28 hours, as shown in Figure 5-4.

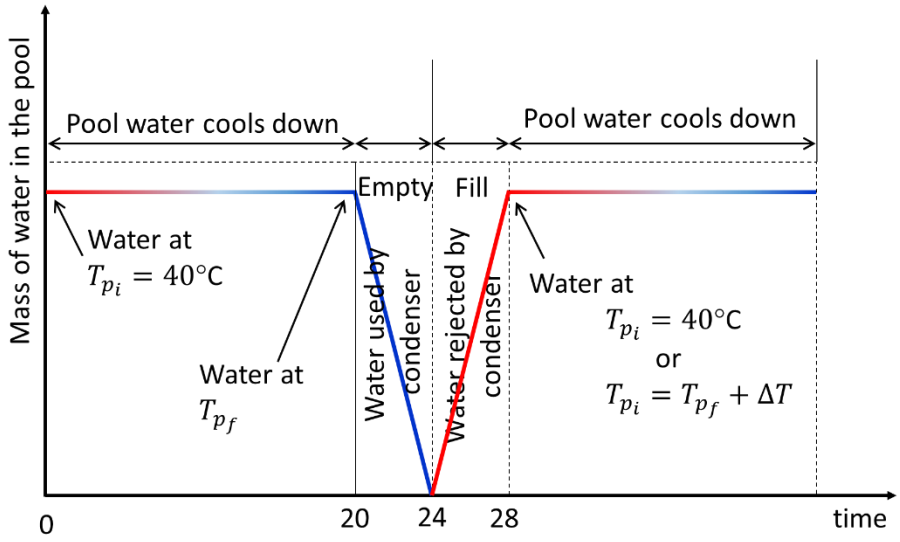

Figure 5-4: Pool filling cycle for the DCS system using one pool.

The performance of the DCS system is evaluated using one pool and actual weather data from April, May and June. Modeling the water temperature in one pool means that the 20 hours cooling, will be followed by 4 hours of emptying the pool and another 4 hours of filling, creating 4 hours shift in the cycle start times of cooling, filling and emptying for every operational day.

We start the 20 hours cooling period at 10 am on the first day, allowing the water in the pond to benefit from radiative cooling throughout the whole night before the 4 hours of water withdrawal from the pool that starts at 6 am the next day. The second cooling cycle starts at 2 pm after filling the pool and water withdrawal from the pool starts at 10 am the following day. The 3rd cycle starts the cooling period at 6 pm, withdrawing water at 2 till 6 pm a day later. The three cycles times are then repeated, assuming multiple pool operation with only one pool being modeled, with cooling starting at 10 am, 2 pm, then 6 pm for the three cycles and the condenser withdrawing water at 6 am, 10 am then 2 pm for the three cycles. For these three cycles, water in the DCS system will benefit from the night sky cooling in full since their 20 hours cooling period all include sunset to sunrise hours (or 7 pm till 5 am for this simulation), which means that the shield is equally removed during the three cycles and water is exposed to the cool night skies.

The 4 hours at the end of each run, when water is withdrawn from the pond to the condenser, at the end of the cooling cycle is the most critical part with the DCS aiming to reach cooler temperatures than air at this point. The start and end of water withdrawal are indicated by the decrease of water depth in the pool as denoted by the arrows in Figure 5-5-a. Even if water temperature is comparable or slightly higher than air, for practicality reasons in equipment selection, sizing, pricing and efficiency, water cooled systems could be more attractive in many applications.

The fact that every 24 hours, the pool receives previously heated water from the condenser with a constant ΔT represents constant heat flux which is more likely to be the typical mode of operation of condensers at constant mass flow rate. However, another possibility is for the reject water to be at a constant temperature and possibly variable flow whether for condenser cooling or any other heat exchanging application as mentioned in the introduction section.

5.3.1: DCS performance during April 11th to 14th, 2017 with constant T (single pool):

For this run, actual measured weather data from the 11th till the 14th of April 2017, at AUC campus in New Cairo (30.02 ° latitude, 31.5 ° longitude), are input as boundary conditions to the model (every minute). This is to estimate the water temperature in the DCS system for the case where the condenser rejects water to the pool at constant temperature, of 40℃, $T_{p_{i_1}}$.

Figure 5-5 (a, b & c) displays the variation of the simulated pool body temperature T_{sim} with time, together with the depth of pool water and shield status, the latter being indicated by the stepped profile at the bottom of the diagram; here the top level denotes shield in upper position(denoted by 4 on the y axis of the graph), the next level down (denoted by 3 on the y axis) indicates the shield resting on the pool rim, whereas the zero level represents removed shield. Also, the ambient temperature T_{ws} is displayed. In addition to that, the shield inside temperature $T_{s,i}$ is displayed in Figure 5-5 (b & c), while both $T_{s,i}$ and $T_{s,o}$ (shield outside temperature) are depicted in Figure 5-5-c. Figure 5-5-d shows the weather data during the simulation period showing the solar radiation, humidity, wind speed and ambient air temperature recorded by the weather station.

The 20 hours cooling period starts at 10 am on the 11th of April and withdrawing water starts at 6 am on the 12th. This allows the water in the pond to benefit from radiative cooling throughout the whole night, reaching comparable temperature to air at the end of the first cycle. The second cooling cycle starts at 2 am on the 12th of April (after the 4 hours of pool filling) and water withdrawal from the pool starts at 10am till 4 pm around noon, with water temperature being slightly higher than air around noon. Finally, the water and air temperatures are very close on the 14th of April.

Figure 5-5-a shows that for the month of April, the water temperature is comparable to air temperature at times when the pool is being emptied to use its water in condenser cooling even though April is one of the cooler months and the run was done in cloudy weather in the city of Cairo, which is not a typical desert climate with clear sky where radiative cooling would be more effective in lowering the water temperature. This is in addition to the fact that every 24 hours, the pool receives previously heated water at constant , $T_{p_{i_1}}$ of 40℃ to simulate possible mode of operation of condensers at constant heat rejection temperature and variable mass flow rate. An 18 $°C$ temperature drop was achieved by the system, which is equivalent to 53 MJ/m^2night of cooling.

Figure 5-5-e shows the predicted heat losses during the simulation period. The figure reveals that evaporation is the biggest loss, followed by radiation and convection for this specific run at AUC campus in New Cairo (30.02 ° N latitude, 31.5 ° E longitude) for the month of April. The spikes in heat flows are coupled to the transient conditions of filling the pool with hot water from the condenser. At the beginning of the filling process, the temperature difference between the hot water and ambient as well as the surface area to volume ratio of the water in the pool are high. Both effects, escalate the losses with evaporation loss being the highest. The increase in heat dissipation continues for a couple of hours after the end of the filling process till the difference between the pool temperature and the ambient gets closer to reaching equilibrium. On April 12th at 7:00 am, there is a sudden increase in ambient temperature, followed by a change in the shield position selected by the model from upper to lower position, to suppress the convection exchange between the pool water and ambient air, which is reflected on Figure 5-5-e, showing no evaporation and only free convection losses for the lower shield position.

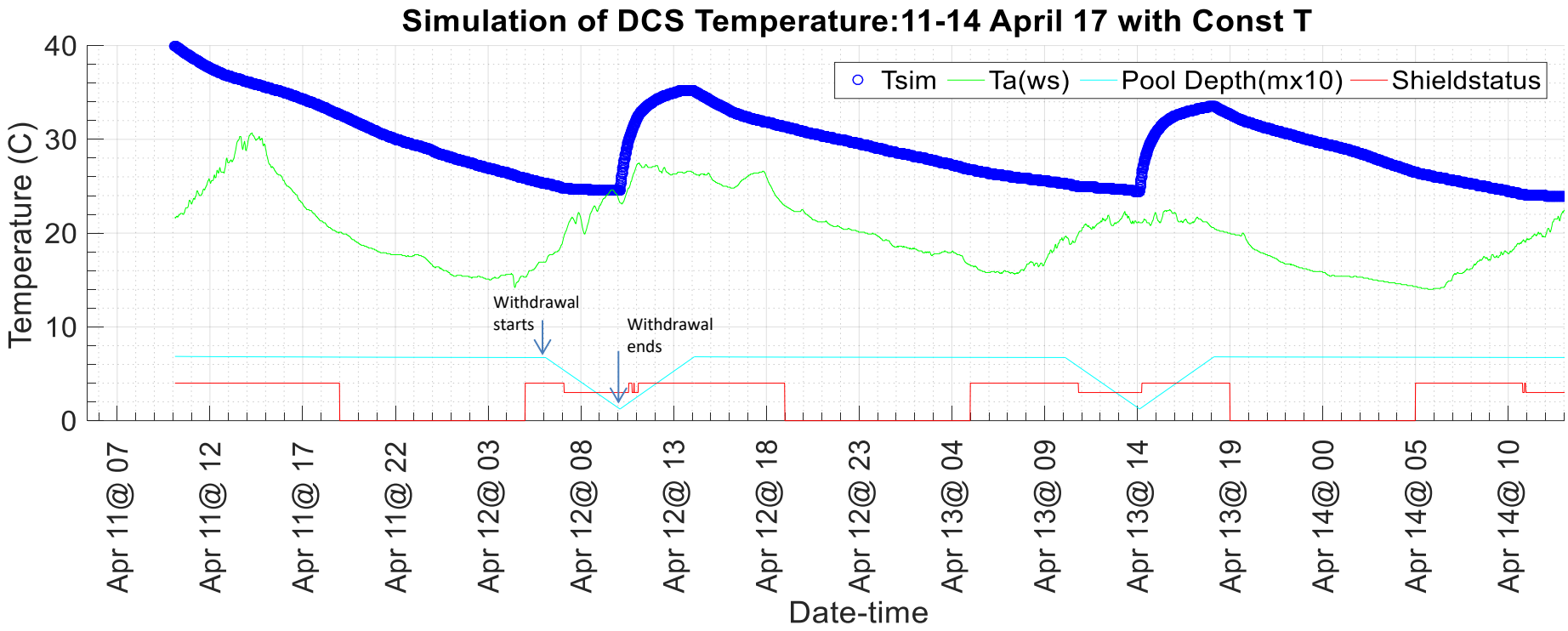
Simulation of DCS Temperature:11-14 April 17 with Const T
Tsim
Ta(ws)
Pool Depth(mx10)
Shieldstatus
Withdrawal starts
Withdrawal ends
Temperature (C)
0
10
20
30
40
Apr 11@ 07
Apr 11@ 12
Apr 11@ 17
Apr 11@ 22
Apr 12@ 03
Apr 12@ 08
Apr 12@ 13
Apr 12@ 18
Apr 12@ 23
Apr 13@ 04
Apr 13@ 09
Apr 13@ 14
Apr 13@ 19
Apr 14@ 00
Apr 14@ 05
Apr 14@ 10
Date-time

Figure 5-5 (a)

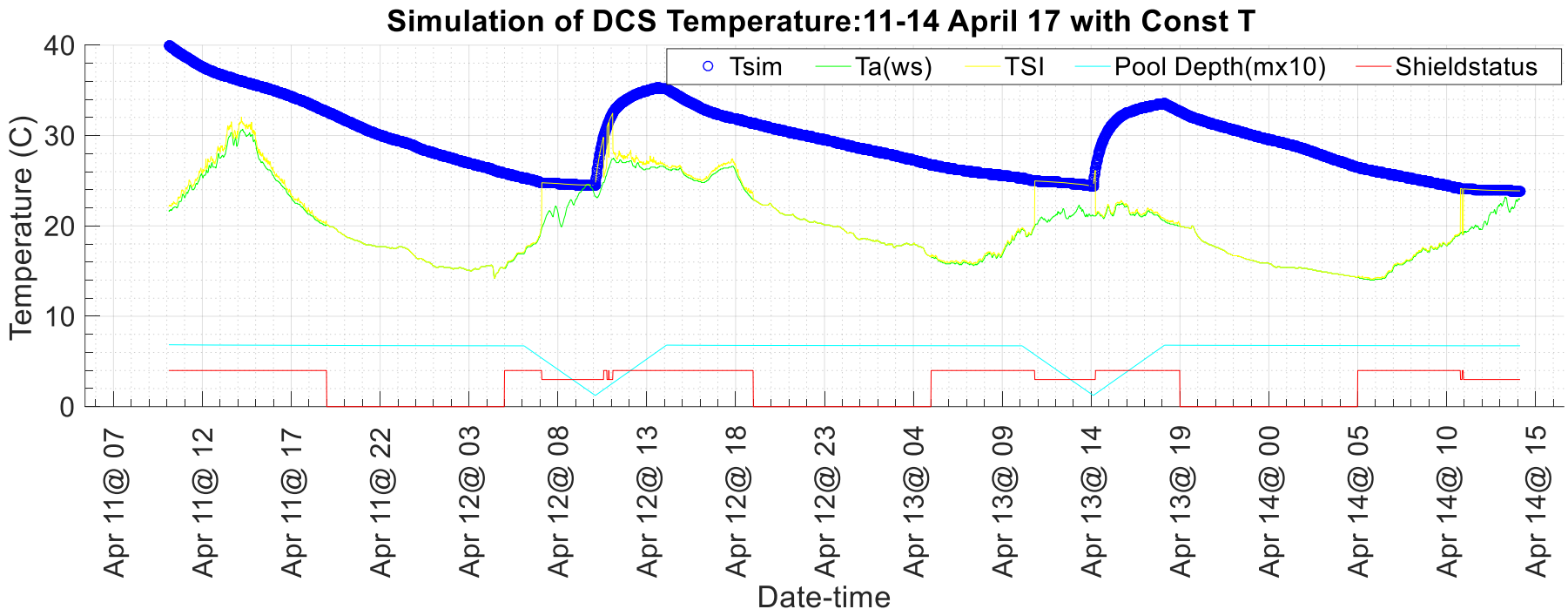
Simulation of DCS Temperature:11-14 April 17 with Const T
Tsim
Ta(ws)
TSI
Pool Depth(mx10)
Shieldstatus
Temperature (C)
0
10
20
30
40
Apr 11@ 07
Apr 11@ 12
Apr 11@ 17
Apr 11@ 22
Apr 12@ 03
Apr 12@ 08
Apr 12@ 13
Apr 12@ 18
Apr 12@ 23
Apr 13@ 04
Apr 13@ 09
Apr 13@ 14
Apr 13@ 19
Apr 14@ 00
Apr 14@ 05
Apr 14@ 10
Apr 14@ 15
Date-time

Figure 5-5 (b)

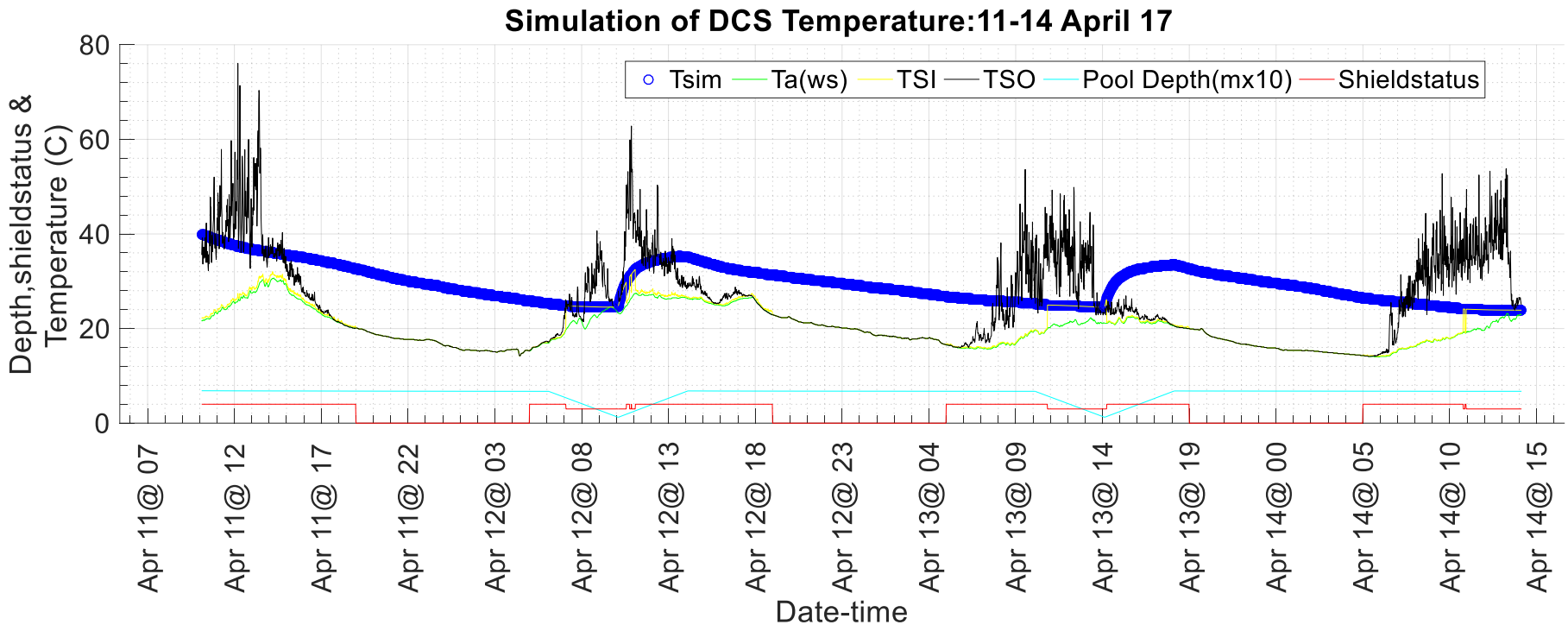
Simulation of DCS Temperature:11-14 April 17
Tsim
Ta(ws)
TSI
TSO
Pool Depth(mx10)
Shieldstatus
Depth,shieldstatus & Temperature (C)
0
20
40
60
80
Apr 11@ 07
Apr 11@ 12
Apr 11@ 17
Apr 11@ 22
Apr 12@ 03
Apr 12@ 08
Apr 12@ 13
Apr 12@ 18
Apr 12@ 23
Apr 13@ 04
Apr 13@ 09
Apr 13@ 14
Apr 13@ 19
Apr 14@ 00
Apr 14@ 05
Apr 14@ 10
Apr 14@ 15
Date-time

Figure 5-5 (c)

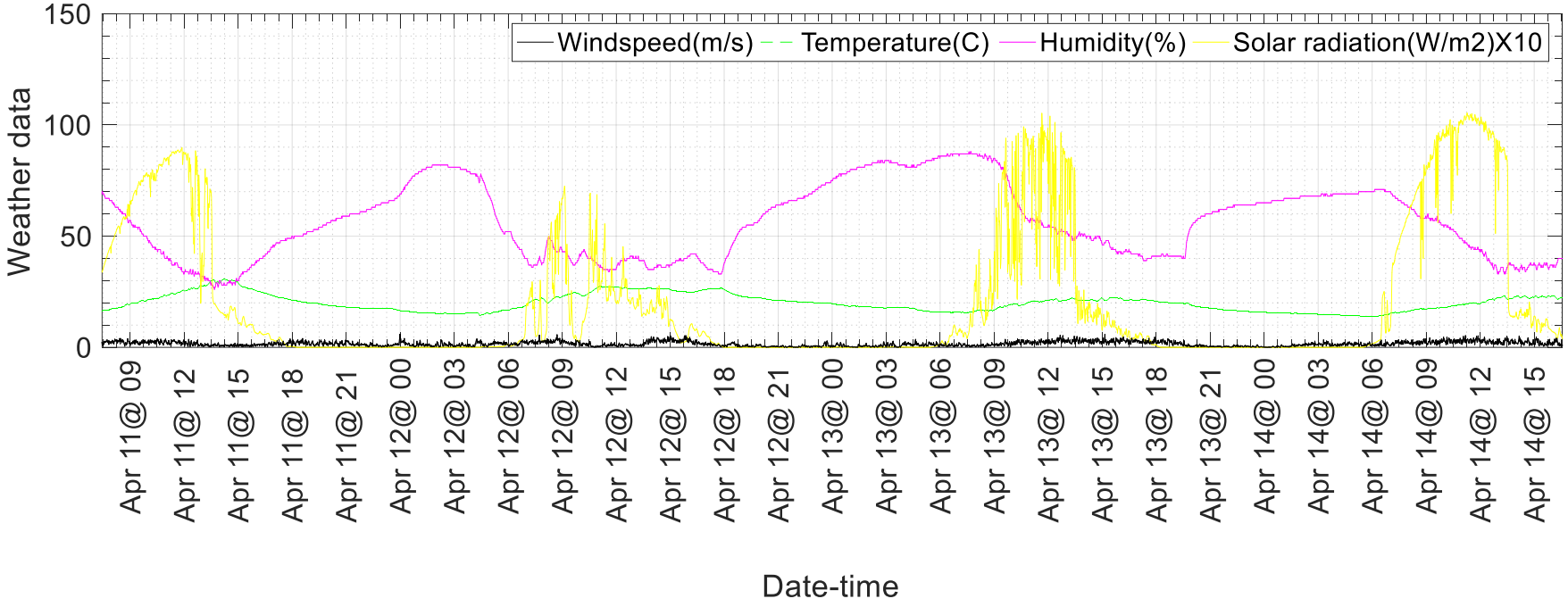
Windspeed(m/s)
Temperature(C)
Humidity(%)
Solar radiation(W/m2)X10
Weather data
150
100
50
0
Apr 11@ 09
Apr 11@ 12
Apr 11@ 15
Apr 11@ 18
Apr 11@ 21
Apr 12@ 00
Apr 12@ 03
Apr 12@ 06
Apr 12@ 09
Apr 12@ 12
Apr 12@ 15
Apr 12@ 18
Apr 12@ 21
Apr 13@ 00
Apr 13@ 03
Apr 13@ 06
Apr 13@ 09
Apr 13@ 12
Apr 13@ 15
Apr 13@ 18
Apr 13@ 21
Apr 14@ 00
Apr 14@ 03
Apr 14@ 06
Apr 14@ 09
Apr 14@ 12
Apr 14@ 15
Date-time
Figure 5-5 (d)

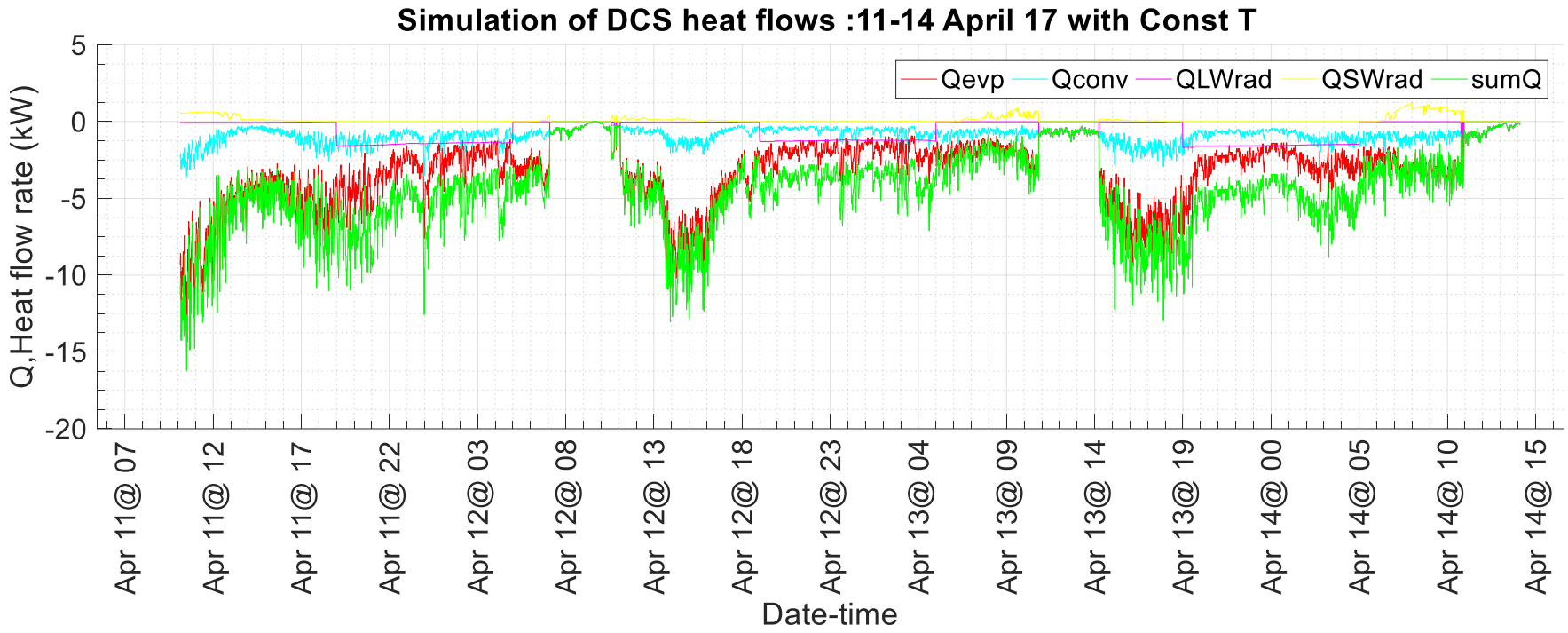

Figure 5-5 (e)

Figure 5-5: Pool temperature, heat flows and weather data of DCS (11th - 14th April 2017)-Const T

5.3.2: DCS performance during April 11th to 14th, 2017 with constant ΔT (single pool):

Figure 5-6 presents the simulation results for the DCS temperatures using actual weather data from April 11th to 14th, 2017 for water rejected to the pool at constant ΔT of 15°C (set at ΔT achieved from the first cycle of this run). This is to simulate constant heat flux which is more likely to be the typical mode of operation of condensers at constant mass flow rate. This figure, when compared to Figure 5-5, shows that both modes of operations, constant ΔT and constant initial temperature ($T_{p_i} = 40$°C), show comparable temperatures for this specific run.

On the other hand, the shield status selected by the model follow similar profiles for both modes of operation with two main exceptions. On the 12th of April at 10:30 and at 18:00, the shield position changed to shield down in the constant ΔT mode (Figure 5-6) instead of shield up in constant T_{p_i} mode (Figure 5-5), indicating a slight increase in the pool temperature as compared to air to render the difference between them greater than the $5°C$ set by the model as a criteria for selecting the shield down position.

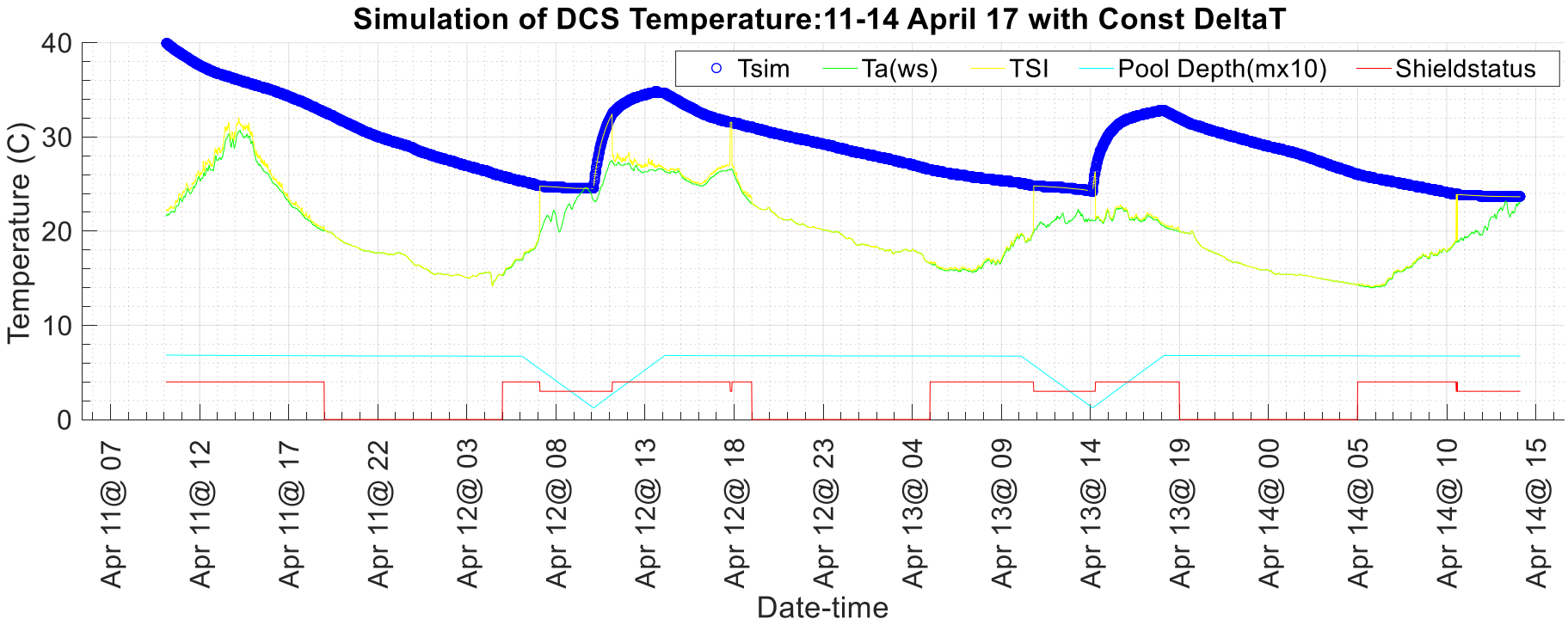
Simulation of DCS Temperature:11-14 April 17 with Const DeltaT
Tsim
Ta(ws)
TSI
Pool Depth(mx10)
Shieldstatus
Temperature (C)
40
30
20
10
0
Apr 11@ 07
Apr 11@ 12
Apr 11@ 17
Apr 11@ 22
Apr 12@ 03
Apr 12@ 08
Apr 12@ 13
Apr 12@ 18
Apr 12@ 23
Apr 13@ 04
Apr 13@ 09
Apr 13@ 14
Apr 13@ 19
Apr 14@ 00
Apr 14@ 05
Apr 14@ 10
Apr 14@ 15
Date-time

Figure 5-6 (a)

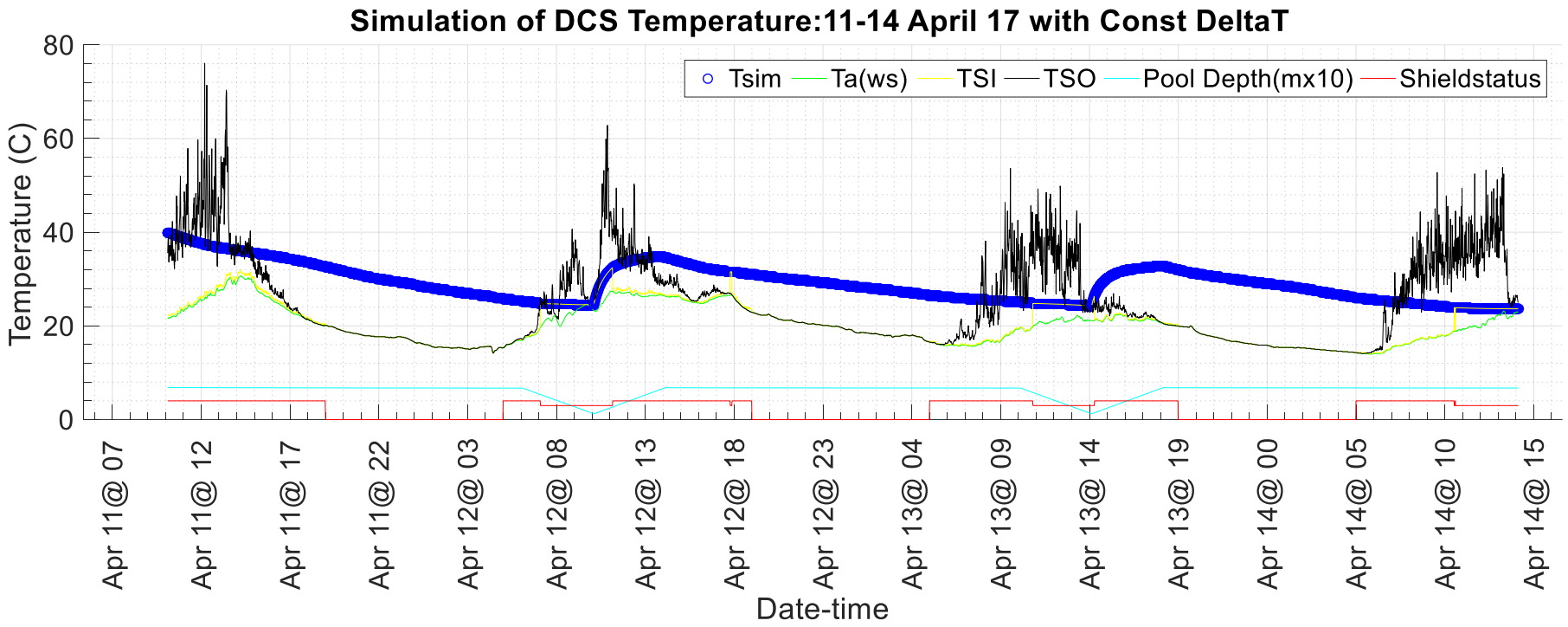
Simulation of DCS Temperature:11-14 April 17 with Const DeltaT
Tsim
Ta(ws)
TSI
TSO
Pool Depth(mx10)
Shieldstatus
Temperature (C)
0
20
40
60
80
Apr 11@ 07
Apr 11@ 12
Apr 11@ 17
Apr 11@ 22
Apr 12@ 03
Apr 12@ 08
Apr 12@ 13
Apr 12@ 18
Apr 12@ 23
Apr 13@ 04
Apr 13@ 09
Apr 13@ 14
Apr 13@ 19
Apr 14@ 00
Apr 14@ 05
Apr 14@ 10
Apr 14@ 15
Date-time

Figure 5-6 (b)

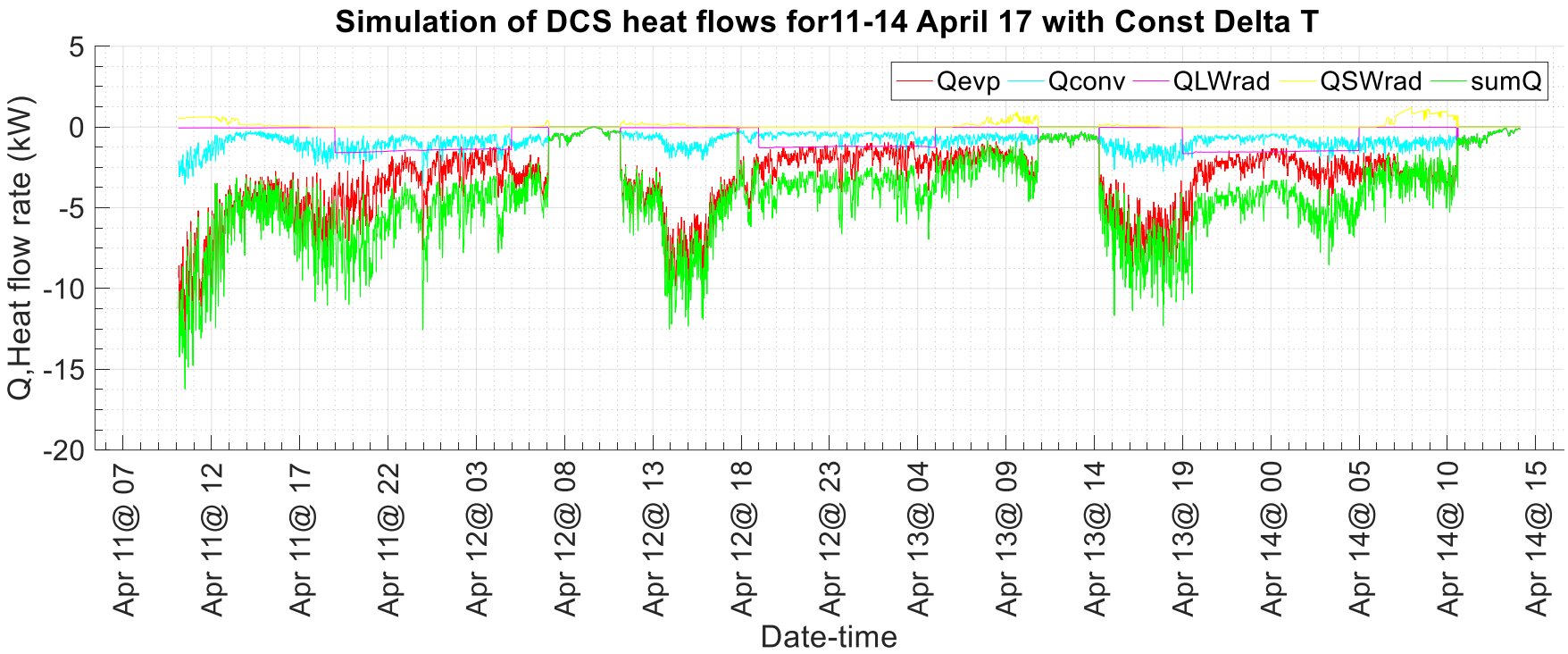

Figure 5-6 (c)

Figure 5-6: Pool temperature and heat flows of DCS for the 11th till the 14th of April 2017-ConstΔT.

5.3.3: DCS performance during May 24th to 27th, 2017 with constant ΔT (single pool):

Figure 5-7 depicts the predicted DCS water temperature T_{sim} , for three days in the month of May. Also shown on the same figure are the ambient temperature T_{ws} , both $T_{s,i}$ and $T_{s,o}$ (shield inside and outside temperature), together with the depth of pool water and shield status.

As displayed Figure 5-7, during the time of water withdrawal to the condenser or for any other cooling purposes, the figure shows that the water temperature is lower than the air temperature by more than five degrees at the end of the 2nd and 3rd cooling cycles. The month of May, being a hotter and drier month than April, better represents the climate in which the DCS system would be used. Thus, showing better DCS system performance. It worth mentioning that there was a problem in the humidity sensor during this run, so the humidity values used in the simulation are taken from (https://www.timeanddate.com/weather/egypt/cairo 2017).

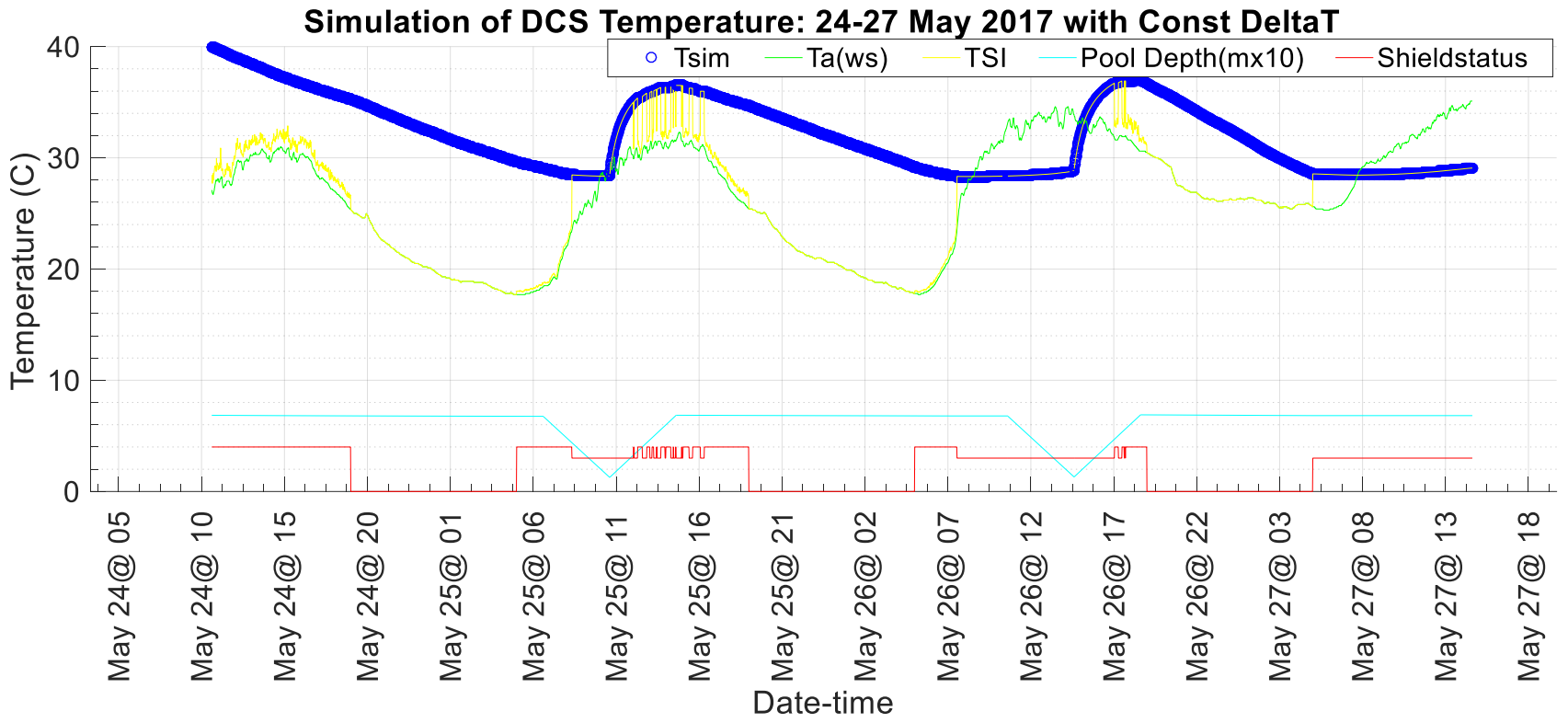
Simulation of DCS Temperature: 24-27 May 2017 with Const DeltaT
Tsim
Ta(ws)
TSI
Pool Depth(mx10)
Shieldstatus
Temperature (C)
0
10
20
30
40
May 24@ 05
May 24@ 10
May 24@ 15
May 24@ 20
May 25@ 01
May 25@ 06
May 25@ 11
May 25@ 16
May 25@ 21
May 26@ 02
May 26@ 07
May 26@ 12
May 26@ 17
May 26@ 22
May 27@ 03
May 27@ 08
May 27@ 13
May 27@ 18
Date-time

Figure 5-7 (a)

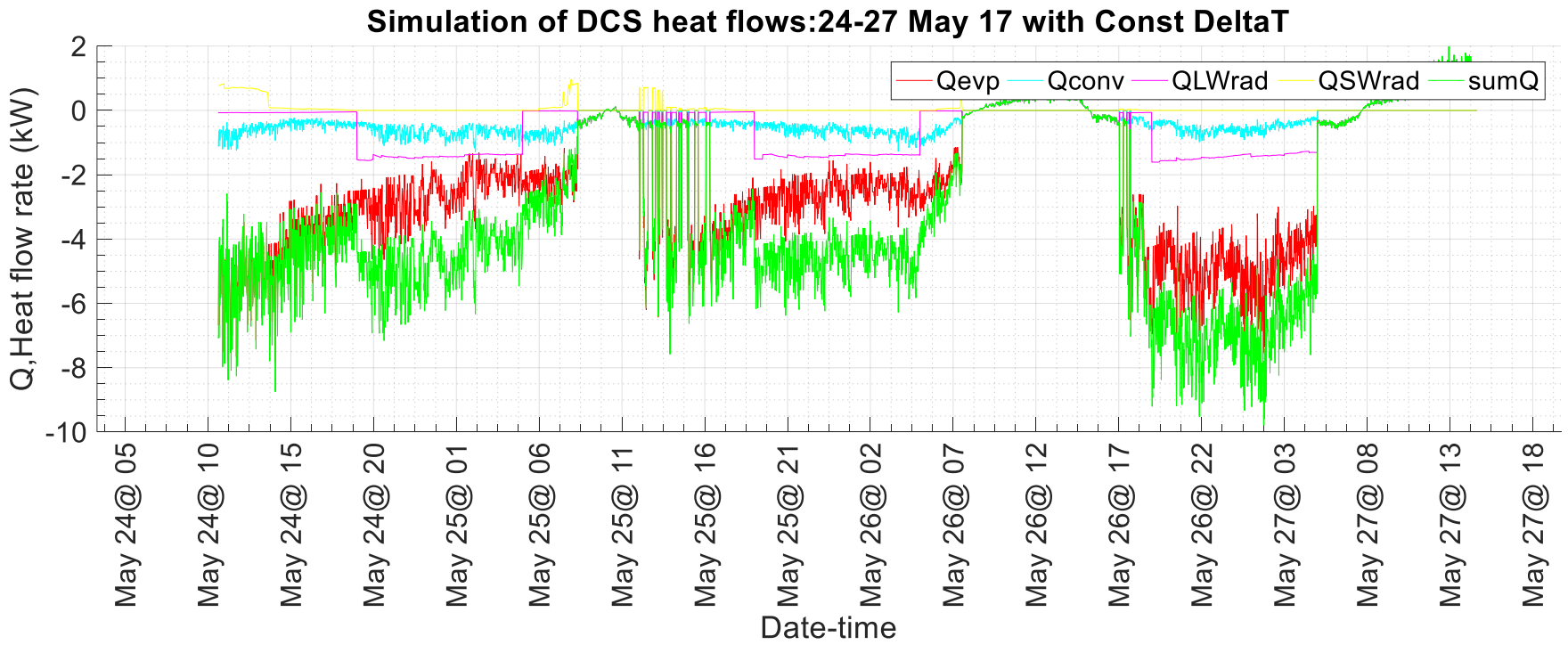

Figure 5-7 (b)

Figure 5-7: Simulation of DCS performance (24-27 May 2017)- constant Tin

5.3.4: DCS performance during June 16th to 20th, 2017 with constant ΔT (single pool):

Similar to the end of May, mid-June results show better DCS performance than the month of April with up to 8 degrees temperature difference between air and water, which favours water cooling produced by DCS as compared to air cooling as demonstrated in Figure 5-8.

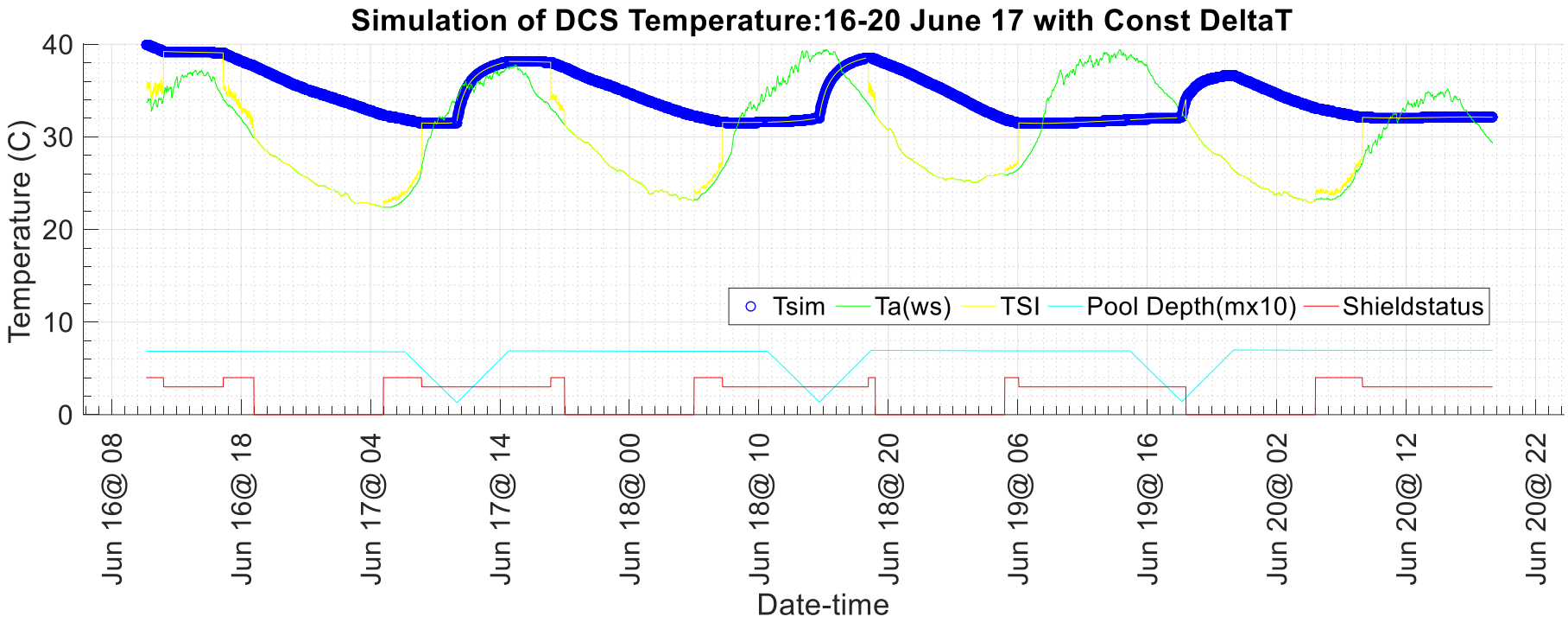
Simulation of DCS Temperature:16-20 June 17 with Const DeltaT
Temperature (C)
40
30
20
10
0
Tsim
Ta(ws)
TSI
Pool Depth(mx10)
Shieldstatus
Jun 16@ 08
Jun 16@ 18
Jun 17@ 04
Jun 17@ 14
Jun 18@ 00
Jun 18@ 10
Jun 18@ 20
Jun 19@ 06
Jun 19@ 16
Jun 20@ 02
Jun 20@ 12
Jun 20@ 22
Date-time
Figure 5-8(a)

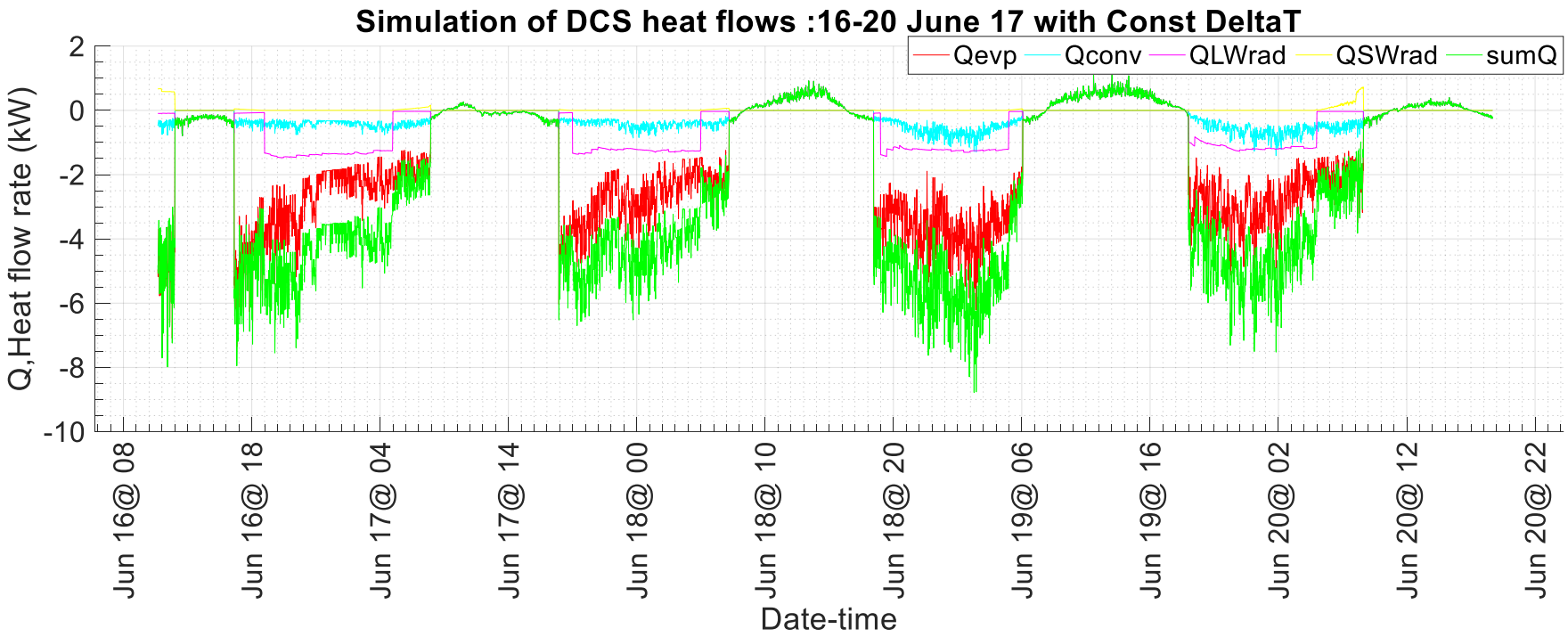

Figure 5-8(b)

Figure 5-8: Simulation of DCS performance for 16th till the 20th 2017 with constant ***ΔT***, 20 hours cooling period

5.4: DCS performance simulation for multiple pools (4 pools for 12 hours operation/day):

5.4.1: DCS performance simulation 11-14 April2017 with constant T (4 pools):

Figure 5-9 presents the simulation of the temperature in the 4 pools for the 12 hours daily cooling operation of the DCS as explained in detail in section 5.1 of this chapter. As seen from the figure, the temperature drop achieved differ slightly from one pool to the other since though they all passed through night cooling from 6 pm till 6 am, they are left to cool for different number of hours and starting at different times during the day. The average temperature drop for the 4 pools is approximately 13$°C$ for pool 1 with a total of 20 hours of cooling, 11$°C$ for pool 2 and 3 with a total of 16 hours of cooling and 8 $°C$ for pool 4 that only receives relatively hot water from the other pools and not directly from the condenser. The details of the cycle filling, emptying and cooling are listed in Table 5-1 .

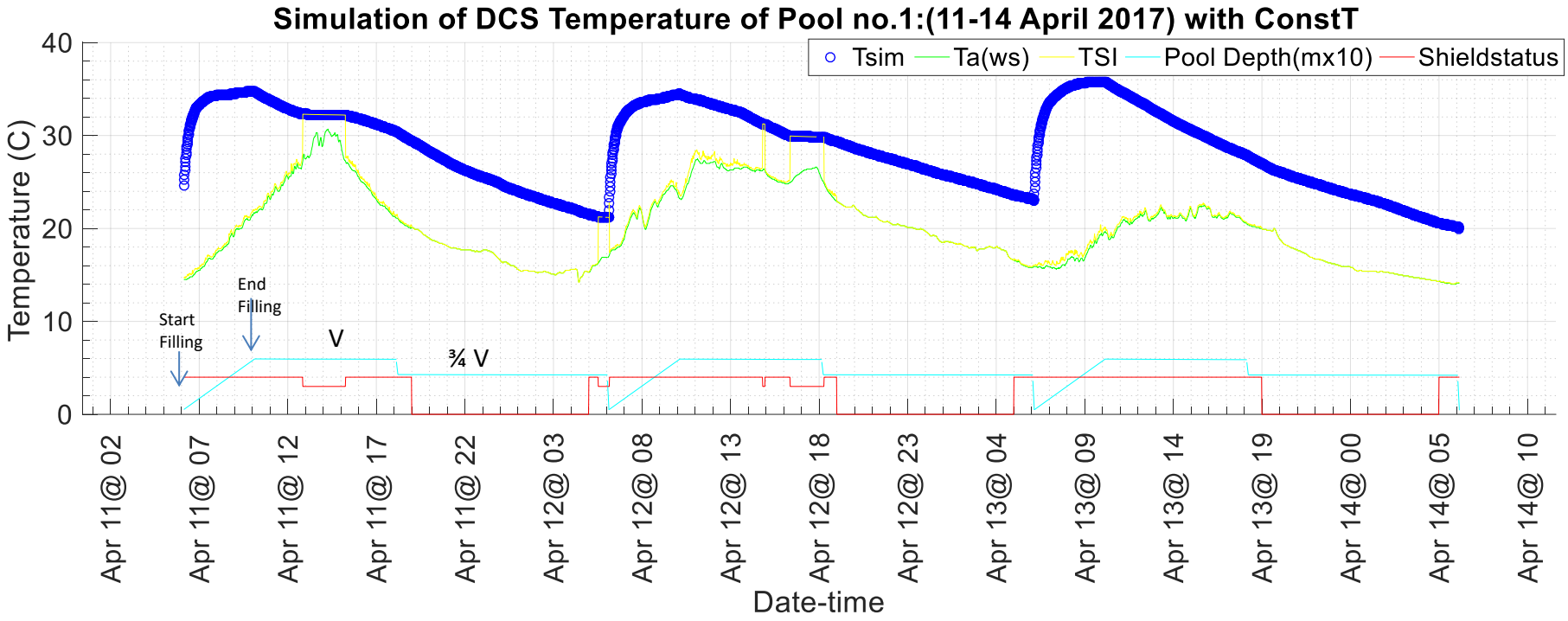
Simulation of DCS Temperature of Pool no.1:(11-14 April 2017) with ConstT
Tsim
Ta(ws)
TSI
Pool Depth(mx10)
Shieldstatus
Temperature (C)
40
30
20
10
0
Start Filling
End Filling
V
¾ V
Apr 11@ 02
Apr 11@ 07
Apr 11@ 12
Apr 11@ 17
Apr 11@ 22
Apr 12@ 03
Apr 12@ 08
Apr 12@ 13
Apr 12@ 18
Apr 12@ 23
Apr 13@ 04
Apr 13@ 09
Apr 13@ 14
Apr 13@ 19
Apr 14@ 00
Apr 14@ 05
Apr 14@ 10
Date-time

Figure 5-9 (a)

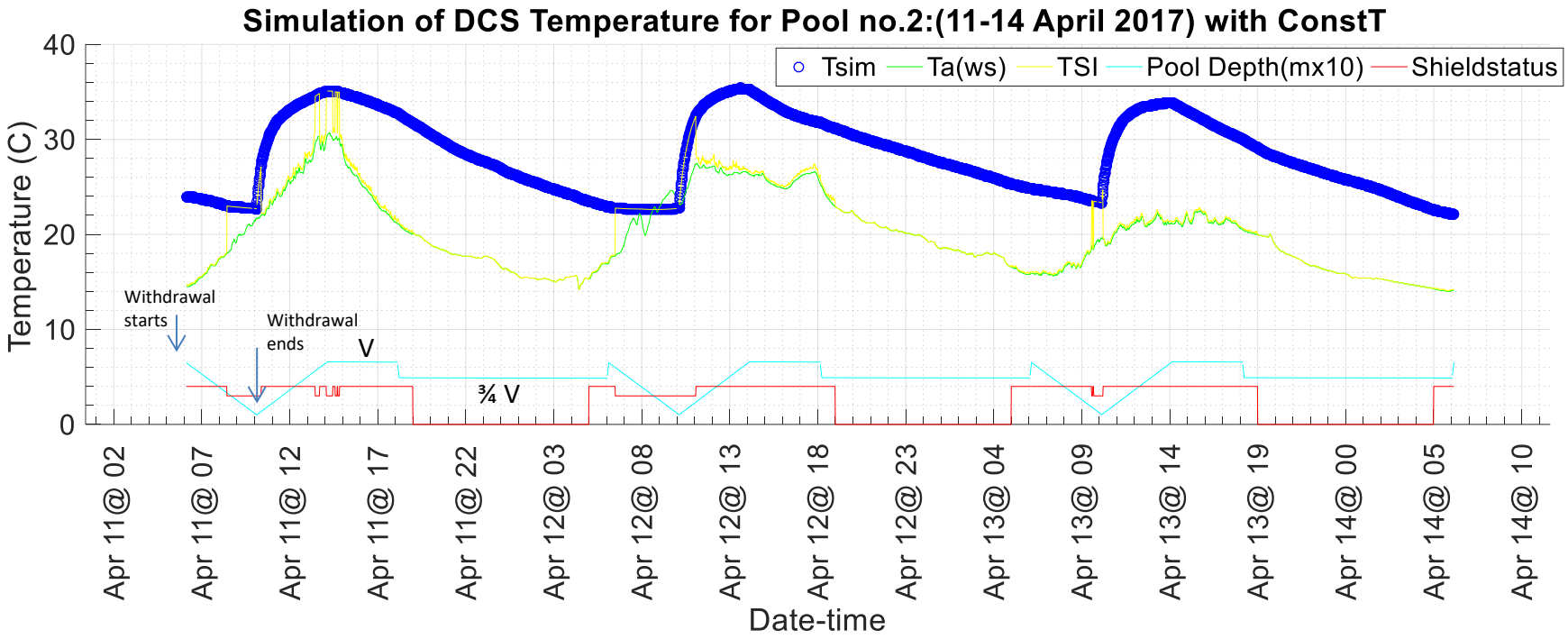
Simulation of DCS Temperature for Pool no.2:(11-14 April 2017) with ConstT
Tsim
Ta(ws)
TSI
Pool Depth(mx10)
Shieldstatus
Temperature (C)
40
30
20
10
0
Withdrawal starts
Withdrawal ends
V
¾ V
Apr 11@ 02
Apr 11@ 07
Apr 11@ 12
Apr 11@ 17
Apr 11@ 22
Apr 12@ 03
Apr 12@ 08
Apr 12@ 13
Apr 12@ 18
Apr 12@ 23
Apr 13@ 04
Apr 13@ 09
Apr 13@ 14
Apr 13@ 19
Apr 14@ 00
Apr 14@ 05
Apr 14@ 10
Date-time

Figure 5-9 (b)

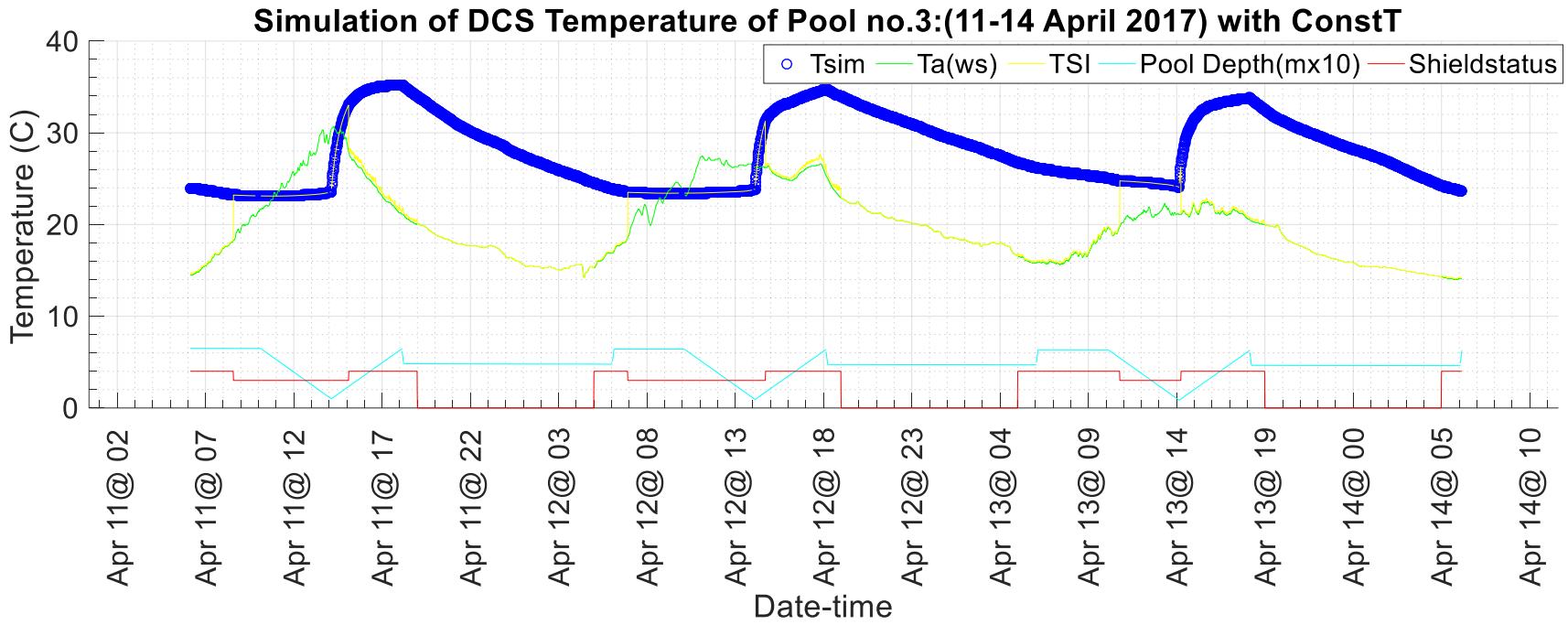
Simulation of DCS Temperature of Pool no.3:(11-14 April 2017) with ConstT
Tsim
Ta(ws)
TSI
Pool Depth(mx10)
Shieldstatus
Temperature (C)
40
30
20
10
0
Apr 11@ 02
Apr 11@ 07
Apr 11@ 12
Apr 11@ 17
Apr 11@ 22
Apr 12@ 03
Apr 12@ 08
Apr 12@ 13
Apr 12@ 18
Apr 12@ 23
Apr 13@ 04
Apr 13@ 09
Apr 13@ 14
Apr 13@ 19
Apr 14@ 00
Apr 14@ 05
Apr 14@ 10
Date-time

Figure 5-9 (c)

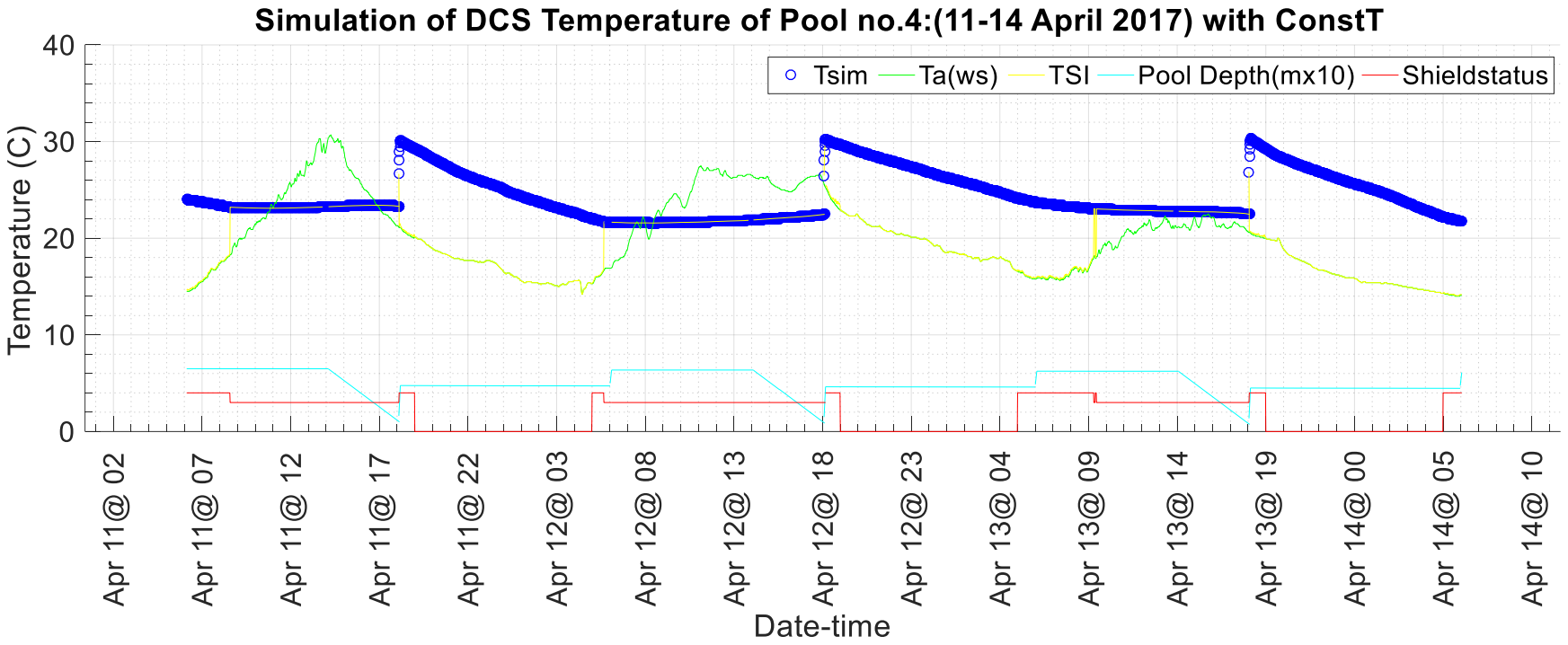

Figure 5-9 (d)

Figure 5-9: DCS performance simulation for 3 days using 4 pools

Figure 5-10 presents the heat flow of pool 1 for the 12 hours operation. The spikes in the heat flow start at 6 am everyday with the filling of the pool with hot water due to the high surface area to volume ratio and the large temperature difference between the hot rejected water out of the condenser and the ambient air temperature that increase the rate of heat loss. Radiation heat loss is of course at its maximum when the shield is removed at night after 7 pm till 5 am in the morning which is the set time of shield removal by the model. On the 11th of April, from shortly before 13 till 15, the model selects lower shield position when the ambient air is too hot (Ta-Tpool>5) to suppress forced convection effects and consequently evaporation is also suppressed.

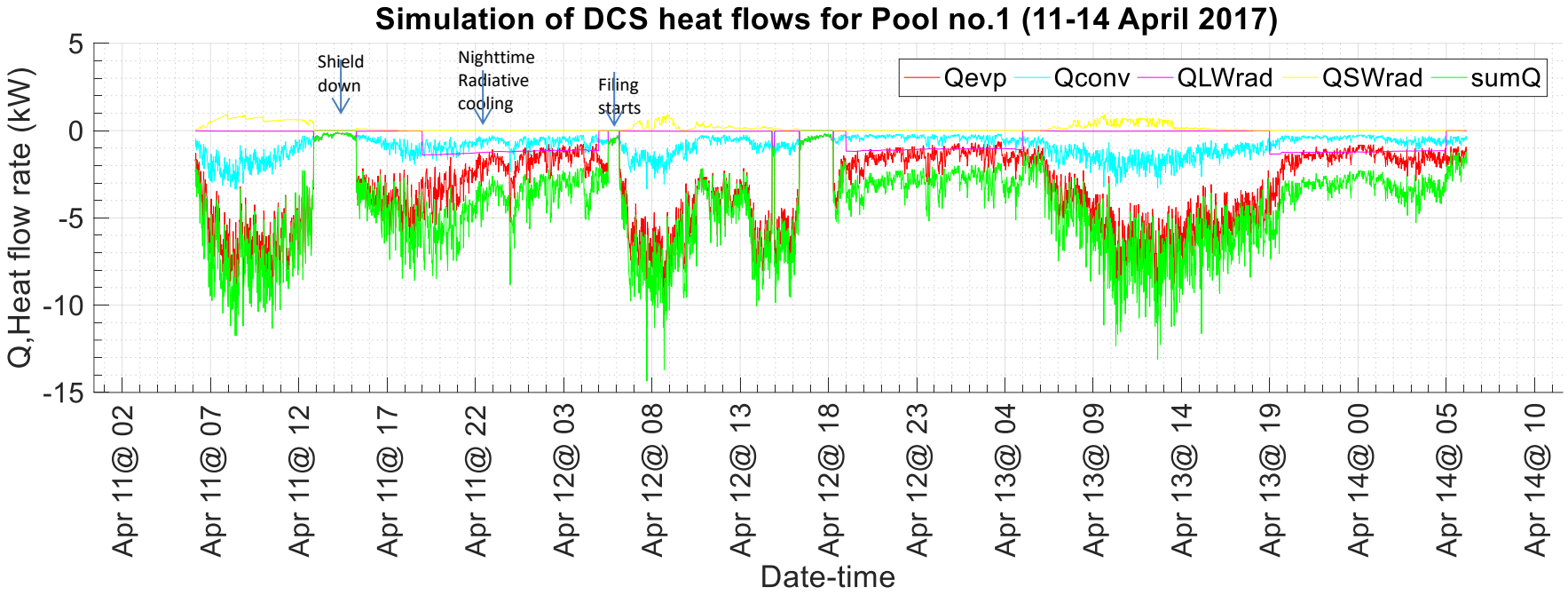

Figure 5-10: Heat flow simulation for 3 days

5.4.2: DCS performance simulation 11-18 April 2017 with constant T (4 pools):

Figure 5-11 presents the simulation of the temperature in the 4 pools for the 12 hours daily cooling operation of the DCS for a week using weather data of New Cairo (30.02 ° N latitude, 31.5 ° E longitude) for the month of April 2017. The maximum temperature drop was on the 13th of April in pool 1 with a value of 16°C, which is equivalent to 47 $\frac{MJ}{m^2.night}$. It is worth mentioning that the discontinuity in the temperature profile of pool 4 is linked with the sudden increase in temperature with fast pumping rate from the other 3 pools right after 6 pm every day. This abrupt change was not reflected on the curve when filling the pool with condenser hot reject water, since the pumping rate was very slow as the duration of filling of one pool from the condenser is 4 hours. The filling of pool 4 from the other 3 pools is simulated to finish in just 5 minutes to reflect the recommended practical implementation discussed in detail earlier in section 5.1.

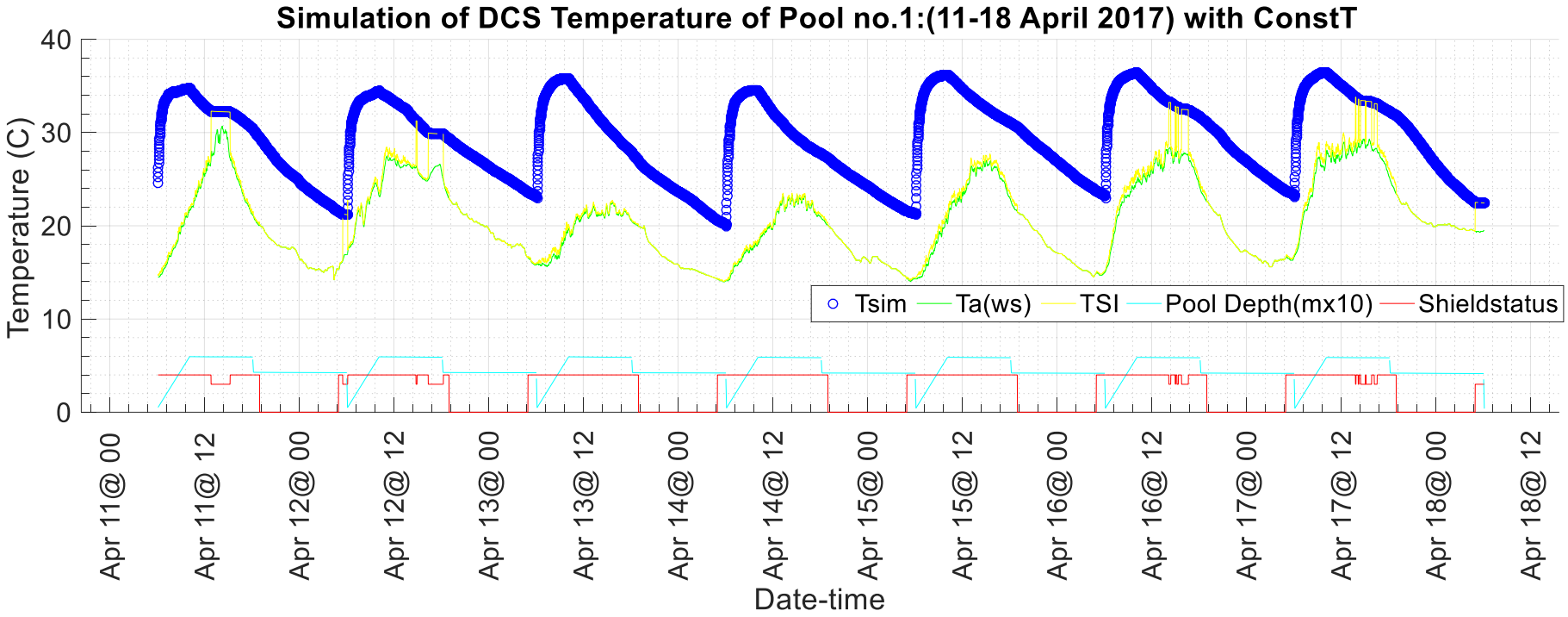
Simulation of DCS Temperature of Pool no.1:(11-18 April 2017) with ConstT
Temperature (C)
40
30
20
10
0
Tsim
Ta(ws)
TSI
Pool Depth(mx10)
Shieldstatus
Apr 11@ 00
Apr 11@ 12
Apr 12@ 00
Apr 12@ 12
Apr 13@ 00
Apr 13@ 12
Apr 14@ 00
Apr 14@ 12
Apr 15@ 00
Apr 15@ 12
Apr 16@ 00
Apr 16@ 12
Apr 17@ 00
Apr 17@ 12
Apr 18@ 00
Apr 18@ 12
Date-time

Figure 5-11 (a)

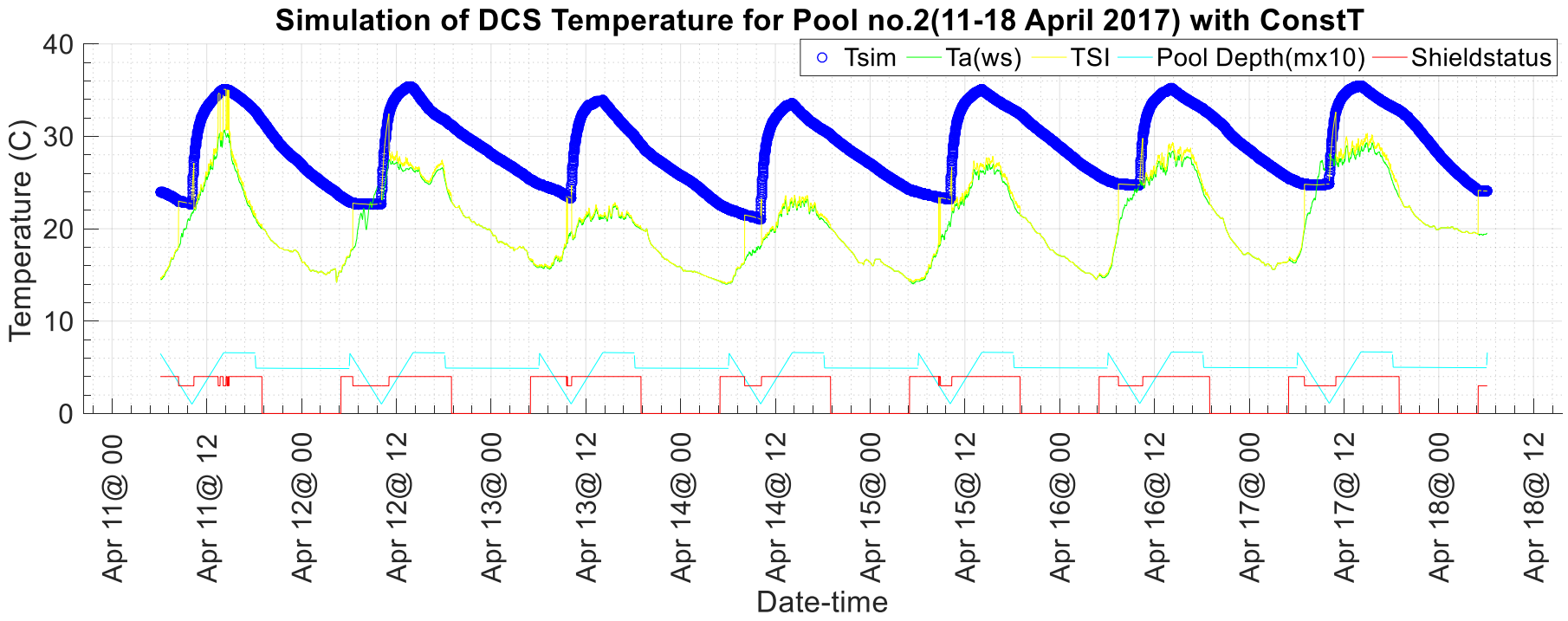
Simulation of DCS Temperature for Pool no.2(11-18 April 2017) with ConstT
Tsim
Ta(ws)
TSI
Pool Depth(mx10)
Shieldstatus
Temperature (C)
40
30
20
10
0
Apr 11@ 00
Apr 11@ 12
Apr 12@ 00
Apr 12@ 12
Apr 13@ 00
Apr 13@ 12
Apr 14@ 00
Apr 14@ 12
Apr 15@ 00
Apr 15@ 12
Apr 16@ 00
Apr 16@ 12
Apr 17@ 00
Apr 17@ 12
Apr 18@ 00
Apr 18@ 12
Date-time

Figure 5-11 (b)

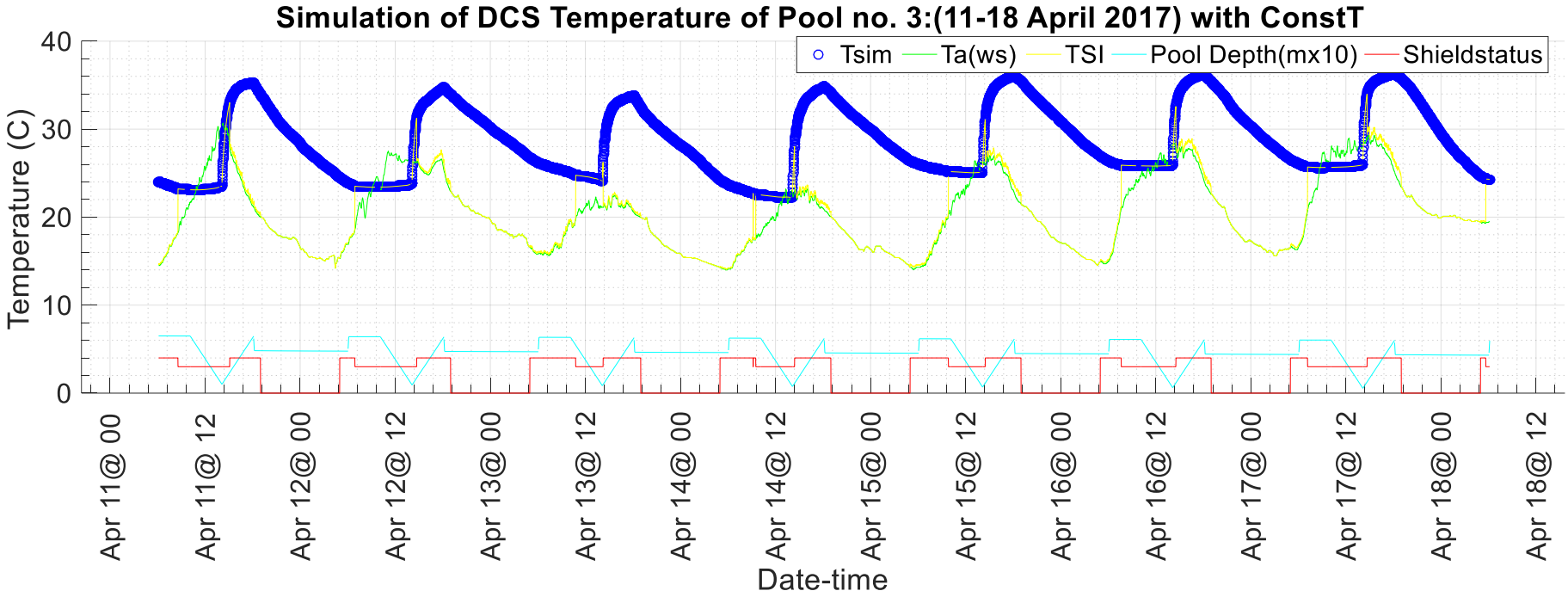
Simulation of DCS Temperature of Pool no. 3:(11-18 April 2017) with ConstT
Tsim
Ta(ws)
TSI
Pool Depth(mx10)
Shieldstatus
Temperature (C)
0
10
20
30
40
Apr 11@ 00
Apr 11@ 12
Apr 12@ 00
Apr 12@ 12
Apr 13@ 00
Apr 13@ 12
Apr 14@ 00
Apr 14@ 12
Apr 15@ 00
Apr 15@ 12
Apr 16@ 00
Apr 16@ 12
Apr 17@ 00
Apr 17@ 12
Apr 18@ 00
Apr 18@ 12
Date-time

Figure 5-11 (c)

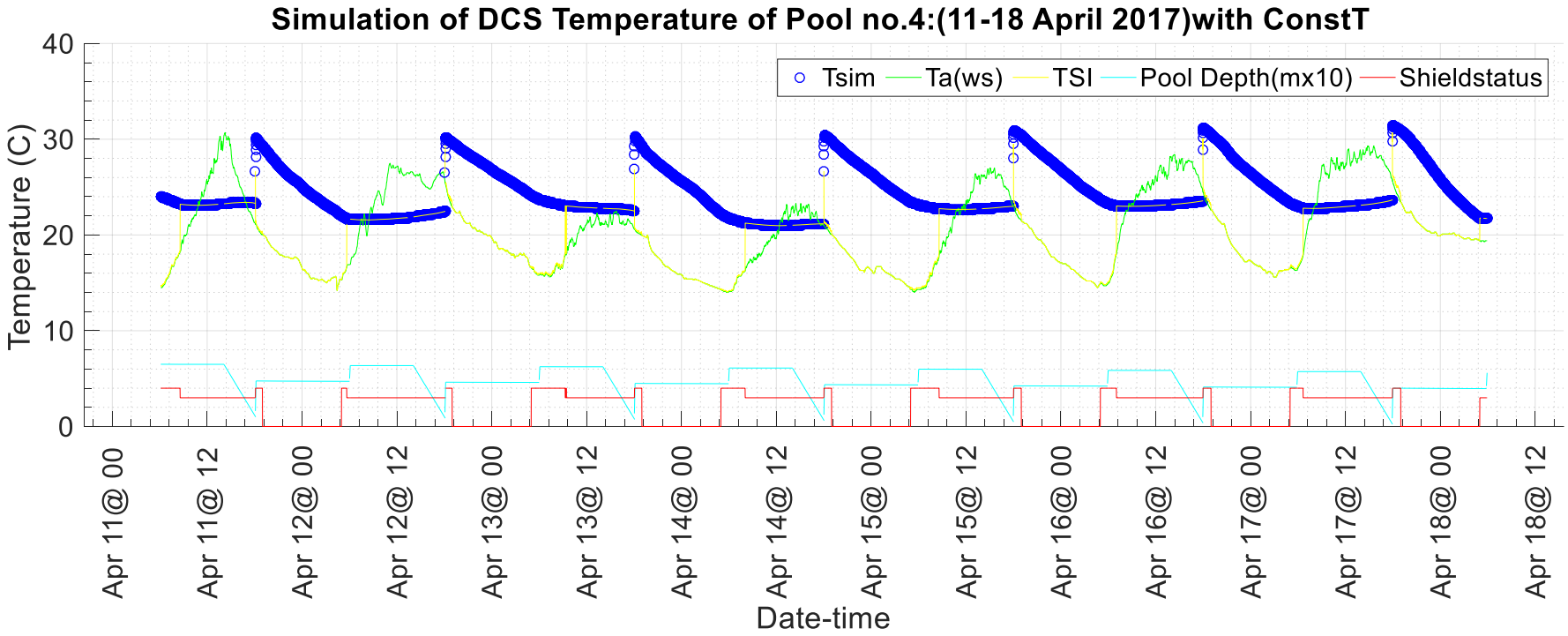

Figure 5-11(d)

Figure 5-11: DCS performance simulation for recorded weather data using 4 pools

Chapter 6: Experimental Rig

This chapter presents the experimental setup that is designed and constructed to gain experience on the operation of the DCs and understand the system behavior in relation with the actual's measured site weather conditions at AUC campus in New Cairo (30.02 ° N latitude, 31.5 ° E longitude). The setup is also used to complement the theoretical model by checking its assumptions and provide means for qualitative comparison.

The experimental setup consists of 4 main parts; a commercial swimming pool, an electric water heater, top shield, and the measuring system, as shown in Figure 6-1 to Figure 6-3. The experiment simply measures real time water temperature in the pool of the DCS for extended periods of time for different shading scenarios, with and without water heating and provides a log for the water temperature in °C every 10 seconds, using a data logger.

Figure 6-1: Experimental setup without the top shield

6.1: Equipment description:

The pool used in the experiments is a commercial 3.66 m diameter swimming pool with maximum depth till rim of 76 cm. The pool is surrounded by an aluminum foil to reflect beam radiation and prevent it from heating the water in the pool from the pool circumference, as shown in Figure 6-3-a. An air gap of around 1 cm is left between the aluminum foil and the pool wall for insulation. It is worth mentioning that during the first runs the aluminum foil was not installed yet around the pool.

In the bottom of the pool, an electric heater is mounted on a wooden bar, as shown in Figure 6-3-b. The heater was 4.8 kW in capacity and was used to act as the heat load that the DCS would be required to cool.

The top of the pool is shielded with a specially designed shield to reflect sun rays away from the pool and prevent the transfer of heat gained at the top part to the bottom layer and consequently to the pool surface. The shield is 3.3 m × 4 m, and is built of 1.1m wide sections, each composed of 4 layers

as in Figure 6-2. From top to bottom, the first layer is made of corrugated galvanized steel 1 mm thick (k=54 W/$m°C$), inside which 5cm foam slabs, made of expanded polystyrene (EPS) beads (k=0.03 W/$m°C$), are fitted for insulation. Finally, the bottom layer is made of a 3 cm thick wooden sheet (k=0.13 W/$m°C$) covered with 5 mm thick polypropylene hollow sheet (k=0.055W/$m°C$), which is made hollow to benefit from the insulation properties of air.

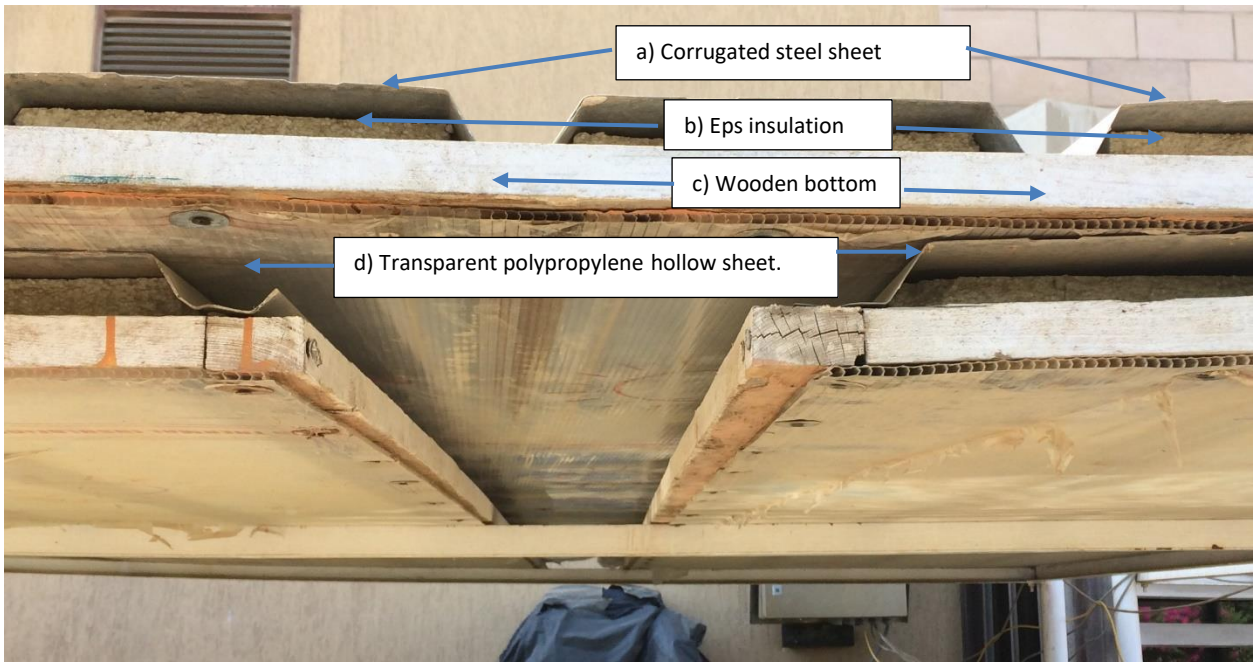

Figure 6-2: Shield components

In its upper position, the distance between the bottom of the shield and the rim of the pool is 90 cm. While, in its lower position the distance was 8 cm.

Figure 6-3(a)

Figure 6-3 (b)

Figure 6-3: Pool with shield in the upper position.

6.2: Measuring system:

The measuring system indicates the outputs for this experiment. These measurements include water temperature measurements, weather measurements and wind speed measurements near the pool surface.

Four thermocouples are mounted in the middle of the pool, to measure the water temperature, using the setup shown in Figure 6-4. The first (T1) and the second (T2) thermocouples are installed at distances 15 cm, and 37.5 cm, respectively from the bottom of the pool. The third thermocouple (T3) is installed at 65 cm from the bottom. It normally starts by measuring the water temperature at the pool surface. However, after some time it measures the ambient air due to depth loss due to evaporation/leakage. The leakage (estimated as 0.065 cm/hour) is due the piercing of the weak rubber material of the pool during equipment mounting. The four thermocouples are connected to a data logger that takes readings every 10 seconds. The data logger model D102 was manufactured by P.A. Hilton Technical (P.A.Hilton.Technical n.d.). A photographic view of the water temperature data logger is shown in Figure 6-5.

All temperature measurements in this experiment are performed using iron-constantan (J-type) thermocouples. The J-type thermocouple has great performance with a Seebeck coefficient of about 52µV/°C, temperature range from 0 to 750°C and tolerance of +/- 2.2°C.

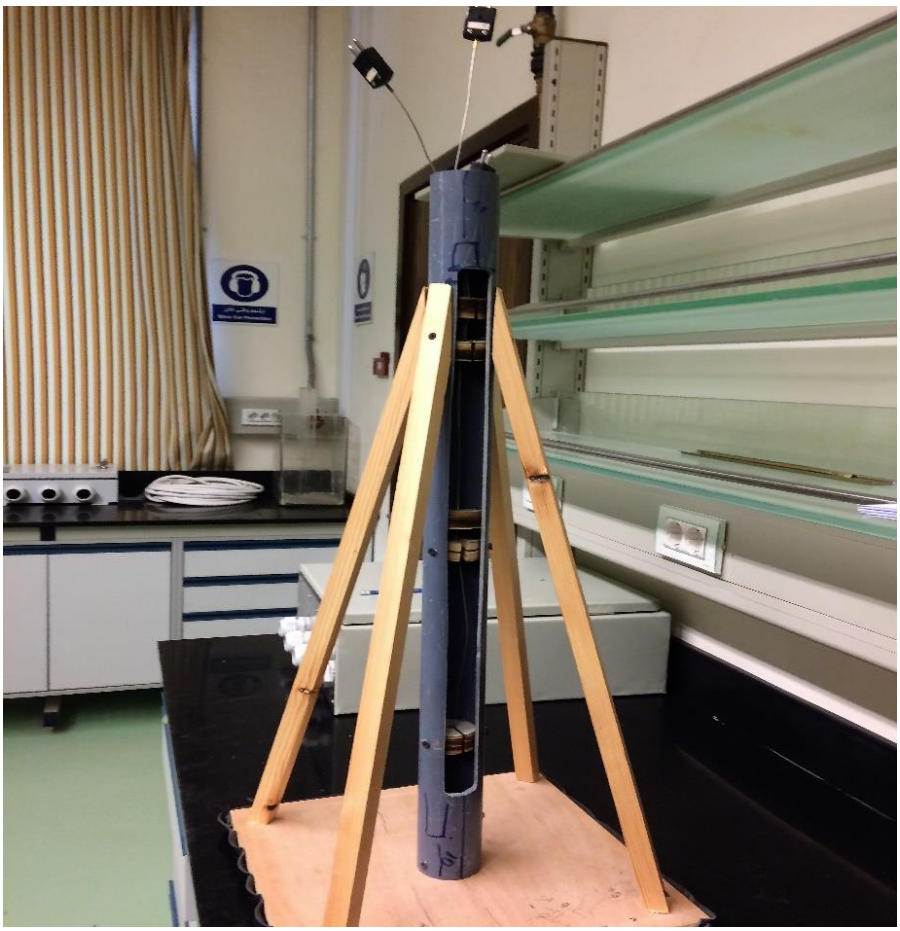

Figure 6-4: A photographic view of the mounting setup for the thermocouples

Figure 6-5 A photographic view of the water temperature data logger

The weather measurements performed in the experiments include solar radiation, ambient temperature, humidity, wind speed and direction. As shown in Figure 6-6 and Figure 6-7, the measuring instrumentation are mounted on a fixture 1m above the pool rim for all instrumentation, expect for wind measuring instruments that are placed on a mounting 2 meters above the pool. The weather instruments horizontal position is intentionally shifted to avoid breakage of the instruments when maneuvering the shield and reduce the effect of physical obstacles on their outputs. The horizontal distance from the right corner of the pool and weather measuring instrument is approximately 0.5 meters for humidity and solar intensity measurements and 4 meters for the wind measuring devices.

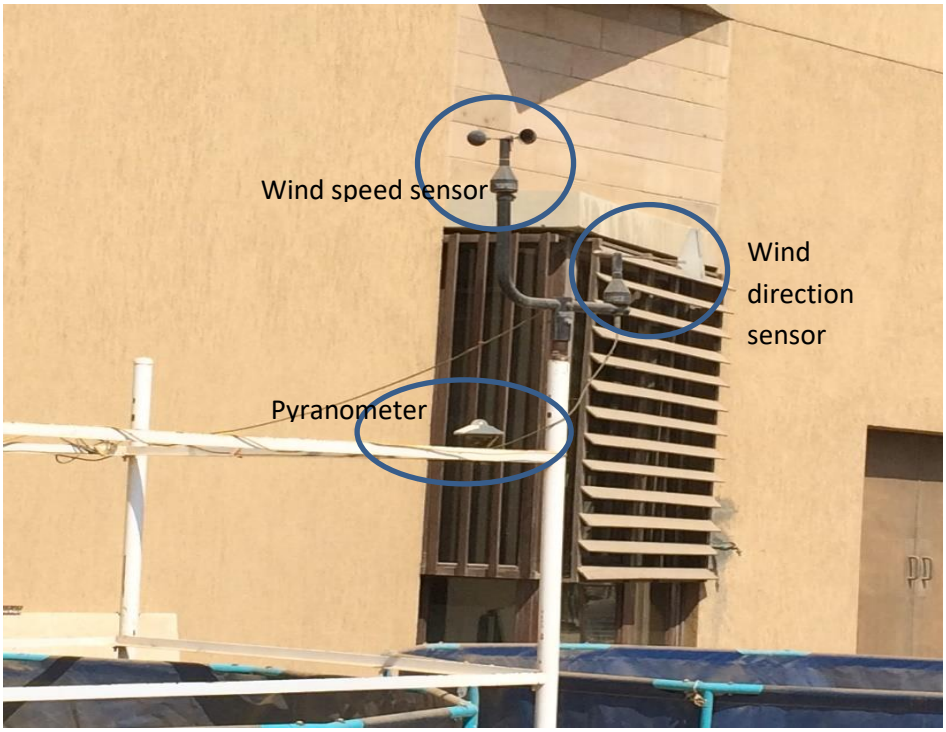

Figure 6-6: Weather Station Instrumentation (wind speed and direction sensors and pyrometer)

A pyrometer, model CMP10 and manufactured by KIPP & ZONEN (kipp & zonen 2017), was used to measure solar radiation. The pyrometer specifications are depicted in Table 6-1. A photographic view of the pyrometer is shown in Figure 6-7.

Table 6-1: Pyrometer specifications

Sensitivity	8.52 µV/W/m^2
Expected daily accuracy	± 2%
Operation temperature	-40 to 80°C
Maximum irradiance	4000 W/m^2
Dimension	Ø150 mm, Height approx. 68 mm

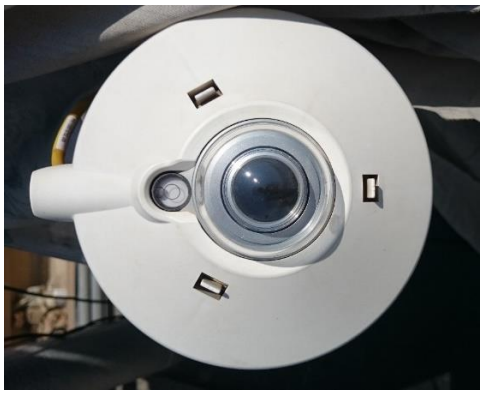

Figure 6-7: A photographic view of the pyrometer

The ambient temperature sensor in shelter, type 3032 and manufactured by Theodor Friedrichs (Theodor Friedrichs n.d.), was used to measure the ambient dry bulb temperature. The sensor specifications are presented in Table 6-2. A photographic view of the ambient temperature sensor is shown in Figure 6-8.

Table 6-2: Ambient temperature sensor specifications

Output	Measuring resistance PT 100
Accuracy at 23°C	+0.2 K
Temp. influence TK	<0.005% K
Operation temperature	-40 to 85°C
Dimension	Ø130 mm, Height approx. 185 mm
Weight	Approx. 780g

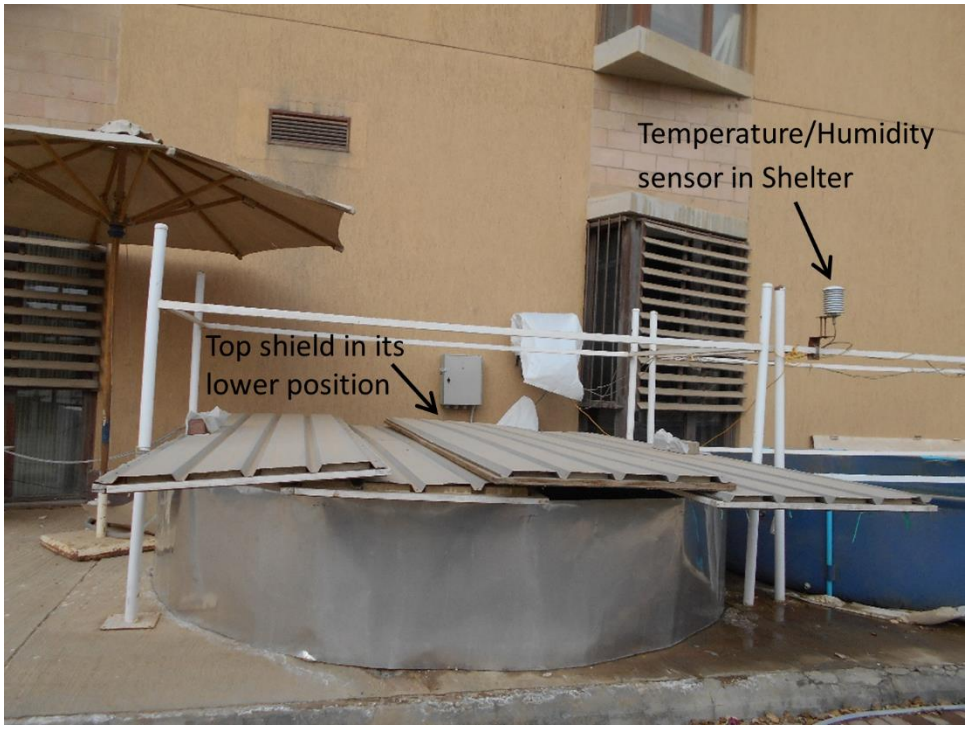

Figure 6-8: A photographic view of the ambient temperature and humidity sensor

A wind speed sensor, type 4035 and manufactured by Theodor Friedrichs (Theodor Friedrichs n.d.), was used to measure wind speed. The sensor specifications are presented in Table 6-3. A photographic view of the wind speed sensor is shown in Figure 6-9.

Table 6-3: Wind speed sensor specifications

Measuring range	0 to 70 m/s
Max. load	100 m/s
Accuracy at 15 m/s	±0.2 m/s
Operation temperature	-25 to 80°C
Dimension	Ø224 mm, Height approx. 275 mm
Weight	Approx. 685g

A wind direction sensor, type 4123 and manufactured by Theodor Friedrichs (Theodor Friedrichs n.d.), was used to determine wind directions. The sensor specifications are presented in Table 6-4. A photographic view of the wind direction sensor is shown in Figure 6-9.

Table 6-4: Wind direction sensor specifications

Measuring range	360°
Max. load	100 m/s
Accuracy	±0.3°
Operation temperature	-25 to 80°C
Dimension	Ø350 mm, Height approx. 370 mm
Weight	Approx. 1015g

Figure 6-9: A photographic view of the wind speed and direction sensors

A data logger, model COMBILOG 1022 and manufactured by Theodor Friedrichs(Theodor Friedrichs 2011), was used to collect data weather data from the solar radiation sensor, wind speed sensor, and wind direction sensor. It has a compact design integrated with LC-display and memory slot. A photographic view of the weather data logger is shown in Figure 6-10. The data logger is developed for the meteorological measurements purpose. The data logger records the data every minute.

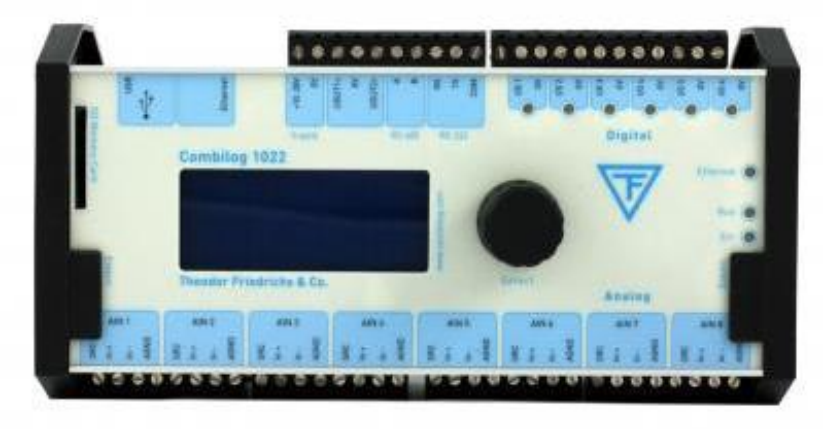

Figure 6-10: A photographic view of the weather data logger

Finally, a handheld hotwire, model AVM430 and manufactured by TSI Alnor(TSI Alnor 2014), was used to measure the wind speed near the pool surface. A photographic view of the hotwire is shown in Figure 6-11.

Figure 6-11: A photographic view of the handheld hotwire

6.3: Experimental Steps:

Several experimental runs were performed of different duration in order to gather data on the pool temperature response under the combined field effect of different weather, shielding and loading conditions.

1. The first set of runs (April to June2017) were done without placing the aluminum foil around the pool or installing the water electric heater, to test the system and for comparison with mathematical model results of various shield positions.
2. The test runs showed that the heating of the walls of the pool by beam radiation will increase the temperature of the pool, therefore a thin aluminum foil was wrapped around the pool.
3. A 4.8 kW heater was installed on wooden fixtures inside the pool to heat the water resembling the heat load of engineering systems to be cooled.
4. The pool was filled with fresh water at the start of every run. The maximum level was around 68.5 centimeter in the middle of the pool, after which water starts to spill from one side of the pool due to a slight ground inclination (on which the pool was installed). This would be 69 centimeters at the left inside corner (next to the wall) and 67 cm on the outside right corner. The pool level was not replenished during the run, instead, depth was measured, at the start, end and during the run to monitor the level.
5. A second set of runs were done both to test the cooling effect of the deferred cooling system after installing the heater and again for comparison purposes with theoretical model that would be used to optimize the system under the different running scenarios.
6. During the shield down run, the wind under the shield was measured manually from time to time to validate the assumption made in the model for the percent of wind that pool would feel under the shield as a result of the unintended relatively small air gap between the pool and the shield as shown in Figure 6-11.

6.4: Project Runs:

Listed below are the runs done during the experiment. These runs are divided into 4 cases, the first three are performed to analyze the effect of shielding the pool in both positions and for comparison purposes with the numerical model. These cases are named with relevance to the existence and the position of the shield during the whole duration of the run, being," no shield ", "Shield down" and "shield up ".

The fourth case was to test the ability of the DCS to absorb the 4.8 kW heat load, even when used at AUC campus in New Cairo (30.02 ° N latitude, 31.5 ° E longitude) which is not a typical desert like climate.

Table 6-5: Project runs

Case/Run	Date	Heater	Shield Position
No shield –Run2	19-26 April 17	Not installed	No shield
No shield –Run4	9-22 May 17	Not installed	No shield
Shield down –Run 7	10-17 December 17	Off	Shield down/Al insulation
Shield down –Run 3	26 April-7 May 17	Not installed	Shield down/No Al Insulation around the pool
Shield up-Run 1	10-18 April 17 Cloudy/Rainy till 14th	Not installed	Shield Up/No Al Insulation around the pool
Shield up-Run 5	24 May-21 June 17	Not installed	Shield Up/No Al Insulation around the pool
Deferred Cooling System-Run 6	14-19 November 17	On-Around 9am to 5pm weekdays ONLY	Shield up-9 am to 5 pm Weekday No shield after 5pm or weekends

Chapter 7: Measurements and their Simulations Results and Discussion

This chapter presents the results of the experimental work conducted to demonstrate the application of the concept of the deferred cooling and to gain experience with practical implementation problems and limitations. Moreover, the experiments were also performed to assess the assumptions made in the model, and in particular to justify the pool lumped capacity treatment.

The chapter also presents the results of the theoretical model after making necessary adjustments to simulate the corresponding experimental conditions as close as possible. A comparison between the numerical results, from the adjusted model, and the experimental results are presented and discussed.

7.1: Model adjustments:

In the numerical model, ideal conditions are simulated in the shield upper position, which assume the shield to be effective enough to block all beam radiation and most diffuse radiation, which turned out not to be the case during the experimental runs.

Also, in the ideal shield lower position, it is assumed that the shield is flush with the rim of the pool thus completely covering the pool and blocking both solar radiation components. It also assumes that condensation and evaporation effects cancel out over the 24 hours, leaving just free convection effects in the enclosed space between the pool and shield. In actual experimental conditions, a gap of approximately 7 cm was present between the shield surface and pool rim, the inevitable presence of air leakage due to the existence of a physical gap between the pool and shield, cause the pool to be subjected to some of the diffuse radiation as well as evaporation and convection. These are accounted for in the adjusted model.

Since the adjustments are not an integral part of the intended model, details of the adjustments are discussed in Appendix B.

7.2: No shield (Runs 2 & 4):

For the no shield scenario two experimental runs were performed as summarized in Table 7-1.The duration of the first run was 7 days, whereas that of the second run was 14 days. Measurements were conducted and recorded throughout the 24 hours, with the aid of a data logger. The measured values are displayed along with the corresponding simulation.

Table 7-1:No shield runs

Case/Run	Date	Heater	Shield Position
Case 1-a: No shield –Run2	19-26 April 17	Not installed	No shield
Case 1-b: No shield –Run4	9-22 May 17	Not installed	No shield

7.2.1: Case 1-a: No shield and no heating :(19-26 April 2017):

Figure 7-1 (a, b & c) presents the experimental data along with the model results for the unshielded scenario, during the period April 19th-26th, 2017. In Figure 7-1-a, T_{bot} and T_{mid} display the measured water temperatures at the bottom and middle of the pool, respectively, while T_{raw} denotes the air temperature right above the pool surface and T_{ws} denotes the ambient air temperature measured by the weather station. Figure 7-1-b shows the weather data during the simulation period displaying the solar radiation in units of w/m^2 , humidity percent, wind speed in m/s and ambient air temperature in $°C$ as recorded by the weather station. Figure 7-1-c shows the predicted heat losses during the simulation period.Figure 7-1-a shows that the temperature of the pool is as high as that of the air during the daytime in days with high humidity where the dry-bulb temperature would be close to the wet-bulb temperature. However, on days with low humidity the water temperature reached temperatures that are ten degrees cooler than air, moreover both water and ambient air temperatures peaked at much closer times in the afternoon (around 3 pm) during the day and reached minimum temperature with a much closer shift during the night (air before sunrise and water in the early morning hours after sunrise). There is around two to three hours lag between minimum and maximum temperatures achieved by water as compared to air, likely to be caused by the large thermal inertia of the water.

The experimental results presented in Figure 7-1-a confirm the validity of the lumped capacity assumption made in the simulation model since the temperature at the bottom and middle of the pool are almost coinciding with less than 0.5$°C$ shift (less than the specified tolerance of the thermocouples used).This is attributed to the influence of strong natural convection currents within the pool.Figure 7-1-c displays the thermal losses for the run, showing the magnitude of solar gain during the day to be overshadowing other losses due to the absence of the shield during the run. On the other hand, the figure shows that evaporation is the biggest thermal loss, followed by long wave radiation then night time convection, which is specific for this site weather data.

Finally, on comparing the numerical predictions to the experimental measurements, Figure 7-1-a shows that the predictions for the pool temperature followed closely the same trend as the experimental measurements, albeit with occasional shifts in time, possibly due to the unaccounted-for thermal inertia effects.

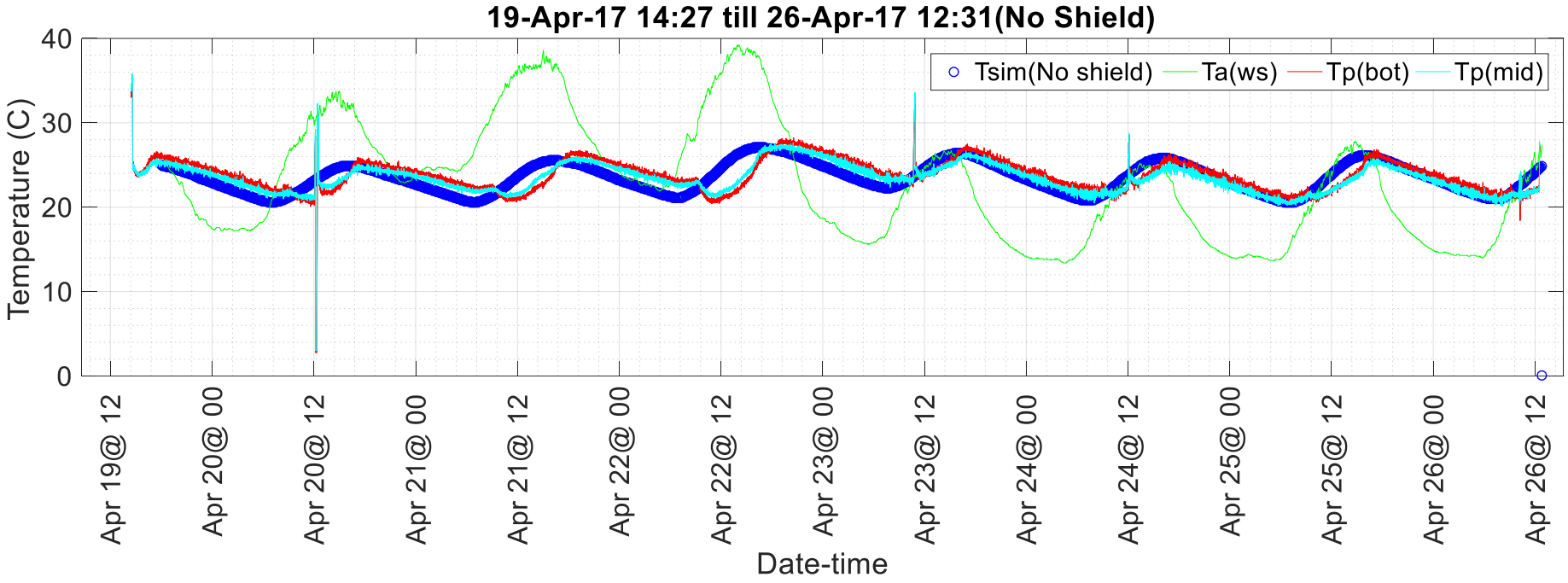
19-Apr-17 14:27 till 26-Apr-17 12:31(No Shield)
Tsim(No shield)
Ta(ws)
Tp(bot)
Tp(mid)
Temperature (C)
0
10
20
30
40
Apr 19@ 12
Apr 20@ 00
Apr 20@ 12
Apr 21@ 00
Apr 21@ 12
Apr 22@ 00
Apr 22@ 12
Apr 23@ 00
Apr 23@ 12
Apr 24@ 00
Apr 24@ 12
Apr 25@ 00
Apr 25@ 12
Apr 26@ 00
Apr 26@ 12
Date-time

Figure 7-1(a)

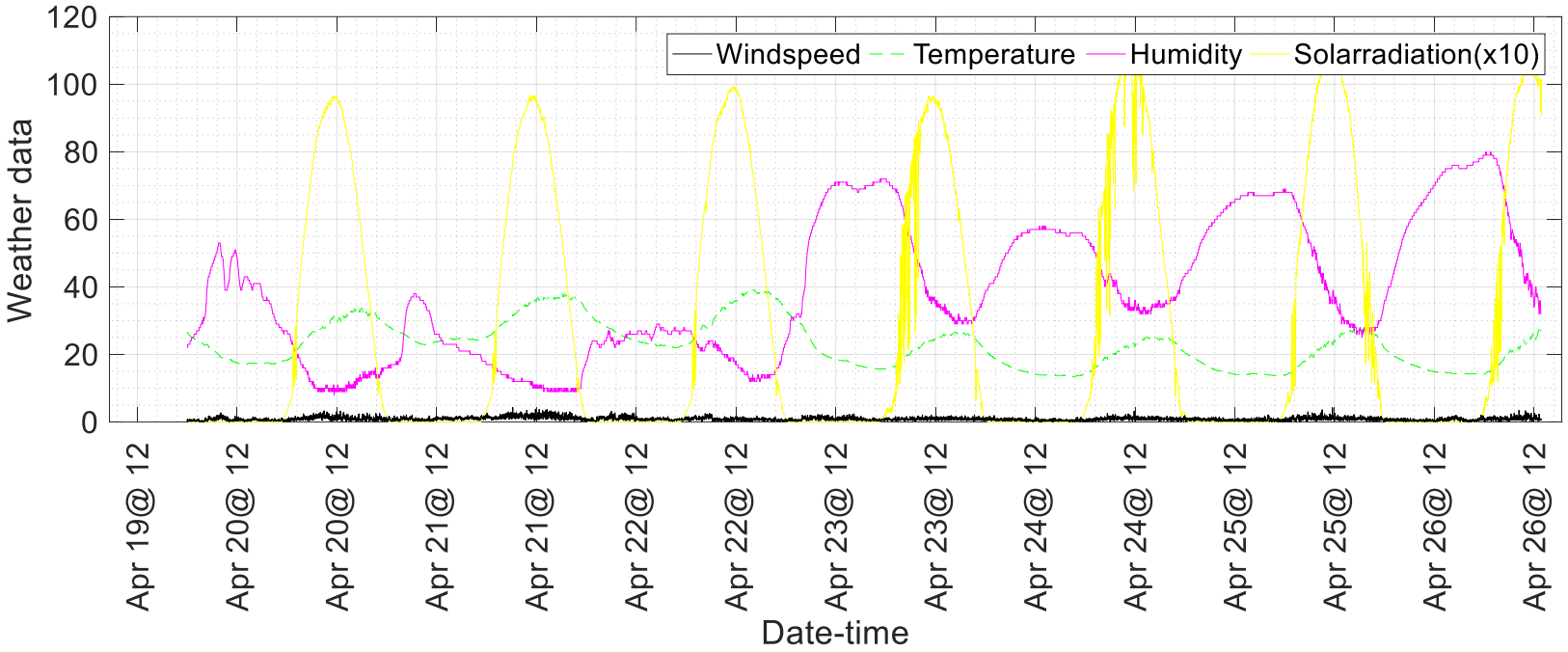
Windspeed
Temperature
Humidity
Solarradiation(x10)
Weather data
120
100
80
60
40
20
0
Apr 19@ 12
Apr 20@ 12
Apr 20@ 12
Apr 21@ 12
Apr 21@ 12
Apr 22@ 12
Apr 22@ 12
Apr 23@ 12
Apr 23@ 12
Apr 24@ 12
Apr 24@ 12
Apr 25@ 12
Apr 25@ 12
Apr 26@ 12
Apr 26@ 12
Date-time

Figure 7-1 (b)

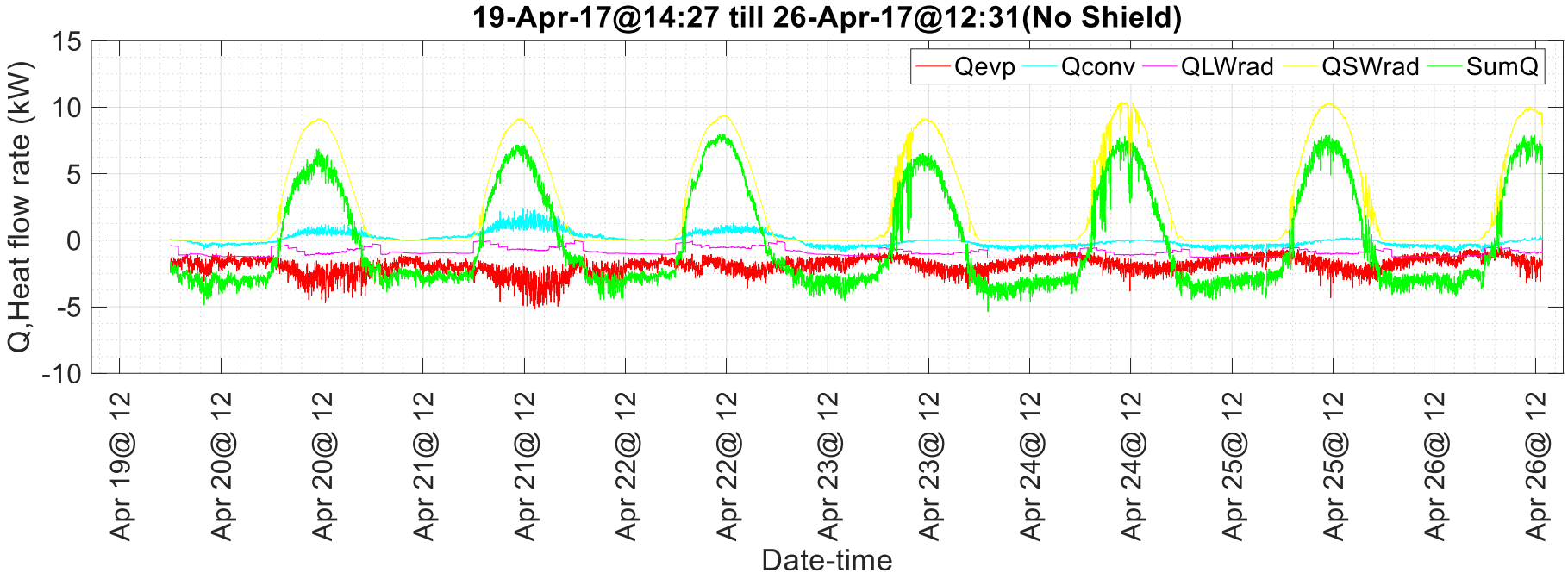

Figure 7-1 (c)

Figure 7-1: Modeling of "No Shield" position versus actual experimental results for the 19th to the 26th of April 2017.

7.2.2: Case1-b: No shield (9-22 May 2017):

Figure 7-2-a presents the experimental data along with the model results for the unshielded scenario, during the period May 9th-22nd, 2017. Similarly, Figure 7-2 confirms the above discussion regarding the peak and minimum temperatures of the pool as compared to ambient air. It worth mentioning that during this run the humidity sensor failed and a constant value of 33% was fed to the numerical model, which had a strong effect on the estimated evaporative cooling.

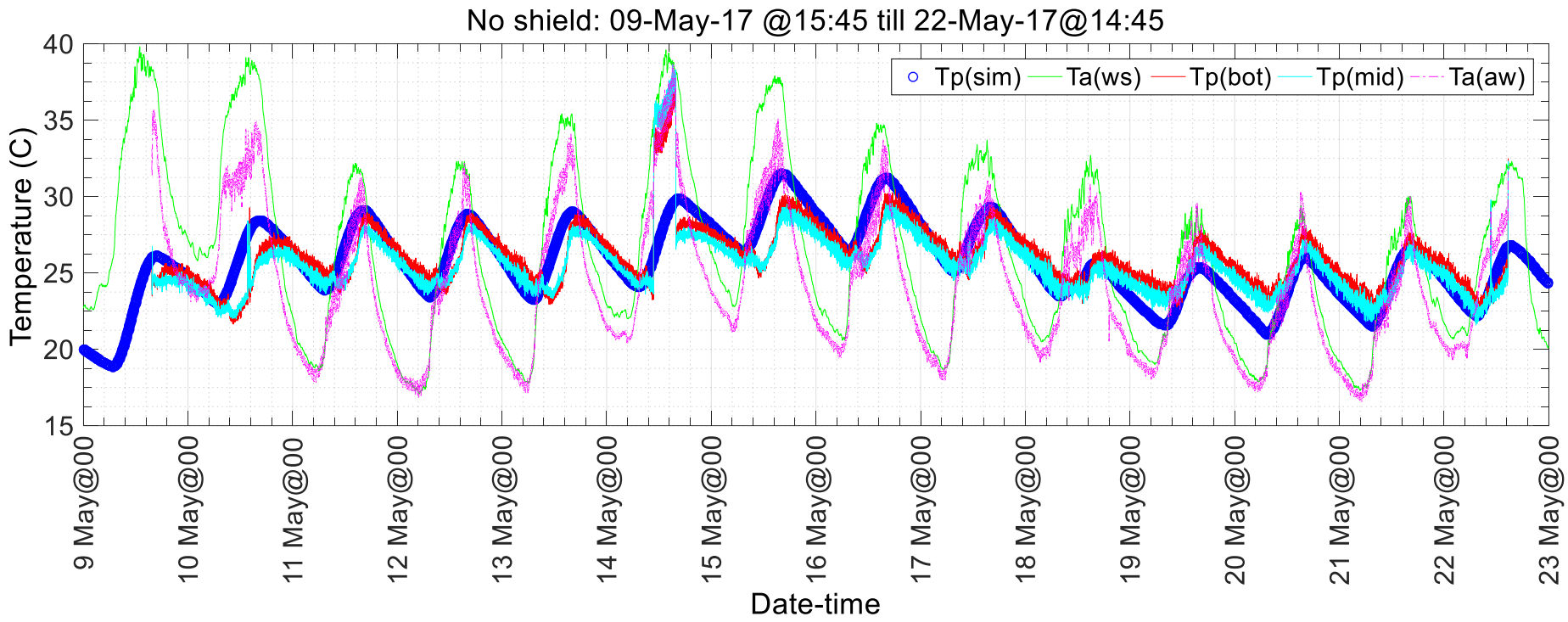
No shield: 09-May-17 @15:45 till 22-May-17@14:45
Tp(sim)
Ta(ws)
Tp(bot)
Tp(mid)
Ta(aw)
Temperature (C)
40
35
30
25
20
15
9 May@00
10 May@00
11 May@00
12 May@00
13 May@00
14 May@00
15 May@00
16 May@00
17 May@00
18 May@00
19 May@00
20 May@00
21 May@00
22 May@00
23 May@00
Date-time
Figure 7-2 (a)

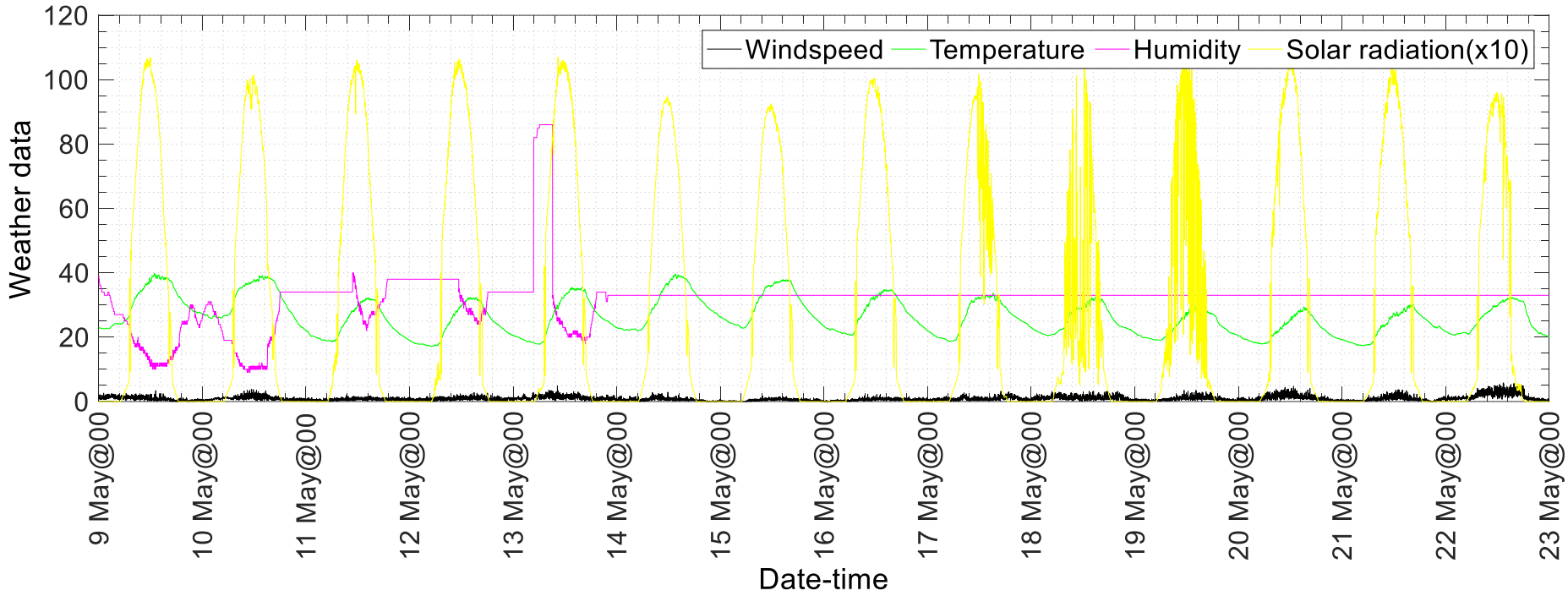

Figure 7-2 (b)

Figure 7-2: No shield Simulated versus actual (9-22May17) with weather data.

7.3: Shield upper position without heating:

For the shield in the upper position scenario two experimental runs were performed as summarized in Table 7-2.

Table 7-2: Shield up experimental runs

Case/Run	Date	Heater	Shield Position
Case 2-a: Shield up -Run 1	10-18 April 17 Cloudy/Rainy till 14th	Not installed	Shield Up/No Insulation around the pool
Case 2-b: Shield up -Run 5	24 May-21 June 17	Not installed	Shield Up/No Insulation around the pool

7.3.1: Case 2-a: Shield upper position (10-18 April 17):

Figure 7-3 presents the model results for the shield in the upper position scenario, along with the experimental data, during the period April 10th-18th, 2017. As shown in Figure 7-3, though the weather was cloudy and rainy during the run, the model was able to predict the general trend with reasonable accuracy for the shield upper position. The model was adjusted to allow for the entrance of a percent of the beam radiation in the pool as demonstrated in appendix B. The adjustment was based on the experimental run in November which would be slightly different in April as per Cairo's sun path diagram in the appendix B. A sensitivity check on the percent area of beam radiation entering the pool as well as the diffuse percent is reported in the last section of this chapter.

The bigger variation between the model prediction and the actual pool temperature is when the temperature is minimum around noon, which could be due to under prediction of evaporation with lower wind speeds (since the formula used is coupled to wind speed), over prediction of solar gain when reflecting the experimental solar gain entering part of the shielded pool during sun shine hours or simply due to the limitation of the Heun's method in predicting the slope of the function (employing trapezoidal rule).

Figure 7-3 displays the thermal losses calculated by the model, showing that the relative magnitude of solar gain for the shield upper position is much higher than radiation and convection losses during the night. Even the radiation and convection heat gain during the day are higher than the radiation and convection losses during the night.

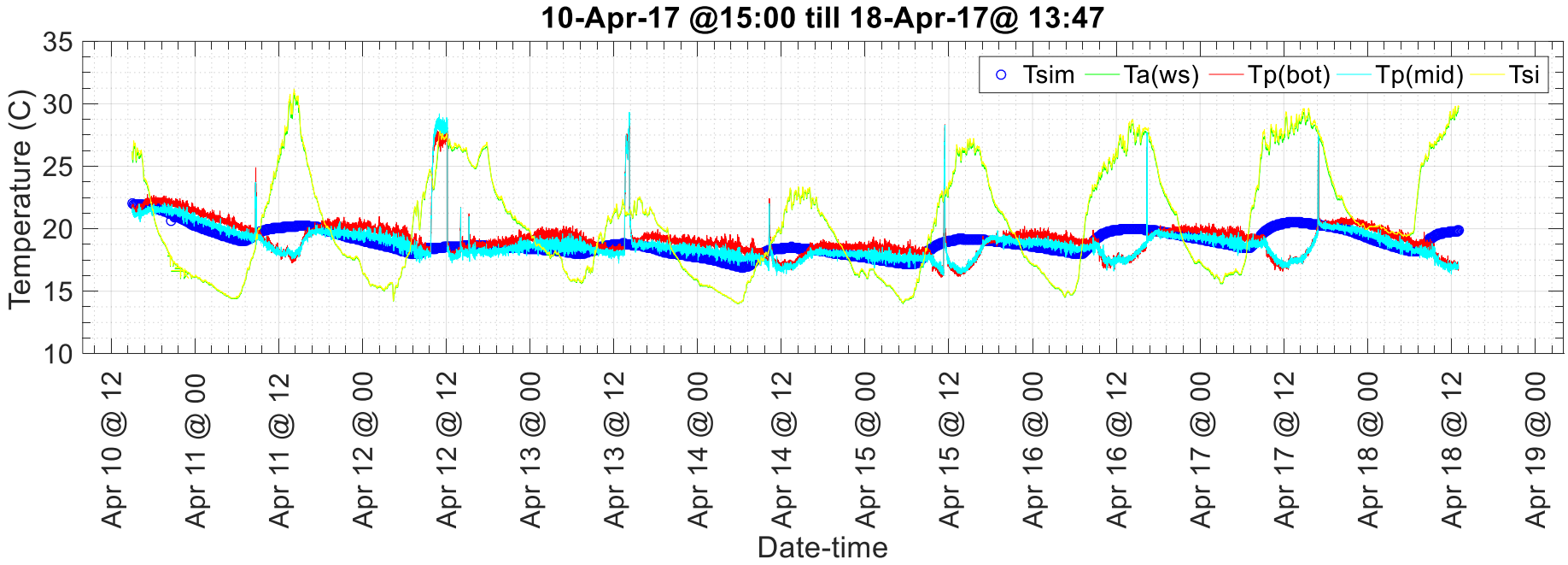
10-Apr-17 @15:00 till 18-Apr-17@ 13:47
Tsim
Ta(ws)
Tp(bot)
Tp(mid)
Tsi
Temperature (C)
35
30
25
20
15
10
Apr 10 @ 12
Apr 11 @ 00
Apr 11 @ 12
Apr 12 @ 00
Apr 12 @ 12
Apr 13 @ 00
Apr 13 @ 12
Apr 14 @ 00
Apr 14 @ 12
Apr 15 @ 00
Apr 15 @ 12
Apr 16 @ 00
Apr 16 @ 12
Apr 17 @ 00
Apr 17 @ 12
Apr 18 @ 00
Apr 18 @ 12
Apr 19 @ 00
Date-time

Figure 7-3 (a)

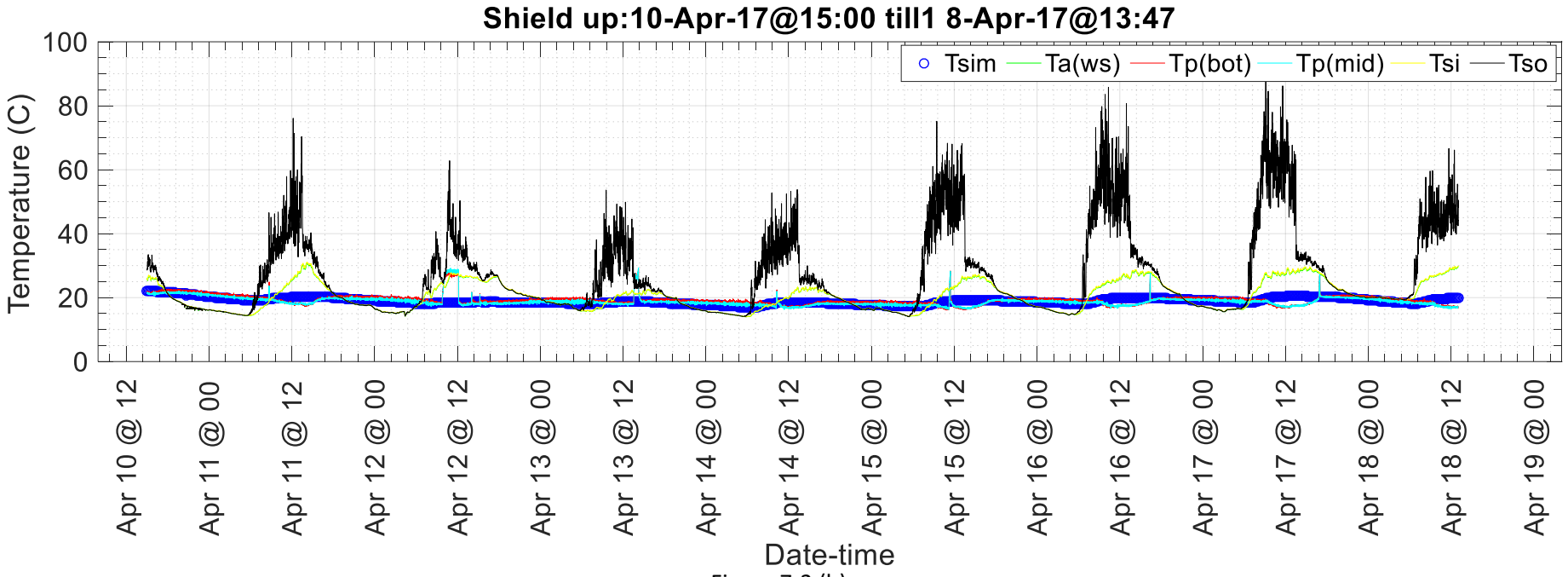
Shield up:10-Apr-17@15:00 till1 8-Apr-17@13:47
Tsim
Ta(ws)
Tp(bot)
Tp(mid)
Tsi
Tso
Temperature (C)
100
80
60
40
20
0
Apr 10 @ 12
Apr 11 @ 00
Apr 11 @ 12
Apr 12 @ 00
Apr 12 @ 12
Apr 13 @ 00
Apr 13 @ 12
Apr 14 @ 00
Apr 14 @ 12
Apr 15 @ 00
Apr 15 @ 12
Apr 16 @ 00
Apr 16 @ 12
Apr 17 @ 00
Apr 17 @ 12
Apr 18 @ 00
Apr 18 @ 12
Apr 19 @ 00
Date-time
Figure 7-3 (b)

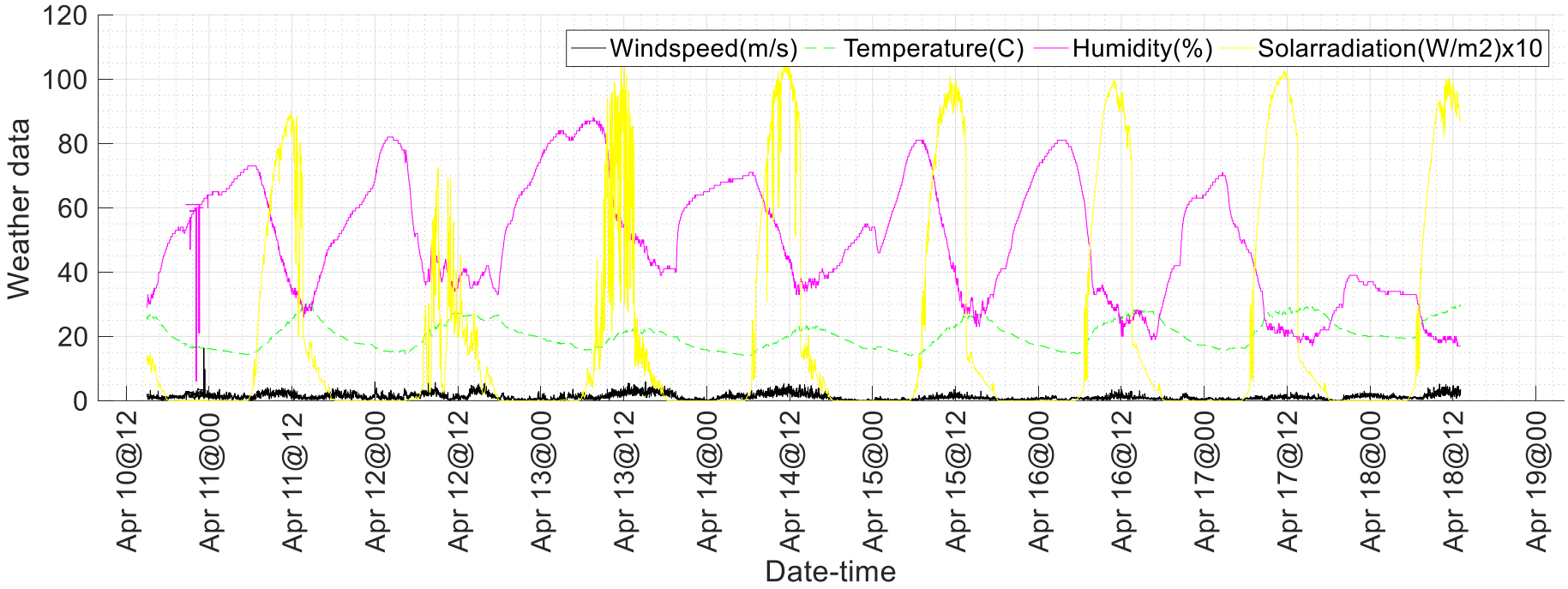
Windspeed(m/s)
Temperature(C)
Humidity(%)
Solarradiation(W/m2)x10
Weather data
120
100
80
60
40
20
0
Apr 10@12
Apr 11@00
Apr 11@12
Apr 12@00
Apr 12@12
Apr 13@00
Apr 13@12
Apr 14@00
Apr 14@12
Apr 15@00
Apr 15@12
Apr 16@00
Apr 16@12
Apr 17@00
Apr 17@12
Apr 18@00
Apr 18@12
Apr 19@00
Date-time

Figure 7-3 (c)

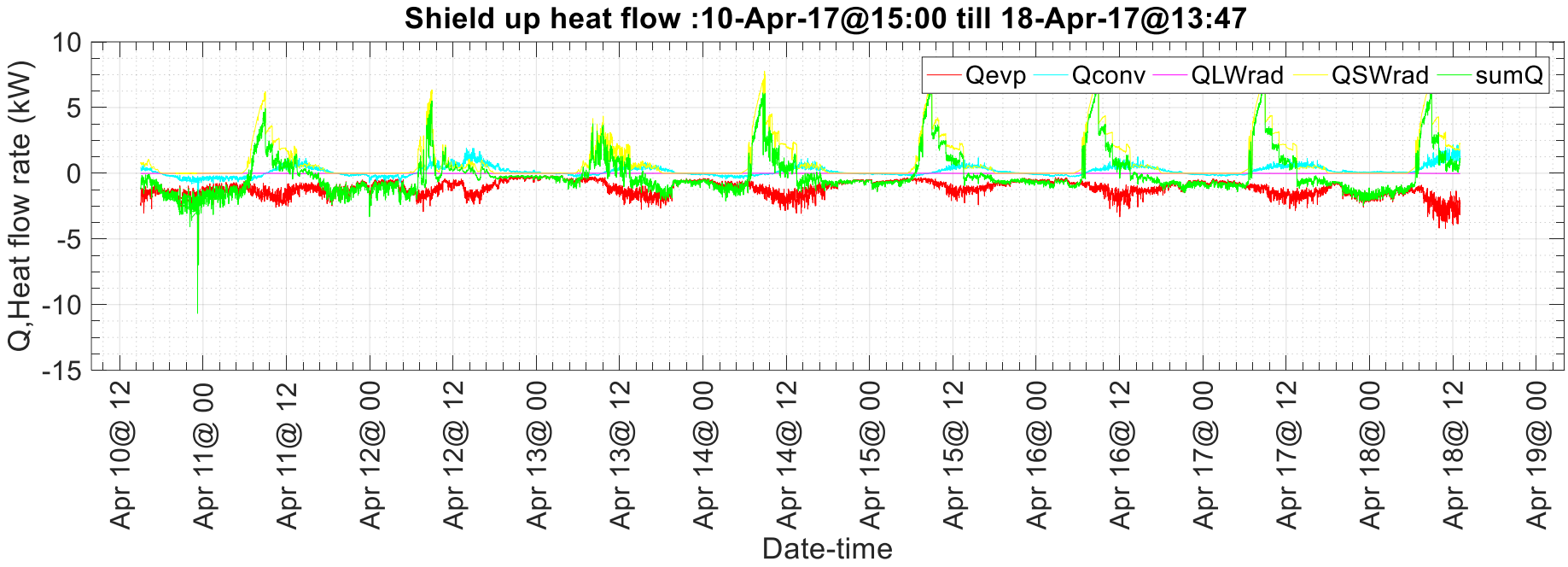

Figure 7-3 (d)

Figure 7-3: Shield up actual temperature versus simulated (10-18 April 17).

7.3.2: Case 2-b: Shield upper position (23May-21 June 17):

Figure 7-4 presents the experimental data during the period May 23rd till June 21st, 2017. The figure highlights the shift between the minimum temperature achieved by the pool and that of air. They had exactly opposite peaks during the whole month confirming the deferred nature of the cooling in the pool as compared to the air. The upper shield position scenario is able to reach a pool temperature cooler than the midnight coolest ambient air at times, but at a deferred phase.

Figure 7-5 and Figure 7-6 zoom on two days, the 7th and 8th of June and the 28th, 29th of May out of the whole run. The figure confirms the validity of the lumped capacity analysis, showing the almost identical temperature profiles at the pool middle and bottom. It also demonstrates the effect of closeness to water on the ambient temperature, reading lower as the sensor gets closer to the water surface, reflecting wet bulb temperature and confirming the sensitivity of the measuring instrumentation.

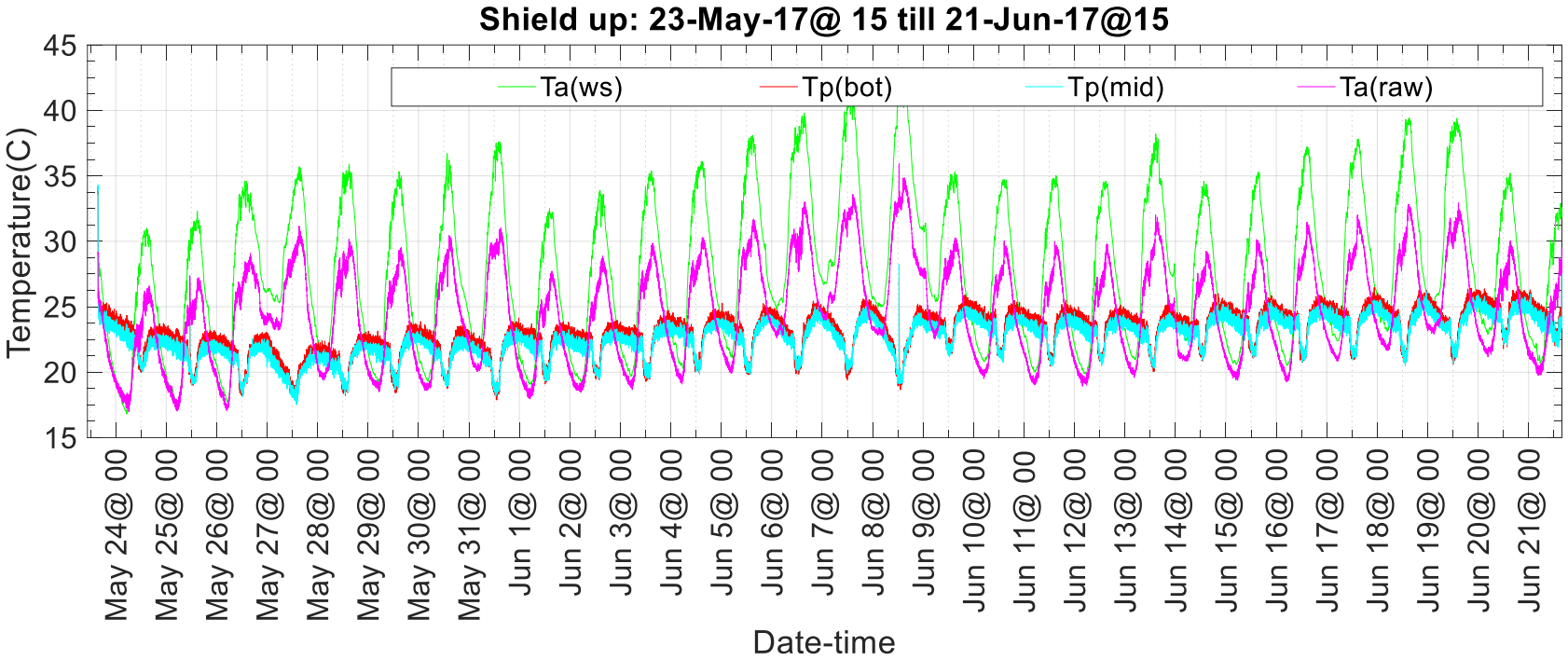

Figure 7-4: Pool and air actual temperature in shield upper position: (23 May-21 June, 2017)

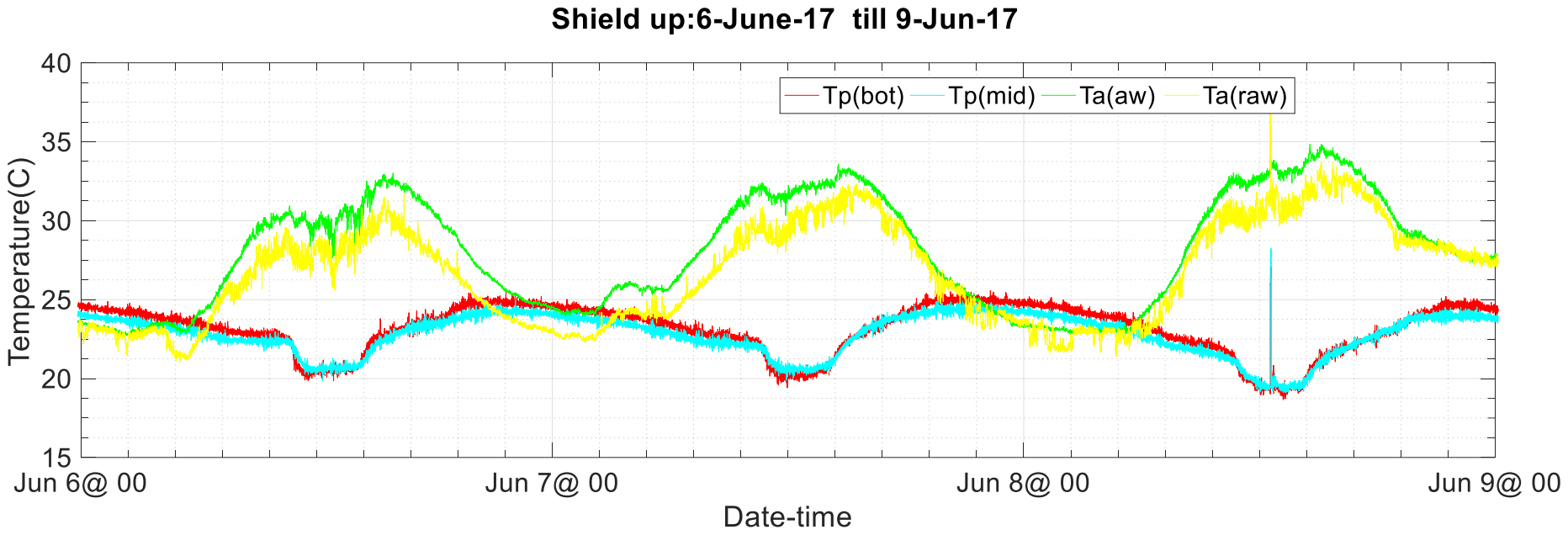

Figure 7-5:Air and water temperature for 6-9 June 2017

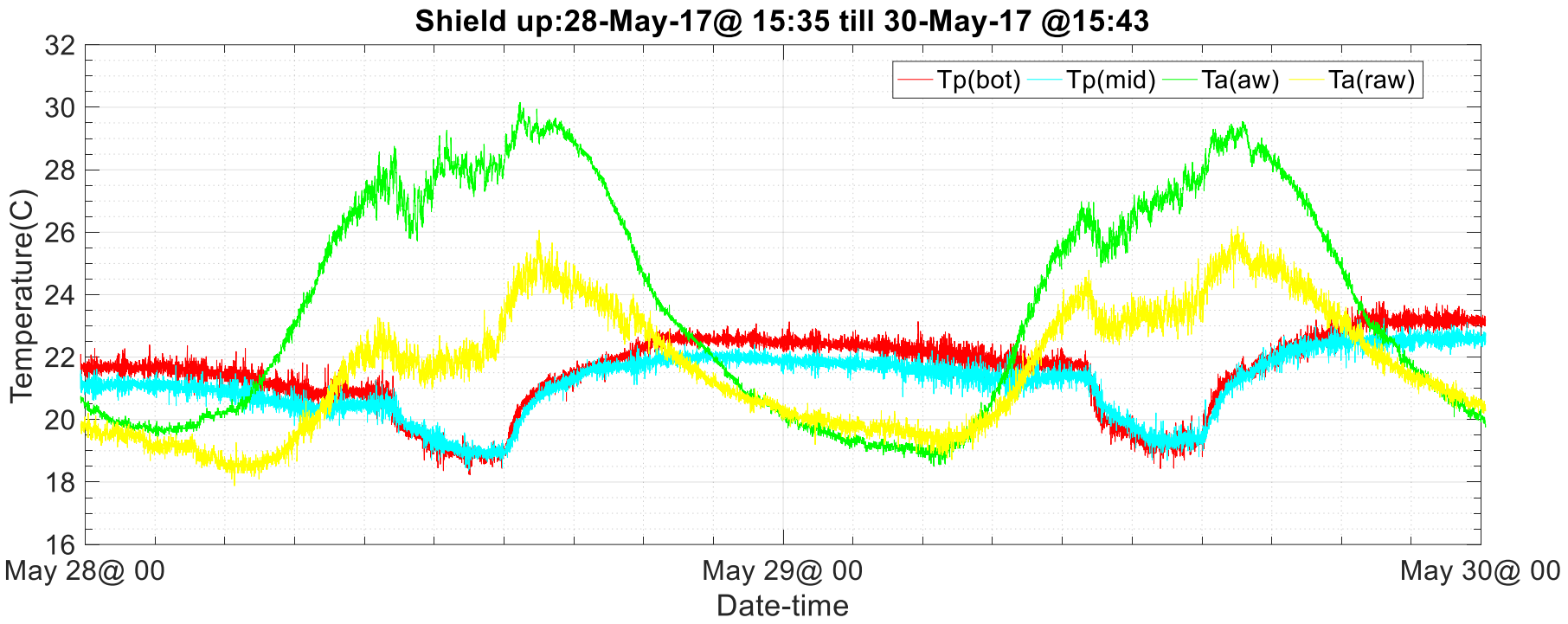

Figure 7-6:Air and water temperature for 28-30 May 2017

7.4: Shield lower position during day and overnight without heating:

For the shield in the lower position scenario, two experimental runs were performed as summarized in Table 7-3.

Table 7-3: Shield down experimental runs

Case/Run	Date	Heater	Shield Position
Case 3-a: Shield down –Run 3	26 April-7 May 17	Off	Shield down/No Insulation around the pool
Case 3-b: Shield down –Run 9	10-17 December 17	Off	Shield down

The following assumptions were used for this run in the model for the experimental shield down position:

i. The wind speed below the shield was assumed to be 20% of wind speed measured by the weather station in free weather stream 2 meters above the pool. The assumption was made based on sample measurements as indicated in appendix B.
ii. Zero % beam and 10 % diffuse radiation were assumed to be entering the pool when covered. Also, there was ground reflected radiation that made it in the small gap between the pool and cover which was taken care off in the long wave radiation model. This was evident when measuring the wind speed in the air gap between pool and cover since there was light in the area as seen from Figure 7-7 .

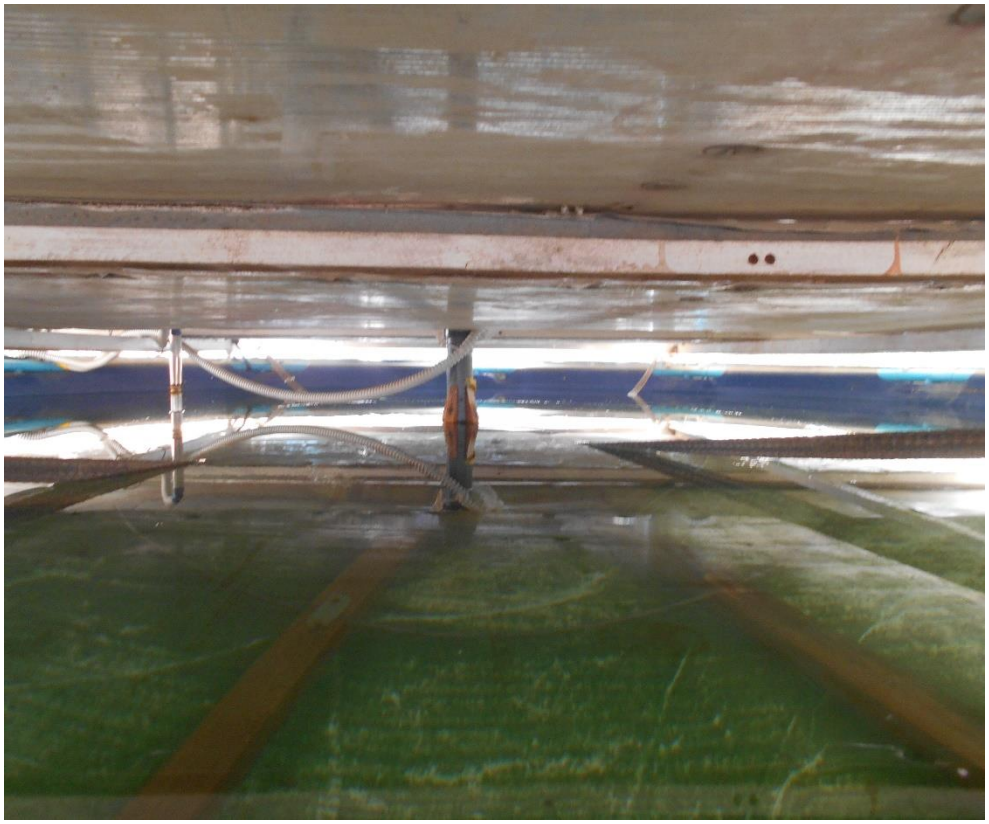

Figure 7-7: View for the pool from under the shield in its lower position

iii. A leakage in the pool was measured and reflected as 0.065 cm/ hour.

iv. Based on the material used in this experiment, emissivity of the shield inside was assumed to be 0.9, conductivity 0.25 $\frac{w}{m°C}$ with a measured thickness of 0.01 m. Emissivity and absorptivity of the shield outside surface were assumed to be 0.25.

Since these assumptions were done to accommodate the issues faced in manufacturing and installation of the field experiment (such as the air gap in the shield down position and the leakage in the pool), they will not affect the ideal model as they should not have been there in the DCS system to start with. They only represent a slight modification to the model for comparison purposes to the field experimental runs.

7.4.1: Case 3-a: Shield lower position (26 April-7 May 17):

As per Figure 7-8-a, the model was able to predict the average temperature of the water in the pool, missing the lowest temperature dips. The figure still shows that in the shield down position (through the day and night), the pool minimum temperature is achieved during the hottest part of the day at noon, with temperature difference greater than 10 degrees between air and water, confirming the concept of the deferred cooling system that aims at using the coolness achieved at night during the day.

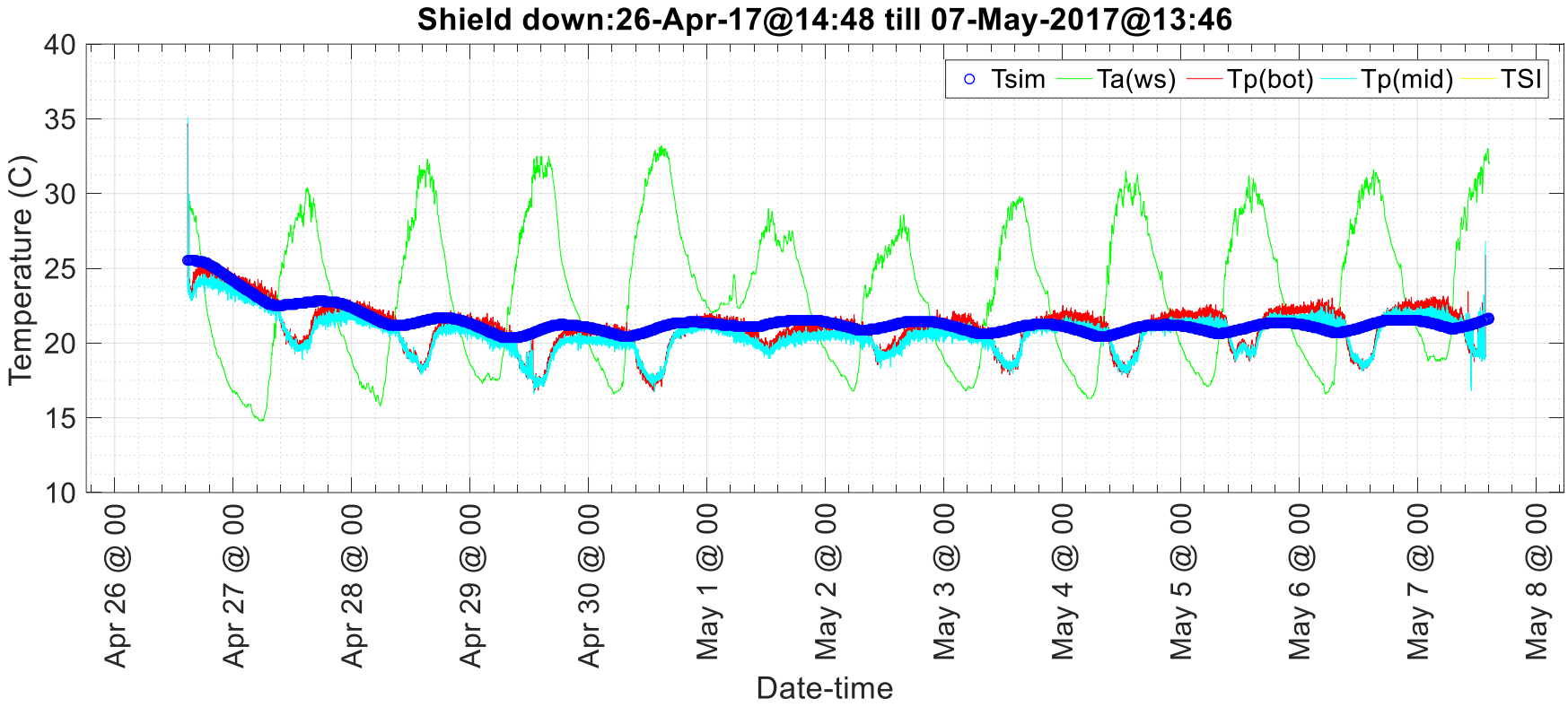
Shield down:26-Apr-17@14:48 till 07-May-2017@13:46
Tsim
Ta(ws)
Tp(bot)
Tp(mid)
TSI
Temperature (C)
40
35
30
25
20
15
10
Apr 26 @ 00
Apr 27 @ 00
Apr 28 @ 00
Apr 29 @ 00
Apr 30 @ 00
May 1 @ 00
May 2 @ 00
May 3 @ 00
May 4 @ 00
May 5 @ 00
May 6 @ 00
May 7 @ 00
May 8 @ 00
Date-time

Figure 7-8 (a)

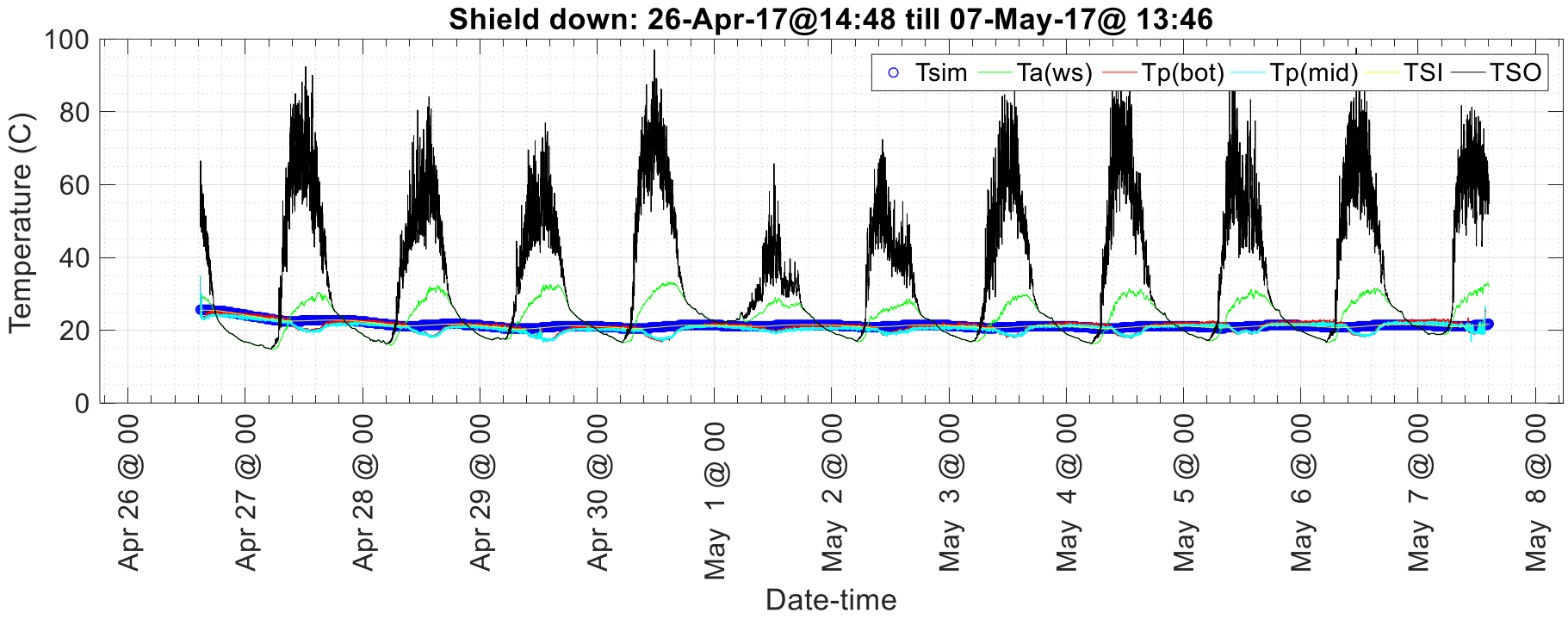
Shield down: 26-Apr-17@14:48 till 07-May-17@ 13:46
Tsim
Ta(ws)
Tp(bot)
Tp(mid)
TSI
TSO
Temperature (C)
100
80
60
40
20
0
Apr 26 @ 00
Apr 27 @ 00
Apr 28 @ 00
Apr 29 @ 00
Apr 30 @ 00
May 1 @ 00
May 2 @ 00
May 3 @ 00
May 4 @ 00
May 5 @ 00
May 6 @ 00
May 7 @ 00
May 8 @ 00
Date-time

Figure 7-8 (b)

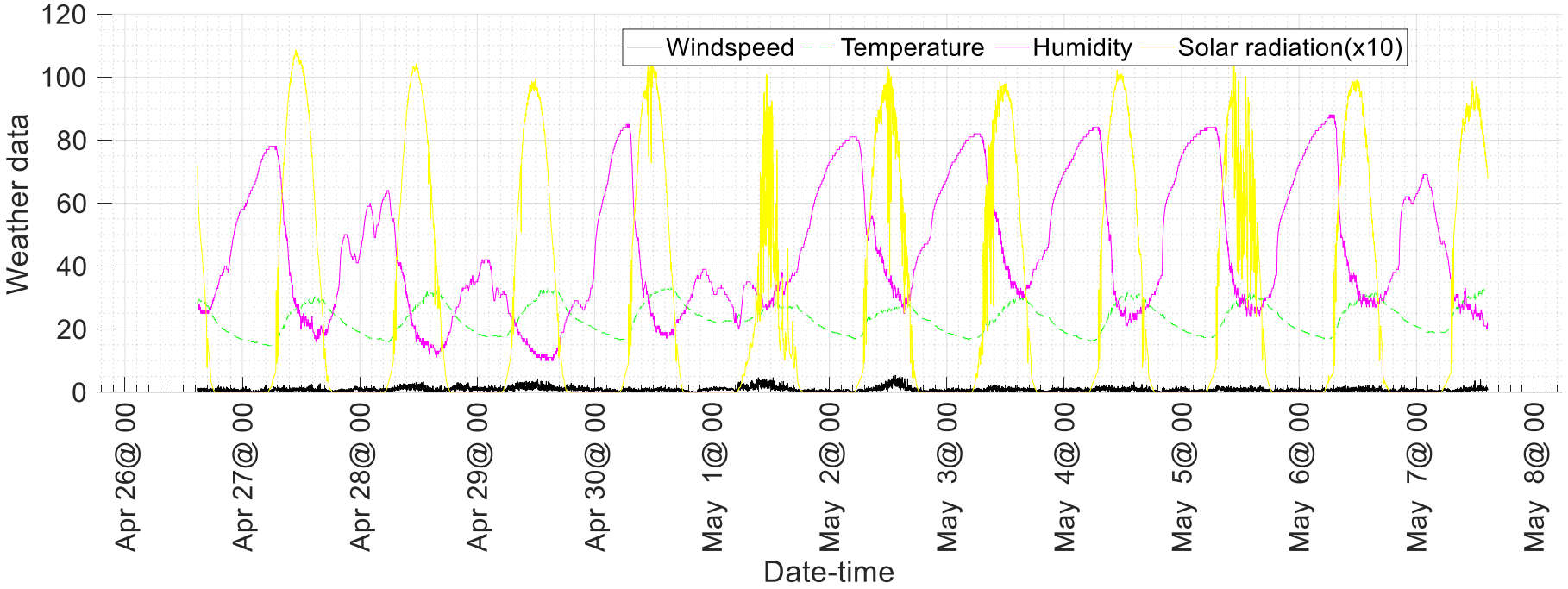
Windspeed
Temperature
Humidity
Solar radiation(x10)
Weather data
120
100
80
60
40
20
0
Apr 26@ 00
Apr 27@ 00
Apr 28@ 00
Apr 29@ 00
Apr 30@ 00
May 1@ 00
May 2@ 00
May 3@ 00
May 4@ 00
May 5@ 00
May 6@ 00
May 7@ 00
May 8@ 00
Date-time

Figure 7-8 (c)

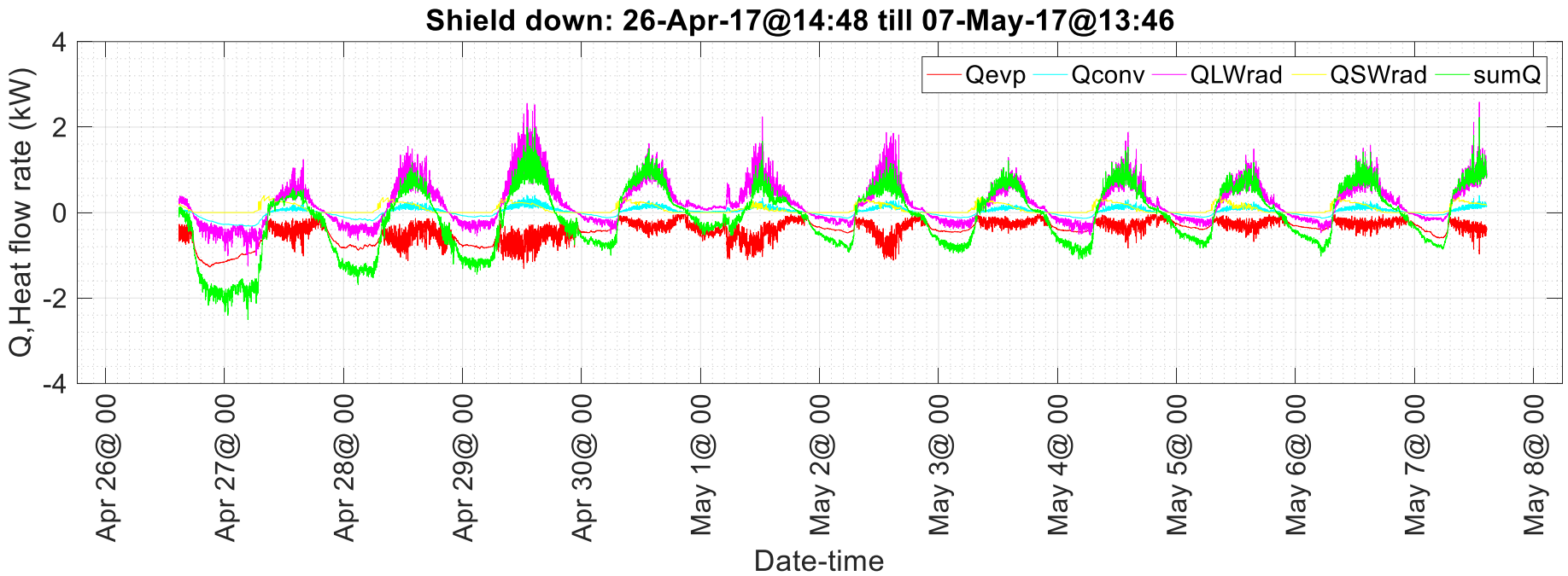

Figure 7-8 (d)

Figure 7-8: Shield down simulation vs. actual (3rd Run:26April-7May)

7.4.2: Case 3-b: Shield lower position (10-17 December 17):

This run was done to demonstrate the ability of the experimental shield down position model to predict the temperature trend in comparison with actual results after installing the heating system and the Aluminium sheets around the pool to insulate its wall from the incident solar radiation on it. The run was done for a week from the 10th till the 17th of December without heating.

As shown Figure 7-9, the experimental results for the “Shield Down” position show that at midnight, the ambient air temperature is less than the pool water temperature, which takes time to cool during the night to reach cooler temperature than the ambient air at a deferred stage during the day, around noon. For example, on the 16th of December at midnight, the pool temperature is about 4 °C higher than ambient air, while at noon, it is about 12 °C cooler. This is the general trend during the whole week, where the air and pool temperatures reach equilibrium in the early morning hours, around sunrise, then the pool temperature start decreasing reaching cooler temperatures in the afternoon (coolest right after midday) till around sunset. The ambient air and water have almost mirror images throughout the day, with different peak points.

So even with the shield down during the night, the water temperature was still preserving almost the same cool temperature that the air reached during the night with a deferred time shift that allow its use during the day. This was the case during the whole run with the temperature difference fluctuating according to the weather condition. This indicates the possible benefit of using the deferred cooling system versus air cooling in engineering applications. It is worth mentioning that in this run, the humidity was high during the night and lower during the day, permitting a larger water temperature drop during the day, as seen in Figure 7-9.

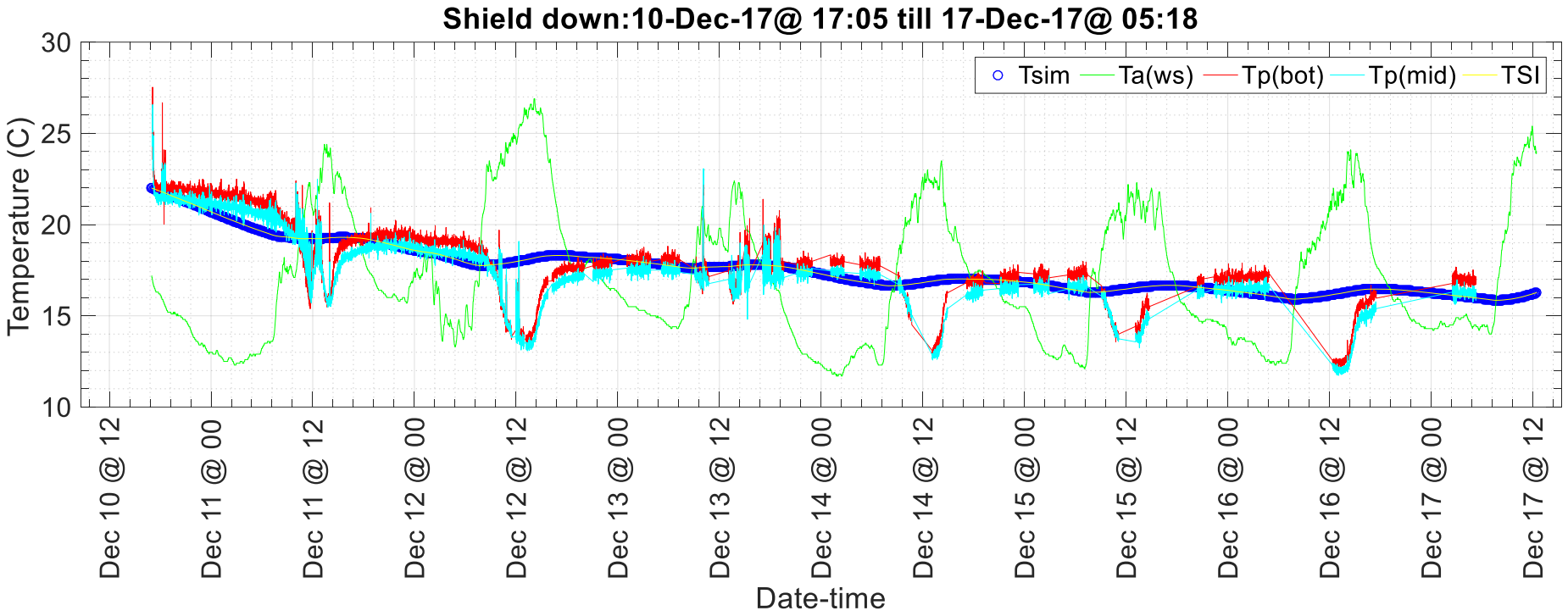
Shield down:10-Dec-17@ 17:05 till 17-Dec-17@ 05:18
Tsim
Ta(ws)
Tp(bot)
Tp(mid)
TSI
Temperature (C)
30
25
20
15
10
Dec 10 @ 12
Dec 11 @ 00
Dec 11 @ 12
Dec 12 @ 00
Dec 12 @ 12
Dec 13 @ 00
Dec 13 @ 12
Dec 14 @ 00
Dec 14 @ 12
Dec 15 @ 00
Dec 15 @ 12
Dec 16 @ 00
Dec 16 @ 12
Dec 17 @ 00
Dec 17 @ 12
Date-time

Figure 7-9 (a)

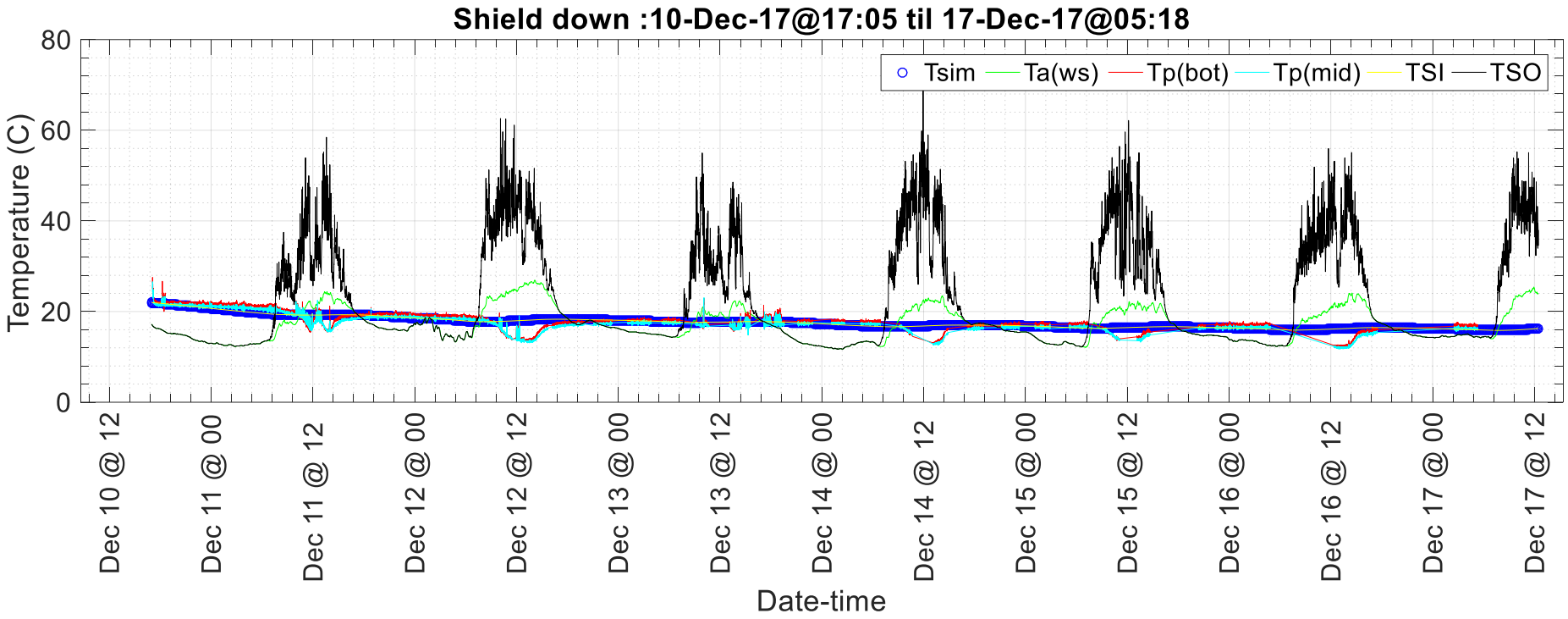
Shield down :10-Dec-17@17:05 til 17-Dec-17@05:18
Tsim
Ta(ws)
Tp(bot)
Tp(mid)
TSI
TSO
Temperature (C)
0
20
40
60
80
Dec 10 @ 12
Dec 11 @ 00
Dec 11 @ 12
Dec 12 @ 00
Dec 12 @ 12
Dec 13 @ 00
Dec 13 @ 12
Dec 14 @ 00
Dec 14 @ 12
Dec 15 @ 00
Dec 15 @ 12
Dec 16 @ 00
Dec 16 @ 12
Dec 17 @ 00
Dec 17 @ 12
Date-time

Figure 7-9 (b)

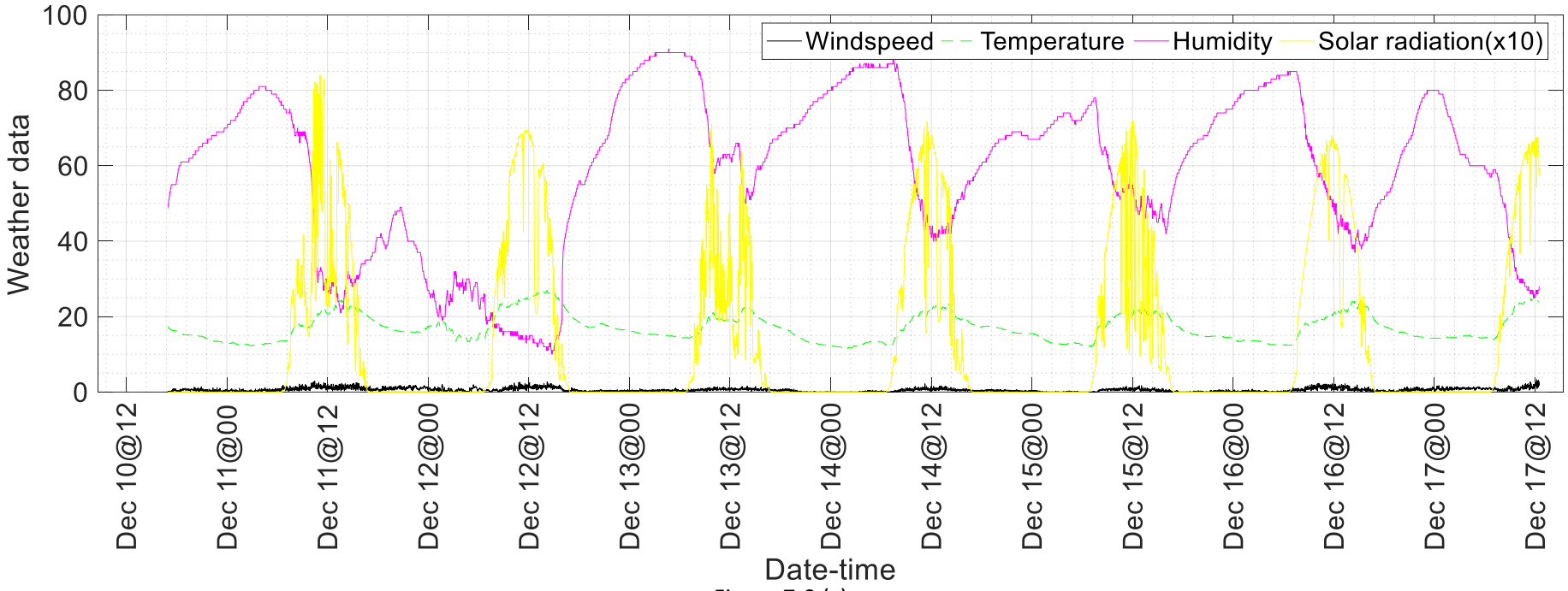
Windspeed
Temperature
Humidity
Solar radiation(x10)
Weather data
100
80
60
40
20
0
Dec 10@12
Dec 11@00
Dec 11@12
Dec 12@00
Dec 12@12
Dec 13@00
Dec 13@12
Dec 14@00
Dec 14@12
Dec 15@00
Dec 15@12
Dec 16@00
Dec 16@12
Dec 17@00
Dec 17@12
Date-time
Figure 7-9 (c)

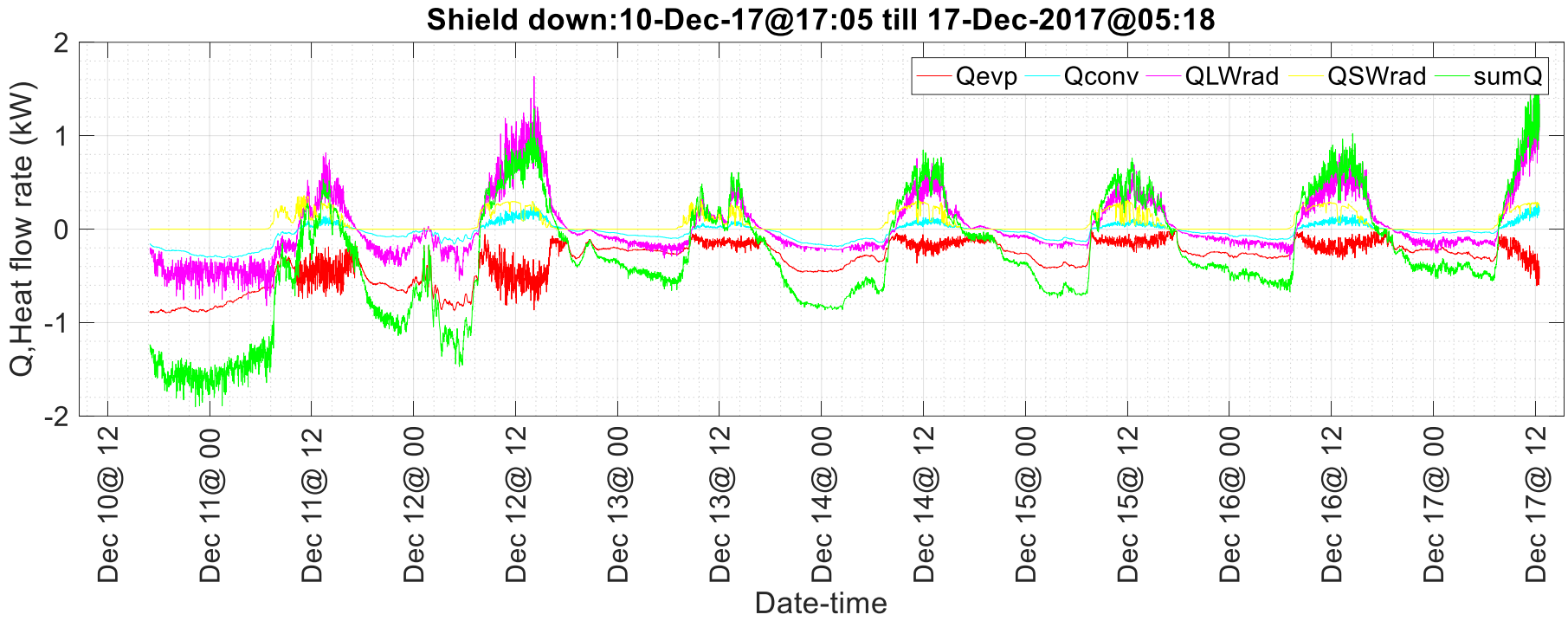

Figure 7-9 (d)

Figure 7-9: Modeling of cooling profile of the pool water with shield in the down position during day and night with aluminum insulation around pool and no heating.

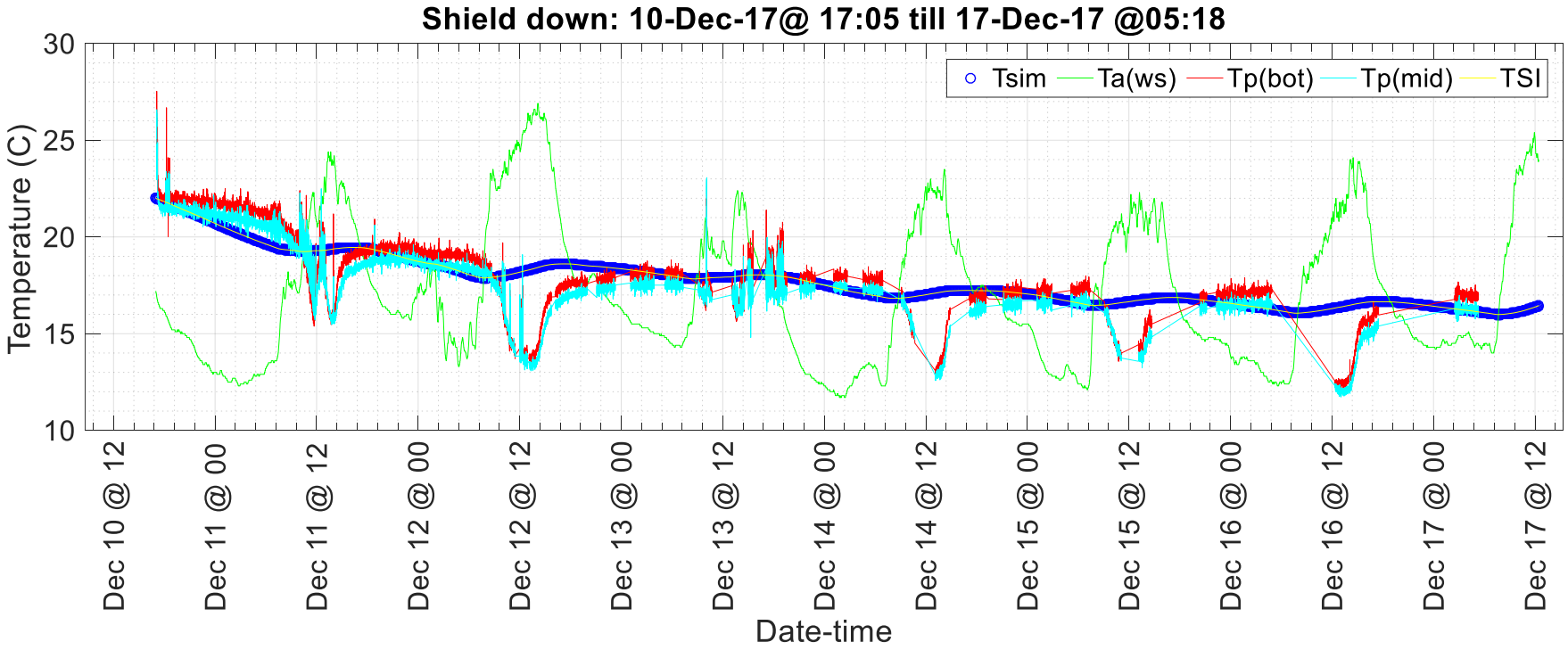

Figure 7-10: Modeling of experimental run of shield down position without heating versus actual (5% wind effect, 10% diffuse, zero beam and 0.07cm/depth leakage).

7.4.3: Discussion:

If the shield were not in the “shield down” position, increasing the beam and diffuse percent increases the temperature and will definitely change the peak positions to follow that of the solar radiation which is clearly not the case as per Figure 7-9 a-c that show the temperature of the pool tend to decrease as the humidity in the air decreases and wind speed increases (due to evaporation).It also shows that the peak pool temperatures are not following neither the peaks of solar radiation nor that of ambient temperatures.

Of course, increasing the wind speed % would lower the temperature, which is not the case in the “shield down “position since the shield tremendously reduces the amount of wind reaching the pool surface to be similar to indoor pools. The sensitivity of the model needs to be improved to reflect a larger effect of the humidity drop on the temperature drop, at this point, it is able to predict the average temperature in the pool without picking up the spikes of temperature drop during the night.

This could be mainly due to:

1) The fact that the model is a zero-dimensional model, while the input weather data boundary conditions are three dimensional and are measured 2 meters above the pool.

2) There is the possibility that the limiting criteria used to define the type of flow regime below the shield is not always matching the real-life situation, especially that the wind below the shield is taken as a percent of the free stream wind speed regardless of the speed or direction of the wind which is a simplification of the actual scenario.

   The model was aimed to be a simple model that would be able to use metrological weather data for any site to model the cooling of the water in the deferred cooling system without the need to measure the wind, humidity and temperature at specific locations, that is why the shield temperature was not measured and not taken as a direct input to the model.

For the shield down position run of the 10-17 December 2017, evaporation is the highest loss, followed by radiation then convection (gain during the day and loss at night). Sum of heat flow range from a loss of 2 Kw to a gain of 1.5 kW at noon.

7.5: Heater on:

After the installation of a 4.8 kW heater, an experimental run was done to demonstrate the DCS performance in the presence of a heat load.

7.5.1: Case 4: Deferred Cooling System: Shield up and heater on week days (9am to 5 pm), No shield or heating after 5 or on weekends:

Table 7-4: DCS experimental run

Case/Run	Date	Heater	Shield Position
Case 4: Deferred Cooling System-Run 6	14-19 November 17	On-Around 9am to 5pm weekdays ONLY	Shield up-9 am to 5 pm Weekday No shield after 5pm or weekends

Figure 7-11 demonstrates the increase of the daily cycle temperature of the pool by 4°C over a 3 days period when heated with the shield in the upper position during the day (14-17 November), while removing the shield and switching off the heater around sunset till 9am (for operational constraints), leaving the water to cool for around 16 hours. It is important to point out that though the water of the DCS did not absorb the full $4.8\ kW$ heat load, at the end of all of the three cooling cycles (at 9 am on the 16th , 17th and 18th),the water temperature was less than air , this is the point at which it would have been used for cooling. In other words, even though the water was heated, and air was not, the water absorbed most of the $4.8\ kW$ heat load and became cooler at the working hours of the day, when it needs to be used to cool. It is quite clear that when the pool is not heated, the temperature of the pool goes back where it started the day before (or even less) depending on the ambient temperature (18th to 19th of November).

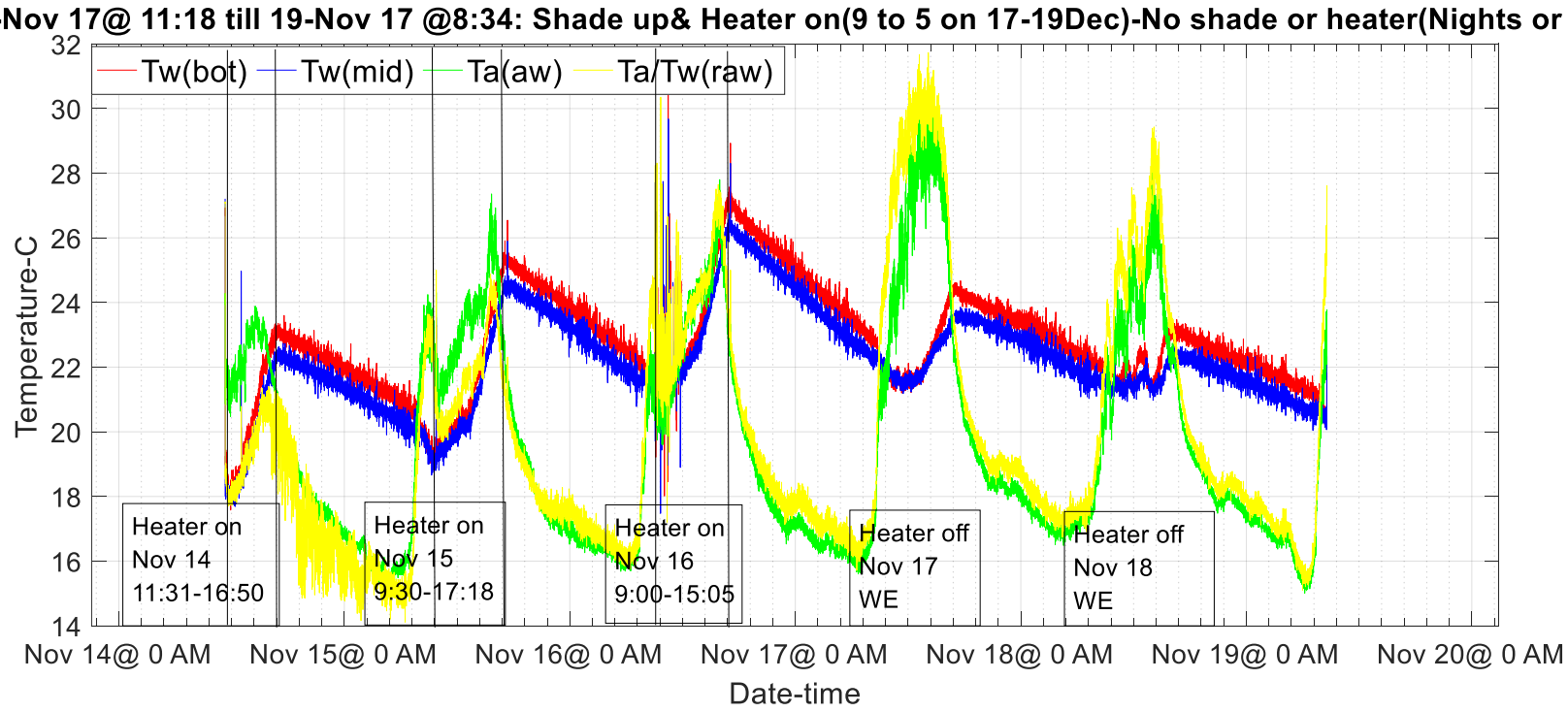

Figure 7-11: Heating and cooling profile of shield-up during day and no shield after sunset position with heater on during the day on week days and shield and heater off weekends.

Table 7-5: DCS run details

Day	Heater On	ΔT (heating) °C	ΔT (Cooling) °C	ΔT (Accumulated) Daily Cycle	Comment
14th -15th Nov:	11:20 am till 16:50 pm	5(18 to 23 °C) Q_{htg}=150.6 MJ (for 5.5 hours, average $\dot{Q}$ of 7.6 kW)	4(Down to 19) Q_{clg}=120.5 MJ (for 16.5 hours, 2.2 kW)	1	Q_{clg}=11.5 MJ/m^2 Additional $\dot{Q}$ of 2.8 kW to the heater 4.8 kW load mainly due to unwanted solar gain
15th -16th Nov:	9:30 am till 17:20 pm	6(19 to 25°C)	4(Down to 21)	2	
16th -17th Nov:	9:00 am till 17:05 pm	6(21 to 27°C)	5(Down to 22)	1	Cooling capacity 14 $\frac{MJ}{m^2.night}$ (A=10.5 m^2)
17th -18th Nov:	No Heating	2	2	0	
18th -19th Nov:	No Heating	1	3	-2	

7.5.2: Discussion:

The cooling capacity in 16 hours that the system was able to achieve was around 14 $\frac{MJ}{m^2.night}$, after being heated during the day for 8 hours with a heating capacity of 4.8 Kw. This cooling rate is calculated from the 5°C drop in temperature of the 10.5 m^2 of water in the pool at an average rate of 2.2kW.

The 4.8 Kw heating rate is equivalent to 17.28 $\frac{MJ}{hr}$ (138$\frac{MJ}{8hrs}$) of heating, which is also equivalent to almost 4.6 °C that the system could have easily absorbed if the thermal gain during the day was not there. The thermal gain was mainly due to the direct beam radiation gain that could have been almost eliminated by altering the shield design to block all beam radiation.

As can be seen form the above table, the maximum cooling achieved on the 3rd day was 14 $\frac{MJ}{m^2.night}$, which is equivalent to 147 $\frac{MJ}{night}$ for a 16 hours cooling period, more than the 138 $\frac{MJ}{8hrs}$ of heating produced by the 4.8 kW heater. If the pool would have been left to cool for the proposed 20 hours

period and a more effective shield was installed just after sunrise (not after 9 am) to avoid direct beam, the temperature of the pool would have been reduced even less .

As seen from Figure 7-11 , when the pool water is heated, it is still much cooler than the ambient temperature during the day though during the night it did not have enough time to cool down to reach ambient air temperature, so using it to cool the condenser cooling water during the day would still be better than using ambient air since they almost follow exactly the same temperature trends with a clear temperature gap in favour of water cooling from the pool, for this specific run. In order to improve the system performance, a second pool would be used as an intermediate storage to allow more time for the system to cool.

In the previous runs with the shield in the upper position without heating, it was noticed that the coolest temperature the pool reached was around noon. On the other hand, for this run since heating started around 9am, the pool did not have enough time to reach its coolest point (with the 16 hours cooling period), which would have been almost two degrees cooler (as seen from the days without heating) had heating started after a longer cooling cycle of 20 hours. This was due to working hours limitation during the experiment.

Figure 7-11 demonstrates the air temperature right above the pool, which is a lot less than those measured by the weather station as demonstrated in Figure 7-12.The figure also demonstrates that though the ambient air temperature was higher than the heated water, by three degrees at times. The coolest temperature of the pool is higher than those of the coolest temperature of the night by up to five degrees at times. This is not like the first two cases without heating in the “shield up “or “shield down” all the time, where the pool temperature came quite close to that of mid night temperature around noon, though the shield was on during the night creating a barrier to temperature loss to the cool night skies. Again, a transient pool would have allowed the temperature to go down more than it did while heating.

7.5.3: Model prediction for the pool performance versus actual results:

In Figure 7-12, the numerical model was used to estimate the performance of the deferred cooling system while ignoring side wall heat gain and losses, which was made possible after placing the Aluminum foil insulation around the pool.

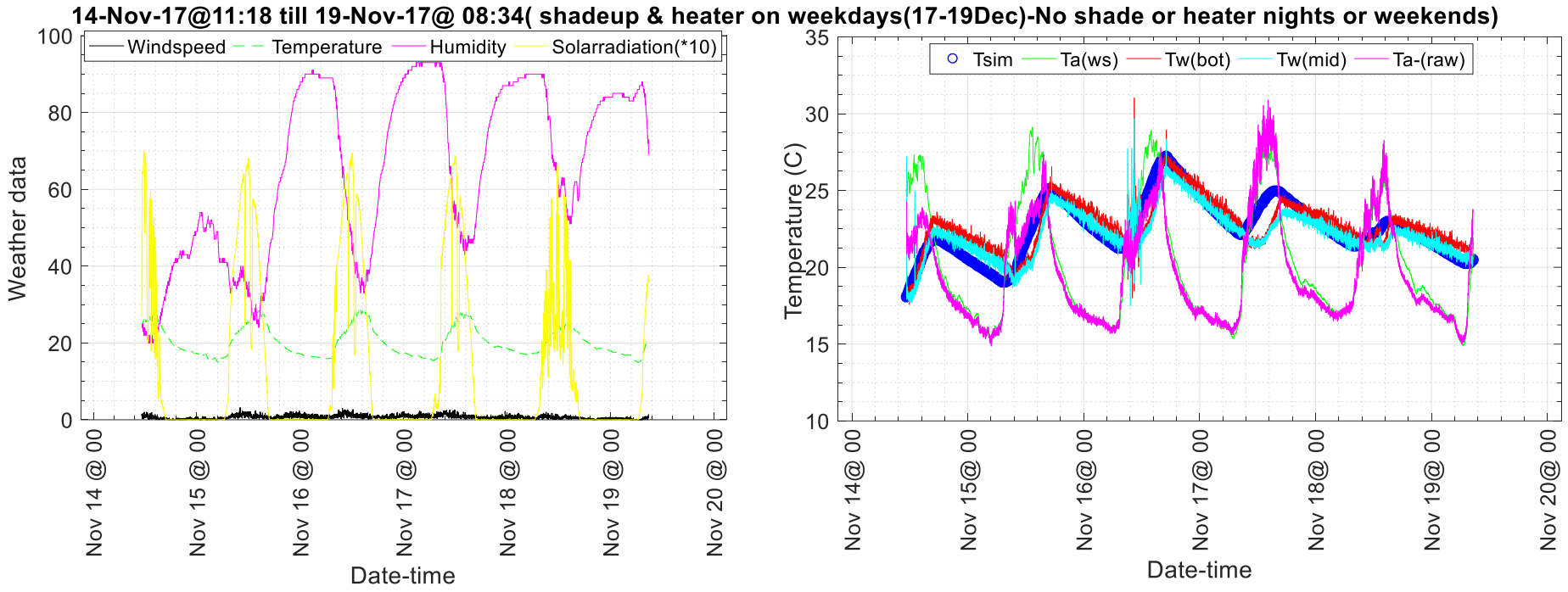

Figure 7-12: Simulation versus actual temperature profile for" shield up/ heater on" during the day

7.5.4: Model assumptions:

i. It was assumed in the model that heating and shield up started after 9 am and stopped before 5pm, though due to practicality, that was delayed or advanced on different days, which could have been reflected in the model, but results were good enough even while ignoring the slight time difference. For example, on the 14th of November the run log shows a 10 minutes advance in shutting off the heater and removing the shield as follows:

Table 7-6: Sample run log

Event	Time
Shield up	11:18
Start logger	11:18
Started heater	11:31
Heater off	16:50
Shield off	16:51

ii. Depth loss of 0.07cm/hour due to leakage

iii. 4.8 Kw heater as measured.

iv. % Area of sun image (Area used to calculate solar gain from beam radiation) was monitored during this run (November), plotted and reflected in the model using curve fitting as demonstrated in Appendix B. The same % A formula was used for modeling the other shield up experimental runs with a possibility to apply a "month correction factor "correction to be deduced from the sun path diagram (as per Appendix B). The images on which these areas were estimated are also shown in Appendix B.

As seen from Figure 7-13 for the thermal losses calculated by the model. The daytime solar gain when the shield was in the upper position on the first 3 days was around 3 kW and peaked at around 6 kW in the early and late hours of the day since the sun was too low that shield allowed all the beam radiation in. It is worth mentioning that 6 kW was the same peak of solar gain for the last two days of the run when the shield was not installed on the weekend, hence a more effective shield design is needed. A retractable, highly reflective shield with adjustable slots to allow the cool air currents to enter when opened, would avoid the cumbersome job of moving a heavy shield between upper and lower positions according to the ambient air temperature and would simply be pulled down during the night.

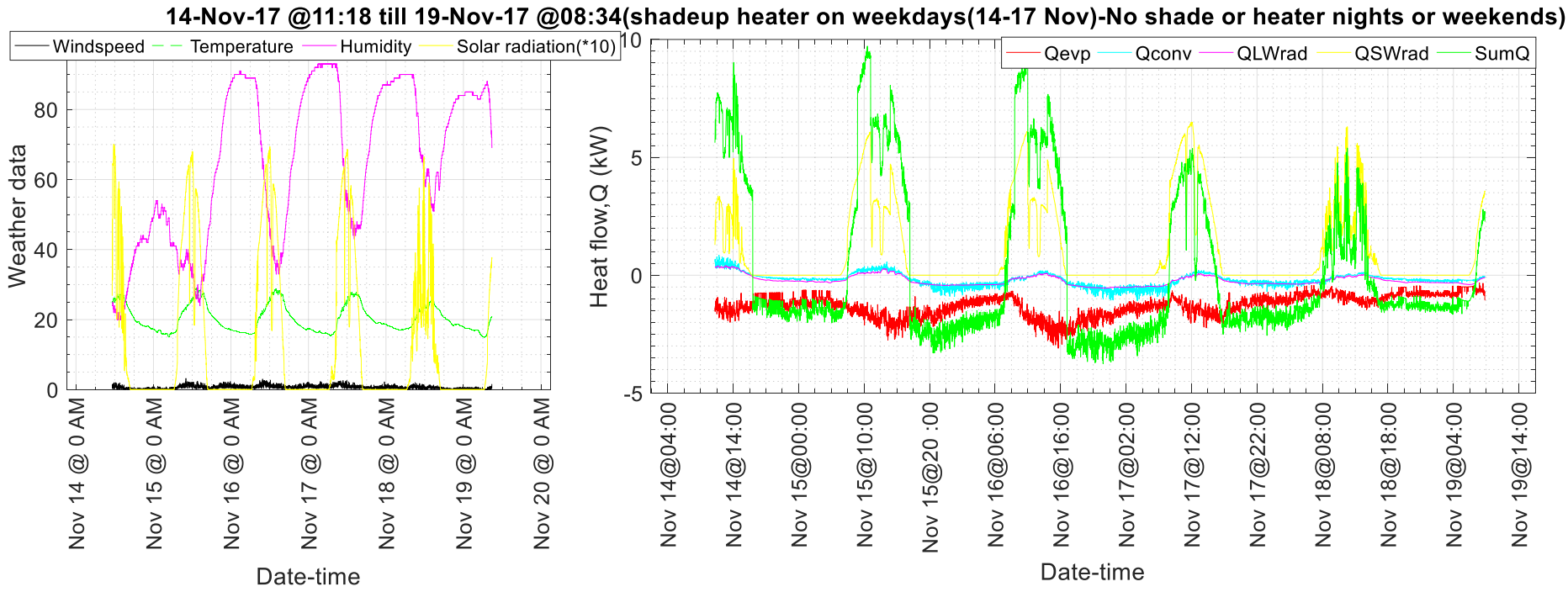

Figure 7-13: Thermal losses of deferred cooling system with shield up & heater on week days 9am to 5 pm

7.6: Sensitivity analysis:

Sensitivity analysis for the simulation of the shield upper position model versus experimental using actual weather data from 10th to 18th April 2017:

7.6.1: Shield up diffuse percent:

In the shield upper position (ideal and experimental), the percent of diffuse radiation entering the pool was assumed to be 30% as displayed in Figure 7-14-a. This assumption was changed to 15% in Figure 7-14-b, showing a slight decrease in the water temperature of the pool.

7.6.2: Shield up beam percent area factor (adjusted model):

In the shield upper position (experimental) model, the percent of beam radiation entering the pool was assumed according to a curve fit from field observations obtained in November experimental run (as per Appendix B) and factored by a" month factor" to adjust for the change in the solar altitude and azimuth angels as per Cairo's sun path diagram. This month factor was changed from 1.15 in Figure 7-14-a to 0.5 as displayed in Figure 7-15, again reflecting a slight decrease in the water temperature of the pool versus actual.

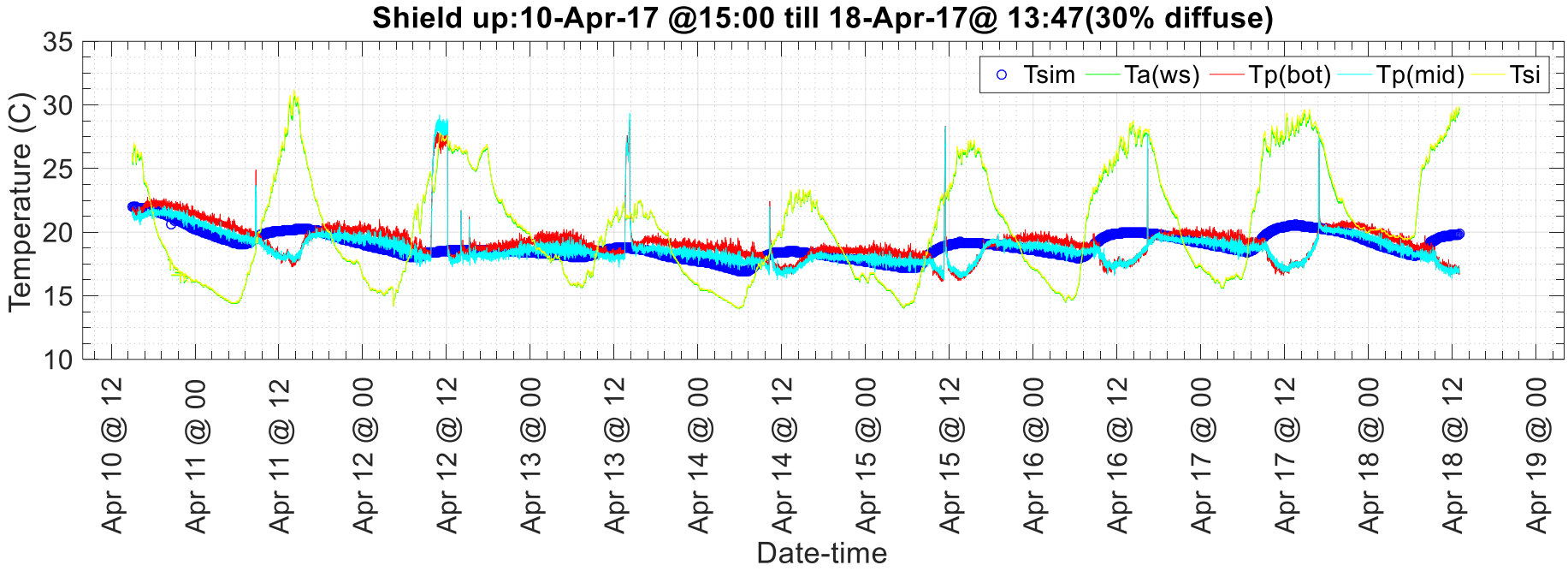
Shield up:10-Apr-17 @15:00 till 18-Apr-17@ 13:47(30% diffuse)
Tsim
Ta(ws)
Tp(bot)
Tp(mid)
Tsi
Temperature (C)
35
30
25
20
15
10
Apr 10 @ 12
Apr 11 @ 00
Apr 11 @ 12
Apr 12 @ 00
Apr 12 @ 12
Apr 13 @ 00
Apr 13 @ 12
Apr 14 @ 00
Apr 14 @ 12
Apr 15 @ 00
Apr 15 @ 12
Apr 16 @ 00
Apr 16 @ 12
Apr 17 @ 00
Apr 17 @ 12
Apr 18 @ 00
Apr 18 @ 12
Apr 19 @ 00
Date-time

Figure 7-14 (a)

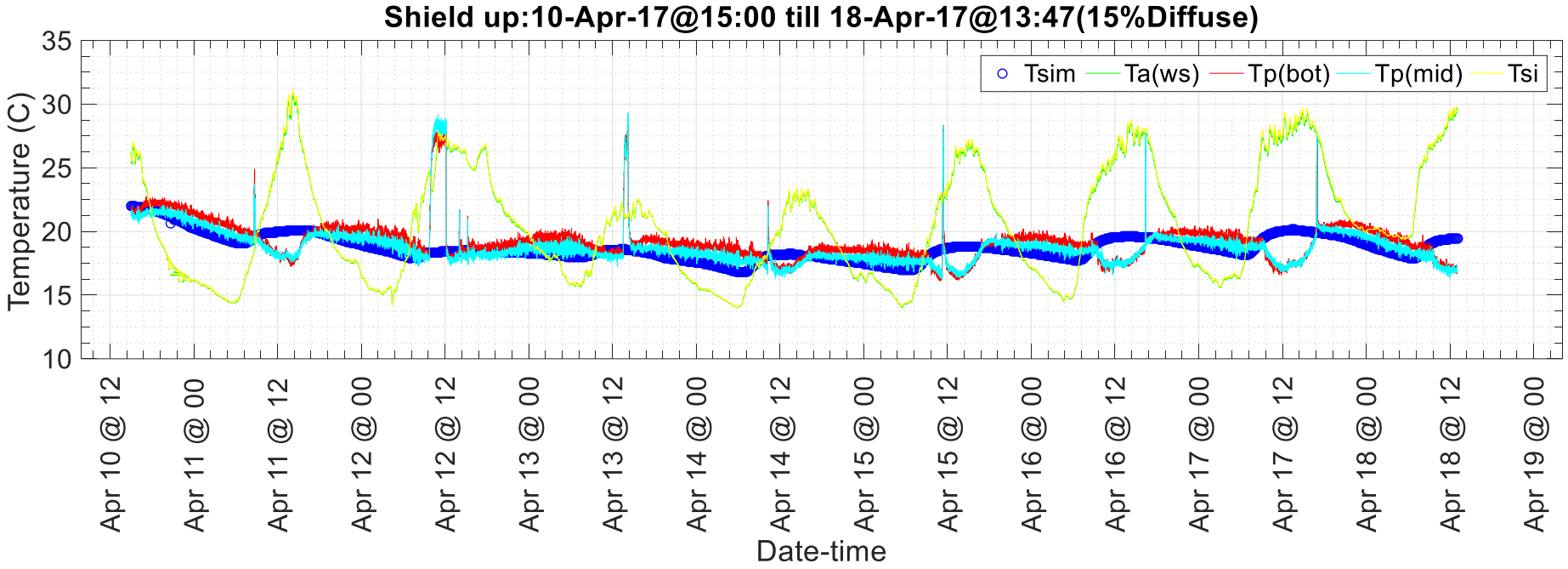

Figure 7-14 (b)

Figure 7-14: Sensitivity check on diffuse % in shield upper position model from 30% in a to 15% in b.

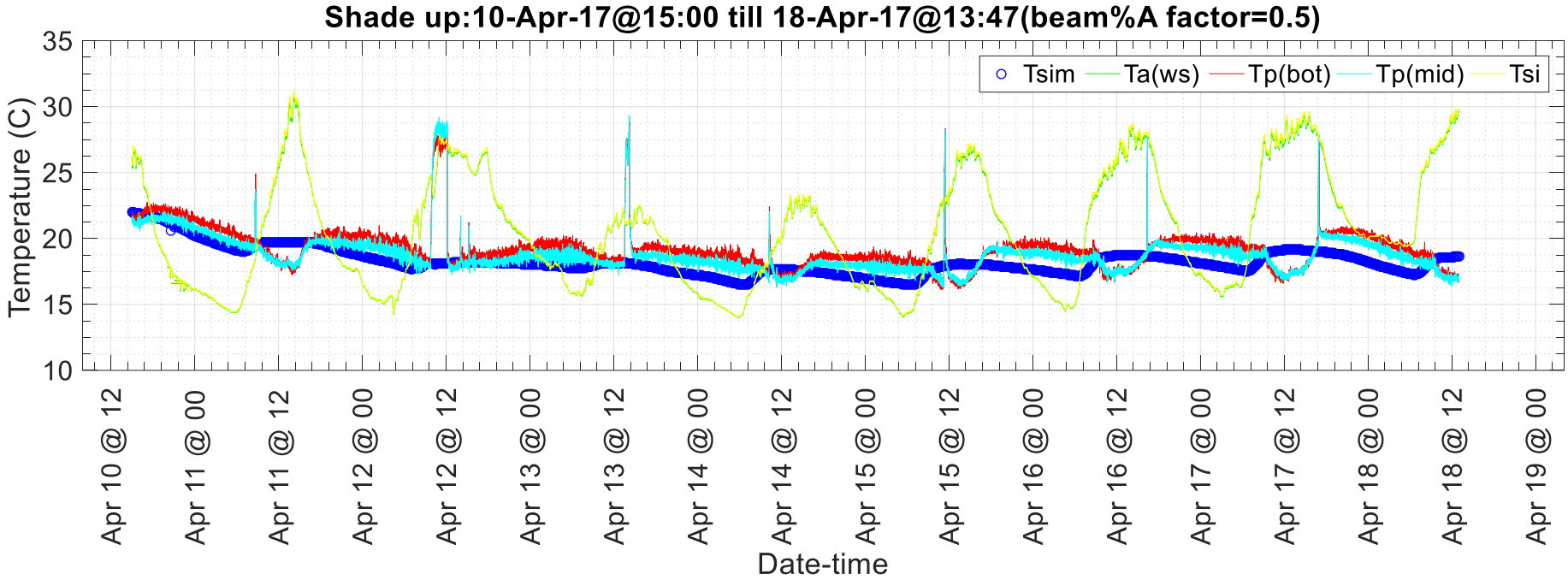

Figure 7-15: Sensitivity check on beam% area entering the pool in the experimental model.

Chapter 8: Conclusion & Recommendations

8.1: Conclusion:

This research work presents a conceptual system for deferring the atmospheric dissipation of the heat rejected from an engine or appliance during the day time, to night time when the ambient conditions are much more favorable for dissipating the heat. It is particularly suitable for desert like climates, where fresh water is scarce, so evaporative cooling is not a viable option and the day time atmospheric temperatures are high, so air-cooling is also not practical; on the other hand, night time cooling by long wave radiation exchange with the sky is particularly effective due to the clear desert skies. As well as revealing the concept, this thesis report describes a practical system design which was implemented in Shallatin, in the southern part of Egypt (23.1 °N latitude, 35.56 °E longitude), and performed successfully.

The thesis report also presents a mathematical model for predicting performance based on actual site weather data. This model can be employed for equipment sizing and operation optimization, as well as performance estimation. The model is applied to predict system response and behaviour for the local weather conditions at a particular test site and demonstrates the ability of the system to dissipate the day time rejected heat during the night time. Moreover, the model can provide an indication for the possible success of any radiative cooling system for any site under consideration by testing the achievable cooling using its relevant weather data. The model allows for testing of any proposed modification such as the use of selective materials.

The experimental work confirmed the validity of the main assumption made in the simulation model, the lumped capacity treatment that is attributed to the influence of strong natural convection currents within the pool. It also suggests a strong link between the use of the shield and the bigger time shift between the daily minimum ambient and water temperatures, hence the demonstration of the concept of cooling deferral.

The recommended operation of the DCS requires the use of effective adjustable solar radiation shield during day-time, which would either allow or block air infiltration according to the temperature difference between the ambient air and water in the DCS. No shield during the night is always the choice for the DCS successful operation. The volume and number of pools to be used is a function of the cooling load (as explained in the DCS operation section) which can be determined using the model. Field testing of the DCS operation showed that this passive system was able to achieve 14 MJ/ (m^2.night) even for an urban site in New Cairo (at AUC campus), though this is not the climate that the DCS is intended for.

The ability of the model to predict performance is demonstrated by comparing its results to the experimental results. Though attempts at comparing corresponding measured and predicted results revealed a great difficulty of trying to predict field data using models, particularly since a large number of phenomena are involved in this application. A small gap in the implementation led to large difference in the output. On comparing the numerical predictions to the experimental measurements for the “No shield” position, the predictions for the pool temperature followed

closely the same trend as the experimental measurements, albeit with occasional shifts in time, possibly due to the unaccounted-for thermal inertia effects. As for the day-time shielded scenarios, the model was able to predict the temperature profile of the deferred cooling system as compared to experimental results, predicting the highest temperature with approximately 5% accuracy, while missing the coolest temperature by approximately 13% for the “Shield up scenario “and 27% for the “Shield down scenario “at times. The bigger variation between the model’s prediction and the actual pool temperature for both shielded scenarios is that the model tends to overestimate the pool temperature when the temperature is minimum around noon, which could be due to under prediction of evaporation with lower wind speeds. This means that the DCS system might be able to achieve cooler minimum temperatures than those predicted by the model, with the model being on the conservative side when predicting the maximum cooling achieved by the system.

Simulating the DCS performance under design conditions by using field measured weather data at the American University in Cairo (AUC) campus in New Cairo (30.02 °N latitude , 31.5 °E longitude) , and comparing the water temperature to ambient temperature at the time of water withdrawal from the pool, showed that the system is able to achieve lower temperature than air during the day by about 8℃ when the pool water is being emptied to be used in cooling ,even though the test site is not a typical desert climate with clear sky where radiative cooling would be more effective in lowering the water temperature. An 18°C temperature drop was achieved by the system, which is equivalent to 53 MJ/m^2night of cooling.

8.2: Recommendation for future work:

1) Practical implementation revealed that the basic design for lifting and lowering the shield was unsatisfactory due to the following:

    a) The design led to large gaps between the shield and pool rim in the lower position. Though in the lower position, as intended, the shield did cut down convection and was successful in creating the shading effect, it was impossible to eliminate air infiltration.

    b) In the upper position, it was unable to completely shield the sun, allowing some of the beam radiation to enter the pool at parts of the day, especially when the sun was low in the sky (low altitude angles) as demonstrated in the photos in appendix B.

    c) The shield was heavy and needed physical effort to change its position when trying to experiment with the field performance of the DCS, which hindered the possibly of performing more field runs while altering the shield position.

Thus, it is proposed that in the future, shutter window louver type design would surround the pool upper rim which when fully closed would prevent infiltration and when open will allow air to go through, while always blocking solar radiation.

Figure 8-1:Pond with louver type shield

2) The use of selective surfaces for the shield material could be investigated in the future to obtain higher temperature drop if needed for critical smaller scale applications.

3) An economic analysis of the DCS system is recommended including both energy and fresh water cost involved in comparison to other cooling alternatives for desert like climates.

References:

Al-Nimr, M.A, Z Kodah, and B Nassar. 1998. “A Theoretical and Experimental Investigation of a Radiative Cooling System.” *Solar Energy* 63(6): 367–73. http://www.sciencedirect.com/science/article/pii/S0038092X9800098X.

Andretta, A et al. 1981. “Selective Surfaces for Natural Cooling Devices.” *Journal de Phsique Colloques* 42(C1): 423–30.

Atwater, Marshall A., and John T. Ball. 1978. “Computation of IR Sky Temperature and Comparison with Surface Temperature.” *Solar Energy* 21(3): 211–16.

Auer, Thomas. 1996. “TRNSYS-TYPE 144 Assessment of an Indoor or Outdoor Swimming Pool.” *TRANSSOLAR Energietechnik GmbH (Strategies for energy efficient design and thermal comfort in buildings)* (November 21).

Bagiorgas, H. S., and G. Mihalakakou. 2008. “Experimental and Theoretical Investigation of a Nocturnal Radiator for Space Cooling.” *Renewable Energy* 33(6): 1220–27.

Bell, Ely E, Leonard Eisner, James Young, and Robert A Oetjen. 1960. “Spectral Radiance of Sky and and Terrain at Wavelengths between 1 and 20 Microns.” *Journal of the Optical Society of America* 50: 1313–20.

Berdahl, Paul and Martin, Marlo. 1984. “Emissivity of Clear Skies.” *Solar Energy* 32(10): 663–64.

Berdahl, Paul, and Richard Fromberg. 1982. “The Thermal Radiance of Clear Skies.” *Solar Energy* 29(4): 299–314.

Bliss, Raymond W. 1961. “Atmospheric Radiation Near the Surface of the Ground: A Summary for Engineers.” *Solar Energy* 59(3): 103–20.

Catalanotti, S. et al. 1975. “The Radiative Cooling of Selective Surfaces.” *Solar Energy* 17(2): 83–89.

Craig, Richard A. 1965. *The Upper Atmosphere*. 1st ed. ed. J. Van Mieghem. Academic Press.

Czarnecki, J.T. 1978. “Swimmimg Pool Heating by Solar Energy.” *CSIRO Division of Mechanical Engineering* (Technical Report TR 19).

Dawoud, B. et al. 2006. “On the Possible Techniques to Cool the Condenser of Seawater Greenhouses.” *Desalination* 195(1–3): 119–40.

Duffie, J. a., and William a. Beckman. 2013. *Solar Engineering of Thermal Processes*. 4th ed. John Wiley & Sons.

Erell, Evyatar, and Yair Etzion. 1996. “Heating Experiments with a Radiative Cooling System.” *Building and Environment* 31(6): 509–17.

———. 2000. “Radiative Cooling of Buildings with Flat-Plate Solar Collectors.” *Building and Environment* 35(4): 297–305.

Etzion, Y., and E. Erell. 1991. “Thermal Storage Mass in Radiative Cooling Systems.” *Building and Environment* 26(4): 389–94.

Faramarzi, Ramin, John Lutton, and Sean Gouw. 2010. “Performance Comparison of Evaporatively-Cooled Condenser versus Air-Cooled Condenser Air Conditioners.” *ACEEE*: 117–27.

Granqvist, C. G., A. Hjortsberg, and T. S. Eriksson. 1982. “Radiative Cooling to Low Temperatures with Selectivity IR-Emitting Surfaces.” *Thin Solid Films* 90(2): 187–90.

Guidati, F. 1992. “Uberprufung von Warme-Und Stoffubergangsbeziehungen an Der Oberflache von Freischwimmbecken Mittels Mebdaten.” *Institut fur Thermodynamik und Warmetechnik* (Studienarbeit Nr.9133).

Hahne, E., and R. Kübler. 1994. “Monitoring and Simulation of the Thermal Performance of Solar Heated Outdoor Swimming Pools.” *Solar Energy* 53(1): 9–19.

Hanif, M. et al. 2014. “Potential Energy Savings by Radiative Cooling System for a Building in Tropical Climate.” *Renewable and Sustainable Energy Reviews* 32: 642–50.

Holman, J.P. and White, P. 1992. *Heat Transfer*. 7th ed. McGraw Hill.

“Https://Www.Timeanddate.Com/Weather/Egypt/Cairo.” 2017.

Huzayyin, O. A., M. S. El Morsi, M. A. Serag-Eldin, and M. F. El-Bedaiwy. 2017. “Prototype for Solar Powered Chip-Ice Production Facility.” In *IMECE2017-72510*, Tampa, Florida, V006T08A100,5

pages. http://proceedings.asmedigitalcollection.asme.org/proceeding.aspx?doi=10.1115/IMECE2017-72510.
Kalogirou, S. A. 2001. “Use of TRYNSYS for Modeling and Simulation of a Hybrid PV– Thermal Solar System for Cyprus.” *Renewable Energy* 23: 247–60.
Kasten, Fritz, and Gerhard Czeplak. 1980. “Solar and Terrestrial Radiation Dependent on the Amount and Type of Cloud.” *Solar Energy* 24: 177–89.
Kimball, B.a. 1985. “Cooling Performance and Efficiency of Night Sky Radiators.” *Solar Energy* 34(1): 19–33.
kipp & zonen. 2017. “Instruction Manual.” *Instruction Manual (CMP series. Pyranometer)*. www.kippzonen.com/Download/72/Manual-Pyranometers-CMP-series-English (December 20, 2018).
Martin, Marlo, and Paul Berdahl. 1984. “Characteristics of Infrared Sky Radiation in the United States.” *Solar Energy* 33(3–4): 321–36.
Matsuta, M., S. Terada, and H. Ito. 1987. “Solar Heating and Radiative Cooling Using a Solar Collector-Sky Radiator with a Spectrally Selective Surface.” *Solar Energy* 39(3): 183–86.
Michell, D., and K. L. Biggs. 1979. “Radiation Cooling of Buildings at Night.” *Applied Energy* 5(4): 263–75.
Naguib, Ramez. 2009. “Total Cost of Ownership For Air Cooled and Water-Cooled Chiller Systems.” *ASHRAE Journal* 51(4): 42–48.
P.A.Hilton.Technical. “Data Logger System D102 Series.” http://www.alfarez.com/frames/hilton/Data logging and Testing/D102_V2.pdf (December 20, 2018).
Richter, D. 1969. “Ein Beitrag Zurr Bestimmung Der Verdunstung von Freien Wasserflachen Dargestellt Am Beispiel Des Stechlinsees.” *Abhandlung des Meteorologischen Dienstes der DDR* 88(XI).
Robaa, S. M. 2006. “A Study of Solar Radiation Climate at Cairo Urban Area, Egypt and Its Environs.” *International Journal of Climatology* 26(13): 1913–28.
Robinson, Brian S., Jordan Dorwart, and M. Keith Sharp. 2015. “US Space Cooling Potentials for Ambient Sources with Thermal Energy Storage.” *International Journal of Ambient Energy* 36(6): 268–81. https://doi.org/10.1080/01430750.2013.864585.
S. Ito and N. Miura. 1989. “Studies of Radiative Cooling Systems for Storing Thermal Energy.” *Journal of Solar Energy Engineering* 111(3): 251–56.
Serag-Eldin, M. A. 2011. “Lowering the Sink Temperature for a Desert Solar Air Conditioning System.” *Sustainable Development and Planning* 150(WIT Transactions on Ecology and the Environment): 227–38.
Serag-Eldin, M. A., and M.S El Morsi. 2015. “Design, Manufacturing and Testing of a Solar Driven Refrigerator Featuring Minimum Energy Waste.” *Egyptian Academy of Scientific Research and Technology(ASRT) Report* (August).
Shah, Mirza Mohammed. 2008. “Analytical Formulas for Calculating Water Evaporation from Pools.” *ASHRAE Transactions* 114(2): 610–18. http://mmshah.org/publications/Pool Evap ASHRAE Tr 2008.
Staley, D. O., and G. M. Jurica. 1972. “Effective Atmospheric Emissivity under Clear Skies.” *Journal of Applied Meteorology* 11: 349–56.
Theodor Friedrichs. 2011. “COMBILOG 1022 Data Logger (Hardware Manual).” http://www.th-friedrichs.de/assets/ProductPage/ProductDownload/ManualE1022V105.pdf (December 20, 2018).
———. “Humidity and Temperature Sensor in Shelter.” http://www.th-friedrichs.de/en/products/humidity/relative-humidity-psychrometer/combined-temperature-humidity-sensor-in-shelter/.
———. “Wind Direction, Heavy-Duty.” http://www.th-friedrichs.de/en/products/wind/wind-speed/

(December 20, 2018b).
TSI Alnor. 2014. “AVM430 Thermal Anometer.” https://tsi.com/alnor-velometer-thermal-anemometer-avm430-a/ (December 20, 2018).
Vall, Sergi, and Albert Castell. 2017. “Radiative Cooling as Low-Grade Energy Source: A Literature Review.” *Renewable and Sustainable Energy Reviews* 77(May): 803–20.
Xu, Xiaolong, Runping Niu, and Guohui Feng. 2015. “An Experimental and Analytical Study of a Radiative Cooling System with Flat Plate Collectors.” *Procedia Engineering* 121(0): 1574–81.

Appendix A: Program Code and Flow Description:

A-1: Program code:

A-1.1: Main program code

```
close all
clear all
clc
[tw,sizecheck_diffuse_percent,diffuse_percent,nrun,shadeday,shademonth,shad
ehour,shadeindicator,weather,windspeed,datetimenum,Ta,humidity,solarradiati
on]=Shade_weather_Run_10_18April2017_shadeup
humidity_percent=humidity/100;
period='11th to 18th April 2017';
mode='DeltaT';
H=0.685;%Height of Pool
row=1000;
R=1.83;
%Depth_loss=0.07/(3600*100);%m/second from cm/hr
V=pi()*R^2*H;
mges=row*V;
mdotleakage=0;
TB_0=40;
mdot_fr=0;    %%mzu = mass flow rate of heating material stream
Tfr=0;     %const DETLA T CONDENSER
%% %%%%%%%%%%%%%%%%%%%%End Initialize---START 1ST DAY%%%%%%%
first_datetime=datestr(datetimenum(1));
start_data_clock=[2017 04 10 15 00 00];
req_startclock=[2017 04 10 10 00 00];
diff=etime(req_startclock,start_data_clock);
if diff>=0
mindiff=(diff/60)+1%%%%1140sec
else
mindiff=(24*60)+(diff/60);
%display(mindiff)
end
u=(mindiff+(20*60))%%2340secmindiff+1200(60*20)
[mges,newdepth,Tfinal,deltaT_Day,Q_kw_Day,Q_KwperM2_Day]=GENERAL_Pool_funct
ion_Template_multiCycle_pos3and4(mindiff,mdotleakage,u,TB_0,mges,mdot_fr,Tf
r,tw,sizecheck_diffuse_percent,diffuse_percent,nrun,shadeday,shademonth,sha
dehour,shadeindicator,weather,windspeed,datetimenum,Ta,humidity,humidity_pe
rcent,solarradiation,period,mode)
%%%%%%%%%%%%%%%%%CYCLE OUTPUT IS INPUT TO NEXT %%%%%%%%%%%%%%%%%%
Tfinal_Day1=Tfinal;
deltaT_Day1=deltaT_Day;
Q_kw_Day1=Q_kw_Day;
Q_KwperM2_Day1=Q_KwperM2_Day;
mass_afterD1=mges
Depth_D1=newdepth
display(mges);
mges=mass_afterD1;
TB_0=Tfinal_Day1;
%% %%%%%%%%%%%%%%%%%%%%%START ClUSTER EMPTY Fill Day
cycle=round((nrun-mindiff-1200)/1680)
cycle=3
for cluster=1:cycle
%% %%%%%%%%%%%%%%%%%%%%End Result 1st Day ---START Empty1%%%%%%%
cc=cluster
mindiff=(mindiff+(20*60))%or minduff=u
```

```
u=(mindiff+(4*60))
diffnu=nrun-u
mdotleakage=0.4
mdot_fr=0;    %%mzu = mass flow rate of heating material stream
[mges,newdepth,Tfinal,deltaT_Day,Q_kw_Day,Q_KwperM2_Day]=GENERAL_Pool_funct
ion_Template_multiCycle_pos3and4(mindiff,mdotleakage,u,TB_0,mges,mdot_fr,Tf
r,tw,sizecheck_diffuse_percent,diffuse_percent,nrun,shadeday,shademonth,sha
dehour,shadeindicator,weather,windspeed,datetimenum,Ta,humidity,humidity_pe
rcent,solarradiation,period,mode)
Tfinal_Day1_empty1=Tfinal;
deltaT_Day1empty1=deltaT_Day;
mass_afterempty1=mges;
Depth_Day1_empty1=newdepth;
TB_0=Tfinal_Day1_empty1
%% %%%%%%%%%%%%%%%%%%%%End Result Empty1%%%%%%%START fill_1
mindiff=(mindiff+(4*60))
u=(mindiff+(4*60));
mdotleakage=0;
mdot_fr=0.4+(7.9999*10^-3);   %%mpktfr= mass flow rate of waterin
%Tfr=40;const T CONDENSER
Tfr=TB_0+abs(deltaT_Day1)  ;  %const DETLA T CONDENSER
[mges,newdepth,Tfinal,deltaT_Day,Q_kw_Day,Q_KwperM2_Day]=GENERAL_Pool_funct
ion_Template_multiCycle_pos3and4(mindiff,mdotleakage,u,TB_0,mges,mdot_fr,Tf
r,tw,sizecheck_diffuse_percent,diffuse_percent,nrun,shadeday,shademonth,sha
dehour,shadeindicator,weather,windspeed,datetimenum,Ta,humidity,humidity_pe
rcent,solarradiation,period,mode)
Tfinal_Day_fill_1=Tfinal;
deltaT_Dayfill_1=deltaT_Day;
mass_afterfill_1=mges;
Depth_fil1_1=newdepth;
mges=mass_afterfill_1;
TB_0=Tfinal_Day_fill_1;
%% %%%%%%%%%%%%%%%%%%%%End Result Empty1%%%%%%%START DAY2
mindiff=(mindiff+(4*60))
u=(mindiff+(20*60));
mdotleakage=0,
mdot_fr=0   %%mpktfr= mass flow rate of waterin
[mges,newdepth,Tfinal,deltaT_Day,Q_kw_Day,Q_KwperM2_Day]=GENERAL_Pool_funct
ion_Template_multiCycle_pos3and4(mindiff,mdotleakage,u,TB_0,mges,mdot_fr,Tf
r,tw,sizecheck_diffuse_percent,diffuse_percent,nrun,shadeday,shademonth,sha
dehour,shadeindicator,weather,windspeed,datetimenum,Ta,humidity,humidity_pe
rcent,solarradiation,period,mode)
%%%%%%%%%%%%%%%%Output Day2 input to empty2
Tfinal_Day2=Tfinal;
deltaT_Day2=deltaT_Day;
Q_kw_Day2=Q_kw_Day;
Q_KwperM2_Day2=Q_KwperM2_Day;
display(mges);
mass_afterDay2=mges;
Depth_Day2=newdepth;
TB_0=Tfinal_Day2;
%% %%%%%%%%%%%%%%%%%%%%End Result 1st Day ---START Empty2%%%%%%%
end
```

A.1.2: Pool Function:

```
function[mges,newdepth,Tfinal,deltaT_Day,Q_kw_Day,Q_KwperM2_Day,OUT_Qv_m,OU
T_Qkon_m,OUT_Qrd_m,OUT_Qsolar_m,OUT_sumQ_m,STOREMATRIX_TB,Ta,shieldstatus]=
GENERAL_Pool_function_Template_multiCycle_pos3and4(mindiff,mdotleakage,u,TB
_0,mges,mdot_fr,Tfr,tw,sizecheck_diffuse_percent,diffuse_percent,nrun,shade
day,shademonth,shadehour,shadeindicator,weather,windspeed,datetimenum,Ta,hu
midity,humidity_percent,solarradiation,period,mode)

%%%%%%%%%%%%%%%%%%%Initialization%%%%%%%%%%%%%%%%%%%%%%%%%%%%%%%%%%%%%%%%%
%%%%%%%%%%
Qv=0;
%TB_0=22;%%%%Temp of pool at time zero
TB_m=0;Mv_m=0;Qzu_m=0;Qv_m=0;Qkon_m=0;Qrd_m=0;Qfr_m=0.;Qsolar=0;DE=0;
simulationtimestep=(1/60);%in hours :one minute time step is used in
simulation
t=simulationtimestep*60;%simulation time step in minutes(dt inside loop in
qr_pool=0;
Store_Max_i_error=0;
count_error=0;
Store_avg_error=0;
%converge(1:6)=[100,100,100,100,100,100];
%%%%%%%%%%%%%%%%%%%%%%End converge initialize%%%%%%%%%%%%%%%%%
%%%%%%%%%%%%%%%%%%%EndInitialization%%%%%%%%%%%%%%%%%%%%%%%%%%%%%%%%%%%%%
%%%%%%%%%%
%%%%%%%%%%%%%%%%%%%CONSTANTS%%%%%%%%%%%%%%%%%%%%%%%%%%%%%%%%%%%%%%%%%%%%
%%%%%%%%%%
row=1000;
cpw=4180;
cp_air=1007;
Cs=5.67;
epsw=0.9;
%%%shade in%%%
eps_shadein=0.9;
Kshade=0.5;
thickness_shade=0.01;
epsshade_out=0.25;
alpha_shadeout=0.25;
%epsshade_out=0.1;
%alpha_shadeout=0.1;
g=9.81;
R=1.83;
Rd=461.519 ;%%%%gas constant of water vapor%%%%%%%%%%%%%%
Lshade=4;
Wshade=3.3;
Xpool_shade=0.2;
Ashade=Lshade*Wshade;
Atot=pi()*R^2;
Ashadecross=(thickness_shade*Wshade);
Rins_shade=thickness_shade/(Kshade*Ashade);%0.003
Rins_shade=(8.72/Ashade)%*1.67%0.66*1.67(delatx*k/A%)
Rsurface_shadein=(1-eps_shadein)/(eps_shadein*Ashade)  ; %surface
resistance of shade
Rsurface_pool=(1-epsw)/(epsw*Atot);%Surface resistance of shade
%H=0.685;%Height of Pool
vlaeq=0.23;
SurfaceHumidity=1;
%Depth_loss=0.07/(3600*100);%m/second from cm/hr
Depth_loss=0;
%V=pi()*R^2*H;
```

```
%Qloss=pi()*R^2*Depth_loss;%Volumertic flow rate of lost depth due to
leakage
%mdotleakage=Qloss*row%kg/sec mass flow rate due to leakage
%mdot_fr=0;%-(Qloss*row); %mpktfr = in kg / s fresh water supply%
%Tfr=25;%const T CONDENSER
%Tfr=TB_0+deltaT_Day1     %const DETLA T CONDENSER
comp_Mv=0;%compensated Mass of evaporation from fresh water
%%%%%%%%%%%%%%%%%%%%%%%%EndConstants%%%%%%%%%%%%%%%%%%%%%%%%%%%%%%%%%%%%%%%%
%%%%%%%%%%
%%%%%%%%%%%%%%%%%%%%%%%%Input%%%%%%%%%%%%%%%%%%%%%%%%%%%%%%%%%%%%%%%%%%%%%%%
%%%%

Lchar=sqrt(Atot);
%Lchar=0.9*(2*R)
fcov=0.00001;
mzu=0;    %%mzu = mass flow rate of heating material stream
Tzu=40;    %%Tzu= the Temp. the heating material stream
fcov=0;
shade_opening=0.000001;
%mges=row*V;

%%%%%%%%%%%%%%%%%%%%%%%%Endinput%%%%%%%%%%%%%%%%%%%%%%%%%%%%%%%%%%%%%%%%%%%%
%%%%%%
%%%%%%%%%%%%%%%%%%%%Estimated Input%%%%%%%%%%%%%%%%%%%%%%%%%%%%%%%%%%%%%%%%
cloudness=0;%%%%%As Observed during run
Exp_shade_down_2_effect_wind=0.2;
Exp_shade_down_2_effect_diffuse=0.1;
Exp_shade_down_2_effect_beam=0;
Exp_shade_up_diffuse_effect=0.3;
ideal_shade_up_4_diffuse_effect=0.3;
month_shade_area_factor=1.15;%%%%

%%%%Initialization after reading weather data %%%;
STORE1=TB_0

%STORE2=TB_0;
n=length(datetimenum);

%%%%%%%%%%%%%%%SKY_TEMPERATURE%%%%%%%%%%%%%%%%%%%%%%%%%%%%%%%%%%%%%%%%%%%%%%
%%%%%%%%%%%%%%%%
%Tsky=(Ta-7)+0.01;

Tdew=(humidity/100).^(1/8).*(112+0.9*Ta)+(0.1*Ta)-112;

Hort=307;
p0=1013;%%%atmopheric pressure in mmbar
const=8005;
Patm = p0*exp(-Hort/const);
esp_sky_nocloud=(0.711+0.0056.*Tdew+0.000073.*Tdew.^2+0.013*cos((2*pi*shade
hour)/24)+(12^-05*(Patm-1013)));

cloud_index_check = 1.4286.*(diffuse_percent-0.3);
cloud_index_check(cloud_index_check<=0)=0.001 ;
cloud_index_check(cloud_index_check>1)=1;
cloud_index =cloud_index_check.^0.5;
```

```
eps_sky =esp_sky_nocloud+(1-esp_sky_nocloud).*cloud_index.*0.8;%%%0.8 is
the largest tow for summer latitude
Tsky = ((Ta+273.15).*eps_sky.^0.25)-273.15;
%%%%%%%%%%%%%SKY_TEMPERATURE%%%%%%%%%%%%%%%
start=mindiff
%for i=start:u
for i=mindiff:u
if i<n
TSO=Ta(i,1)
TSI=Ta(i,1)
%%%%%%%%%%%%%%%%%% CONVERGE INITIALIZE%%%%%%%%%%%%%%%%%%%%%%%%%%%%%%%%%%%%%%%%
prev_shadeposition=8;
TB=STORE1;
TGr=Ta(i,1);
thisshadehour=shadehour(i,1)
iequal=i;
counterip=0;
for ip=1:2
if counterip<100;
counterip=counterip+1;
if ip==1;
TB_IP1=TB;
end
TB=TB_IP1;
TB_m=0;Mv_m=0;Qzu_m=0;Qv_m=0;Qkon_m=0;Qrd_m=0;Qfr_m=0.;Qsolar=0;DE=0;sumQ_m
=0;
for k=1:t
%%%%%%%%%%shade position as function of day hour%%%%%%%%%%%%%%%%
if (shadehour(i,1)>=5)&& (shadehour(i,1)<19)  %%%%%%
Qheater=0;%(j/s)
cloudness=0;
if (Ta(i,1)+5)<TB
shadeposition=4%%%4ideal shield up position
if prev_shadeposition==0
TSO=Ta(i,1)
TSI=Ta(i,1)
end
else
shadeposition=3%%%3ideal shield lower position
if prev_shadeposition==0
TSO=Ta(i,1);
TSI=Ta(i,1)
end
end
elseif (shadehour(i,1))>=19||(shadehour(i,1)<5)
shadeposition=0
Qheater=0;
cloudness=0 ;
%else
% shadeposition=0;
% cloudness=0;
%Qheater=0;
end%%%%%00000ifshadeposition
%thisshadehour=shadehour(i,1);
prev_shadeposition=shadeposition;
shieldstatus(i)=shadeposition;
%%%%%%%%%%%%End shade position as function of day hour%%%%%%%%%%
%% %%Heun method%%%%loop%%%%%%
heunn_error=100;
heunn_iter=0;
while(abs(heunn_error)>0.1)&&(heunn_iter<100)
```

```
for Heunn=1:2
if heunn_iter>0
Heunn=2;
end
%   MASSSS=mges
if (Heunn==2)&&(i<n) %This is to take boundary conditions at the end of the
minute in the 2nd
heunnequal=Heunn;
i=i+1;
end
heuniter=heunn_iter;
%% %%%%%%%%%%%%%%%%%%%%RADIATION EXCHANGE WITH SKY%%%%%%%%%%%%%%%%%%%%%%%%
%$$$$$$$$$$$$$$$%%%%%%%EQUATIONS%%%%%heat balance for shade out then shade in
for shapeup positions%%%%%%%%%%%%
if (shadeposition>0)%%%%%%%%%Radiation calculation for shade position >0 (2
or 3 down , 1 or 4 up)or else <0
%%%%%%%%%%%%%%%%%% CONVERGE INITIALIZE%%%%%%%%%%%%%%%%%%%%%%%%%%%%%%%%%%%%
%count_converge=0;
count_converge=0;
old_heat_a11=0;
old_heat_a22=0;
old_heat_b1=0;
old_heat_b2=0;
old_rad_b1=0;
old_rad_b2=0;
if (shadeposition==2)||(shadeposition==3)%%%initialize converge coeff shade
down ideal 3 and exp 2
converge(1:6)=[100,100,100,100,0,0]
coeff=6;
elseif (shadeposition==1)||(shadeposition==4)%%%shade up ideal(4) or exp(1)
converge(1:6)=[100,100,100,100,100,100]
coeff=6;
end%%%endintialize converge coeff
%count_converge=1

All_icheck_converge=(converge(1:coeff));
%%%%%%%%%%%%%%%%%% END CONVERGE
INITIALIZE%%%%%%%%%%%%%%%%%%%%%%%%%%%%%%%%%%%%
% while (any((converge(1:coeff)))>0.1&&(count_converge<400))
while
((converge(1))>0.1||(converge(2))>0.1||(converge(3))>0.1||(converge(4))>0.1
1||(converge(5))>0.11||(converge(6))>0.1)&&(count_converge<400)
hconv_shadeout=(3.1+4.1*windspeed(i,1));
%% Cramer's Coefficients of shade out equation%%%%%%%%
functionTSO=epsshade_out*Ashade*Cs*10^-
8*(TSO^2+(Tsky(i,1))^2)*(TSO+Tsky(i,1));
heat_a11=((1/(Rins_shade*Ashade))+(hconv_shadeout*Ashade)+functionTSO);
heat_a12=-(1/(Rins_shade*Ashade));
heat_b1=Qsol_shade+(hconv_shadeout*Ashade*Ta(i,1))+(functionTSO*Tsky(i,1));
%%%%%%%%%%%%%shadein_heat_balance%%%%%%%%%%%%
%q_(cond(s,o-s,i)  )= q_(forced/natural  conv(s,i-amb) )-q_LWrad(s,i-pool)
-q_LWrad(?(s,i-Ground @&))
hconv_shadein=(3.1+4.1*windspeed(i,1));%%%%if forced TOBE REVISED
%hconv_shadein=(5.7+3.8*windspeed(i,1));%%%%if mixed RE book appendix
heat_a21=-(1/(Rins_shade*Ashade));
if shadeposition==1||(shadeposition==4)%%%shade up ideal(4) or exp(1)
heat_a22=((1/(Rins_shade*Ashade))+(hconv_shadein*Ashade)+((Cs*10^-
8*TSI^3))/Rsurface_shadein);
F_poolshade=0.55;
```

```
%%%%TO ALTERNATE SOLUTION OF Js ANd Jp (recalaculate )after calculating Tso
and TSI from previous Js And Jp
[qr_shade,qr_pool,Js,Jp,rad_b1,rad_b2]=New_Qrad_Fps(TB,TSI,TGr,Tsky(i,1),At
ot,Ashade,epsw,eps_shadein,F_poolshade);
%[Js,Jp]=New_Qrad_Fps(TB,TSI,TGr,Tsky(i,1),Atot,Ashade,epsw,eps_shadein,F_p
oolshade);
heat_b2=(hconv_shadein*Ashade*Ta(i,1))+(Js/(Rsurface_shadein));
%display(TB)
jees1=Js
%jeep1=Jp
TSO=((heat_a22*heat_b1)-(heat_a12*heat_b2))/((heat_a11*heat_a22)-(heat_a12-
heat_a21))
TSI=((heat_a11*heat_b2)-(heat_a21*heat_b1))/((heat_a11*heat_a22)-
(heat_a12*heat_a21))
Esi=Cs*(TSI)^4*10^-8;
Eso=Cs*(TSO)^4*10^-8;
[qr_shade,qr_pool,Js,Jp,rad_b1,rad_b2]=New_Qrad_Fps(TB,TSI,TGr,Tsky(i,1),At
ot,Ashade,epsw,eps_shadein,F_poolshade);
heat_b2=(hconv_shadein*Ashade*Ta(i,1))+(Js/(Rsurface_shadein));
qqqqeeepool=qr_pool
converge_heatradb1=(abs(old_rad_b1-rad_b1)/rad_b1)*100;
converge_heatradb2=(abs(old_rad_b2-rad_b2)/rad_b2)*100;
converge(5)=converge_heatradb1;
converge(6)=converge_heatradb2;
coeff=6;
%%%elseif shadeposition>1%solving a22 and b2 for shield upper position up1
elseif (shadeposition==2)||(shadeposition==3)%%%a22 and b2 for  shade down
ideal 3 and exp 2
functionTSI=(Cs*(TSI^2+TB^2)*(TSI+TB))/(Rsurface_shadein+(1/Atot)+Rsurface_
pool)
heat_a22=((1/(Rins_shade*Ashade))+(hconv_shadein*Ashade)+functionTSI);
heat_b2=(hconv_shadein*Ashade*Ta(i,1))+(functionTSI*TB);
%Tsssky=Tsky(i,1)

TSO=((heat_a22*heat_b1)-(heat_a12*heat_b2))/((heat_a11*heat_a22)-(heat_a12-
heat_a21))
TSI=((heat_a11*heat_b2)-(heat_a21*heat_b1))/((heat_a11*heat_a22)-
(heat_a12*heat_a21))
qr_pool=-functionTSI*(TSI-TB)%%%%-ve sign??
end %%%end differentiate between calculation for shadeposition up and down
1 or2
converge_heata11=(abs(old_heat_a11-heat_a11)/heat_a11)*100;
converge_heata22=(abs(old_heat_a22-heat_a22)/heat_a22)*100;
converge_heatb1=(abs(old_heat_b1-heat_b1)/heat_b1)*100;
converge_heatb2=(abs(old_heat_b2-heat_b2)/heat_b2)*100;
converge(1)=converge_heata11;
converge(2)=converge_heata22;
converge(3)=converge_heatb1;
converge(4)=converge_heatb2;
i_step_converge=(converge(1:coeff));
%%%%%Store the old coefficent value before calculating new ones
old_heat_a11=heat_a11;
old_heat_a22=heat_a22;
old_heat_b1=heat_b1;
old_heat_b2=heat_b2;
if shadeposition==1||(shadeposition==4)%%%shade up ideal(4) or exp(1)
old_rad_b1=rad_b1;
old_rad_b2=rad_b2;
end
count_converge=count_converge+1;
%display(count_converge)
```

```
All_icheck_converge(count_converge,1:coeff)=(converge(1:coeff));
%plot(1:con,check_con)
%hold on
end %%%%converged
%countingcovv=count_converge
if (count_converge==400)
display Did_not_converge_after_400_iterations
i=n+1;
end
Final_i_check_converge=i_step_converge;
Max_i_error=max(Final_i_check_converge);
if shadeposition>1
Avrg_i_error=mean(Final_i_check_converge(1:4));
elseif shadeposition==1
Avrg_i_error=mean(Final_i_check_converge);
end
count_error=count_error+1;
Store_avg_error=Store_avg_error+Avrg_i_error;
if (Max_i_error>Store_Max_i_error);
Store_Max_i_error=Max_i_error;
end
iofncheck=i;

count_converging(i)=count_converge;
Max_count_coverge=max(count_converging);
Avg_count_coverge=mean(count_converging);
%end%%%%%%%%%shadeposition>0 solve for Tsi and Tso
%Check convergence of heat_a11,heat_b1,heat_a22,heatb2,rad b1, radb2
%end %%% END OF LOOP iTJ
Qrd=(1-fcov)*qr_pool/1000;
else%%%%%%%%44444444if:NOSHADE
CTSKY=Tsky(i,1);
Qrd=(1-fcov)*Cs*epsw*Atot*(((TB+273.15)/100)^4-
((Tsky(i,1)+273.15)/100)^4)/1000;
end %%%%%%%%Radiation calculation for shade position>0 and else 0

%% %%%%%%%%%BETA EVAPORATION AND CONVECTION HT FOR
SHADEDOWN(SHADEPOSITION=2)%%%%

if shadeposition>=2%:IF SHADEDOWN_POSITION2 EVAPORATION CONVECTION
BETA%%%%%%%

Tf=(Ta(i,1)+TB)/2;
humidity_f=(SurfaceHumidity+humidity_percent(i,1))/2.;
kin=Kinematic_Viscosity(Tf);
dense=Density_Humid_Air(TB,SurfaceHumidity,psat(TB));
div=(Kinematic_Viscosity(Tf)^2*Density_Humid_Air(TB,SurfaceHumidity,psat(TB
)));
shade_velocity=(windspeed(i,1)*Exp_shade_down_2_effect_wind)+0.01;
%shade_velocity=vlaeq;
Gr=g*Lchar^3*(Density_Humid_Air(Ta(i,1),humidity_percent(i,1),psat(Ta(i,1))
)-Density_Humid_Air(TB,SurfaceHumidity,psat(TB)))/div;
%Ar=7.9405e10 is Gr
Pr=Kinematic_Viscosity(Tf)/Thermal_Diffuisivity(Tf);
Sc=Kinematic_Viscosity(Tf)/Diffusion_Coeff(Tf);
Re=Lchar*shade_velocity/Kinematic_Viscosity(Tf);
%Re=811319.6 if use vleaq
Ra=(Gr*Pr);
Richardson_No=Gr/Re^2;
```

```
end%1111111111SHADEDOWN:POSTION>2: properties cal for shade 3 and 2 for
EVAPORATION CONVECTION BETA for 2/N for 3
if shadeposition==2; %666666666666:if Qv.Mv and Qkon ShadeDown%%%%%%%%
if (Richardson_No < 0)%22222222:IF RICHARDSON NO.:DECIDE FREE/MIXED OR
FORCED CONVECTION
Sh=0.151*Re^(2./3.);%%%FORCED CONVECTION:TEMP POOL LESS THAN AMBIENT:
%VERY WEAK FREE CONVECTION CURRENT (PLATE HEATED FROM DOWN), AIR
%CURRENTS FROM WIND HAS MORE EFFECT
elseif (Richardson_No>2)
% Sh=0.13*Re^(2./3.)*Richardson_No^(1./3.);%==Sh2=0.13*(Gr)^(1/3)
Sh=0.15*(Gr*Sc)^(1/3);
else
%%%%MIXED CONVECTION:Max of forced  and free or sum of two  Nu to certain
poweR
hilf=0.000906785*Richardson_No^4;
Sh=Re^(2./3.)*(0.151-0.000429704*Richardson_No^2+hilf);
end%22222222222222:IF RICHARDSON NUMBER%%%%%%%%%%%%%%%%%%%%%%%%%
Beta=Sh*Diffusion_Coeff(Tf)/Lchar;%SHADEEDOWN(Sh=KX/D or sh=Beta*Lchar/D)
%if shadeposition==2; %666666666666:if Qv.Mv and Qkon ShadeDown%%%%%%%%
Mv=(1-fcov)*Beta*Atot/(Rd*(Tf+273.15))* 1.e5*(psat(TB)-
(humidity_percent(i,1)*psat(Ta(i,1))));
Qv=Mv*delhv(TB)/1000;
%%%%%%%%%%%%CONVECTION%%%%%%%%%%%%%%%%%
alpha=cp_air*Density_Humid_Air(Tf,humidity_f,psat(Ta(i,1)))*Beta*(Thermal_D
iffuisivity(Tf)/Diffusion_Coeff(Tf))^(2./3.);
Qkon=alpha*Atot*(TB-Ta(i,1))/1000.;
elseif  (shadeposition<2)||(shadeposition==4) %66666666:if Qv and Mv for
SHADE UP AND NO SHADE
Qv=(1-fcov)*Atot*(((4.523+5.088*windspeed(i,1).^0.84)))*(psat_rev(TB)-
(humidity_percent(i,1).*psat_rev(Ta(i,1))));
Qv=Qv/1000;
Mv=Qv/delhv(TB)*1000;
Qkon=Atot*(3.1+4.1*windspeed(i,1))*(TB-Ta(i,1))*1*10^(-3);
%disp(n)
elseif shadeposition==3  %IF SHADEDOWN_POSITION3 EVAPORATION CONVECTION
BETA: cover right over pool%%%%%%%
TfP_S=(TSI+TB/2);
Gr3=(g*Lchar^3*(TB-TSI))/Kinematic_Viscosity(TfP_S)^2;
Pr3=Kinematic_Viscosity(TfP_S)/Thermal_Diffuisivity(TfP_S);
humidity_TfP_S=(humidity_percent(i,1)+humidity_f/2);
Thermal_Conductivity_TfP_S=Thermal_Diffuisivity(TfP_S)*cp_air*Density_Humid
_Air(TfP_S,humidity_TfP_S,psat(TfP_S));
Ra3=(Gr3*Pr3);
if Ra3<1700;
Nu3=1;
elseif (Ra3>=1700)&&(Ra3<7000);
Nu3=0.059*(Ra3)^(0.4);
elseif (Ra3>=7000)&&Ra3<(3.2*10^5);
Nu3=0.212*(Ra3)^(1/4);
elseif Ra3>=(3.2*10^5);
Nu3=0.061*(Ra3)^(1/3);
end
hconvsi_p=(Nu3*Thermal_Conductivity_TfP_S/Xpool_shade);
Qkon=Atot*hconvsi_p*(TB-TSI)*10^(-3);
Qv=0;
Mv=0;
end%%%%%%%%%%%%66666666:IF SHADE POSITION2 (SHADEDOWN) CONV COND EVAP%%%%%
%%%%END calculation of Evap & Conv according to shadeposition%%%%%%%%%%%%%
%% %%%%%%%%%%%%%%%%%%%%DIRECT SOLAR GAIN%%%%%%%
beam_percentArea=((4.8379*(shadehour(i,1)^2))-
(113.52*shadehour(i,1))+681.08)/100;
```

```
if shadeposition==1 && shadeindicator(i,1)==1 && cloudness==0
beam_percentArea=((4.8379*(shadehour(i,1)^2))-
(113.52*shadehour(i,1))+681.08)/100;
beam_percentArea=beam_percentArea*month_shade_area_factor;
Qs=(((diffuse_percent(i,1)*Exp_shade_up_diffuse_effect)+((1-
diffuse_percent(i,1))*(shade_opening+beam_percentArea))))*(1-
fcov)*epsw*Atot*solarradiation(i,1)/1000;
elseif shadeposition==1 && shadeindicator(i,1)==1 && cloudness==1
Qs=((0.6*Exp_shade_up_diffuse_effect)+(0.4*(shade_opening++beam_percentArea
)))*(1-fcov)*epsw*Atot*solarradiation(i,1)/1000;
elseif shadeposition==2
shade_opening=0.0000001;
Qs=((Exp_shade_down_2_effect_diffuse*diffuse_percent(i,1)+((1-
diffuse_percent(i,1))*Exp_shade_down_2_effect_beam)))*(1-
fcov)*epsw*Atot*solarradiation(i,1)/1000 ;
elseif shadeposition==4
shade_opening=0.0000001;
Qs=((ideal_shade_up_4_diffuse_effect*diffuse_percent(i,1))*(1-
fcov)*epsw*Atot*solarradiation(i,1))/1000;
elseif shadeposition==3
Qs=0;


% Qsnoshade=(1-fcov)*epsw*Atot*solarradiation(i,1)/1000
%kk=1
%sh=shadeindicator(i,1)
% month=shademonth(i,1)
%h=shadehour(i,1)
%d=diffuse_percent(i,1)
%c=cloudness
else
Qs=(1-fcov)*epsw*Atot*solarradiation(i,1)/1000;
end %%Qsolar
%% %%%%%%%%%%%%% Calculation of the supplied heat flow
%%%%%%%%%%%%%%%%%%%%%%Calculation of the required fresh water%%%%%%%
mfr=(mdot_fr+comp_Mv)*dt;
masslossevapation=Mv;
Qzu=mzu*cpw*(Tzu-TB)/1000;
%%%%%%%% Calculation of heat losses by fresh water supply
Qfr=(mdot_fr+comp_Mv)*cpw*(TB-Tfr)/1000.;
%% %%%%%%%%%%%% Heat Balance:
if Heunn==1
TB_a=(mges*TB+mfr*Tfr)/(mges+mfr);
QTERM=-(-Qheater-Qzu-Qs+Qv+Qrd+Qkon);
TB=TB_a-(dt/(mges*cpw)*1000*(-Qheater-Qzu-Qs+Qv+Qrd+Qkon));
TB_H1=TB;
end
sumQ=(-Qheater-Qzu-Qs+Qv+Qrd+Qkon);
Qstore(Heunn,1)=sumQ;
if (Heunn==2) &&(i<n)
Av_slope=(Qstore(1,1)+Qstore(2,1))/2;
Tb_a=TB_a;
TB=TB_a-(dt/(mges*cpw)*1000*Av_slope);
i=i-1;
dtbh1=TB_H1;
heunn_error=(((TB-TB_H1)/TB)*100);
TB_H1=TB;
end
end %%%%%Heunn end 1:2
if (heunn_iter==100);
display(heunn_did_not_converge);
```

```
i=n;
end
heunn_iter=heunn_iter+1;
dispI=i;
end %Heunn loop
TB_m=TB_m+TB;
TBMNOW=TB_m;
Qzu_m = Qzu_m+Qzu;
Qv_m  = Qv_m+Qv;
Mv_m  = Mv_m+Mv;
Qkon_m= Qkon_m+Qkon;
Qrd_m = Qrd_m+Qrd;
Qfr_m = Qfr_m+Qfr;
Qsolar= Qsolar+Qs;
sumQ_m= sumQ_m+ sumQ;
end %%%end k
%display(ip)
Ratemassloss=mdotleakage+Mv;
mchange=(-Mv+mzu)*dt+mfr;
Massloss=((mdotleakage+Mv)*dt)-mfr;%mass loss in a minute(or during
simulation time in minutes if t not 1)
shadestatus(i,1)=shadeposition;
prevshadestatus(i,1)=prev_shadeposition;
thisshadehour=shadehour(i,1);

TB_m  = TB_m/t;
Qzu_m = Qzu_m/t;
Qv_m  = Qv_m/t;
Mv_m  = Mv_m/t;
Qkon_m= Qkon_m/t;
Qrd_m = Qrd_m/t;
Qfr_m = Qfr_m/t;
Qsolar= Qsolar/t;
sumQ_m= sumQ/t;
%%%%%%%%%%%%%%%%%%%%%%%%%%%%%%%%%%%%%%5
if ip==1
TB_ip1=TB;
%TB_m_ip1   = TB_m;
Qzu_m_ip1 = Qzu_m;   Qv_m_ip1 = Qv_m;   Mv_m_ip1   = Mv_m;   Qkon_m_ip1=
Qkon_m;   Qrd_m_ip1 = Qrd_m;   Qfr_m_ip1 = Qfr_m;  Qsolar_ip1= Qsolar;
sumQ_m_ip1= sumQ;
else
TB_ip2=TB;
TB_m_ip2   = TB_m;
%%%%%%%%%%%%%%%%%%%%%%%%%%%%%%%%%%%%%%%%%%%%%%%%%%%%%%%%%%%555
Qzu_m_ip2 = Qzu_m;   Qv_m_ip2 = Qv_m;   Mv_m_ip2   = Mv_m;   Qkon_m_ip2=
Qkon_m;   Qrd_m_ip2 = Qrd_m;   Qfr_m_ip2 = Qfr_m;  Qsolar_ip2= Qsolar;
sumQ_m_ip2= sumQ;
%%%%%%%%%%%%%%%%%%%%%%%%%%%%%%%%%%%%%%%%%%%%%%%%%%%%%%%%%%%%
if ((TB_ip1-TB_ip2)/TB_ip1)*100<0.1
AverageTB=(TB_ip1+TB_ip2)/2;
TB=AverageTB
%%%%%%%%%%%%%%%%%%%%%%%%%%%%%%%%%%%%%%%%%%%%%%%%%%%%%%%%%%%555
Qzu_m=(Qzu_m_ip1+Qzu_m_ip2)/2 ;
Qv_m= (Qv_m_ip1+Qv_m_ip2)/2 ;
Mv_m=(Mv_m_ip1+Mv_m_ip2)/2  ;
Qkon_m= (Qkon_m_ip1+Qkon_m_ip2)/2 ;
Qrd_m= (Qrd_m_ip1+Qrd_m_ip2)/2  ;
Qfr_m=  (Qfr_m_ip1+Qfr_m_ip2)/2 ;
Qsolar= (Qsolar_ip1+Qsolar_ip2)/2 ;
sumQ= (sumQ_m_ip1+sumQ_m_ip2)/2;
```

```
%%%%%%%%%%%%%%%%%%%%%%%%%%%%%%%%%%%%%%%%%%%%%%%%%%%%%%%%%%%%%%%%%%%%%%%%
else
ip=1;
end %%TB OF IP CONVERGED
end
end%%%%end averge ip
end %%% end of ip

%Calculation of the difference of the stored energy
DE=mges*cpw*(TB-TB_0);
%%%%%%%%%%5The storage temperature is place into the storage array%%% -----
------------------------------
STORE1=TB;
STOREMATRIX_TB(i,1)=STORE1;
STORE3=TSI;
STORE4=TSO;
STOREMATRIX_TSI(i,1)=STORE3;
STOREMATRIX_TSO(i,1)=STORE4;
%end
OUT1(i,1)= TB_m;
mges=mges-Massloss;
newdepth=mges/(row*Atot);
Pool_Depth(i)=newdepth*10;
%%%%%%%
%%%This output averaged over number of minutes in t , in our case t=1Qin
kj/s and Mv in kg/s
OUT_TB(i,1)= TB_m;
%OUT_Qzu_m = Qzu_m;
OUT_Qv_m(i,1)   = -Qv_m;
OUT_Mv_m(i,1)   = Mv_m;
OUT_Qkon_m(i,1)= -Qkon_m;
OUT_Qrd_m(i,1) = -Qrd_m;
OUT_Qfr_m(i,1) = Qfr_m;
OUT_Qsolar_m(i,1)= Qsolar;
OUT_sumQ_m(i,1)=-sumQ_m;
end%%%%if i<n
end
Tfinal=TB;
deltaT_Day=TB-TB_0;
Q_kw_Day=(mges*cpw*deltaT_Day);
Q_KwperM2_Day=Q_kw_Day/Atot;
%% %%%% PLOT
if (u>=n)%%%to be able to plot last data
u=n-1;
end
s=mindiff;
subplot 132
grid on
grid MINOR
hold on
set (gca,'fontsize',18,'fontname','arial')%,'ylabel','Rotation',0)
plot(tw(s:u),OUT_Qv_m(s:u),'DatetimeTickFormat','MMM d@ HH','r-')
hold on
plot(tw(s:u),OUT_Qkon_m(s:u),'DatetimeTickFormat','MMM d@ HH','c-')
hold on
plot(tw(s:u),OUT_Qrd_m(s:u),'DatetimeTickFormat','MMM d@ HH','m-')
hold on
plot(tw(s:u),OUT_Qsolar_m(s:u),'DatetimeTickFormat','MMM d@ HH','y')
hold on
plot(tw(s:u),OUT_sumQ_m(s:u),'DatetimeTickFormat','MMM d@ HH','g')
hold on
```

```
legend('Qevp','Qconv','QLWrad','QSWrad','sumQ','orientation','horizontal');
Titleform=['Simulation of DCS heat flows for',period, mode];
%Titleform=['Simulation of DCS heat flows for',period,'with Const DeltaT'];
title(Titleform);
xlabel('Date-time');
ylabel('Q,Heat flow rate (kW)');
tw1=exceltime(tw) ;
subplot(133)
grid on
grid MINOR
hold on
set (gca,'fontsize',18,'fontname','arial')%,'ylabel','Rotation',0)
plot(tw(s:u),STOREMATRIX_TB(s:u),'DatetimeTickFormat','MMM d @HH ','bo')
hold on
plot(tw(s:u),Ta(s:u),'DatetimeTickFormat','MMM d @HH ','g')
hold on
plot(tw(s:u),STOREMATRIX_TSI(s:u),'DatetimeTickFormat','MMM d @ HH a','Y')
hold on
plot(tw(s:u),Pool_Depth(s:u),'DatetimeTickFormat','MMM d @HH ','c')
hold on
plot(tw(s:u),shieldstatus(s:u),'DatetimeTickFormat','MMM d@ HH ','r-')
hold on
legend('Tsim','Ta(ws)','TSI','Pool
Depth(mx10)','Shieldstatus','orientation','horizontal');
Titleform=['Simulation of DCS Temperature:',period,' with Const',mode];
title(Titleform);
xlabel('Date-time');
ylabel('Temperature (C)');
%% %%%%%%%%%%%%%%%%%%%%Results
Hfinal=mges/(row*Atot);
if (shadeposition>0) &&(i<n)
shadestatus(i)=shadeposition;
prevshadestatus(i)=prev_shadeposition;
thisshadehour=shadehour(i,1);
display(All_icheck_converge(1:count_converge,1:coeff));
if (count_converge>400)
display Coefficients_did_not_converge_after_400_iterations
else
display count_converge_is ;display(count_converge);
end
display ErrorAnalysis:
Matrix_count_converge=count_converging;
Maximum_converge=max(count_converging);
Mod_Matrix_count_converge=Matrix_count_converge(Matrix_count_converge>0);
Mod_Average_converge=mean(Mod_Matrix_count_converge);
Max_error=Store_Max_i_error;
Avg_error=Store_avg_error/count_error;
countofLoop_error=count_error;
checking_iofn=iofncheck;
Mod_Average_converge=mean(Mod_Matrix_count_converge);
end
```

A.1.3: Program sub functions:

A.1.3.1: Qradiation function:

```
function[qr_shade,qr_pool,Js,Jp,rad_b1,rad_b2]=New_Qrad_Fps(TB,TSI,TGr,Tsky
,Atot,Ashade,epsw,eps_shadein,F_poolshade)
L=4;
W=3.3;
R=1.83;
Cs=5.67*10^-8;
%%%%%%%%%%%%%%%
Esi=Cs*(TSI)^4;%%%%Eb1
Ep=Cs*(TB)^4;%%%%Eb2
Esky=Cs*(Tsky^4);%%%%Eb3
Egr=Cs*(TGr)^4;%%%%Eb3
%%%%%%Shape factors%%%%%%%
F_shadepool=F_poolshade;
F_poolsky=1-F_poolshade;
F_shadeground=1-F_poolshade;
%%%%%%%Resistance
Rsurface_shade=(1-eps_shadein)/(eps_shadein*Ashade);%Surface resistance of
shade
Rsurface_pool=(1-epsw)/(epsw*Atot);%Surface resistance of shade
Rspace_poolshade=1/(Atot*F_poolshade);
Rspace_shadepool=Rspace_poolshade;
Rspace_poolsky=1/(Atot*F_poolsky);
Rspace_shadeground=1/(Ashade*F_shadeground);
 %%%%%%%Cramer's solution%%%%%%%%
alpha1=Rsurface_shade;
beta1=Rspace_shadeground;
gamma1=Rspace_poolshade;
alpha2=Rsurface_pool;
beta2=Rspace_poolsky;
gamma2=Rspace_poolshade;
a11=(1/alpha1)+(1/beta1)+(1/gamma1);
a12=-(1/alpha1);
rad_b1=(Esi/alpha1)+(Egr/beta1);
a21=(-1/alpha2);
a22=(1/alpha2)+(1/beta2)+(1/gamma2);
rad_b2=(Ep/alpha2)+(Esky/beta2);
cramer_Js=((a22*rad_b1)-(a12*rad_b2))/((a11*a22)-(a12*a21));
cramer_Jp=((a11*rad_b2)-(a21*rad_b1))/((a11*a22)-(a12*a21));
A=[a11,a12;a21,a22];
AINV=A^-1;
ainv=inv(A);
size(AINV);
B=[rad_b1;rad_b2];
Jmatrix=AINV*B;
qr_shade_cramer=((Esi-cramer_Js)/Rsurface_shade)
qr_pool_cramer=(cramer_Jp-Ep)/(Rsurface_pool)
qr_shade_matrix=((Esi-Jmatrix(1,1))/Rsurface_shade)
qr_pool_matrix=(Jmatrix(2,1)-Ep)/(Rsurface_pool)
qr_shade=qr_shade_cramer;
qr_pool=qr_pool_cramer;
%qr_pool=qr_pool_matrix
Jp=cramer_Jp;
Js=cramer_Js;
Tshieldinside=TSI;
display(TSI);
```

A.1.3.2: Property functions:

Thermal Diffusivity:

```
function [alpha]=Thermal_Diffuisivity(T)

alpha=(1.8843*10^(2)+1.2789*T+1.7619*10^(-3)*T^2)*10^(-7)
end
```

Saturation pressure:

```
C1=6.1087;
C2=17.08085;
C3=234.175;
psaturated=C1*exp((C2*T)/(C3+T));
```

Density of Humid Air:

```
function
[density_HumidAir]=Density_Humid_Air(T,humidity_percent,psaturated)
Rw=461.5 ;
patm=1.013e5;
xh=humidity_percent/((patm/psaturated)-humidity_percent);
density_HumidAir =patm/(Rw*(T+273.15))*(xh+1.6077)/(xh+1.);
end
```

Enthalpy of Evaporation:

```
function [deltahv]=delhv(T)

deltahv=(2.5006*10^(3)-2.366*T)*1000;
```

Kinematic Viscosity:

```
function [Visco]=Kinematic_Viscosity(T)

Visco=(1.3505e-5+9.06524e-8*T+8.09524e-10*T^2);
End
```

Diffusion Coefficient :

```
function [D]=Diffusion_Coeff(T)

D=1.179968*10^-9*(T+273.15)^1.75;
End
```

A.1.4: Program input functions:

A.1.4.1: Weather and shade indicator input function:

```
function[tw,sizecheck_diffuse_percent,diffuse_percent,nrun,shadeday,shademo
nth,shadehour,shadeindicator,weather,windspeed,datetimenum,Ta,humidity,sola
rradiation]=Shade_weather_Run_10_18April2017_shadeup
fid = fopen('Weather(10-18April)shadeup.CSV');
readdata=textscan(fid,'%s %f %f %f %f %f
%f','headerlines',1,'delimiter',',');
%%%%%%%%%%%%%%%%%%%%Extract Data from readdata%%%%%%%%%%%%%5
Datetime=readdata{1};
windspeed=readdata{3};
Ta=readdata{4};
humidity=readdata{5};
solarradiation=readdata{6};
% check=solarradiation(326:400)
 datetimenum=datenum(Datetime,'dd/mm/yyyy HH:MM:SS');
nrun=length(datetimenum);
shadehour=hour(datetimenum);
shademonth=month(datetimenum);
shadeday=day(datetimenum);
[sizecheck_diffuse_percent,diffuse_percent]=diffuse_k(shademonth,shadehour,
nrun);
shade_month_ith=shademonth(nrun,1);
[shade_begin,shade_end]=shade_hour(shade_month_ith);
for i=1:nrun
if (shade_end>shadehour(i,1) && shadehour(i,1)>shade_begin)
shade=1;
else
shade=0;
end
shadeindex(i,1)=shade;
end
shadeindicator=shadeindex;
shade_size_check=size(shadeindicator);
weather=[datetimenum,Ta,windspeed,humidity,solarradiation];
fclose(fid);
solarradiation_plot=solarradiation/10
tw=datetime(Datetime);
subplot(131)
start=1
u=nrun
grid on
grid MINOR
hold on
set (gca,'fontsize',18,'fontname','arial')%,'ylabel','Rotation',0)
plot(tw(start:u),windspeed(start:u),'DatetimeTickFormat','MMM d @ HH ','k-
')
hold on
plot(tw(start:u),Ta(start:u),'DatetimeTickFormat','MMM d @HH','g--')
hold on
plot(tw(start:u),humidity(start:u),'DatetimeTickFormat','MMM d@HH ','m-')
hold on
plot(tw(start:u),solarradiation_plot(start:u),'DatetimeTickFormat','MMM
d@HH','y-')
hold on
legend('Windspeed(m/s)','Temperature(C)','Humidity(%)','Solarradiation(W/m2
)x10','orientation','horizontal');
xlabel('Date-time');
ylabel('Weather data');
```

A.1.4.2: Measured pool temperature input& calibration function:

```
function[tpw,recordstarttoend,recorddatetimenum,t1,t2,t3,t4,t5]=poolweather
_Run_10_18April2017_shadeup_graph
clc
%%%%%%%%%%%%%%%%open weather data File%%%%%%%%%%%%%%%%%%%%%%%%%%%%
fid =fopen('Record_10_18April_shadeup.csv')
readdata=textscan(fid,'%s %s %s %f %f %f %f
%f','headerlines',1,'delimiter',',');
%%%%%%%%%%%%%%%%%%%%Extract Data from readdata%%%%%%%%%%%%%5
recorddatetimestring=readdata{3};
ncheck=size(recorddatetimestring);
slope1=0.7943;slope2=0.7887;slope3=0.7922;slope4=0.7867;slope5=0.7939;
intercept1=2.7968;
intercept2=3.0123;intercept3=2.9826;intercept4=2.8241;intercept5=3.0158;
t1=(readdata{4}*slope1)+intercept1;
t2=(readdata{8}*slope2)+intercept2;
t3=(readdata{5}*slope3)+intercept3;
t4=(readdata{6}*slope4)+intercept4;
t5=(readdata{7}*slope5)+intercept5;
recorddatetimenum=datenum(recorddatetimestring,' dd/mm/yyyy  HH:MM:SS')
recorddatetimenumbegin=recorddatetimenum(1:30);
checkdatebegin=datestr(recorddatetimenumbegin);
checkdatemiddle=round(ncheck/2);
recorddatetimenummiddle=recorddatetimenum((checkdatemiddle-
10):checkdatemiddle);
checkdatemiddle=datestr(recorddatetimenummiddle);
recorddatetimenumend=recorddatetimenum((ncheck-10):ncheck);
checkdateend=datestr(recorddatetimenumend);
sizerecorddatetime=size(recorddatetimenum);
%recorddatetimestring=datestr(recorddatetime)
%datetime=datestr(datenum(Datetime,'dd.mm.yyyy HH:MM:SS'))
%weather=[datetimenum,Ta,windspeed,humidity,solarradiation]
fclose(fid);
recorddatetimestring1=datestr(recorddatetimenum);
n1=length(recorddatetimestring1);
n=length(recorddatetimestring);
sizedatetimestring=size(recorddatetimestring);
sizedatetimestring1=size(recorddatetimestring1);
recordstartdatetime=recorddatetimestring1(1,1:20);
recordenddatetime=recorddatetimestring1(n1,1:20);
%recordstarttoend=[recordstartdatetime,' till ',recordenddatetime,'-
(Shadeup)']
recordstarttoend=[recordstartdatetime,' till ',recordenddatetime];
tpw=datetime(recorddatetimestring,'Inputform','dd/MM/yyyy HH:mm:ss')
plot(tpw,t1,'DatetimeTickFormat','MMM d  @H a','r-')
plot(tpw,t2,'DatetimeTickFormat','MMM d @ H a','b-')
hold on
      %
```

A.1.4.3: Diffuse% for Month and hour of the day input function:

```
Function[sizecheck_diffuse_percent,diffuse_percent]=diffuse_k(shademonth,sh
adehour,nrun)
fid =fopen('Diffuse.csv');
readdata=textscan(fid,'%f %f %f %f %f %f %f %f %f %f %f %f
%f','headerlines',1,'delimiter',',');
for month=1:13
prep=cell2mat(readdata(month));
diffuse(:,month)=prep;
end
for month=1:12
for hour=1:24
lastdiffuse(month,hour)=diffuse((hour+1),(month+1));
end
end
for d=1:nrun
checkmonth=shademonth(d);
checkhour=shadehour(d);
if checkhour~=.0
checkdiffuse=lastdiffuse(checkmonth,checkhour);
diffusematrix(d)=checkdiffuse;
else
diffusematrix(d)=0;
end
end
diffuse_percent=transpose(diffusematrix)/100;
sizecheck_diffuse_percent=size(diffuse_percent);
```

A.1.4.4:Shade begin and end from sun path diagram input function:

```
function[shade_begin,shade_end]=shade_hour(shade_month_ith)
fid =fopen('shade_hour.csv');
readdata=textscan(fid,'%f %f %f %f %f %f %f %f %f %f %f
%f','headerlines',1,'delimiter',',');
for month=1:12
prep=cell2mat(readdata(month));
sh_hour(:,month)=prep;
size(sh_hour);
end
for month=1:12
shadebegin(month)=sh_hour(1,month);
shadeend(month)=sh_hour(2,month);
end
for d=1:12
checkmonth=shade_month_ith;
if checkmonth==d;
shade_begin=shadebegin(d);
shade_end=shadeend(d);
end
end
```

A-2: Program flow description:

A-2.1: Pool function Flow Description:

After reading constants and variable initialization, the program starts reading the measured weather data every minute as a function of time of the day from a separate function "The weather data function", creating the weather data matrix. The weather data function also gathers input from two other functions, the "Diffuse-K" function and the "shield hour" function. The diffuse function inputs the diffuse versus beam % of measured radiation as obtained from previous research on radiation over Cairo (Robaa 2006), while the shield hour function obtains information from the sun path diagram on the hour where the shading of beam radiation over the pool begins and the hour at which it ends, giving a shield indicator of zero or one to be used later in case of shield upper position. In between those hours, the beam radiation could enter certain area of the pool according to the shield position as explained earlier in the solar gain section. Then the main loop of the program starts for n number of runs, where n equals the number of minutes in the weather data file for this run. Inside the main loop, there is another loop for the number of minutes in a simulation time step t (in case different than a minute). In case the simulation time step in minutes is different from the frequency at which the data is read, the bigger loop needs to be adjusted accordingly to read the relevant weather data for the simulation time step.

Inside the main loop, heat flow rates into and out of the pool are calculated, whether losses due to convection, evaporation, long wave radiation or heat gains from short wave solar radiation and electric heating. Conduction losses to the ground and to side walls are neglected.

At the end of every loop, heat balance equation ($mc_p dT/dt = \sum Q$) is applied to calculate the change in temperature over the time of the loop (dt=60seconds) and the temperature of the pool at the end of the loop minute becomes the initial temperature of the next loop. An average of all calculated values of heat flows and pool temperature is calculated every loop, which would be more useful in case simulation time is different than a single minute. The change in internal energy is also calculated. Figure 4-4 and Figure 4-5 illustrate the method of solution of the shield upper and lower positions.

There are 4 main loops in the program as follows:

1) Weather data loop (i=1: n): This is the first loop that reads the i^{th} value of ambient temperature , humidity , wind speed and global radiation from the weather data matrix generated by the weather data function This loop is followed by :
2) Pool temperature convergence and averaging loop (ip=1:2 ,if not converged ip is set back to 1): This is the loop that provides an average of at least two calculated values of pool temperature after checking that the values converged to less than 0.1% error.
3) Main interval calculation loop (k=1 to t): This is the main interval calculation loop for every interval of time t, where t is the number of minutes in a loop, currently one minute is used. If different than a minute, the heat flow and temperature are calculated every minute, then averaged. Inside this loop is the Heun's loop
4) Heun's loop(Heun=1:2): The main calculation loop is executed twice every minute to get an average slope (which is the sum of heat flow in our case) at the beginning and end of the minute, this slope is then used to calculate the pool temperature from the value calculated in the previous time step.

The main interval calculation loop starts by:

a) Shield position:

Determining whether there is a shield or no shield as a function of the hour of the day, placing a shield from 9am to 5 pm to avoid the sun from entering the pool during the hottest parts of the day and exposing the pool to the night time sky to cool down by radiation exchange to the cold sky. It is possible to relate placing the shield to sun rise and sun set according to the day of the month, however for practicality the time is fixed to the "7 to 7" interval, after which the shield pool is removed. During the day and between those times, the shield is placed in the upper position if the ambient air temperature is less than the pool temperature by 5 degrees (to benefit from cool convection currents), otherwise it is placed in the lower position right above the pool.

In the model, shield positions are assigned values between 0 and 4, with no shield position reference value of 0, experimental upper shield position a value of 1 , experimental lower shield position value of 2, ideal lower shield position with a value of 3 and finally ideal upper shield position a value of 4.

b) Heun's first loop starts by looking at the shield position and calculating heat flows as follows:

Radiation heat flow:

If shield position is greater than zero, that means the shield is installed (position 1, 2, 3 or 4) . For the upper position (1 and 4), the program starts to calculate the radiation heat loss for the relevant position by preparing the coefficients of the two heat balance equations for the inside and outside of the shield by using the previous values of TSO and TSI (or initial for the first loop) , then calculating Js and Jp performing the resistance network method in a separate function called Qrad that is called for the first time to output both values(Js and Jp only) to be used in calculating TSI and TSO to get Esi and Eso . Esi and Eso are then returned back to the Qrad function as inputs to recalculate the radiation heat flow of the pool and shield, Js , Jp and the radiation equations coefficients b1 and b2 needed to solve the heat balance equations.

The six variable coefficients are then checked for convergence and the while loop is then repeated until the values converge to less than 0.1%. The equations are solved using Cramer's rule as explained in Figure 4-4 .Figure 4-5 illustrates the procedure for the shield down position (2,3).

Else if shield position is zero, long wave radiation heat flow is calculated using the simple equation for no shield as explained earlier in the mathematical model. The split between diffuse and beam radiation obtained from (Robaa 2006) is also used as a measure of cloudiness that is used by the model to reflect the impact of the existence of clouds on the sky temperature used to calculation night time sky radiation losses.

Evaporation and convection heat flows are then calculated as follows:

Shield lower position

Heun's first loop starts by looking at the shield position and calculating evaporation and convection for either the ideal shield position 3, assuming free convection only as explained in the mathematical model or for the experimental shield position 2 with Richardson number as the defining criteria for the type of flow, being free, forced or mixed. Sherwood number is then calculated, followed by the mass transfer coefficient, evaporation mass flow rate and then evaporation heat flow. Heat transfer coefficient is then calculated from Reynolds –Colburn analogy that links both coefficients.

Shield upper position and no shield:

The calculation of mass and heat transfer coefficients are calculated in the same manner for shield up and No shield positions, with two empirical formulas as function of wind speed, followed by evaporation and convection heat flow as well as mass flow of evaporation.

Direct solar gain:

Direct solar gain is then calculated for different shield positions. The No shield position is normally not applicable when the sun is up, however it is bound to happen during long weekends when the system is not operating. In this case, the whole area of the pool receives radiation.

As for the shield upper and lower positions, the global radiation obtained from the weather data function is split into diffuse and beam using the diffuse function as obtained from previous research on radiation over Cairo(Robaa 2006) .It is assumed that 30% of the diffuse radiation enters the pool in the shield upper position for both the experimental and ideal model , while 10% in the shield experimental lower position and zero % in the ideal lower position. As for the beam radiation, it should not enter the pool in both cases, however during the experimental work, the shield upper position allowed part of the beam radiation to enter which had to be reflected in the model. For the experimental shield upper position, the shield hour function obtains information from the sun path diagram on the hour where the shading of beam radiation over the pool begins and the hour at which it ends, giving a shield indicator of zero or one. In between those hours, the beam radiation enters certain area of the pool and is multiplied by a percent area obtained from experimental work as a function of the hour.

c) Heun's method application:

Heun's method is then applied by calculating the pool temperature (TB) if Heun's loop is equal 1, the sum of heat flows that represents the first derivative is then calculated and stored to be used in the second loop (where Heun's equals two) to get the average slope and recalculate TB using the initial pool temperature TB-a at the start of the main program loop(k loop) as well as the average slope. It is important to note that the boundary conditions represented in the weather data for the first loop were taken from i^{th} value of the weather matrix, while for the second loop, i was taken as i+1 in order to pull the weather data at the end of the calculation interval. This had to be reversed at the

end of Heun's loop for the next iteration. Heun's loop is then repeated until the pool temperature value converges to less than the specified error (0.1%).
Now the main calculated loop is repeated at least twice (ip=1:2) while checking for convergence of the pool temperature to less than 0.1%. In case the pool temperature converged, an average of the two loops is obtained, otherwise, ip is set back to 1, thus the pool averaging loop (ip) is repeated till the convergence criteria is satisfied (or maximum number of Heun's iterations are reached). The average pool temperature is then reported back to the outer most loop to become the input to the next iteration pulling the next weather data i^{th} value from the weather matrix.

A-2.1: Main Functions Descriptions:

Radiation exchange with the sky:

For the shield up position radiation losses are calculated with a separate function , Qrad_Fps that uses radiation network method as per Holman (Holman, J.P. and White 1992) to solve two equations for radiation exchange between the pool, shield inside, ground and sky.

Shape factors are input into Qrad_FPS function as 0.55 for shield upper postion (position 1 and 4). Listed below is the function header in MATLAB code with its inputs and outputs for its second call.

```
[qr_shield,qr_pool,Js,Jp,rad_b1,rad_b2]=New_Qrad_Fps(TB,TSI,TGr,Tsky(i,1),A
tot,Ashield,epsw,eps_shieldin,F_poolshield)
```

Shading Hour from sun path diagram*:*

This function builds the matrix that has the beginning and the end of shield hour for every month of the year by reading it from Excel sheet.
This function is called by another function," shield_weather_run" of the relevant weather data file. The later function provides the shield month input to the shield hour function after reading it from the weather file and also includes its results of shield begin and end to create a shield indicator matrix for every entry in the weather data that is included among its outputs to be transferred to the main body of the program. This function is called by the following code:
[shield_begin,shield_end]=shield_hour(shield_month_ith);

Function Name: *shield_hour*

Input:
1) *shield_month_ith:* This is the month matrix read from the weather data file by the,"shield_weather_run"
Output:
shield_begin: The shield beginning as input from the sun path diagram into the excel sheet.
shield_end: *The shield end as input from the sun path diagram into the excel sheet.*

```
function[shield_begin,shield_end]=shield_hour(shield_month_ith)
```

Diffuse% for every month and hour of the day:

Description:

This function creates diffuse % matrix for every entry in weather data according to month and day; as if there is an additional column in weather data.
This function is called by another function,"the shield_weather_run" of the relevant weather data file. The later function provides the weather data input to the diffuse_k function after reading it to the weather file and also includes its results in its outputs to be transferred to the main body of the program. This function is called by the following code:

```
function[sizecheck_diffuse_percent,diffuse_percent]=diffuse_k(shieldmonth,s
hieldhour,nrun)
```

Function Name: diffuse _K
Input:
1)shieldmonth: the month of every entry in the weather data files
2)shieldhour: the hour of each row in the weather data file
3)nrun: the length of the weather data file(ie: the number of rows)

Output:
diffuse_percent: This is a diffuse % matrix that indicates the diffuse percent of every entry in the weather data file. This is used in the shield up position to calculate the amount of beam radiation the shield is hiding every hour of the day.
sizecheck_diffuse_percent: This is just a check the diffuse % matrix is the same size of the length of weather data. This output is optional.

Shield Weather Run:

This function does three main tasks:

1- Reads the weather data file to be used by the main program. Provides these weather data for two sub functions inside it, diffuse K and shield hour.
2- Uses the shield begin and end output of the shield hour to create the shield indicator matrix for every entry in the weather data and passes on this information along with the diffuse% matrix it obtained from the diffuse k function to the main program.
3- Plots the weather data.

The function is called by then following code

```
[sizecheck_diffuse_percent,diffuse_percent,nrun,shieldday,shieldmonth,shiel
dhour,shieldindicator,weather,windspeed,datetimenum,Ta,humidity,solarradiat
ion]=Shield_weather_Run_26April_7May_shielddown
```

Function Name: `Shield_weather_Run_(datafilename)`

Output*:*

weather,windspeed,datetimenum,Ta,humidity,solarradiation: These are all weather data read from the weather file. Weather output has all the five-weather data combined in one matrix.

nrun,shieldday,shieldmonth,shieldhour,shieldindicator: They are all outputs related to the shield up position indicating the length of the weather run ,the day , month and hour in the data weather date

field and finally the shield indicator for every hour of the run being zero before the shield begins and one after the shield ends as obtained from sun path diagram.

diffuse_percent& sizecheck_diffuse_percent: This is a diffuse % matrix that indicates the diffuse percent of every entry in the weather data file. This is used in the shield up position to calculate the amount of beam radiation the shield is hiding every hour of the day. This size check is just a check that the diffuse % matrix is the same size of the length of weather data. This output is optional.

Short Wave Radiation Exchange with the Sky:

Shielded Pool:

Since the solar radiation incident on any surface is composed of both beam and diffuse radiation, with the shield aiming to block most of the beam part, it was necessary to differentiate between both parts for every hour of each day of the year. A study done on solar radiation in Cairo provided details on its components and the diffuse fraction of it. The work was based on actual measurements on horizontal surface of hourly global and diffuse radiation from 1992 till 2003. The annual average diffuse percent (Kd) of the global radiation was found to be 35%, with this value changing according to cloudiness and the quality and quantity of particulate matter in the atmosphere. The diffuse percent (Kd) for a cloudless sky was found to change for every hour of the day, starting with highest values at sun rise and decreasing to the minimum at noon, then increasing back to almost the same value it started from at sunset. Of course, the value depended also on the month of the year, so for every hour of the day in every month of the year, the study reported a diffuse percent that could be used based on the 12 years measurements collected. This information was necessary for modeling the deferred cooling system, since the weather station used in our study, provided global radiation measurements every minute, while the shield could only aim at blocking the beam part. Since global radiation is maximum around noon (averaging from a minimum of 1.48 MJ/m^2 at noon in December to a maximum of 3.39 MJ/m^2 in June) and minimum at sun rise and sunset in a nearly symmetrical way, it was clearly necessary to block the beam radiation close to noon that has the maximum energy that could heat up the pool. (Robaa 2006)For example, since only around 20 percent of solar radiation in June at noon is diffuse and this is when global radiation is reported to be maximum , we are more concerned in blocking the beam part of radiation around noon , than blocking either diffuse radiation around that hour or beam radiation at early or late hours of the day.

When the shield is in the lower position, touching the pool side edges, with an air gap between the shield lower surface and the pool water surface, the beam radiation is completely blocked and only an insignificant part of the diffuse radiation makes it to the pool surface.

Appendix B: Numerical Model Adjustments to Match Experimental Setup

B.1: Short wave radiation gain model adjustment for shield upper position:

Due to an imperfection in the shield design, solar beam radiation made it in the gap between the pool rim and the shield in the experimental setup. The % area of the pool that absorbed the beam radiation measured is estimated and input to the adjusted numerical model to be used when comparing results from the model with experimental results. The % area estimation is based on the following experimental observations as per Figure B-1 and Figure B-2.

Sun 's image inside pool in the shield upper position and estimation %A beam entering the pool:

(a)

Sun Image-Shade up@10:00-Nov15th 2017 A sun image-35-%(-34°ys ,32 °Θs)

Shade from east and south are starting to separate at the edge of the pool and crescent area is decreasing to around 30% of Pool area

(b)

Sun Image-Shade up@11:00-Nov15th 2017 A sun image-15-%

Shade from east and south are separated , east image starting to reduce as sun moves more to the south (towards zero azimuth) , overall sun image in pool declining to around 15%

(c)

Sun Image-Shade up@11:15-Nov15th 2017 A sun image-13-%

Image from east side starting to disappear as sun moves more to the south (towards zero azimuth) , sun image reducing further to around 13%

(d)

Sun Image-Shade up@12:00-Nov15th 2017 A sun image-12-%(0°ys ,41°Θs)

Image from east side completely disappeared as sun passed zero azimuth, image from west side starting to appear , while image from south still there , sun image around 12%

(e)

Sun Image-Shade up@12:30 to 14:00 - Nov15th 2017 A sun image-13-%

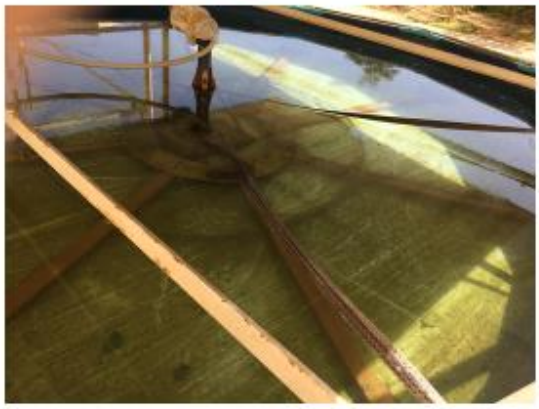

At 12: 30 Image from west side increasing , sun image around 20%

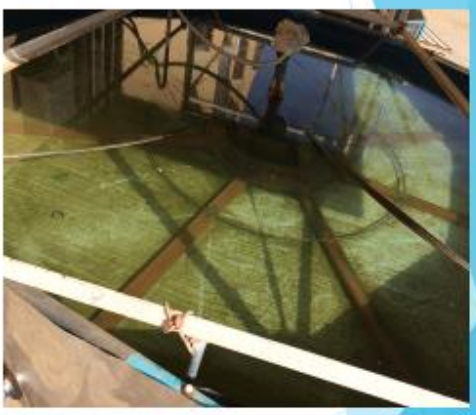

At 14: 00 Image from west side continue to increase as azimuth angle increases and areas from west and south join to make a big crescent from the opposite west side as opposed to early morning , sun image around 40%

(e)

Sun Image-Shade up@14:15 to 15:15- Nov15th 2017 A sun image

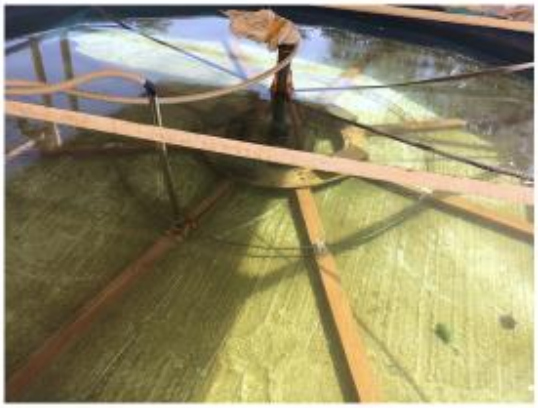

At 14:15 Image from west side increasing further , sun image around 50%

At 15:15 Image from west side still increasing and passing the center of the pool , sun image around 70%

(f)

(g)

Figure B-1:Sun's image on the pool surface in November at different time of the day

Area Estimation:

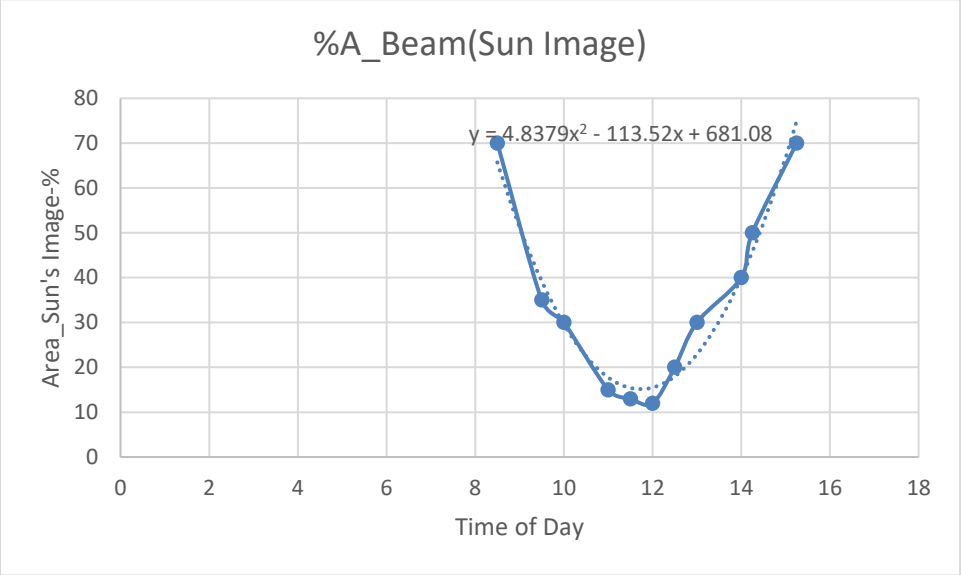

Figure B-2: %A Beam (sun's image) versus time of the day for November 14th

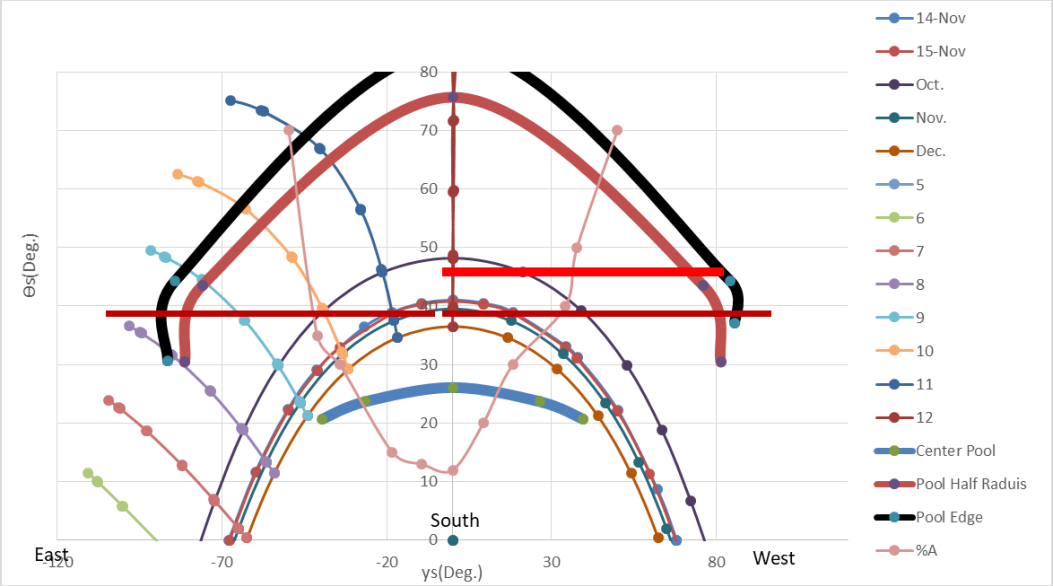

Figure B-3: %A Beam versus time of the day for November 14th on Cairo's sun path diagram,

Figure B-3 shows %A Beam (sun image) versus time of the day for November 14th on the sun path diagram, showing Month of October and November and reflecting 3 lines in the center and middle and edge of the pool.

It is clear that the %A and the shape of the images in appendix B, depend on:

1-The dimensions and the shape of the shield and pool.

2-The sun path at the relevant day of the month that is the altitude and the azimuth of the sun.

3-The obstacles, buildings and trees around the pool.

Commercial programs are available that could draw the sun image in the pool and estimate the area of the beam‘s image of the pool. For the sake of the program the percentage area was determined from observation that accurately represented the period of the month. Ideally, the shield should block the beam radiation from entering the pool by extending to the sides, however this was not possible in the experimental set up, so the estimated area would differ if the set up was different. Further development of this program could include that part into Matlab code with respect to dimensions of the pool and sun path, however as explained earlier the aim is to block the beams for the deferred cooling system, that is why it was not embedded in the code of this study.

B.2: Evaporation and convection estimation for the experimental lower shield position:

Due to a manufacturing error that led to the presence of unintended gap between the pool rim and the shield in the experimental set, air infiltration occurred, and convection and evaporation differ from the theoretical model that had to be adjusted when comparing results from the model with experimental results

Measuring wind % under the shield relative to free stream:

Wind under shield versus free stream speed (Average 12%):

Table B-1: Wind speed measured under the shield as compared to free stream wind.

Date/ Time	Wind Below Shield(m/s)	Free stream wind(m/s)	%wind
12/3/17 14:36	0.06	0.4	0.14
12/3/17 14:37	0.04	0.4	0.10
12/3/17 16:04	0.02	0.2	0.10
12/3/17 16:05	0.03	0.2	0.13
12/4/17 14:24	0.12	0.8	0.15
12/4/17 14:25	0.10	0.5	0.20
12/4/17 14:26	0.01	0.7	0.02
12/4/17 14:27	0.12	0.7	0.17
12/4/17 14:28	0.03	0.6	0.04
12/4/17 15:15	0.06	0.2	0.30
12/4/17 15:16	0.16	0.6	0.26
12/4/17 15:17	0.09	0.3	0.29
12/4/17 15:18	0.01	0.4	0.03
12/4/17 16:48	0.01	0.3	0.03
12/4/17 16:49	0.05	0.5	0.10
12/5/17 11:32	0.07	0.6	0.12
12/5/17 11:33	0.10	0.7	0.14
12/5/17 11:34	0.03	0.2	0.17
12/5/17 11:35	0.04	1.1	0.04
12/5/17 13:47	0.06	0.7	0.08
12/5/17 13:48	0.06	0.8	0.07
12/5/17 13:49	0.08	0.9	0.09
12/5/17 15:05	0.08	0.8	0.10
12/5/17 15:06	0.07	0.7	0.10
12/5/17 15:07	0.14	0.7	0.20
12/5/17 15:08	0.11	0.7	0.16
12/5/17 15:09	0.05	0.6	0.08
12/10/17 14:43	0.06	0.9	0.07
12/10/17 14:44	0.05	0.8	0.06

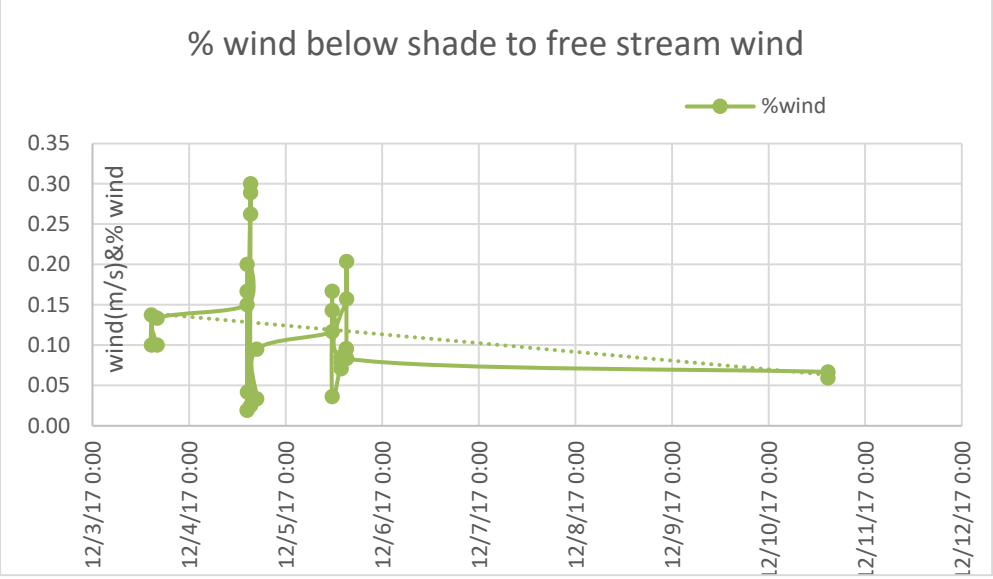

Figure B-4: Percent wind speed measured under the shield as compared to free stream wind.

Table B-2: Wind speed measured under the shield as compared to free stream wind for a windy day.

Date/ Time	Wind Below Shield(m/s)	Free stream wind(m/s)	%wind
12/13/17 16:09	0.19	0.8	0.23
12/13/17 16:10	0.20	0.7	0.28
12/13/17 16:11	0.19	0.9	0.21
12/13/17 16:12	0.20	1	0.20

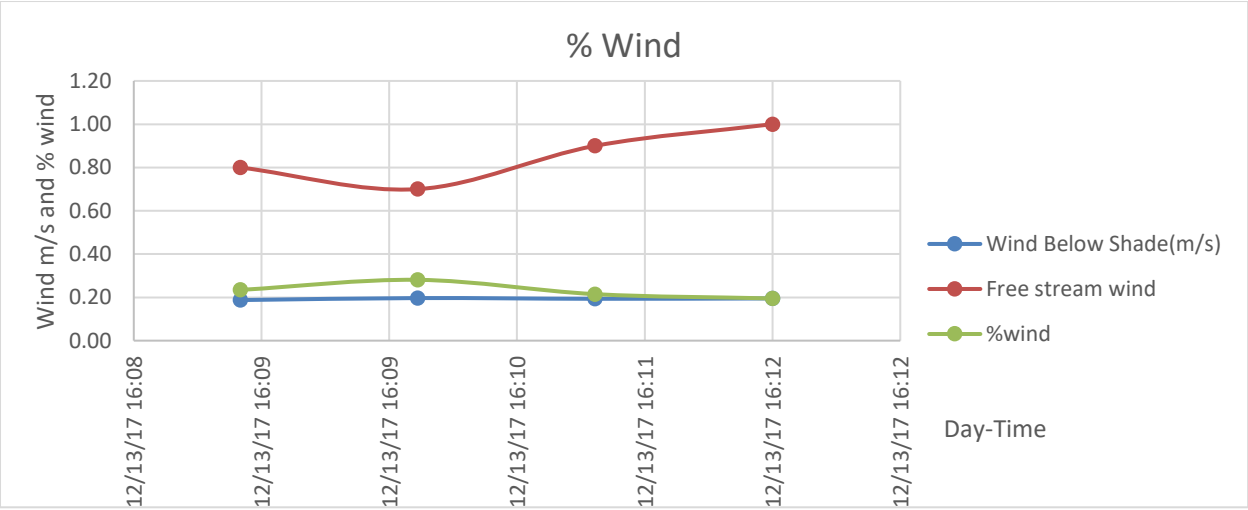

Figure B-5: Wind % measured under the shield as compared to free stream wind.

Experimental shield lower position:

1-If the ambient Temperature is the same as the temperature of water surface (Ta=Tpool), air reaches saturation with moisture content as it touches the pool surface. Moist air, being lighter, creates convection currents when it moves upward due to the effect of buoyancy with drier heavier air from above replacing it. (Shah 2008)

2-If the ambient temperature is less than the temperature of the pool(Ta<Tpool), the buoyancy effects are higher because air is heated when it touches the surface of the pool making the density increase greater than the first case and thus natural convection is even stronger. (Shah 2008)

3-If the ambient temperature is greater than the temperature of the pool (Ta>Tpool), natural convection has much less effect due to the heat loss by air at the pool surface. Saturation will occur at the temperature of the pool surface with lower density difference between the moist air at the surface and the drier air above it. (Shah 2008)

a) If the density difference are less than or equal 0.02, the sideways air movements and stray currents are more pronounce in transferring heat than natural convection. The density of humid air is calculated at the pool surface temperature (Shah 2008)

b) In the case when density of ambient air is less than the density of saturated humid air at the surface, mostly when the pool temperature is much less than the ambient, Gr number and Ri number consequently are less than zero, the heat transfer profile could be estimated by that of the bottom of a hot plate (hot plate being the ambient air), unlike the first 3 cases where it is a case of top of a heated plate (the plate being the pool surface humid air).

So to summarize, the evaporation/convection governing equations can be approximated to that of the top heated plate except when Grashof number is negative, it would be that of a reversed plate.

Criteria Used to determine type of flow below the shield (Ri):

In order to determine the type of convection currents below the shield in the shield down position, $Richardson\ Number(Ri) = Gr/Re\text{^}2$ could be used. Two alternative approaches were found:

1) The domination of forced, natural or mixed convection can be set according to Richardson number as follows (Holman, J.P. and White 1992)

a) For very low Ri <0.1, forced convection dominates

b) For very High Ri >10, natural convection (Holman, J.P. and White 1992)

c) For Ri close to unity (0.1<Ri<10), mixed convection

In this case forced convection can either aid, oppose or be perpendicular to free convection currents. Nusselt Number(Nu) in that case can be approximated by adding Nu of both free and forced to some power n being for horizontal surfaces and 4 for spheres.

$$N^n = Nu^{nforced} + Nu^{nfree}$$

2) According to this study in the interpretation of TRNSYS 2017 code (Auer 1996) ,the domination of forced, natural or mixed convection is also set according to Richardson number with different limits as follows

a) For very low Ri <0, forced convection dominates. It is assumed to be the case of reversed plate as it should correspond to Gr<0 and negative density difference.

b)For higher Ri >2, natural convection

c)For Ri close to unity (0<Ri<2), mixed convection

B.3: Calculation of thermal conductivity of the shield:

As discussed in chapter 3, each section the shield is composed of 4 layers of different materials as listed in the following table.

Material	K in $\frac{w}{m\,^{\circ}C}$(Holman, J.P. and White 1992)	Thickness in m (δx)	Resistance per unit Area ((δx)/k($m^{2}{}^{\circ}C/w$)
Corrugated Galvanized steel	54	0.001	0.0000154(1.2 Area factor-Corrugated)
Foam	0.03	0.05	2.2(0.75 Area factor)
Wood	0.13	0.03	0.23
Polypropylene hollow sheet	0.055 (0.16(polypropylene)-25% & 0.02624(air)-75%)	0.005	0.09
			∑=2.52/A A : Total Area of shield sections used(Each section is 1.1 wX4 L) $\sum R = 0.57$ per section($^{\circ}C/w$)